

A Proportional Timing Generator
for Measuring Intermodulation
Product Distortion
on Television Transposers

by

Paul Frederick Bouwer

Submitted in partial fulfilment of the
requirements for the degree of
Doctor of Philosophy
in the
Department of Electronic Engineering
University of Natal
Durban.

1989

PREFACE

The experimental and theoretical research described in this thesis was carried out by the author in the Electronic Engineering Department of the University of Natal at Durban during the period January 1983 to October 1989 under the supervision of Professor A.D. Broadhurst.

These studies represent original work by the author and have not been submitted in any form to another University for any degree. Where use was made of work carried out by others, it has been duly acknowledged in the text.

Signed



Date

31st October 1989

ABSTRACT

Broadcasting authorities presently measure intermodulation distortion by applying a three tone simulation of a composite video and sound signal to the transposer and then measuring the relative amplitude of the major in-band intermodulation product (nominally at vision carrier frequency plus 1,57 *MHz* in the 625 line I/PAL System) on a spectrum analyser. This method is slow and requires a skilful operator to achieve repeatable results. Furthermore it tests the common RF amplification equipment at one luminance level and one chrominance level and therefore does not subject the transposer equipment to operation over its full range.

A new sampling measurement technique has been proposed which overcomes all these problems by selectively mixing, while transmitting a colour bar test pattern, the demodulated output video signal of the frequency transposer with a pulse train coinciding with a particular colour. This thesis describes the design of a very stable proportional timing generator and its application to the measurement of intermodulation distortion on frequency transposers.

The timing generator, which locks automatically onto the video signal and produces narrow sampling pulses which coincide accurately with a particular section of each line over a 50 °C temperature range, is applicable to all PAL and NTSC TV Systems.

DEDICATION

To Almighty God

Creator of Heaven and Earth and all that is in them

Who implanted the ear and invented the eye [Psalm 94:9]

Whose Designs are evident in all of Nature

and To His Son Jesus Christ The Lord

To Whom all Praise and Glory is due

and

without Whose help this project would not have been completed.

ACKNOWLEDGEMENTS

I would like to thank Prof. A.D. Broadhurst for his diligent supervision, many helpful discussions, and for providing clear guidance and encouragement throughout this project.

My sincere thanks are also extended to the following:

Prof. H.L. Nattrass, Head of the Department of Electronic Engineering, for encouraging the use of departmental facilities and participation of his staff in the project.

Mr. G. Vâth, whose practical advice and professional construction of the prototype helped to produce a reliable and versatile instrument.

Mr. R.C.S. Peplow, for providing computer aided design support for printed circuit mask manufacture and schematic circuit diagram drafting, and for assistance with the Kidron Laser Octave used for producing this document.

The South African Broadcasting Corporation for financing and directing this research through their Senior Director, Technical, Mr. P.J. Theron.

Mr. A.L. Curle, Head of Research, for proposing the research programme, for providing much valuable information on the three tone test measurement technique, and his careful practical assessment of the analyser.

Mr. P. Fraser, Head of Transmitter Operations, and Mr. J. Hind, Regional Technical Director, for their support. Mr. S.W. Freemantle, Transmitter Manager, Natal, and his technical staff who spent many hours testing the distortion analyser and explaining the intricacies of transmitter performance testing.

Mr. F. van Vloten for assistance with quartz crystal specifications and crystal oscillator designs.

Messrs. T. Watts and A. Munnik for procuring many components for the manufacture of the prototype, and for their helpful discussions and suggestions.

Finally, Messrs. H. Tibaud and P. Facoline who provided drafting support and demonstrated their expertise with the Gerber CAD equipment.

Any typographical and spelling errors are my own.

TABLE OF CONTENTS

	Page
TITLE _____	i
PREFACE _____	ii
ABSTRACT _____	iii
DEDICATION _____	iv
ACKNOWLEDGEMENTS _____	v
TABLE OF CONTENTS _____	vi
COLOUR PHOTOGRAPHS _____	xiv
LIST OF PRINCIPAL SYMBOLS _____	xv

CHAPTER 1

INTRODUCTION

Introduction to the Sampling Type

Intermodulation Distortion Analyser _____ 1

CHAPTER 2

METHODS OF MEASURING TV TRANSPOSER

INTERMODULATION DISTORTION

2.1	Introduction to Testing Methods _____	7
2.2	The Three Tone Test _____	8
2.2.1	Introduction _____	8
2.2.2	Theory of the Three Tone Test _____	8
2.2.3	Three Tone Test Signal Levels _____	12
2.2.4	Three Tone Test Procedure _____	14
2.2.5	Limitations of the Three Tone Test _____	15
2.3	Flor's Measurement Technique _____	16
2.3.1	Introduction _____	16
2.3.2	Flor's Measurement Procedure _____	18
2.3.3	Limitations of Flor's Method _____	21
2.4	Swiss PT&T Three Tone Test for Measuring Intermodulation Product Distortion _____	22
2.4.1	Introduction _____	22

2.4.2	Theory of the Swiss PT&T 3TT	25
2.4.3	Instantaneous Sideband Noise Amplitudes	28
2.4.4	Swiss PT&T Test Results	30
2.5	A Sampling Technique for Measuring Intermodulation Product Distortion in Television Transposers	31
2.5.1	Introduction	31
2.5.2	The Original Sampling I.M. Analyser	31
2.5.3	Theory of the Sampling Measurement Technique	36
2.5.4	I.M. Measurement using the I.M. Analyser	47

CHAPTER 3

SYSTEM DESIGN CONSIDERATIONS FOR A SAMPLING TYPE TELEVISION INTERMODULATION DISTORTION ANALYSER

3.1	Practical Problems Associated with the Original Sampling Concept	49
3.1.1	Introduction	49
3.1.2	The Need for a Wide Initial Bandwidth	49
3.1.3	Identical Low Pass Filters	51
3.1.4	Sampling Pulse Timing Tolerances	51
3.1.5	Phase Alternation of Chrominance "V"	52
3.1.6	Applicability to all TV Systems	53
3.2	A Proposed Time Division Multiplexed Intermodulation Distortion Analyser	54
3.2.1	Introduction	54
3.2.2	Intermodulation Signal Down-Conversion	56
3.2.3	Active Low Pass Filters	56
3.2.4	Intermodulation Signal Amplitude Detection	57
3.2.5	Analogue-to-Digital Conversion	59
3.2.6	Logarithmic Digital dBp Display	59
3.3	System Design Philosophy	60
3.3.1	Optimum Noise Performance	60
3.3.2	Selection of a Down-Conversion Mixer	60
3.3.3	Choice of a Pulse Timing Generator	61
3.3.4	A Temperature Compensation Technique	61

3.4	Multiplexed System Gain Estimation	61
3.5	Theoretical Relationship between I.M. Measurement Error, System Rise Time and Sampling Pulse Delay	65
3.6	Crystal Reference Oscillator	68

CHAPTER 4

PROPORTIONAL TIMING PULSE GENERATOR THEORY AND DETAILED CIRCUIT DESIGN

4.1	Operation of the Phase Lock Loop Based Sample Timing Pulse Generator	69
4.1.1	Introduction	69
4.1.2	Operation of the Phase Lock Loop Based Sample Timing Pulse Generator	70
4.1.3	Phase Lock Loop Synchronisation	72
4.2	Phase Lock Loop System Design	73
4.2.1	Initial Parameter Estimates	73
4.2.2	Choice of VCO Timing Component Values	76
4.2.3	Selection of Low Pass Filter Components	79
4.2.4	Measured VCO Transient Performance	81
4.2.5	PLL VCO Phase Error Estimates	84
4.2.6	Frequency Spectrum of the Ramp Modulated VCO Output Signal	90
4.3	PLL Status Indication Circuits	94
4.3.1	Introduction	94
4.3.2	PLL Status: Video Present	94
4.3.3	PLL Status: Locked or Unlocked	96
4.3.4	LM556 Dual Monostable Status Timer	96
4.3.5	Synchronisation of Histogram Display	97
4.4	Timer Circuit Stability	98
4.4.1	Introduction	98
4.4.2	Sync Separator Timing Stability	99
4.4.3	Design Philosophy for Temperature Stable CMOS Monostable Pulse Generators	100
4.4.4	Monostable Pulse Circuit Designs	102
4.4.4.1	Choice of Timing Resistors	102
4.4.4.2	5,6 μ s Delay Monostable Designs	103

4.4.4.3	1,8 μ s Sampling Monostable Designs	104
---------	---	-----

CHAPTER 5

TIMING GENERATOR CALIBRATION, I.M. ANALYSER TESTS, APPLICATIONS AND ERROR vs SYSTEM RISE TIME		
5.1	Timing Generator Calibration	106
5.1.1	Introduction	106
5.1.2	Test and Calibration Procedure	106
5.2	Comparative Tests Performed at 25°C	
	I.M. Analyser vs Three Tone Test	112
5.2.1	Introduction	112
5.2.2	Preliminary Checks and Precautions	113
5.2.3	Comparison Test Procedure	114
5.2.4	Results of the Comparative Tests Performed at 25°C	115
5.3	Comparative Tests Performed at 0°C, 25°C and 50°C	
	I.M. Analyser vs Three Tone Test	118
5.3.1	Test Procedure	118
5.3.2	Test Results	118
5.3.3	Test Equipment Requirements	122
5.4	Acceptance Tests Performed by the Swiss Institute for Posts, Telephones and Telegraphs	123
5.4.1	Introduction	123
5.4.2	Test Procedures	123
5.4.3	Colour Burst Measurements	124
5.4.4	I.M. Analyser Frequency Bandwidth	125
5.4.5	Internal Reference Oscillator Check	125
5.5	Practical I.M. Measurements on TV Transposers using the I.M. Analyser	126

CHAPTER 6

CONCLUSIONS AND RECOMMENDATIONS	_____	
6.1 Barlows Communications Test Results	_____	128
6.2 Swiss PT&T Institute Test Results	_____	128
6.3 Errors due to System Rise Time	_____	130
6.4 Stability of Sampling Delay Time	_____	130
6.5 Applications of the Sampling I.M. Analyser	_____	131

APPENDIX A

INTERMODULATION DISTORTION ANALYSER FUNCTIONING AND SPECIFICATIONS	_____	A.1
---	-------	-----

APPENDIX B

THEORY OF INTERMODULATION DISTORTION IN TELEVISION TRANSPOSERS DUE TO NON-LINEAR COMMON AMPLIFICATION		
B.1 Introduction	_____	B.1
B.2 I.M. Distortion Theory	_____	B.2
B.3 Prediction of I.M. Distortion for a Thomson CSF Type TH382 Power Tetrode	_____	B.4
B.3.1 Constant Current and Mutual Characteristics	_____	B.4
B.3.2 Transfer Characteristic Modelling	_____	B.6
B.4 I.M. Distortion Power Amplitudes	_____	B.10
B.5 Conclusions	_____	B.13

APPENDIX C

CMOS CD4046 PHASE LOCK LOOP PHASE COMPARATOR CIRCUITS: DETAILED ANALYSIS OF OPERATION		
C.1 Phase Lock Loop Theory	_____	C.1
C.1.1 Introduction to Phase Lock Loop Theory	_____	C.1
C.1.2 Derivation of the Phase Lock Loop System Transfer Function STF(s)	_____	C.4
C.2 Phase Lock Loop Feedback System Stability Considerations	_____	C.6

C.2.1	A System Analysis Problem	C.6
C.2.2	The Root Locus Approach	C.6
C.2.3	Type 1 Second Order Systems using a Passive R-C Low Pass Filter	C.8
C.2.4	Type 1 Second Order Systems using a Passive Lag-Lead Filter	C.10
C.3	CMOS CD4046 Phase Lock Loop	C.11
C.4	CMOS CD4046 Phase Comparator I	C.12
C.4.1	Basic Operation	C.12
C.4.2	Phase Difference Operation	C.13
C.4.3	Frequency Locked – not Phase Locked	C.14
C.4.4	The Problem of Harmonic Locking	C.14
C.5	CMOS CD4046 Phase Comparator II	C.15
C.5.1	Basic Operation of Phase Comparator II	C.15
C.5.2	Phase Difference Operation	C.19
C.5.3	Frequency Difference Operation	C.24
C.6	Phase Comparator Gain K_d	C.25
C.7	Observations and Conclusions	C.26

APPENDIX D

MEASUREMENT OF PERFORMANCE PARAMETERS FOR THE CMOS CD4046 PHASE LOCK LOOP CHIP

D.1	Introduction	D.1
D.2	Phase Comparator II Gain Factor K_{d2}	D.1
D.3	VCO Gain Factor K_o	D.2
D.4	PLL Capture and Lock Range	D.9
D.5	Measurement of Phase Shift Error when using Phase Comparator II	D.13
D.6	Summary and Observations	D.13

APPENDIX E

TEMPERATURE COMPENSATION THEORY
FOR CMOS MONOSTABLE PULSE TIMERS

E.1	Introduction	E.1
E.2	Timer Circuit Design Procedure	E.1
E.3	Temperature Compensation Theory	E.2
E.3.1	Temperature Behaviour of R-C Components	E.2
E.3.2	Pulse Width vs Temperature Performance:	
	CMOS Dual Monostable Chips	E.3
E.3.3	Pulse Width Temperature Compensation	E.4
E.4	Effective Temperature Coefficient	
	for Two Like Elements	E.5
E.4.1	Two Resistors in Series	E.5
E.4.2	Two Resistors in Parallel	E.6
E.4.3	Linearisation of a Thermistor	E.6
E.4.4	Two Capacitors in Parallel	E.8
E.4.5	Two Capacitors in Series	E.8
E.5	Passive Component T.C. Specifications	E.9
E.6	Polynomial Curve Fitting	E.10
E.6.1	The Least Squares Technique	E.10
E.6.2	Application to CD4528 and CD4538	
	CMOS Monostable Timer Chips	E.11
E.7	Conclusions	E.13

APPENDIX F

DETERMINATION OF NOISE LEVELS
DUE TO THE SAMPLING OF THE
LUMINANCE AND CHROMINANCE SIGNALS

F.1	Introduction	F.1
F.2	Noise Produced when Sampling a	
	Constant Luminance Signal	F.3
F.2.1	System I/PAL Luminance Sampling Noise	F.3
F.2.2	System M/NTSC Luminance Sampling Noise	F.9
F.2.3	Luminance Noise Reduction Techniques	F.9
F.3	Noise Produced when sampling	
	the Colour Subcarrier	F.14

F.3.1	Chrominance Sampling Noise Theory	F.14
F.3.2	Chrominance Noise Reduction Techniques	F.16
F.3.3	Low Pass Filter Design Options	F.17
F.3.4	Filter Component Values	F.17
F.3.5	Response of Passive Butterworth Filter	F.20
F.4	Conclusions	F.21

APPENDIX G

SABC TV SPECIFICATIONS FOR TV COLOUR BAR SIGNALS AND TV CARRIER FREQUENCY TOLERANCES

G.1	TV Colour Bar Specifications	G.1
G.1.1	Introduction	G.1
G.1.2	Field Sync Pulse Specifications	G.3
G.1.3	Line Sync Pulse Specifications	G.5
G.1.4	Colour Burst and White Bar Specifications	G.6
G.2	Estimated Tolerances in Expected Intermodulation Product Frequencies	G.7
G.2.1	Introduction	G.7
G.2.2	Expected Frequency Tolerances	G.7
G.3	Compatible Pulse Timer Specifications	G.9
G.4	Conclusions	G.9

APPENDIX H

PAPERS PUBLISHED ON THE SAMPLING TYPE INTERMODULATION DISTORTION ANALYSER

Copies of two published papers	
co-authored by the writer	
and referred to in references [8] and [9].	H.1

REFERENCES	REF.1
------------	-------



Fig. 0.1 Prototype Television Intermodulation Analyser
A New Sampling Type Instrument with Unique Features



Fig. 0.2 Prototype Television Intermodulation Analyser
with OKF Monitor showing Histogram Display of
Intermodulation Distortion within each Colour Bar

LIST OF PRINCIPAL SYMBOLS

A_v	Voltage gain factor
BW	Bandwidth in radians/second or hertz (as specified)
C	Capacitance in farads (unless otherwise indicated)
$C(t)$	Counter input signal to the phase lock loop phase comparator
C_T	VCO timing capacitance in farads
dB	Power ratio in decibels relative to some reference power
dBp	Power ratio in decibels relative to peak sync power
dBm	Power ratio in decibels relative to 1 mW into 50 Ω
f_c	Filter -3 dB cut-off frequency in hertz
f_{IM}	Intermodulation distortion difference frequency within the video frequency band (i.e. $f_s - f_{SC}$) in hertz
f_{SC}	Colour subcarrier frequency in hertz
f_s	Sound subcarrier frequency in hertz
f_v	Video carrier frequency within the intermediate frequency band in hertz
$F(s)$	System transfer function in the frequency domain
f_z	Frequency in hertz of first sideband with zero amplitude
$I(t)$	External input signal to the phase lock loop phase comparator
i_A	Power tetrode instantaneous anode current in amperes
i_{ch}	Phase lock loop filter capacitor charging current in amperes
i_{dis}	Phase lock loop filter capacitor discharge current in amperes
K_{pw}	Ratio of monostable pulse generator pulse width to R-C time constant
K_o	Phase lock loop voltage controlled oscillator gain factor in radians/volt-second
K_d	Phase lock loop phase comparator gain in volts/radian
L	Inductance in henrys (unless otherwise indicated)
m	Modulation index
n_z	Number of first sideband with zero amplitude
P	Power dissipation in watts
$P_i(t)$	Fourier series representation of a pulse waveform
PW	Monostable pulse width in seconds
Q	General quality factor of a resonant (tuned) circuit
Q_w	Working or loaded quality factor of a resonant circuit

R	Resistance in ohms (unless otherwise indicated)
R_1	Mark-to-space ratio of a pulse waveform
t	Time in seconds
T	Temperature in degrees celsius
T_H	Television horizontal line period in seconds
$v_d(t)$	Phase lock loop phase comparator output signal in the time domain
$v_i(t)$	Instantaneous input voltage in the time domain in volts
$v_F(t)$	Fourier series representation of the effective field pulse waveform due to loss of video signal during field synchronisation
$v_f(t)$	Phase lock loop instantaneous filter output signal in volts
$v_k(t)$	Phase lock loop counter output signal in the time domain
$v_{LO}(t)$	Fourier series representation of the local oscillator signal
$V_{mix}(t)$	Instantaneous mixer output signal voltage
$V_{miximd}(t)$	Instantaneous down-converted intermodulation distortion component of the mixer output signal voltage
$v_{Lum}(t)$	Fourier series representation of the sampled luminance component in the video signal
$V_o(s)$	Output voltage in the frequency domain in volts
$v_o(t)$	Instantaneous output voltage in volts
$V_s(s)$	Source voltage in the frequency domain in volts
$v_s(t)$	Instantaneous source voltage in volts
$v_{Sa}(t)$	Fourier series representation of the sampling pulse waveform
α	Half the bandwidth of a tuned circuit in radians/second
α_r	Temperature coefficient of resistance in ohms/ohm-degree
ζ	Damping factor of a resonant circuit or second order system
θ	Phase angle in radians
θ_e	phase detector input phase angle error in radians
τ_r	Rise time of system in seconds
ϕ	Phase shift in radians
ω_n	Natural frequency of a resonant circuit or second order system
ω_f	Phase lock loop VCO free running frequency in hertz
ω_H	Television horizontal line frequency in radians/second
$\omega_{1/2H}$	Half the television line frequency in radians/second
ω_o	Centre or resonant frequency of a resonant circuit or second order system in radians/second
ω_{Sa}	Fundamental frequency of sampling pulse waveform in radians/second

CHAPTER 1

Introduction to the Sampling Type Intermodulation Distortion Analyser

This thesis represents a contribution by the author to the design and implementation of an intermodulation distortion analyser for testing the linearity of television transposers. It reports on original research by the author into the design of a proportional timing generator with the stability required for the implementation of a sampling type intermodulation (I.M.) distortion analyser. The initial concept and theoretical development of the sampling measurement technique was due to A.D. Broadhurst [1]. The theory was extended by the author to determine the noise contributions of unwanted sidebands produced by the sampling process that fell within the measurement frequency window.

In Broadhurst's original I.M. distortion analyser, six separate channels were required to allow I.M. distortion produced within each bar of a standard colour bar test signal to be measured, and displayed, simultaneously. An improved system, proposed by the author, used time division multiplexing of a single channel. This multiplexed system was adopted for the final prototype I.M. analyser described in this thesis after a theoretical analysis, and measurements on a two-channel, breadboarded system, had revealed serious matching problems between channels in attempting to achieve an accuracy of $\pm 0,5 \text{ dB}$.

As a prelude to patent applications for the new measurement system an extensive literature search was conducted through the South African Inventions Development Corporation of the Council for Scientific and Industrial Research. It revealed only one other I.M. distortion measurement system remotely similar to Broadhurst's sampling concept. This technique, described in a paper by Flor [2], was sufficiently different in principle to allow patent applications to proceed in Britain [3], Western Europe, the United States of America, Canada and Japan. Flor's method of measuring I.M. distortion is

discussed in Chapter 2, together with the new sampling technique and the standard three tone test.

The sampling technique used in the multiplexed I.M. analyser for measuring I.M. distortion level is based upon selectively mixing the demodulated output of the frequency transposer, when modulated with a colour bar test pattern or similar waveform, to produce a 200 *Hz* component proportional to The I.M. distortion amplitude. This low frequency component is then filtered, rectified, and its amplitude converted to digital form for display in *dBp* (ie. *dBs* relative to peak sync power). A detailed description of the multiplexed instrument and problems associated with its operation are presented in Chapter 3. The design of the sample pulse timing generator is given in Chapter 4. Appendix C has the relevant phase lock loop theory and a comprehensive description of the operation and performance of the phase comparators in the **CD4046** CMOS phase lock loop chip. Appendix D records the empirical values of, and the measurement techniques for determining, the chip's major performance parameters.

The functioning of the I.M. Analyser is summarised in Appendix A. Simultaneous outputs are available, which give the I.M. distortion levels corresponding to the various colours in the colour bar test pattern. These distortion levels may be displayed on a monitor as a histogram to facilitate the adjustment of frequency transposer pre-correctors for optimum I.M. distortion performance. Typical histograms, calibration information and test results obtained from the use of the I.M. distortion analyser appear in Chapter 5.

Television relay stations are designed to receive signals in one frequency band and then re-transmit the information either on another channel in the same band, or in another band altogether. Those relay stations receiving at VHF and re-transmitting at UHF frequencies are usually used to provide local coverage in poor VHF reception areas, where problems have arisen due to geographical features such as mountains and high hills. This relay technique obviates the need for high quality land line links between TV transmitters, but any non-linearity in the transposer equipment degrades the information transmitted.

A typical up-converter type relay station has a VHF receiving antenna directed towards another broadcast television station for use by the frequency transposing equipment in the television relay station to receive a VHF transmission. A nearly identical signal is then transmitted at UHF by the transposer equipment from a separate UHF transmitting antenna. The frequency transposer equipment selects the appropriate channel for reception and frequency converts the whole vestigial sideband signal up in frequency to the desired channel for re-transmission. The received VHF television signal is not demodulated at any stage during the relay process.

Any non-linearities in the characteristics of the amplifiers of the frequency transposing equipment cause intermodulation products to be produced. This is particularly prevalent in the final output stage. These intermodulation products are generated by the interaction of the vision and sound signals and cause visible and audible distortion. The most visible product produces a "fishbone" or Moiré type pattern on the TV receiver's screen which is caused by beats between the vision carrier, colour subcarrier and sound subcarrier. The cause of I.M. distortion, and a numerical technique for predicting the I.M. level produced within an amplifier with a known transfer characteristic, is discussed in Appendix B.

Comprehensive tests have been performed to determine the subjective effect of intermodulation distortion on various types of scene displayed on a television monitor. Shelswell [4] has shown that scenes with little saturated colour could withstand high I.M. levels equivalent to -40 dBp on the three tone test without much degradation. Those scenes containing high frequency components were particularly critical because of the presence of Moiré patterns, although in some cases cross colour effects tended to predominate and mask these patterns. For scenes with large areas of saturated colour a consistent relationship between subjective degradation and I.M. level has been found, with -52 dBp giving a "just perceptible" pattern. Saturated red areas were the most susceptible to intermodulation distortion, as was confirmed independently by Newell and Geddes [5] and Rösler [6].

Picture interference was claimed to be less perceptible with the sound carrier modulated as the coherence of the Moiré pattern was reduced. It was observed during comparative tests, however, that a low frequency modulation of 40 Hz

caused the Moiré pattern to move and thus become more visible. Speech modulation is said by local transmitter engineers to produce even more disturbing results.

Harvey [7] has performed similar subjective tests on the effects of intermodulation distortion. He has shown that the visibility of the Moiré pattern is dependent on the sound/vision intercarrier frequency, with optimum conditions (ie.least visibility) occurring with a sound subcarrier frequency set to $6\text{ MHz} - 400\text{ Hz}$, or $5\,999\,600\text{ Hz}$. This latter frequency is used for the sound carrier during normal TV broadcasts in South Africa, but 6 MHz is usually used during the three tone testing of transposers. The I.M. Analyser was designed to automatically cope with both these frequencies.

It should be noted that the mean operating points of the output devices, which are usually vacuum tetrodes, are determined by the luminance component within the TV signal. A large luminance component will give a different average operating point on the device static characteristic to that due to a low luminance level, and the non-linearities of the output devices will differ correspondingly. It follows that the intermodulation distortion levels will vary with both luminance and chrominance levels. This fact is not easily exploited in the two main measurement techniques that have been used thus far. The proposed sampling technique, however, makes use of the colour bar signal or similar waveform with a wide range of combined luminance and chrominance components. This allows the transmitter to be tested over almost its full dynamic range.

This new sampling approach to I.M. measurement was presented at the 11th International Broadcasting Convention held at Brighton, England, during September 1986 [8]. Some results of tests performed using the I.M. Analyser were included in that presentation. A more detailed description of the analyser's operation and its application to I.M. measurements was presented at the IEEE Broadcasting Symposium held at Washington D.C. in September 1987 [9]. These papers, co-authored by the writer, are included as Appendix H.

Originality is claimed for the following aspects of the sampling I.M. distortion analyser described in this thesis:

1. Development of a phase lock loop based digital state machine for division of each video line into ten equal parts. This proportional subdivision of the video line is essential for the correct positioning of sample pulses within the standard colour bar test waveform used in conjunction with the analyser. Details of the colour bar signals used by the South African Broadcasting Corporation, together with sync pulse and frequency tolerance specifications, may be found in Appendix G. Proportionality is ensured irrespective of the system (PAL or NTSC) line frequency by phase locking the state machine to the line sync pulses. [see Chapter 3, Section 3.3]
2. Conversion of A.D. Broadhurst's original concept of the sampling I.M. distortion analyser into a time division multiplexed system for ease of practical implementation [see Chapter 3, Section 3.2].
3. The formulation and experimental verification of sampling noise theory applicable to this sampling measurement system [see Appendix F].
4. Development of an averaging sample-and-hold circuit [see Chapter 3, Section 3.2.4].
5. Development of a mechanism for recovering continuous line pulses [see Chapter 4, Section 4.1.2].
6. Derivation of the theoretical relationship between I.M. distortion measurement error, system rise time, and sampling pulse delay time. A simple computer programme facilitates the determination of measurement error for different combinations of system rise time and sample pulse delay [see Chapter 3, Section 3.5].

In addition to the above, related work was carried out on the temperature compensation of electronic timer circuits used in the sample pulse generator. The theory developed in this regard may also be original:

7. Derivation of temperature compensation theory involving non-linear temperature coefficients (T.C.s) for the timer integrated circuit, and linear T.C.s for the passive timing elements. The theory allows the use of combinations of resistors and capacitors with differing T.C.s for accurate temperature compensation of these timing circuits [see Appendix E].

When considering the theory of intermodulation distortion presented in Appendix B the author decided to perform a numerical simulation of a Class B Television power amplifier using the least squares approach to quantify the coefficients of the polynomial representing the amplifier transfer characteristic. Hence originality is claimed for:

8. The prediction of intermodulation distortion in a Class B amplifier stage with Thomson CSF TH382 power tetrodes using a numerical simulation technique.

It should be noted that, unless otherwise indicated, all parameters quoted in this dissertation are for the I/PAL system current in use in South Africa.

CHAPTER 2

Methods of Measuring TV Transposer Intermodulation Distortion

2.1 INTRODUCTION TO TESTING METHODS

A general introduction to the cause of intermodulation (I.M.) distortion in common amplification TV transmitters is presented in Appendix B. The problem is avoided in transmitters having separate amplifiers for the vision and sound signals, but is prevalent in low power transposers (or repeaters) with common amplification.

A number of methods are available for measuring the I.M. distortion level in broadcast equipment. In this chapter, a few selected tests are described together with their basic theory. The measurement technique most commonly used among broadcasting authorities is the Three Tone Test (3TT) [10, 11], while that due to Flor [2] is closest in concept to the new sampling method proposed by A.D. Broadhurst [1]. A variation of the 3TT performed by the Swiss Posts, Telephones and Telegraphs (PT&T) is included [17], as it represents the accepted standard in Europe. A wobulation technique is also used by the Swiss PT&T but is not discussed as insufficient details are known.

Japan appears to be the only country that requires three tone tests to be conducted at each of six modulation levels corresponding to the six colour bars in a standard colour bar signal [15]. Indeed the I.M. distortion specifications applicable to TV broadcasters in many countries appear to be rather loosely defined.

2.2 THE THREE TONE TEST

2.2.1 Introduction

A typical test configuration for conducting the Three Tone Test (3TT) is shown overleaf in block diagram form in Fig. 2.1. The main difference between this test configuration and that performed on a practical transposer is that no frequency conversion occurs in the test. Other possible arrangements are described by Best [10] and Heydel und Vogt [11].

2.2.2 Theory of the Three Tone Test

The spectrum of a transmitted I/PAL television signal modulated with a 100/0/75/0 colour bar test pattern is shown in Fig. 2.2. Three dominant frequency components are evident. They are:

1. Vision carrier at frequency f_v
2. Colour subcarrier at frequency f_{sc}
3. Sound carrier at frequency f_s

These three frequencies are used to simulate a transmitted television signal in order to be able to measure frequencies and levels of intermodulation products generated by any non-linearities of the transmitter. A typical spectrum of such a three tone signal is shown in Fig. 2.3.

A television picture will have, in addition to the discrete frequency components in Fig. 2.3, sidebands of smaller amplitudes at multiples of both the half-line frequency $\frac{1}{2}f_H$ in a PAL system because of phase alternation each line, or the line frequency f_H in the NTSC System, and the field frequency of 50 Hz (Europe and RSA) or 60 Hz (USA) as can be seen from Fig. 2.2. When the three principal frequencies f_v , f_{sc} and f_s are passed through a transmitter with a non-linear transfer function, intermodulation (I.M.) terms are produced.

Considering System I/PAL, the three most significant of these intermodulation terms are:

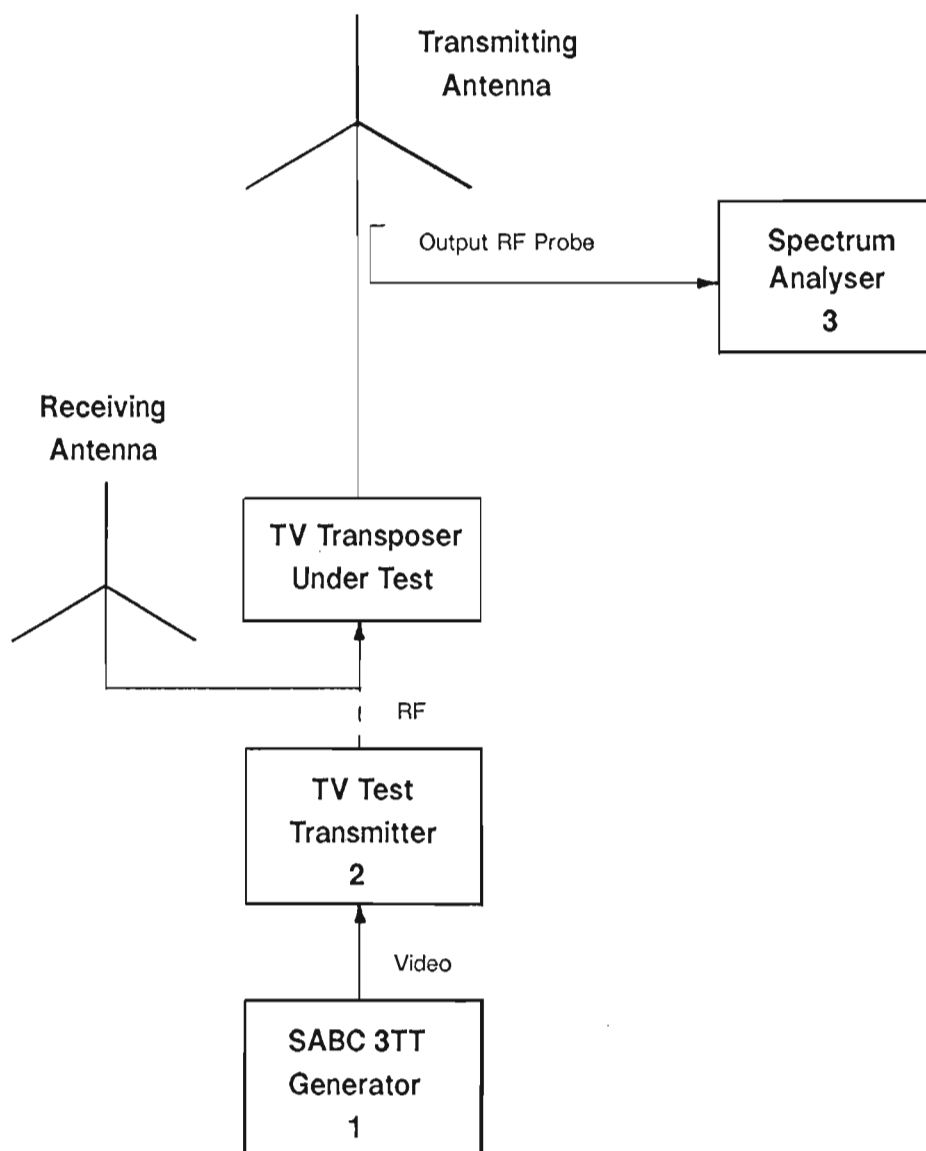
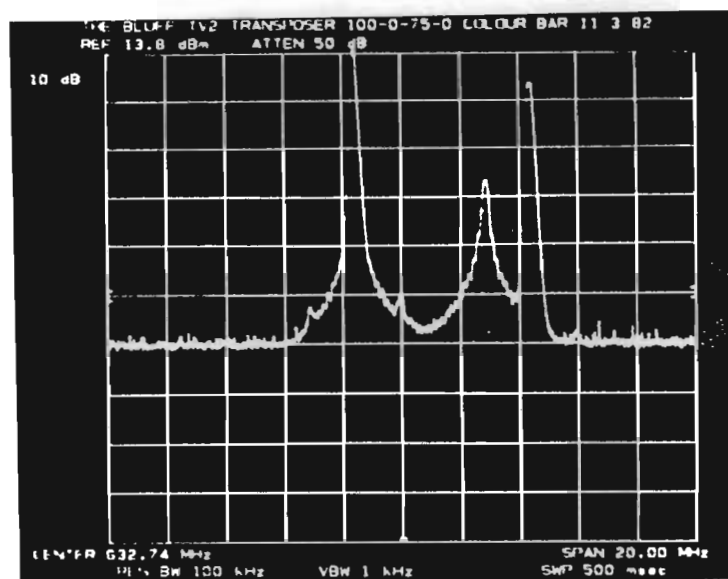


Fig. 2.1 Block Diagram for I.M. Measurement
Using the Three Tone Test Method

Equipment Required:

- | | | |
|----|----------------------|-------------------------|
| 1. | Three Tone Test Gen. | Rohde & Schwarz |
| 2. | TV Test Transmitter | Rohde & Schwarz SBUF |
| 3. | Spectrum Analyser | Hewlett-Packard Hp 141T |



↑
 f_{IM}

Fig. 2.2 Spectrum of Transmitted TV Signal
modulated with a 100/0/75/0 colour bar signal

REF -13.3dBm

10dB/ AT5dB RBW100kHz VBW300kHz

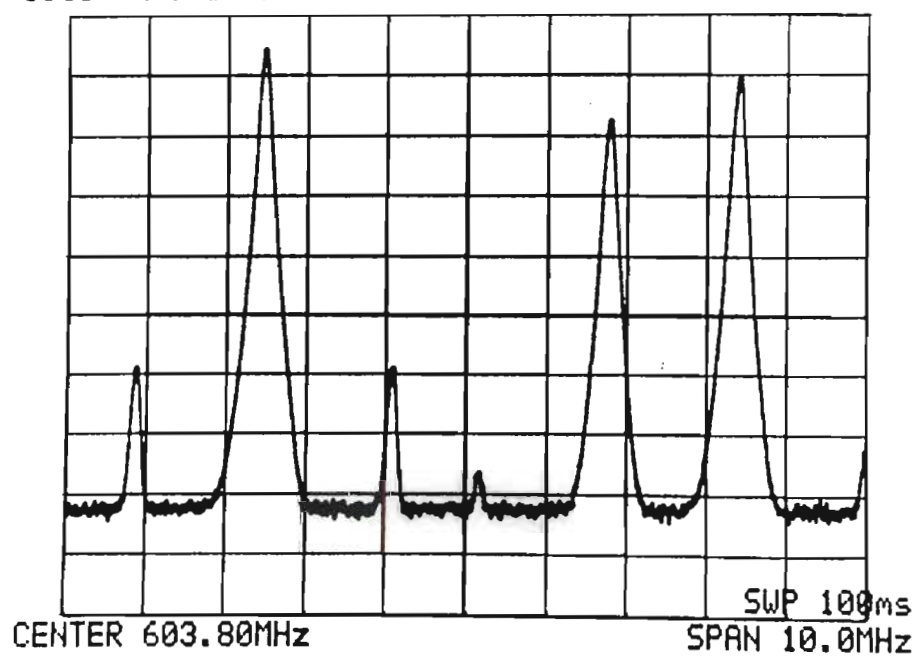


Fig. 2.3 Spectrum of Three Tone Test TV Signal

$$-f_s + f_v + f_{sc} = f_v - 1,57 \text{ MHz} \quad (2.1)$$

$$f_s + f_v - f_{sc} = f_v + 1,57 \text{ MHz} \quad (2.2)$$

$$-f_s + 2f_{sc} = f_v + 2,80 \text{ MHz} \quad (2.3)$$

The first two terms represent sidebands situated at the 1,57 MHz difference frequency on either side of the vision carrier f_v . The most visible in-band I.M. component is the upper sideband at 1,57 MHz, or more accurately at

$$f_{im} = f_v + f_s - f_{sc} \quad (2.4)$$

The lower sideband component at $f_v - f_s + f_{sc}$ may be attenuated by the vestigial sideband filter.

As the vision carrier frequency varies from channel to channel, it is convenient to quote the frequency difference f_{im} relative to the carrier frequency where

$$f_{im} = f_s - f_{sc} \quad (2.5)$$

The most common difference frequencies for various TV Systems are given in Table 2.1.

Table 2.1
Intermodulation Product Frequency f_{im}
Broadcast Conditions

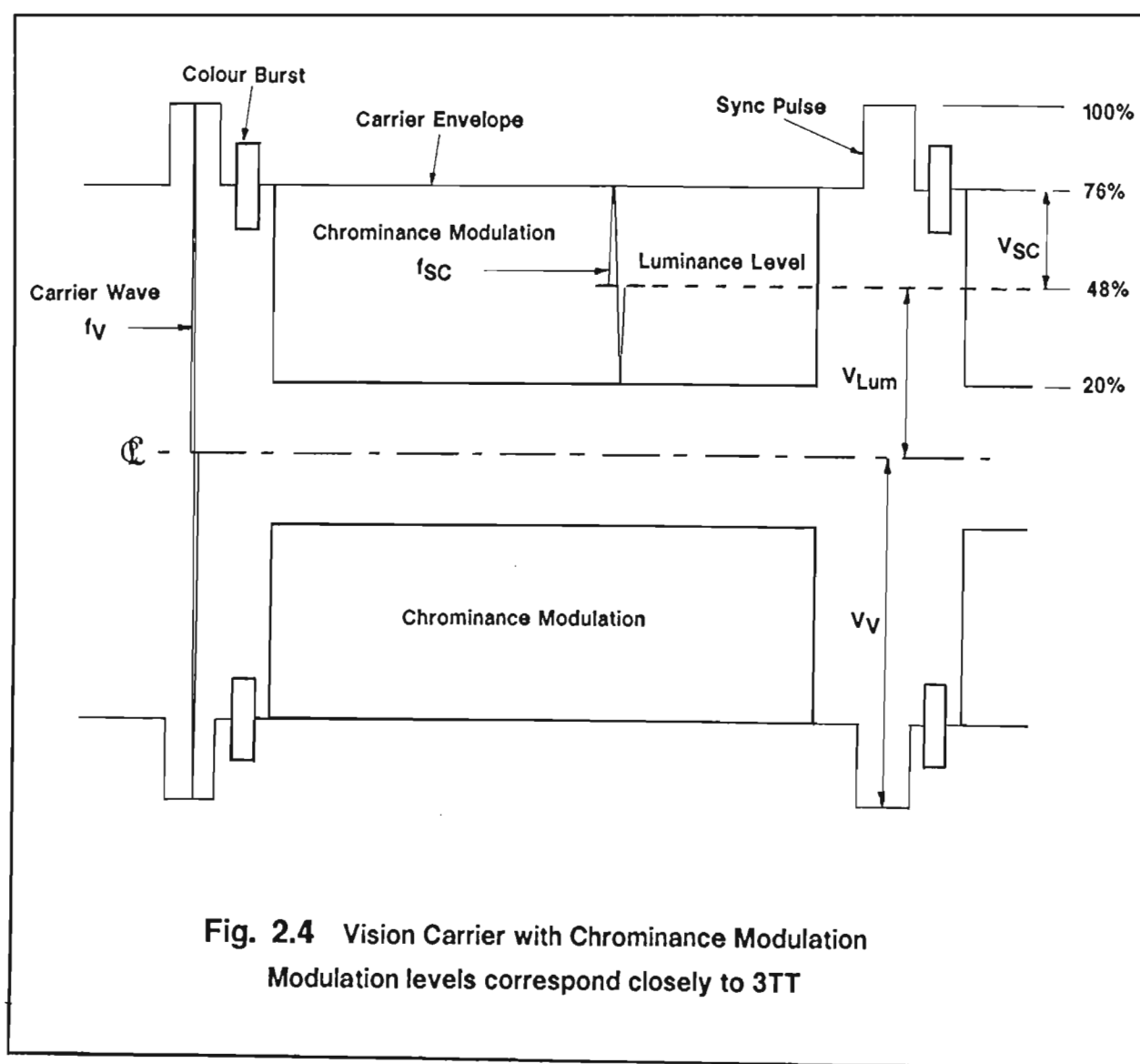
Broadcast TV System	Sound Subcarrier f_s (Hz)	Colour Subcarrier f_{sc} (Hz)	Intermodulation Product f_{im} (Hz)
B/PAL	5500000	4433618,75	1066381,25
G/PAL	5500000	4433618,75	1066381,25
I/PAL	5999600	4433618,75	1565981,25
M/PAL	4500000	3575611,49	924388,51
M/NTSC	4500000	3579545,00	920455,00

The first three of these in-band intermodulation frequencies are commonly referred to as the 1,07 MHz and 1,57 MHz I.M. components respectively. The corresponding I.M. component in the M/NTSC System is at 920 kHz. In the

RSA, the maximum I.M. level permitted by the SABC for System I/PAL transmissions is -53 dBp (relative to peak sync power).

2.2.3 Three Tone Test Signal Levels

Fig. 2.4 below illustrates a vision carrier modulated with a chrominance subcarrier to correspond to the typical 3TT test levels. It should be noted that the 3TT is a carrier test, and no synchronising pulses would be present in the signal as vision carrier modulation. For the sake of simplicity, the sound carrier is not shown.



The amplitudes of the input signal components are set according to the data in Table 2.2 which follow the South African Standards [14]. The vision carrier is usually adjusted to have an amplitude corresponding to mid-grey. In System I/PAL, black corresponds to 20% of the peak vision carrier amplitude, and white to 76%. Thus the vision carrier peak amplitude is set to

$$\frac{1}{2}(76\%-20\%) + 20\% = 48\% \quad (2.6)$$

of peak sync amplitude, or $-6,375 \text{ dBp}$ relative to peak sync power. This is usually taken as -6 dBp for convenience.

The colour subcarrier signal is adjusted in amplitude to modulate the vision carrier from the black level to the white level. This modulation has a peak-to-peak amplitude corresponding to

$$\begin{aligned} (76\%-20\%) &= 56\% \\ &= 200 \text{ m \%} \end{aligned} \quad (2.7)$$

where m is the modulation index. The amplitude modulated vision carrier may thus be expressed as:

$$f_v(t) = V_v \cos(\omega_v t) [1 + m \cos(\omega_{sc} t)] \quad (2.8)$$

Referring to Fig. 2.4 it will be seen that 56% also refers to the peak-to-peak chrominance signal amplitude which, in terms of a demodulated video signal, is equivalent to the white pulse at 0,7 Volts peak. Thus the peak sync or vision carrier amplitude V_v on Fig. 2.4 is 1,25 Volts. *This 1,25 Volt level is used as reference throughout for all dBp calculations.*

Two sidebands are produced by this modulation having identical peak-to-peak magnitudes of $100 \text{ m } V_v$ or 28% of peak sync amplitude at frequencies $(\omega_v \pm \omega_{sc})$. The sideband levels correspond to a peak value of 14% of peak sync, or $-17,08 \text{ dBp}$, which is taken as -17 dBp .

The sound carrier level is usually set to the same order of magnitude as the vision carrier for the relevant TV System [see Table 2.2].

Table 2.2
Input Carrier Levels Relative to Peak Sync Power

COEFF	RSA (dBp)	UK (dBp)	DIN 45 004 (dBp)
A_V	-6	-8	-8
A_{SC}	-17	-17	-17
A_S	-10	-7	-10

2.2.4 Three Tone Test Procedure

The first part of this test is performed with the transposer in service. Because transposers have automatic gain control (AGC) circuits that operate on peak sync, the AGC must be disabled to allow the unmodulated carriers of the 3TT to be accepted. To do this the transmitter output power is set on "AGC disabled" to be the same as with "AGC enabled". AGC is then disabled and a spectrum analyser connected to the output radio frequency (RF) probe. The spectrum analyser is tuned to the transposer vision output frequency and the vision peak sync output level is noted (say A dBm). The spectrum analyser is then disconnected.

The transposer is now taken out of service. The receiver antenna feeder is disconnected from the transposer and connected to the spectrum analyser. On tuning the spectrum analyser to the vision input frequency the peak sync input level is measured at B dBm. The magnitude of the received signal is being used as a reference.

The spectrum analyser is now disconnected from the receiver antenna feeder and connected to the output of the TV Test transmitter which is excited by the 3TT generator. This generator is set to give -6 dB, -17 dB and -10 dB levels relative to the received peak sync level B dBm for the vision carrier, and colour and sound subcarriers respectively. The spectrum analyser is then disconnected from the TV Test transmitter.

The TV Test transmitter is then connected to the transposer input and the spectrum analyser to the transposer output RF probe, and the level of the intermodulation is measured at $C \text{ dBm}$.

The difference between the peak sync power ($A \text{ dBm}$) measured at the output RF probe and the intermodulation level ($B \text{ dBm}$) measured at the probe is the required relative level of the intermodulation distortion in dB .

2.2.5 Limitations of the Three Tone Test

The 3TT is Complicated to Perform: It should be evident that the procedure is complicated and tedious, taking a long time to perform.

The 3TT is a Carrier Test: It cannot therefore be used directly to test a common amplification transmitter. The test signals must be injected at the IF stage of the transmitter, and this is no trivial task for the average technician. Lack of line sync pulses makes it impossible to use the 3TT with the I.M. analyser for direct comparison purposes.

Spectrum Analyser Limitations: The expected accuracy is only about $\pm 3 \text{ dB}$ because the I.M. level to be measured is in practice almost at the noise floor of the typical type of spectrum analyser used. Measurement range is limited to about 58 dB by the dynamic range of the spectrum analyser. The spectrum analyser itself must not be driven too hard or its own mixer will generate intermodulation products.

The 3TT is a Static Test: Measurement of I.M. distortion is performed at only one of many possible combinations of luminance and chrominance levels. This is its severest limitation.

2.3 FLOR'S MEASUREMENT TECHNIQUE

2.3.1 Introduction

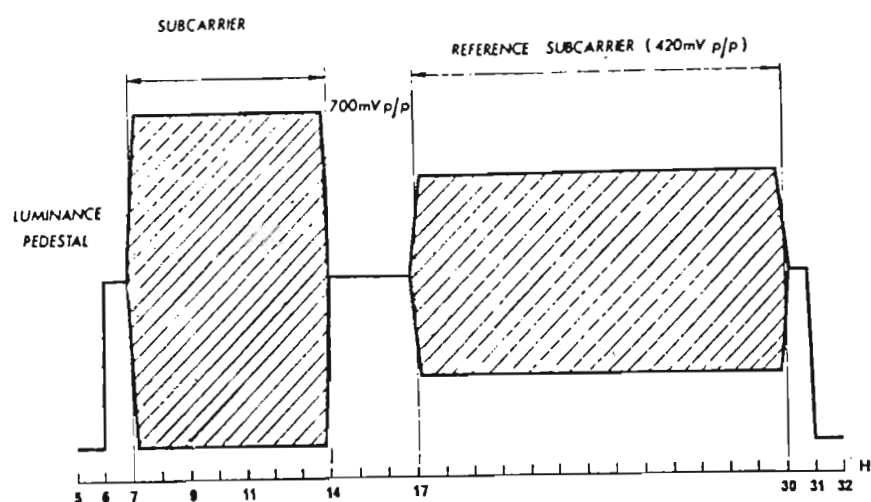
Various lines within each TV frame are used internationally for the transmission of special test signals. Two alternative versions of test line 331, which comply with CCIR International Standard Specifications [13], are used in Austria. The leading sections of these two waveforms have either stepped or unstepped modulations of the colour subcarrier, as shown overleaf in Figs. 2.5 (a) and (b) respectively.

For his I.M. measurements, Flor [2] used the third, modified test line 331 shown in Fig 2.5 (c). With a fully modulated 4,43 MHz burst signal, a 25% synchronisation pulse and 10% residual carrier, this signal produced a ratio of carrier levels almost the same as that used for the three tone test for System B+G/PAL in Europe, as is confirmed from Table 2.3.

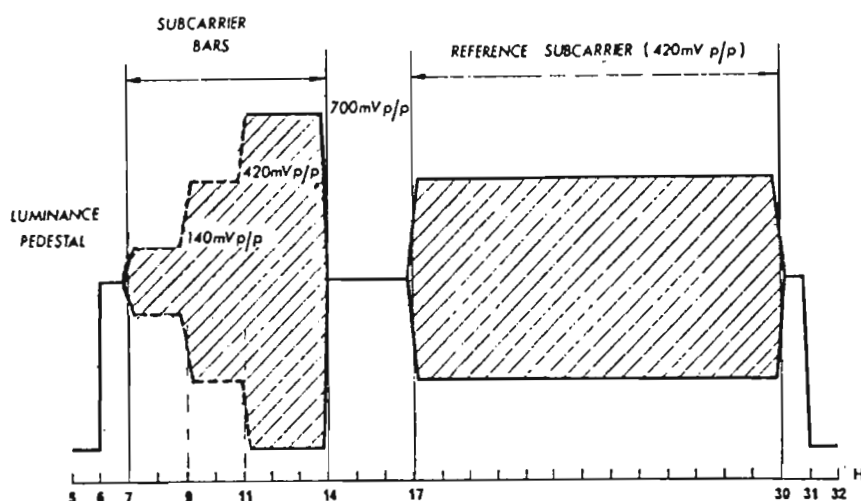
Table 2.3
Relative Carrier Levels
3TT and Flor's Burst Signal
Flor's Levels according to DIN 45 004 Standard

CARRIER:	CARRIER LEVELS:	
	FLOR'S BURST (dBp)	3TT (dBp)
Vision	-7,4	-8
Colour	-15,8	-17
Sound	-10,0	-10

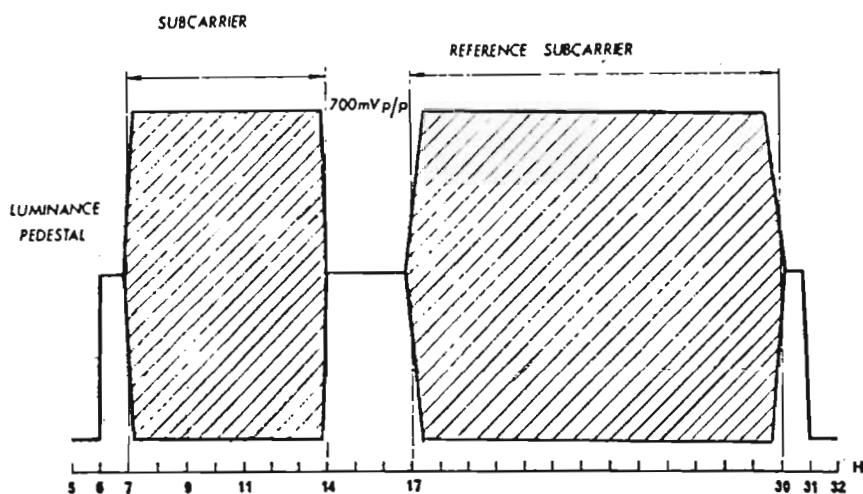
Note that the vision carrier amplitude was 1,4 dB lower than that used by the SABC in local three tone tests (see Table 2.2).



(a) Standard Unstepped Test Line 331



(b) Standard Stepped Test Line 331



(c) Flor's Modified Non-Standard Test Line 331

Fig. 2.5 Variants of Test Line 331 Waveform

2.3.2 Flor's Measurement Procedure

Using the test equipment configuration shown in block diagram form in Fig. 2.6, the third non-standard version of line 331 was continuously broadcast as part of the transmitted TV signal. The I.M. distortion component in the transmitter output was then fed through Chebyshev filter and 20 dB amplifier to a standard OKF type waveform monitor. By triggering the video monitor horizontal sweep at the commencement of line 331, the I.M. distortion component associated with line 331 was observed. The peak amplitude of the signal displayed within the latter half of line 331 was used to determine the I.M. distortion level.

Flor's test was conducted in the time domain, and his test results, reproduced in Fig. 2.7, show large transients and some ringing within the two chrominance modulation burst regions. His test equipment arrangement included a Chebyshev filter with a bandwidth of 200 kHz centred at 1.07 MHz for System B/PAL or G/PAL. The filter order and passband ripple, however, were not specified. This filter had an effective working quality factor Q_w of over 5, and transients were to be expected when such a system was subjected to an input with step changes present. A value of Q_w an order of magnitude smaller would have been necessary for such transients to be avoided [20 to 24].

A further problem associated with Flor's measurement technique was the rather slow filter response. The rise time was expected to be 5 μs for the 200 kHz bandwidth, and practical measurements with a Krohn-hite active filter having separate four pole, tunable, low and high pass sections in cascade confirmed this estimate. Settling and delay times were at least 5 μs in the 8th order case. This means that a colour burst signal having a width of at least 10 μs would be necessary for reasonable accuracy and measurement range. Flor's measurement approach could therefore not be used for accurate intermodulation distortion measurements with a standard colour bar signal having widths of only 6.4 μs .

A significant noise level is evident in the silent section between the two bursts in Fig. 2.7. This noise sets the threshold at which intermodulation measurements may be made. To achieve a reasonable degree of accuracy the minimum I.M. distortion level should be 10 dB above the noise threshold. Again appropriate

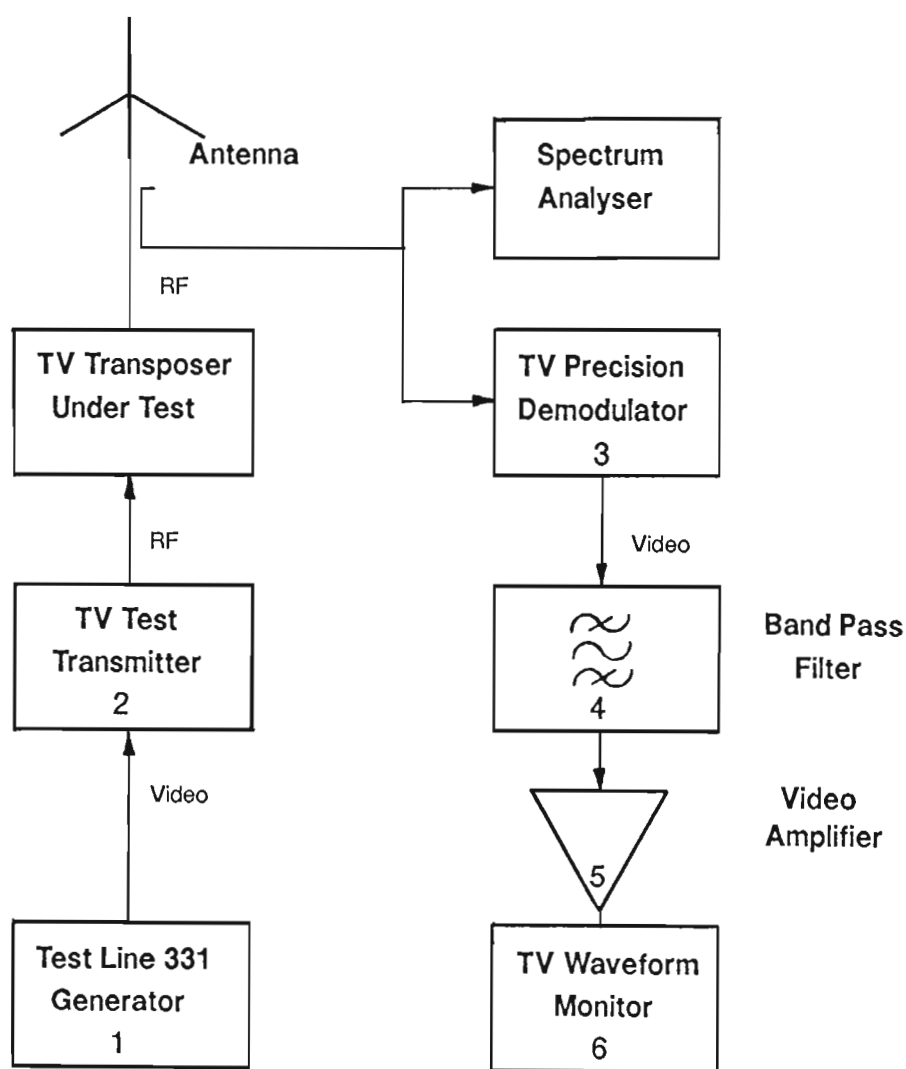
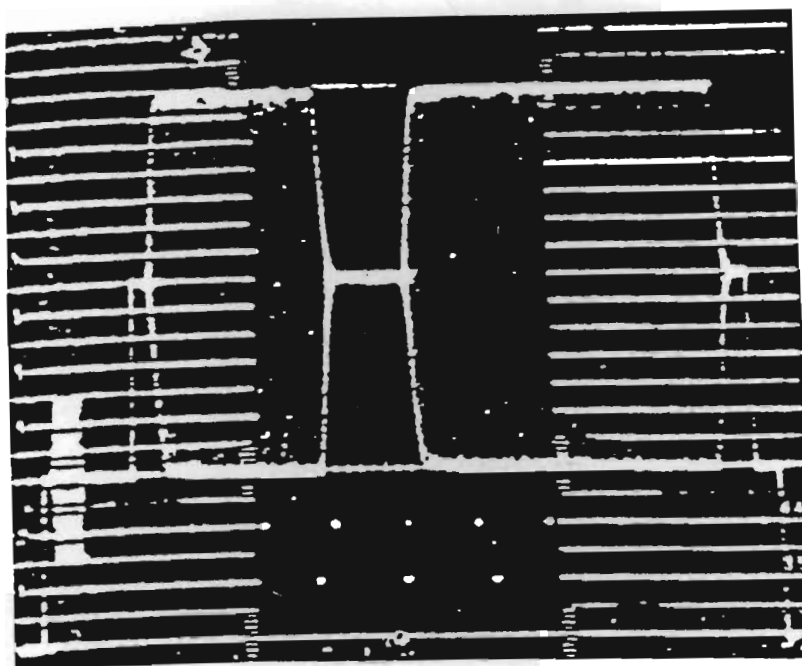


Fig. 2.6 Block Diagram for I.M. Measurement
Flor's Method using Test Line 331

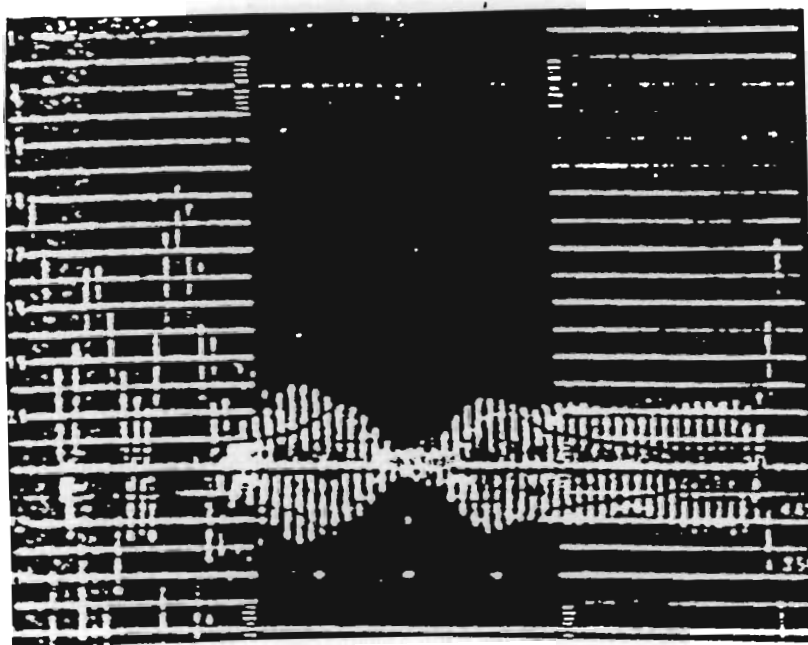
Suggested Equipment Required:

1. Line 331 Generator
2. Test Transmitter
3. TV Demodulator
4. Band Pass Filter
5. Video Amplifier
6. Oscilloscope

Rohde & Schwarz SBUF
 Rohde & Schwarz AMF 2
 Chebychev: 200 kHz band width
 centred on f_{IM} of 1,07 MHz
 Voltage Gain; 20 dB
 Rohde & Schwarz OKF



(a) Flor's Modified Test Line 331



(b) Output of 200 kHz Band Pass Filter

Fig. 2.7 Flor's Published Results
Using Flor's non-standard test line 331 waveform

details were not given in Flor's paper.

2.3.3 Limitations of Flor's Method

Flor's method was considered inadequate for the following reasons:

A Special Pattern Generator is required: This measurement method requires a complex, specially modified pattern generator to insert the required test signal at line 331.

Band Pass Filter Dynamic Response: A bandwidth of 200 kHz at f_{IM} , or $1,07\text{ MHz}$, gives an effective working Q_w of 5,33 which is high enough to make some ringing inevitable. The settling time of the system (to within 1%) should be considerably less than the $27\text{ }\mu\text{s}$ signal duration in order that measurements with reasonable accuracy may be made.

Noise and f_{IM} Filter Bandwidth: Video picture components having frequencies within the same 200 kHz pass band are also monitored on the OKF display. Noise present within the system became evident in the interval between the two modulated sections of line 331. These components determine the noise floor, which is seen to be more than 20% of the peak signal amplitude in Fig. 2.7 (b) or only 12 dB down. Measurement range is therefore limited to about -50 dBp , which is a major limitation and does not meet South African TV I.M. distortion specifications. The noise floor level is also dependent on picture content, which is not an ideal measurement situation.

Measurements are Performed at one Luminance Level Only: The measurement of I.M. amplitudes at six different luminance levels covering the broadcast luminance range, which correspond closely to the levels within the six colour bars, would require the transmission of six test lines during each frame with a staircase progression of luminance level from one test line to the next. This situation would require a change in the world TV signal transmission standards, and is therefore not a practical proposition.

2.4 SWISS PT&T THREE TONE TEST FOR MEASURING I.M. DISTORTION

2.4.1 Introduction

The sampling I.M. analyser was subjected to tests at the Swiss Institute for Posts, Telephones and Telegraphs (PT&T) and a private report of its performance [14] was returned with the instrument. These Swiss PT&T tests form an important part of the acceptance procedure for all broadcast instrumentation used in Europe. Appropriate analyser internal frequencies were selected for their System B/PAL (for VHF TV transmissions) and G/PAL (for UHF TV transmissions).

Two tests were used at the Swiss PT&T for measuring I.M. distortion: a 3TT and a wobulation test. Despite written requests for information on the 3TT waveforms, and the wobulation test instrumentation configuration, no details were received. The only detail available on the wobulation test is the block diagram which included for interest as Fig. 2.8 while the waveform assumed for the analysis of the PT&T 3TT that follows is based on one of the waveforms included in their reported results.

The Swiss 3TT instrumentation configuration is represented in the block diagram of Fig. 2.9. Two main differences between the carrier 3TT normally used, and that applied at the Swiss PT&T, are the following.

Firstly, use was made of a signal similar to that previously illustrated in Fig. 2.4 but which lacks the colour burst signal. This assumed waveform is illustrated in Fig. 2.10. It has a constant luminance level, constant colour subcarrier modulation, and a sound carrier (not shown). Such a signal would produce a display having uniform colour and intensity on a TV screen. Details of the actual modulation pulse widths, etc. are unfortunately not available, but Fig. 2.10 gives the figures assumed for this theoretical analysis.

Secondly, the measurement technique employed various digital and analogue spectrum analysers, including one of the latter with a 100 kHz bandwidth, to determine the frequency content at the transmitter output and thus measure

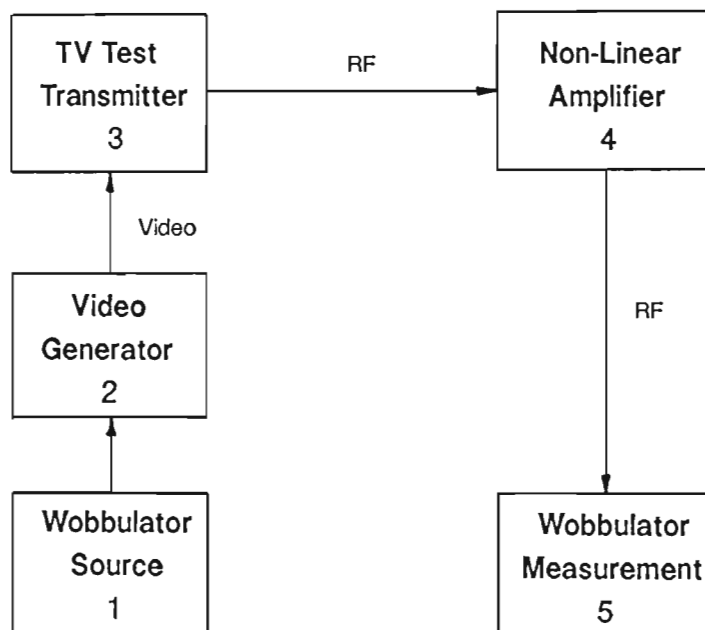
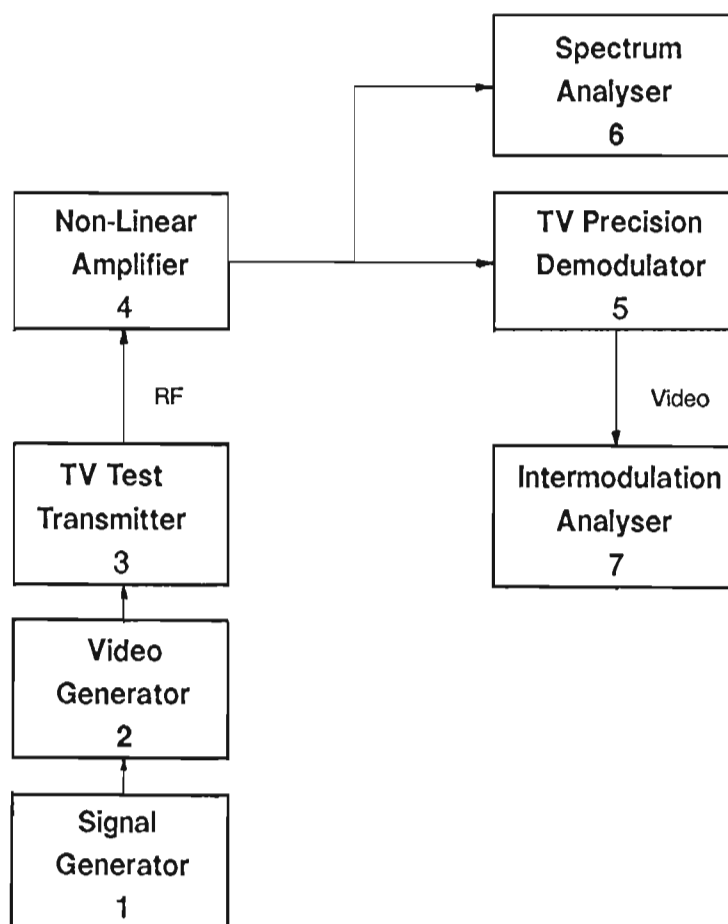


Fig. 2.8 Block Diagram for I.M. Measurement
Swiss PT&T Wobulation Test Block Diagram

Equipment Required:

1. Wobulator
2. Video Generator
3. Test Transmitter
4. Amplifier
5. Wobulation Meas.

Rohde & Schwarz SWOF3
 Rohde & Schwarz SPF2
 Rohde & Schwarz SBUF
 Hewlett-Packard Hp 8447E
 Rohde & Schwarz SWOF3-Z

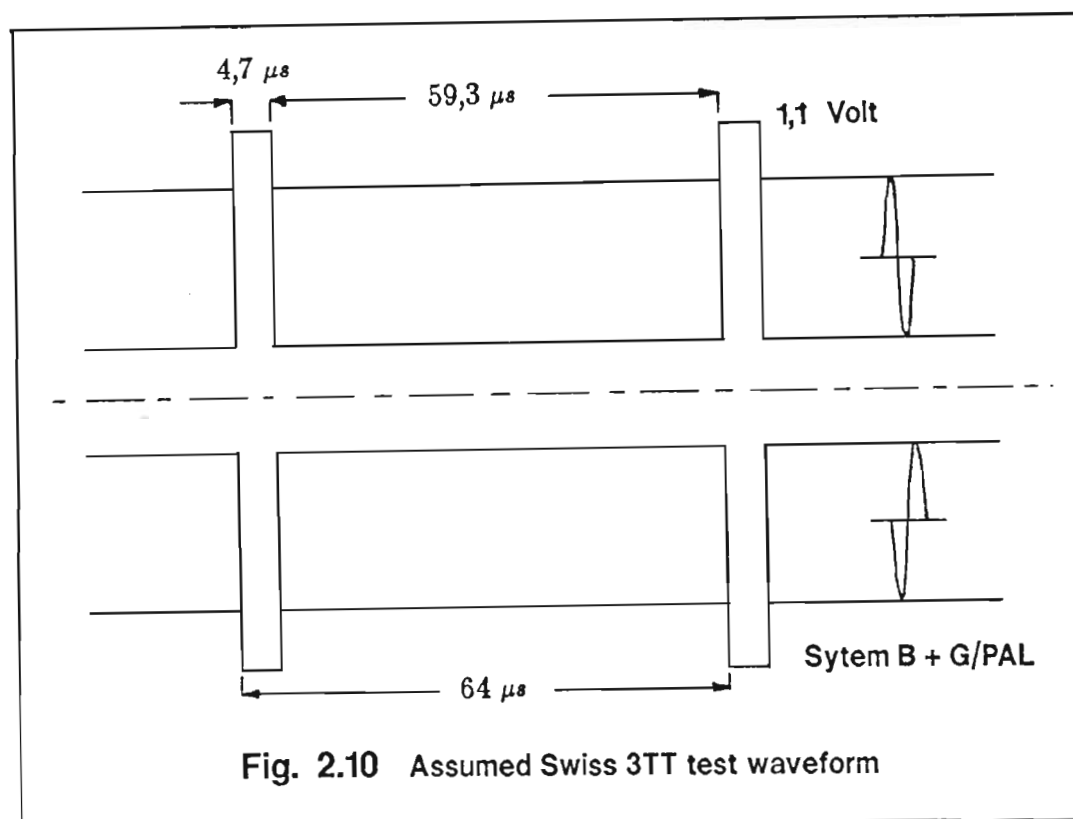


**Fig. 2.9 Block Diagram for I.M. Measurement
Swiss PT&T Three Tone Test**

Equipment Required:

- | | | |
|----|---------------------|--------------------------|
| 1. | Signal Generator | Rohde & Schwarz SMG |
| 2. | Video Generator | Rohde & Schwarz SPF2 |
| 3. | Test Transmitter | Rohde & Schwarz SBUF |
| 4. | Amplifier | Hewlett-Packard Hp 8447E |
| 5. | TV Demodulator | Rohde & Schwarz AMF 2 |
| 6. | Spectrum Analysers: | |
| | Digital | Takeda-Riken TR 4172 |
| | Analogue | Tektronix 7 L 13 |
| 7. | I.M. Analyser | |

the I.M. distortion. A recorder with a writing speed capable of reproducing a 30 kHz sinewave was used to plot the amplitude spectrum measured with the wide-band analyser. The average of these I.M. distortion measurements was then taken as the standard or reference value to which the I.M. analyser reading was compared.



If the above waveform is passed through a non-linear transmitter or transposer an I.M. distortion signal will be produced only during the time period between sync pulses as a result of the lack of chrominance modulation within the sync pulse.

2.4.2 Theory of the Swiss PT&T 3TT

The modulation of the assumed 3TT test waveform shown in Fig. 2.10 can be broken up into two sections: one between the sync pulses, and a second consisting only of the sync pulses themselves. Ignoring the chrominance modulation initially these two regions correspond to pulses, shown within the square brackets, having standard forms that can be expressed as Fourier Series in terms of the $\text{sinc}(x)$ function [20] and their mark-space ratios R_1 and R_2 where

$$\text{sinc}(x) = \frac{\sin(x)}{x} \quad (2.9)$$

$$R_1 = \frac{59,3}{64} \quad (2.10)$$

and

$$R_2 = \frac{4,7}{64} \quad (2.11)$$

The Fourier Series representations of two pulse waveforms are:

$$\begin{aligned} P_1(t) &= \quad \text{[Waveform: A periodic pulse train with a period of } 64 \mu s \text{. Each cycle contains a high pulse of } 59,3 \mu s \text{ and a low pulse of } 4,7 \mu s \text{. The high pulse is centered at } 32 \mu s \text{ within each cycle.}] \\ &= R_1 + 2R_1 \sum_{n=1}^{\infty} \text{sinc}(n \pi R_1) \cos(n \omega_H t) \end{aligned} \quad (2.12)$$

with the origin centred in the $4,7 \mu s$ sync pulse, and

$$\begin{aligned} P_2(t) &= \quad \text{[Waveform: A periodic pulse train with a period of } 64 \mu s \text{. Each cycle contains a high pulse of } 4,7 \mu s \text{ and a low pulse of } 59,3 \mu s \text{. The high pulse is centered at } 32 \mu s \text{ within each cycle.}] \\ &= R_2 + 2R_1 \sum_{n=1}^{\infty} \text{sinc}(n \pi R_2) \cos(n \omega_H t) \end{aligned} \quad (2.13)$$

with its origin centred in the $59,3 \mu s$ pulse region between sync pulses. This origin is delayed by $32 \mu s$, or half a line period, relative to the previous one used for v_1 , and a phase shift term of $-2\pi n \times 32/64$ radians (or $-n\pi$ rad) must be introduced into equation (2.13) to allow both series to be referenced to the centre of the sync pulse. Hence equation (2.13) becomes:

$$P_2(t) = R_2 + 2R_1 \sum_{n=1}^{\infty} \text{sinc}(n \pi R_2) \cos(n \omega_H t - n \pi) \quad (2.14)$$

If the chrominance modulation is now included the two sections of the signal in Fig. 2.10 have frequency components described by the following equations:

Between the sync pulses:

$$V_1 = V_{\text{Chr}} \cos(\omega_v t) [1 + m \cos(\omega_{\text{SC}} t)] \times P_1(t) \quad (2.15)$$

which has sideband components at frequencies of $\omega_v \pm n\omega_H$ and $\omega_v \pm \omega_{\text{SC}} \pm n\omega_H$.

The sync pulses alone:

$$V_2 = V_{\text{sync}} \cos(\omega_v t) \times P_1(t) \quad (2.16)$$

which has sideband components at frequencies of $\omega_v \pm n\omega_H$ only. These may be added to the corresponding frequency components from equation (2.15).

If the waveform in Fig. 2.10 is passed through a non-linear amplifier within a frequency transposer, an I.M. distortion component will result. Again the I.M. distortion signal is modulated by the pulse waveform with the larger mark-space ratio R_1 because of the lack of chrominance component within the sync pulses, so that this third component may be represented by the following expression:

$$v_3 = V_{\text{IM}} \cos(\omega_{\text{IM}} t) \times P_1(t) \quad (2.17)$$

with its own sidebands at frequency spacings of $\omega_H \text{ rad/s}$.

Thus the composite waveform presented to the spectrum analysers at the transposer output consists of the sum, or superposition, of the three components:

$$v_{\text{SA}} = v_1 + v_2 + v_3 \quad (2.18)$$

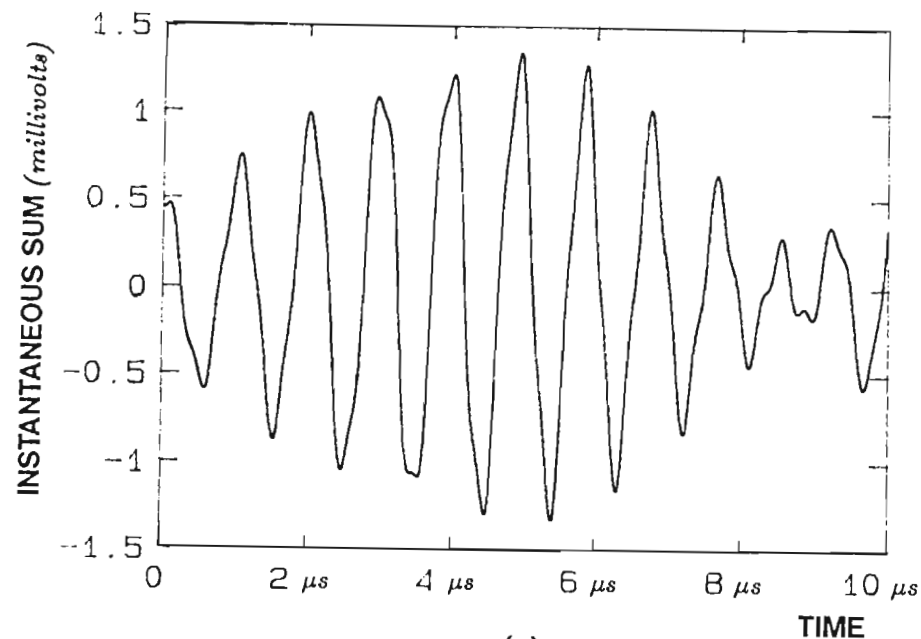
where v_3 is the component that is to be measured, and the sum $v_1 + v_2$ represents unwanted noise.

2.4.3 Instantaneous Sideband Noise Amplitudes

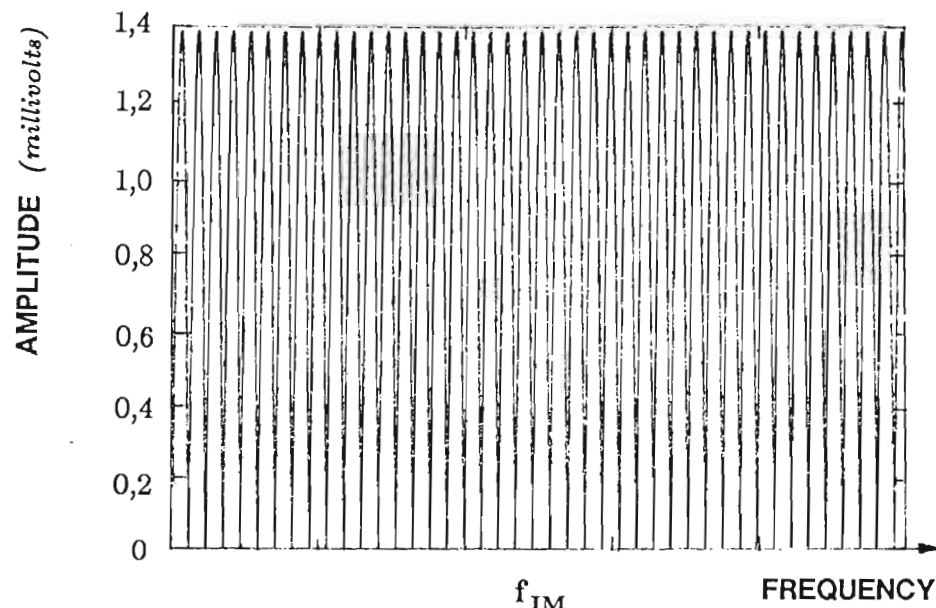
For the I/PAL and G/PAL Systems, video noise sidebands spaced at line frequency intervals f_H or 15625 Hz will occur near to f_{IM} when $n \simeq 68$ for components at $\omega_V + n\omega_H$ and $n \simeq 215$ for components at $\omega_V + \omega_{SC} - n\omega_H$. These two groups of sidebands do not coincide in frequency.

The displayed spectrum of the transposer output signal will depend on the I.F. filter bandwidth setting for the spectrum analyser. Individual spectral lines will be visible with a narrow bandwidth of a few kilohertz, while a maximum of seven sidebands spaced at f_H can pass with little attenuation through the 100 kHz band pass filter in the wide-band spectrum analyser. An ideal filter was assumed for the spectrum analyser, allowing seven sidebands to pass through with no attenuation and zero phase shift. A computer programme was written to sum all the noise components within the filter pass band surrounding f_{IM} over a $10\text{ }\mu\text{s}$ period at 10 ns intervals. Instantaneous cancellation of the sidebands occurs at regular, short time intervals of $9,699\text{ }\mu\text{s}$, giving a "zero" spectrum analyser noise floor, but only when the I.M. distortion component at f_{IM} is not included within the pass band. The resulting waveform, shown in Fig. 2.11 (a), has large amplitude variations due to harmonic beating.

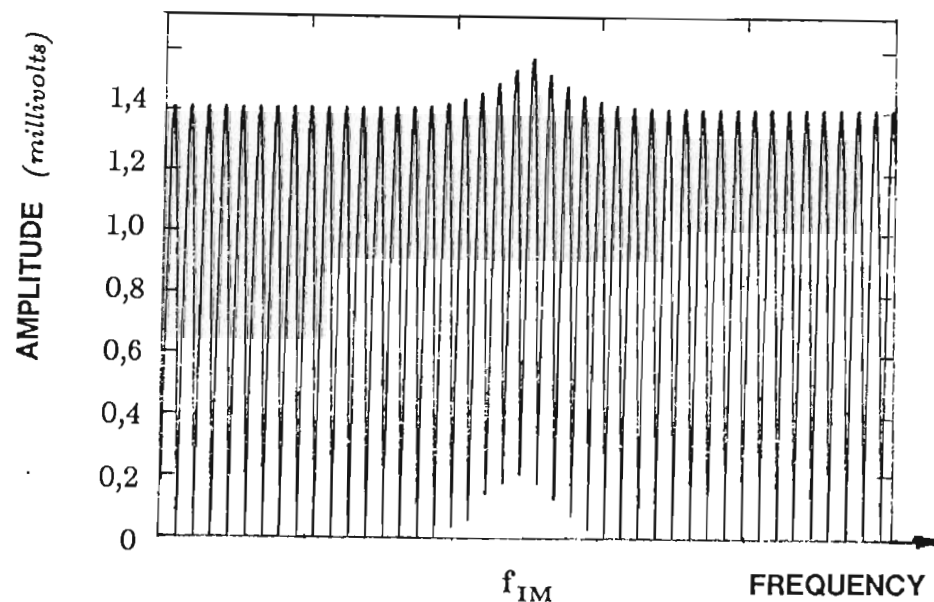
If such an ideal filter scans the frequency spectrum slowly the noise components will sum to zero at regular time intervals, producing a picture similar to the amplitude diagram in Fig. 2.11 (b). The presence of any other signal, such as an I.M. signal, will be manifested when the recorded display does not reach "zero". The height of the resultant lower limit of the display will therefore correspond to the amplitude of the I.M. signal being measured, as shown in Fig. 2.11 (c). Thus the change in "noise floor" may be used to determine the magnitude of v_3 which is the I.M. signal level.



(a)



(b)



(c)

Fig. 2.11 Simulation of Swiss PT&T Three Tone Test

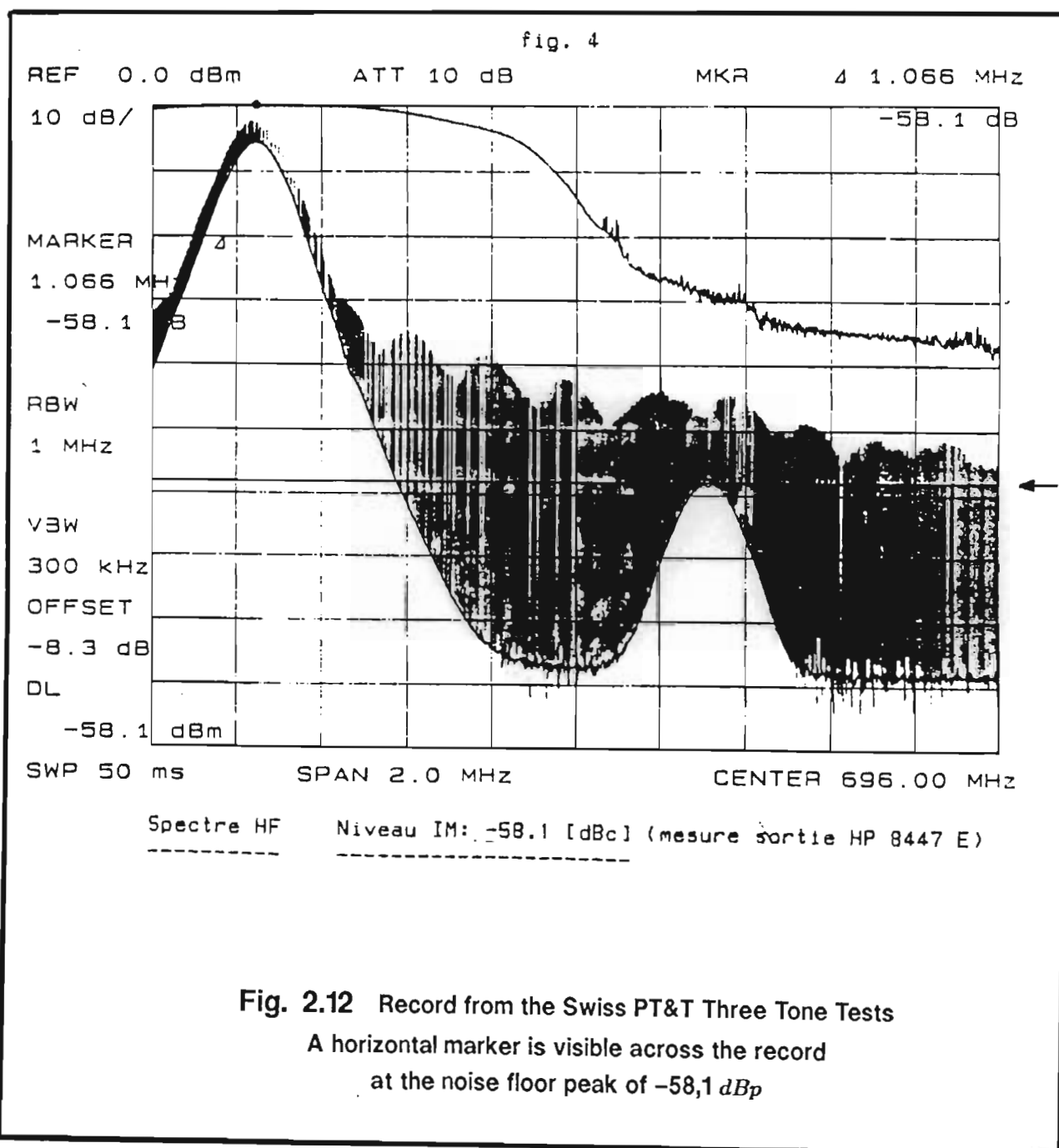
(a) Sum of seven video sidebands about f_{IM} as a function of time

(b) Magnitude of sideband sum as the 100 kHz bandwidth filter sweeps through the video band with no I.M. distortion component present.

(c) Magnitude of sideband sum as the 100 kHz bandwidth filter sweeps through the video band with the I.M. distortion component present.

2.4.4 Swiss PT&T Test Results

Fig. 2.12 shows a typical graphical record obtained during the 3TT measurements, and comparative results obtained by this spectrum analyser technique, and the I.M. analyser, are presented in Table 5.12 of Chapter 5. Results from the wobble test were used to check the 3TT results, as shown in Table 5.11.



2.5 A SAMPLING TECHNIQUE FOR MEASURING INTERMODULATION PRODUCT DISTORTION IN TELEVISION TRANSPOSERS

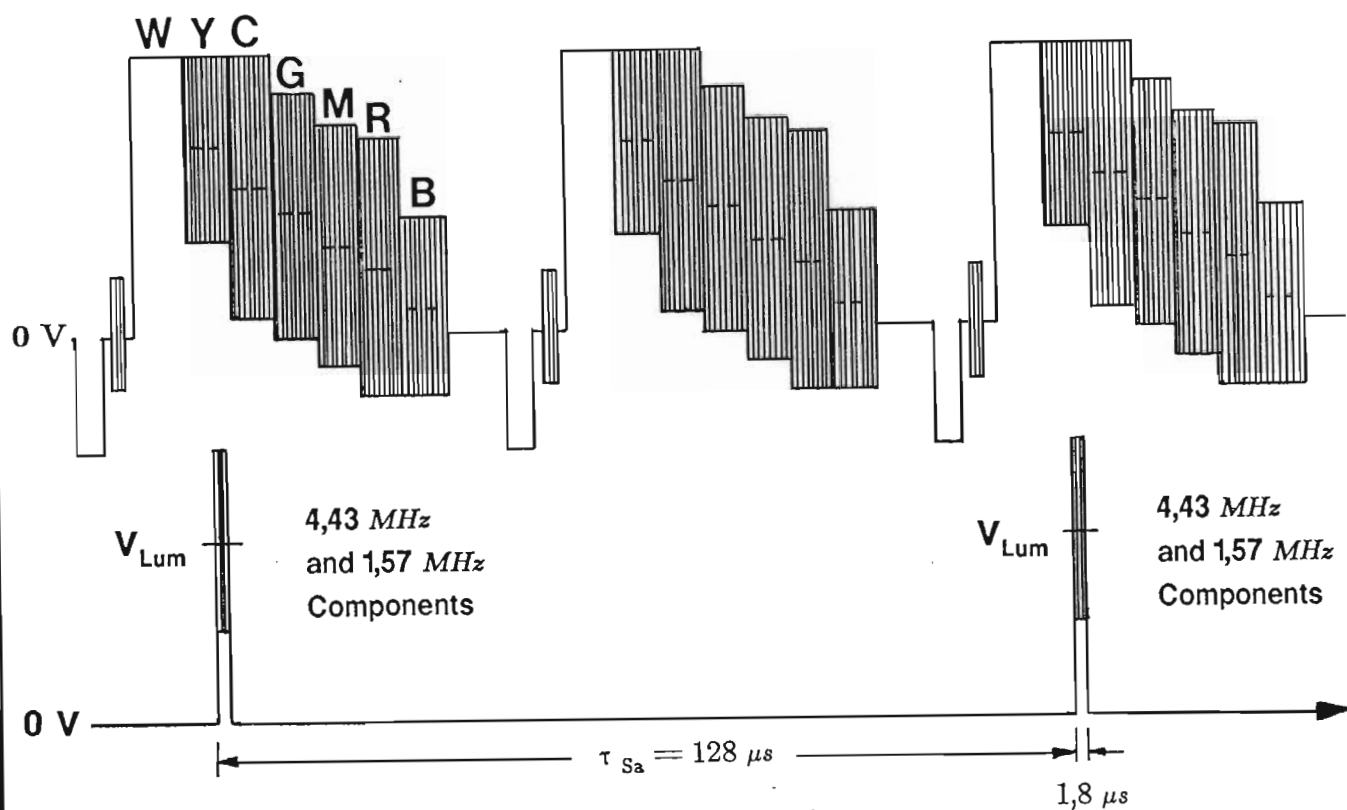
2.5.1 Introduction

Conceptually, the original sampling I.M. distortion measurement technique as proposed by Broadhurst [1] was very simple. The vision carrier of the transmitter under test was modulated with a standard colour bar signal. Figs. G.1 and G.2 in Appendix G show two colour bar waveforms used locally for testing TV transmitters. The output was then demodulated to produce a video signal which included the I.M. distortion signal. This video signal was then sampled repetitively within a particular colour bar and typical sampler outputs, when used with a 100-0-75-0 colour bar signal, are illustrated in Figs. 2.13 (a) and (b) for the I/PAL and M/NTSC Systems respectively. The amplitude of the I.M. component contained within the measurement frequency window was then measured. The measurement was performed by down-converting the 1,57 MHz I.M. component to a low frequency of 200 Hz, low frequency filtering (with a 500 Hz low pass filter) to reject the adjacent line harmonics, and the amplitude determined using a precision full-wave rectifier and averaging circuit.

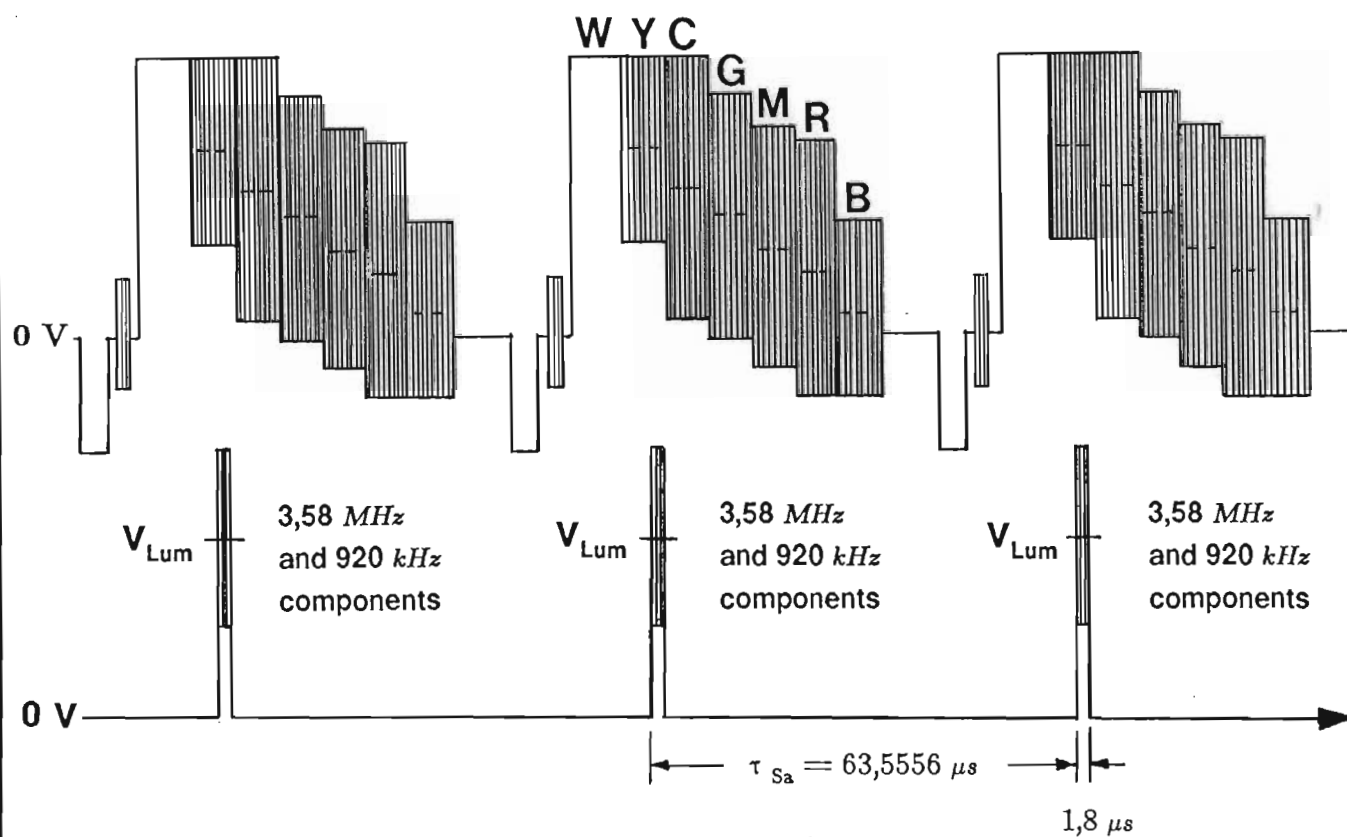
If the signal amplitudes and phase within the sampled colour bar are continuous, the effective input video signal appears (to the sampler) to have constant luminance, chrominance and I.M. component levels. This facilitates an understanding of both the sampling process and its analysis. Unless otherwise indicated I/PAL parameters are used in the following analysis.

2.5.2 Operation of the Original Sampling I.M. Distortion Analyser

The original apparatus developed for sampling the video signal consisted of two basic functional divisions. One section, represented in block diagram form in Fig. 2.14, determined both the duration and positioning of the sampling pulses



(a) Output for System I/PAL



(b) Output for System M/NTSC

Fig. 2.13 Demodulated Video Sampler Output

Input signal is a 100-0-75-0 colour bar

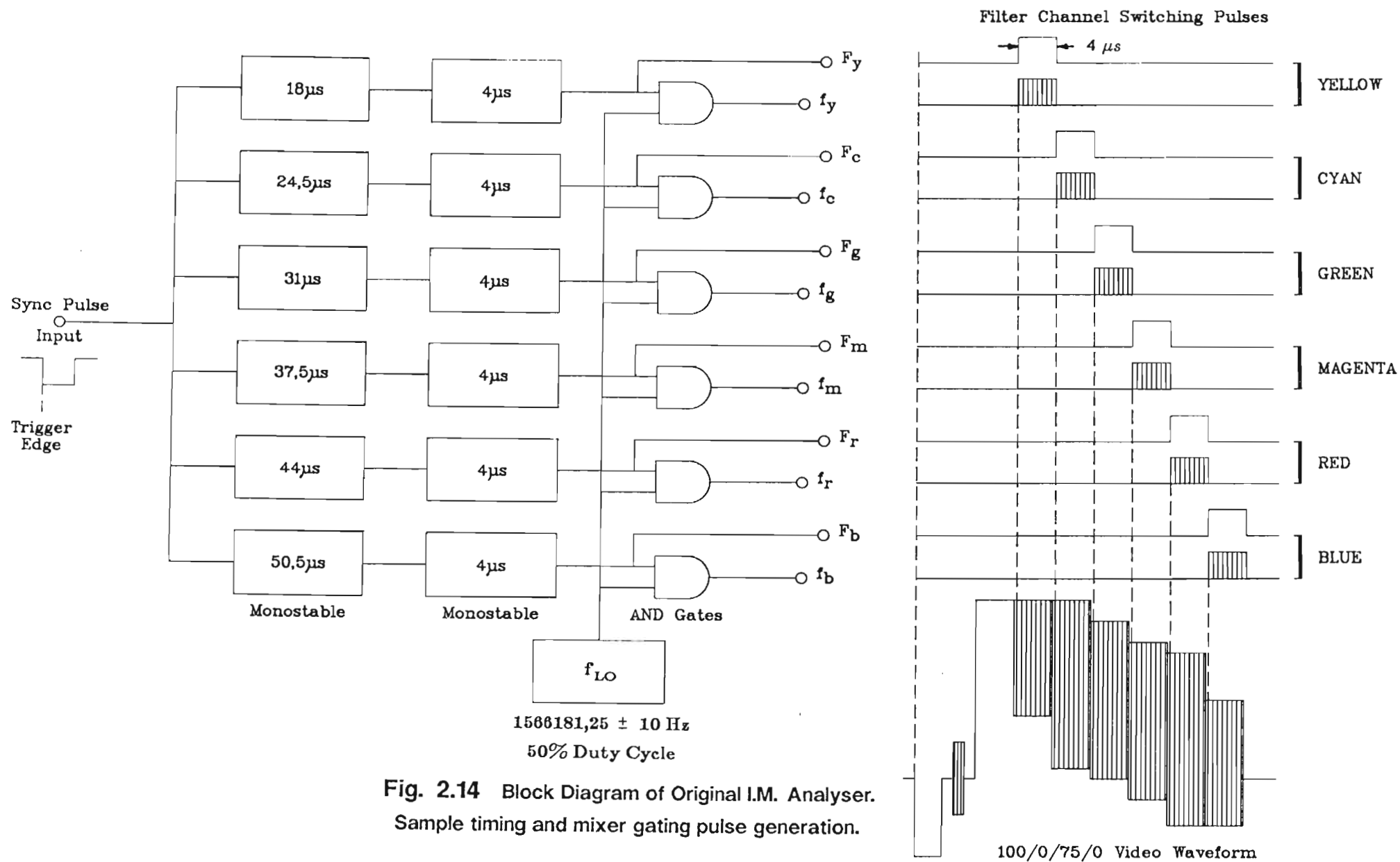


Fig. 2.14 Block Diagram of Original I.M. Analyser.
Sample timing and mixer gating pulse generation.

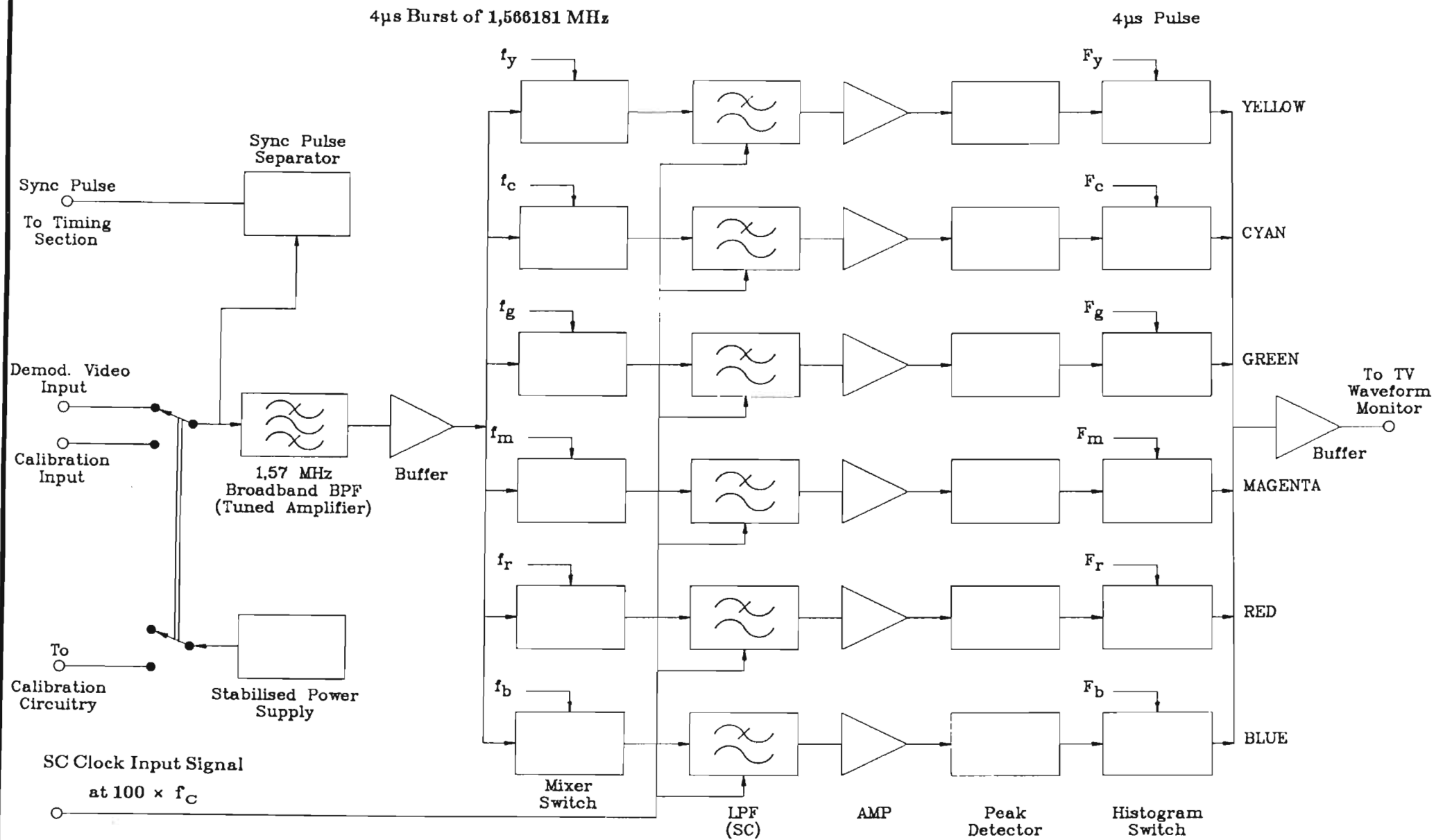


Fig. 2.15 Block Diagram of Original I.M. Analyser.

Signal filtering, down-conversion and detection
and histogram display generation

SC = Switched Capacitor Filter
 f_C = SC Filter cut-off frequency

used to control the mixing pulses applied to the down converters. A second section, illustrated in Fig. 2.15, consisted of a band pass filter feeding six down-converters, one for each of six channels corresponding to the six colour bars. The I.M. distortion signals were detected and their amplitudes measured with a self-contained tracking digital voltmeter.

A demodulated video output signal from the frequency transposer under test was applied to the analyser video input, feeding both the filter and down-converter section and the sync pulse separator which provided synchronisation for the timing section.

Fig. 2.15 also illustrates the production of the gated local oscillator pulses and the timing pulses required for the mixer and histogram switches. All six delay monostables produced pulses synchronised to the leading edge of the line sync pulse. Each delay pulse trailing edge triggered a $4\ \mu\text{s}$ monostable to produce sampling pulses designated as F_y (yellow), F_c (cyan), F_g (green), F_m (magenta), F_r (red) and F_b (blue) which corresponded in time to the central region of their respective colour bars. These $4\ \mu\text{s}$ pulses gated the local oscillator signal to produce the timed local oscillator mixer input pulses f_y (yellow), f_c (cyan), f_g (green), f_m (magenta), f_r (red) and f_b (blue) respectively.

Fig. 2.15 includes the input band pass filter section which selected the I.M. component to be measured, and attenuated the three principal frequency components of the colour bar signal. The initial bandwidth chosen to select the $1.57\ \text{MHz}$ intermodulation product was approximately $30\ \text{kHz}$. The output signal from the band pass filter was fed to the mixer whose function was to down-convert the intermodulation frequency f_{IM} to a frequency of about $200\ \text{Hz}$. This was achieved using a local oscillator with a frequency $200\ \text{Hz}$ above (or below) the intermodulation frequency. In fact both conditions arise as two sound carrier frequencies are used, one at $5.9996\ \text{MHz}$ for broadcasting and one at $6\ \text{MHz}$ for three tone testing.

The input band pass filter was buffered and fed the six channels in parallel. Each channel had a separate down-converter, its mixer being active for only $4\ \mu\text{s}$ during the particular colour bar associated with that channel. Selective mixing was achieved with timing pulses f_y (yellow), f_c (cyan), f_g (green), f_m (magenta), f_r (red) and f_b (blue). Digital pulses applied to the mixer consisted of

a burst of local oscillator pulses $4,0 \mu s$ wide, with the position of the burst arranged to coincide with a particular selected colour on the colour test pattern [see Fig. 2.14]. This allowed the I.M. distortion signal amplitude to be determined at a particular section of the transmitter's characteristic or depth of modulation. It was clearly necessary to transmit a colour bar or other similar test pattern for these measurements to be performed.

A low pass filter passed the difference frequency $f_{LO} - f_{IM}$ via a buffer to a peak detector which produced a DC output voltage corresponding to the I.M. level within the particular colour bar. These peak detector dc outputs were selected sequentially every line by means of the $4 \mu s$ timing pulses F_y, F_c, F_g, F_m, F_r and F_b and combined by the switches for display as a histogram.

2.5.3 Theory of the Sampling Measurement Technique

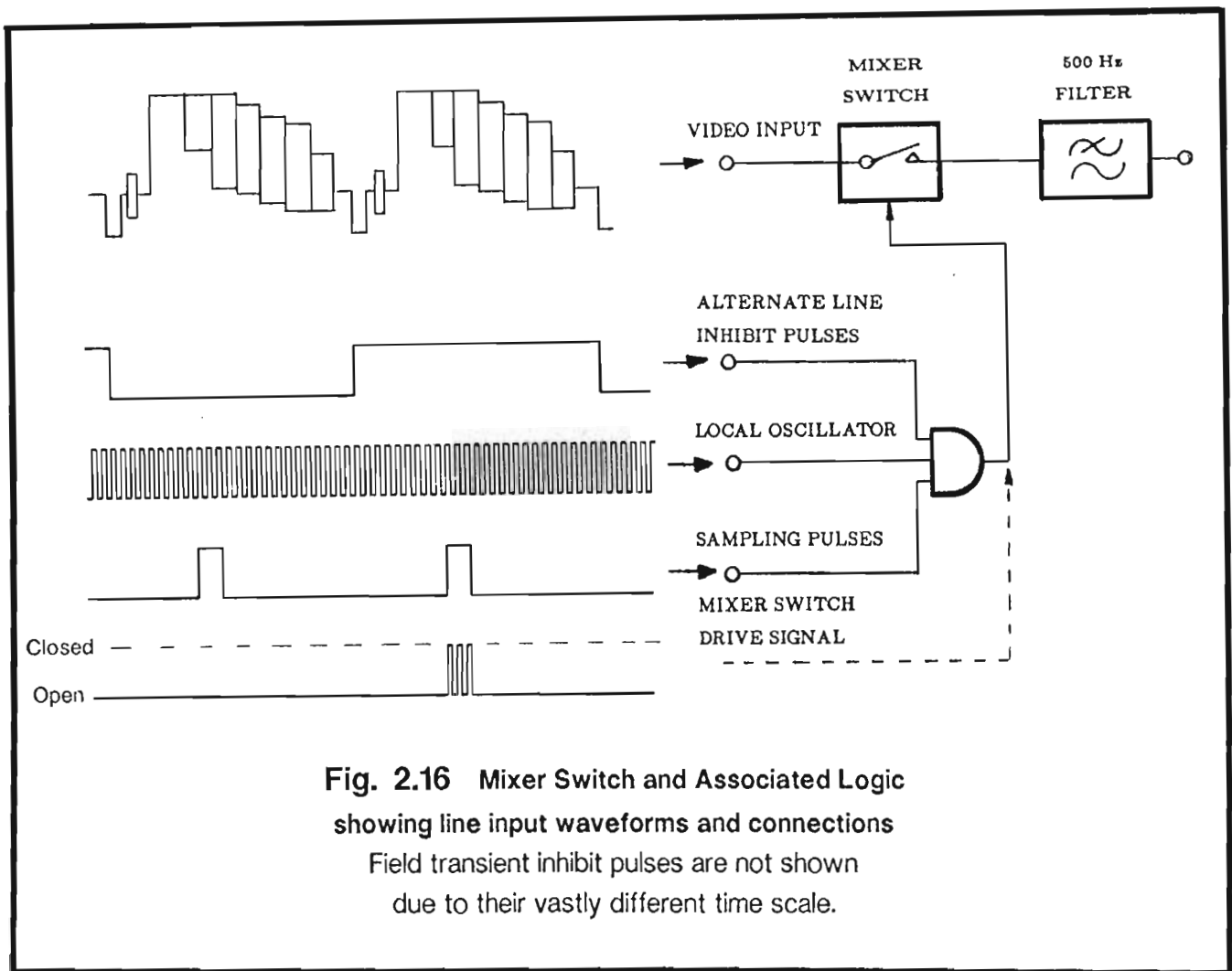
The basic concept of the sampling I.M. analyser was developed into the multiplexed system which is described later in Chapter 3. For this new system the sampling pulse width was reduced to $1,8 \mu s$ to allow distortion measurements to be performed within the colour burst. Hereafter $1,8 \mu s$ will be used in place of $4,0 \mu s$ for the sampling pulse width in the theory that follows.

Fig. 2.16 overleaf illustrates the basic mixer circuit with control logic and input waveforms. The multiplexed system has a single analogue type switching mixer to which the video signal is applied. Three LOGIC level signals are combined in an AND gate to control the opening and closing of the mixer switch. These latter three signals are the local oscillator squarewave, the $1,8 \mu s$ sampling pulse waveform, and the alternate line inhibit signal.

A simplified analysis of the mixing process shown in Fig. 2.16 follows.

- 1 The analogue intermodulation distortion signal at ω_{IM} , present in the video signal applied to the mixer, is assumed to be a sinewave of amplitude V_{IM} represented by

$$v_{IM}(t) = V_{IM} \cos \omega_{IM} t \quad (2.19)$$



- 2 A LOGIC level local oscillator signal which switches the mixer on and off with a 1:1 mark-space ratio at the local oscillator frequency ω_{LO} . This process is equivalent to multiplication by a square wave having unit amplitude and represented by the Fourier Series [26 to 34]:

$$v_{LO}(t) = \frac{1}{2} + \frac{2}{\pi} \left[\sum_{n=1,3,5 \text{ etc.}}^{\infty} \frac{1}{n} \cos(n \omega_{LO} t) \right] \quad (2.20)$$

- 3 The LOGIC level sampling waveform $v_{sa}(t)$, which represents the product of the alternate line inhibit pulses and the sampling pulses shown in Fig. 2.16, consists of $1.8 \mu s$ wide pulses with a mark-space ratio of R_3 and unit amplitude. Again, sampling is equivalent to multiplication by a wave of unit amplitude having the following familiar Fourier Series representation:

$$v_{sa}(t) = R_3 + 2R_3 \sum_{n=1}^{\infty} \text{sinc}(n \pi R_3) \cos n \omega_{sa} t \quad (2.21)$$

The origin used for this Fourier analysis is centred in the 1,8 μs sampling pulse. The mark-space ratio R_3 of the sampling waveform is

$$R_3 = \frac{1,8}{128} \quad (2.22)$$

for the PAL System, and

$$R_3 = \frac{1,8}{64} \quad (2.23)$$

for the NTSC System, and

$$\text{sinc}(x) = \frac{\sin(x)}{x} \quad (2.24)$$

Note that in the PAL System the sampling frequency ω_{sa} is given by:

$$\begin{aligned} \omega_{sa} &= \frac{1}{2} \omega_H \\ &= \omega_{1/2H} \end{aligned} \quad (2.25)$$

which is the half-line, or alternate line, frequency.

- 4 Video information is present for 290,5 lines or 18,59 ms , and absent for 22 lines or 1,41 ms during each field period in the I/PAL System. This is equivalent to multiplying the mixer input signal by a LOGIC level gating waveform $v_F(t)$, synchronised to the field sync pulses, which has a mark-space ratio of R_4 and unit amplitude. Again the Fourier Series representation of $v_F(t)$ has similar form to that for the previous unit amplitude sampling pulse waveform, with the origin for this analysis being centred on the 290,5 lines with video information present.

$$v_F(t) = R_4 + 2R_4 \sum_{n=1}^{\infty} \text{sinc}(n \pi R_4) \cos n \omega_F t \quad (2.26)$$

with

$$\begin{aligned} R_4 &= \frac{312,5 - 22}{312,5} \\ &= 0,93 \end{aligned} \quad (2.27)$$

and

$$\omega_F = 2\pi \cdot 50 \text{ rad/s} \quad (2.28)$$

for the I/PAL System, while the corresponding figures for the M/NTSC System are

$$\begin{aligned} R_4 &= \frac{262,5 - 16}{262,5} \\ &= 0,94 \end{aligned} \quad (2.29)$$

and

$$\omega_F = 2\pi \cdot 60 \text{ rad/s} \quad (2.30)$$

Note that 60 *Hz* is nominally used for the actual frequency of 59,94 *Hz*.

The rise time of the 500 *Hz* filter at the mixer output [see Fig. 2.16] is approximately 2 *ms*, and therefore the intermodulation component $v_{IM}(t)$ has ample time to settle during the 290,5 active lines provided that this filter has little overshoot. Thus $v_F(t)$ has little effect on the amplitude, and hence the accuracy of the distortion measurements. But $v_F(t)$ does influence the system noise produced by the sampling process, and this is taken into account in Appendix F where 50/60 *Hz* sidebands produced by the field pulses are considered in detail.

It is instructive to examine the frequency spectra at the output of the mixer shown in Fig. 2.16 with the local oscillator inhibited, i.e. with

$$v_{LO}(t) = 1$$

$$v_F(t) = 1$$

In this case the spectra would not be down-converted.

Consider the effect of the sampling waveform on the input video signal. The process of sampling repeatedly within the same colour bar makes the input signal to the mixer switch, within that colour bar, appear to be a continuous video signal with constant luminance level, chrominance modulation depth and intermodulation distortion amplitude. Expressed in terms of superposition, three constant amplitude signals are apparently present, and each is sampled by the mixer switch. This sampling process is described mathematically in the following equations:

Sampling the Luminance Component:

Sampling of the luminance component produces a signal given by the expression

$$v_{\text{Lum}}(t) = V_{\text{Lum}} \cdot v_{\text{Sa}}(t) \cdot v_{\text{LO}}(t) \cdot v_{\text{F}}(t)$$

This reduces to

$$v_{\text{Lum}}(t) = V_{\text{Lum}} \left[\mathbf{R}_3 + 2\mathbf{R}_3 \sum_{n=1}^{\infty} \text{sinc}(n\pi \mathbf{R}_3) \cos(n\omega_{\text{Sa}}t) \right] \quad (2.31)$$

which has components spaced at $\omega_{1/2H} \text{ rad/s}$, or $\omega_H \text{ rad/s}$, relative to the vision carrier ω_V respectively for the PAL and NTSC TV Systems. The resulting PAL spectrum is shown in Fig. 2.17 (a).

Sampling the Intermodulation Component $V_{\text{IM}}(t)$:

Sampling of the intermodulation signal produces components given by the equation

$$v_{\text{SIM}}(t) = V_{\text{IM}}(t) \left[\mathbf{R}_3 + \mathbf{R}_3 \sum_{n=1}^{\infty} \text{sinc}(n\pi \mathbf{R}_3) \times \cos(\omega_{\text{IM}} \pm n\omega_{\text{Sa}})t \right] \quad (2.32)$$

with sidebands at $(\omega_{\text{IM}} \pm n\omega_{1/2H}) \text{ rad/s}$ for the PAL TV System, or at $(\omega_{\text{SC}} \pm n\omega_H) \text{ rad/s}$ for the NTSC TV System. The corresponding PAL spectrum is shown in Fig. 2.17 (b).

Sampling the Chrominance Component $V_{\text{Chr}}(t)$:

Sampling of the chrominance signal produces components given by the equation

$$v_{\text{SChr}}(t) = V_{\text{Chr}}(t) \left[\mathbf{R}_3 + \mathbf{R}_3 \sum_{n=1}^{\infty} \text{sinc}(n\pi \mathbf{R}_3) \times \cos(\omega_{\text{SC}} \pm n\omega_{\text{Sa}})t \right] \quad (2.33)$$

which has sidebands at frequencies at $(\omega_{\text{SC}} \pm n\omega_{1/2H}) \text{ rad/s}$ for the PAL TV System, or at $(\omega_{\text{SC}} \pm n\omega_H) \text{ rad/s}$ for the NTSC TV System. The corresponding PAL spectrum is shown in Fig. 2.17 (c).

Sampling the Sound Component $V_s(t)$:

If any of the sound carrier signal were present a situation analogous with that represented in equation (2.33) would result, with the colour subcarrier ω_{sc} replaced by sound subcarrier ω_s as shown in equation (2.34).

$$v_{ss}(t) = V_s \left[R_3 + R_3 \sum_{n=1}^{\infty} \text{sinc}(n \pi R_3) \times \cos(\omega_s \pm n \omega_{sa})t \right] \quad (2.34)$$

where V_s is the peak voltage of the residual sound subcarrier at the selected colour bar. A precision demodulator normally removes the sound subcarrier almost completely from its video output.

In all four cases, sampling produces sidebands with line frequency spacing about the sampled carrier for NTSC System signals, or with half-line frequency spacings for PAL System signals. Sideband amplitudes follow the $\text{sinc}(x)$ function with the first zero amplitude at frequency f_z (or n_z sidebands), where

$$f_z = 1/\tau_{sa}$$

with

$$\tau_{sa} = 1,8 \mu s$$

Hence

$$\begin{aligned} f_z &= 555\,555 \text{ Hz} \\ &= 35,5556 \times f_H \end{aligned}$$

giving

$$n_z = 35,5556 \quad (2.35)$$

for the NTSC System, and

$$\begin{aligned} f_z &= 555\,555 \text{ Hz} \\ &= 71,1111 \times f_{1/2H} \end{aligned}$$

so that

$$n_z = 71,1111 \quad (2.36)$$

for the PAL System.

The spectra shown in Figs. 2.17 (a), (b), (c) and (d) summarise the sideband data for the I/PAL System with half-line frequency spacings, or 7812,5 Hz, computed from equations (2.31), (2.32), (2.33) and (2.34) recorded in Tables 2.4 to 2.7

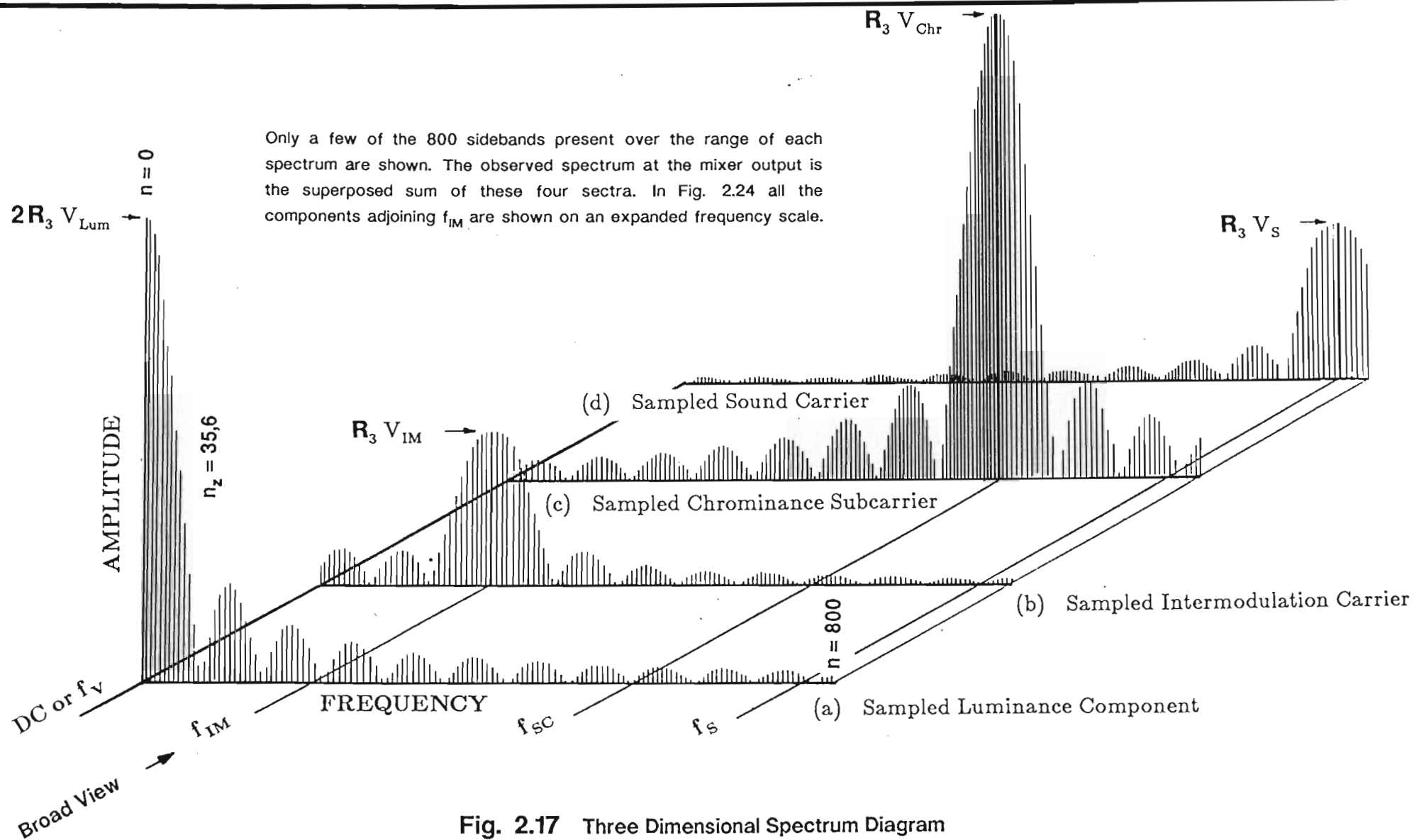


Fig. 2.17 Three Dimensional Spectrum Diagram
Video components sampled every alternate line

SIDEBAND NUMBER	SIDEBAND FREQUENCY (Hz)	SIDEBAND AMPLITUDE (Volts)	SIDEBAND AMPLITUDE (dB)
0	0	.028125	0
10	78125	.027219	-1.2844063
20	156250	2.460569E-02	-1.16114
30	234375	.0205847	-2.710959
40	312500	1.560969E-02	-5.113969
50	390625	1.022676E-02	-8.787093
60	468750	5.001676E-03	-14.99954
70	546875	4.462498E-04	-35.99029
80	625000	-3.045298E-03	-19.30926
90	703125	-5.241158E-03	-14.59331
100	781250	-6.092072E-03	-13.28655
110	859375	-5.724812E-03	-13.82662
120	937500	-4.411084E-03	-16.09094
130	1015625	-.0025176	-20.96212
140	1093750	-4.457123E-04	-36.00076
150	1171875	1.429806E-03	-25.87631
160	1250000	2.813489E-03	-19.99695
170	1328125	3.525915E-03	-18.03642
180	1406250	3.519746E-03	-18.05162
190	1484375	2.873932E-03	-19.81232
200	1562500	1.768434E-03	-24.03007
210	1640625	4.44818E-04	-36.0182
220	1718750	-8.400042E-04	-30.49622
230	1796875	-1.858817E-03	-23.59712
240	1875000	-2.450666E-03	-21.19617
250	1953125	-2.543412E-03	-20.87352
260	2031250	-2.159417E-03	-22.29512
270	2109375	-1.404569E-03	-26.03099
280	2187500	-4.435661E-04	-36.04268
290	2265625	5.334002E-04	-34.44079
300	2343750	1.346225E-03	-26.3995
310	2421875	1.856443E-03	-23.60822
320	2500000	1.989437E-03	-23.00725
330	2578125	1.743932E-03	-24.15126
340	2656250	1.187846E-03	-27.48665
350	2734375	4.4196E-04	-36.07419
360	2812500	-3.449959E-04	-38.22558
370	2890625	-1.024958E-03	-28.76774
380	2968750	-1.477496E-03	-25.59133
390	3046875	-1.630392E-03	-24.73601
400	3125000	-.0014704	-25.63315
410	3203125	-1.042751E-03	-28.61824
420	3281250	-4.400035E-04	-36.11273
430	3359375	2.172368E-04	-42.24319
440	3437500	8.038339E-04	-30.87853
450	3515625	1.213437E-03	-27.30151
460	3593750	1.377292E-03	-26.20133
470	3671875	1.275331E-03	-26.86939
480	3750000	9.378304E-04	-29.53937
490	3828125	4.37695E-04	-36.15842
500	3906250	-1.247989E-04	-47.05763

Table 2.4

Calculated amplitudes of every tenth sideband produced by the alternate line sampling of a 1 Volt Luminance signal are shown to the left. The dB values are relative to a reference of $2R_3$ Volts or 0,028125 Volts.

Amplitudes of eleven sidebands in the region of f_{IM} are shown below.

SIDEBAND NUMBER	SIDEBAND FREQUENCY (Hz)	SIDEBAND AMPLITUDE (Volts)	SIDEBAND AMPLITUDE (dB)
195	1523438	2.364463E-03	-21.5072
196	1531250	2.25119E-03	-21.93361
197	1539063	2.134696E-03	-22.39513
198	1546875	2.015236E-03	-22.89533
199	1554688	1.893063E-03	-23.43855
200	1562500	1.768434E-03	-24.03007
201	1570313	1.641615E-03	-24.67643
202	1578125	1.512861E-03	-25.38587
203	1585938	1.382438E-03	-26.16894
204	1593750	1.250612E-03	-27.0394
205	1601563	1.117641E-03	-28.01581

SIDEBAND NUMBER	SIDEBAND FREQUENCY (Hz)	SIDEBAND AMPLITUDE (Volts)	SIDEBAND AMPLITUDE (dB)
0	1566381	.0140625	0
10	1644506	.0136095	-.2844057
20	1722631	1.230284E-02	-1.16114
30	1800756	1.029235E-02	-2.710959
40	1878881	7.804842E-03	-5.113969
50	1957006	5.113379E-03	-8.787091
60	2035131	2.500838E-03	-14.99954
70	2113256	2.231249E-04	-35.99029
80	2191381	-1.522649E-03	-19.30926
90	2269506	-2.620578E-03	-14.59331
100	2347631	-3.046036E-03	-13.28655
110	2425756	-2.862406E-03	-13.82662
120	2503881	-2.205542E-03	-16.09094
130	2582006	-.0012588	-20.96212
140	2660131	-2.228561E-04	-36.00076
150	2738256	7.14902E-04	-25.87632
160	2816381	1.406744E-03	-19.99695
170	2894506	1.762958E-03	-18.03642
180	2972631	1.759873E-03	-18.05162
190	3050756	1.436966E-03	-19.81232
200	3128881	8.842184E-04	-24.03006
210	3207006	2.22409E-04	-36.0182
220	3285131	-4.200021E-04	-30.49622
230	3363256	-9.294073E-04	-23.59713
240	3441381	-1.225333E-03	-21.19617
250	3519506	-1.271706E-03	-20.87352
260	3597631	-1.079709E-03	-22.29512
270	3675756	-7.022856E-04	-26.03098
280	3753881	-2.21783E-04	-36.04268
290	3832006	2.667001E-04	-34.44079
300	3910131	6.731117E-04	-26.39951
310	3988256	9.282216E-04	-23.60822
320	4066381	9.947184E-04	-23.00725
330	4144506	8.719661E-04	-24.15126
340	4222631	5.939228E-04	-27.48665
350	4300756	2.2098E-04	-36.07419
360	4378881	-1.724971E-04	-38.22562
370	4457006	-5.124774E-04	-28.76776
380	4535131	-7.387481E-04	-25.59132
390	4613256	-8.151961E-04	-24.73601
400	4691381	-7.352004E-04	-25.63314

Table 2.5

Calculated amplitudes of every tenth sideband produced by the alternate line sampling of a 1 Volt Intermodulation signal at frequency f_{IM} are shown to the left. The dB values are relative to a reference of R_3 Volts or 0.0140625 Volts which is the sampled "carrier" amplitude.

SIDEBAND NUMBER	SIDEBAND FREQUENCY (Hz)	SIDEBAND AMPLITUDE (Volts)	SIDEBAND AMPLITUDE (dB)
0	4433619	.0140625	0
10	4355494	.0136095	-.2844057
20	4277369	1.230284E-02	-1.16114
30	4199244	1.029235E-02	-2.710959
40	4121119	7.804842E-03	-5.113969
50	4042994	5.113379E-03	-8.787091
60	3964869	2.500838E-03	-14.99954
70	3886744	2.231249E-04	-35.99029
80	3808619	-1.522649E-03	-19.30926
90	3730494	-2.620578E-03	-14.59331
100	3652369	-3.046036E-03	-13.28655
110	3574244	-2.862406E-03	-13.82662
120	3496119	-2.205542E-03	-16.09094
130	3417994	-.0012588	-20.96212
140	3339869	-2.228561E-04	-36.00076
150	3261744	7.14902E-04	-25.87632
160	3183619	1.406744E-03	-19.99695
170	3105494	1.762958E-03	-18.03642
180	3027369	1.759873E-03	-18.05162
190	2949244	1.436966E-03	-19.81232
200	2871119	8.842184E-04	-24.03006
210	2792994	2.22409E-04	-36.0182
220	2714869	-4.200021E-04	-30.49622
230	2636744	-9.294073E-04	-23.59713
240	2558619	-1.225333E-03	-21.19617
250	2480494	-1.271706E-03	-20.87352
260	2402369	-1.079709E-03	-22.29512
270	2324244	-7.022856E-04	-26.03098
280	2246119	-2.21783E-04	-36.04268
290	2167994	2.667001E-04	-34.44079
300	2089869	6.731117E-04	-26.39951
310	2011744	9.282216E-04	-23.60822
320	1933619	9.947184E-04	-23.00725
330	1855494	8.719661E-04	-24.15126
340	1777369	5.939228E-04	-27.48665
350	1699244	2.2098E-04	-36.07419
360	1621119	-1.724971E-04	-38.22562
370	1542994	-5.124774E-04	-28.76776
380	1464869	-7.387481E-04	-25.59132
390	1386744	-8.151961E-04	-24.73601
400	1308619	-7.352004E-04	-25.63314
410	1230494	-5.213754E-04	-28.61824
420	1152369	-2.200017E-04	-36.11273
430	1074244	1.08617E-04	-42.2433
440	996118.8	4.019169E-04	-30.87853
450	917993.8	6.067186E-04	-27.30151
460	839868.8	6.886459E-04	-26.20133
470	761743.8	6.376656E-04	-26.86939
480	683618.8	4.689152E-04	-29.53937
490	605493.8	2.188475E-04	-36.15842
500	527368.8	-6.239946E-05	-47.05763

Table 2.6

Calculated amplitudes of every tenth sideband produced by the alternate line sampling of a 1 Volt Chrominance subcarrier signal at frequency f_{SC} are shown to the left. The dB values are relative to a reference of R_3 Volts or 0.0140625 Volts which is the sampled subcarrier amplitude.

Amplitudes of eleven sidebands in the region of f_{IM} are shown below.

SIDEBAND NUMBER	SIDEBAND FREQUENCY (Hz)	SIDEBAND AMPLITUDE (Volts)	SIDEBAND AMPLITUDE (dB)
365	1582056	-3.534036E-04	-31.99583
366	1574244	-3.872081E-04	-31.20236
367	1566431	-4.200749E-04	-30.49472
368	1558619	-4.519469E-04	-29.85951
369	1550806	-4.827653E-04	-29.28653
370	1542994	-5.124774E-04	-28.76776
371	1535181	-5.410334E-04	-28.29677
372	1527369	-5.683817E-04	-27.86845
373	1519556	-5.944771E-04	-27.47855
374	1511744	-6.19277E-04	-27.12356
375	1503931	-6.427385E-04	-26.80057

SIDEBAND NUMBER	SIDEBAND FREQUENCY (Hz)	SIDEBAND AMPLITUDE (Volts)	SIDEBAND AMPLITUDE (dB)
0	6000000	.0140625	0
10	5921875	.0136095	-1.2844057
20	5843750	1.230284E-02	-1.16114
30	5765625	1.029235E-02	-2.710959
40	5687500	7.804842E-03	-5.113969
50	5609375	5.113379E-03	-8.787091
60	5531250	2.500838E-03	-14.99954
70	5453125	2.231249E-04	-35.99029
80	5375000	-1.522649E-03	-19.30926
90	5296875	-2.620578E-03	-14.59331
100	5218750	-3.046036E-03	-13.28655
110	5140625	-2.862406E-03	-13.82662
120	5062500	-2.205542E-03	-16.09094
130	4984375	-1.0012588	-20.96212
140	4906250	-2.228561E-04	-36.00076
150	4828125	7.14902E-04	-25.87632
160	4750000	1.406744E-03	-19.99695
170	4671875	1.762958E-03	-18.03642
180	4593750	1.759873E-03	-18.05162
190	4515625	1.436966E-03	-19.81232
200	4437500	8.842184E-04	-24.03006
210	4359375	2.22409E-04	-36.0182
220	4281250	-4.200021E-04	-30.49622
230	4203125	-9.294073E-04	-23.59713
240	4125000	-1.225333E-03	-21.19617
250	4046875	-1.271706E-03	-20.87352
260	3968750	-1.079709E-03	-22.29512
270	3890625	-7.022856E-04	-26.03098
280	3812500	-2.21783E-04	-36.04268
290	3734375	2.667001E-04	-34.44079
300	3656250	6.731117E-04	-26.39951
310	3578125	9.282216E-04	-23.60822
320	3500000	9.947184E-04	-23.00725
330	3421875	8.719661E-04	-24.15126
340	3343750	5.939228E-04	-27.48665
350	3265625	2.2098E-04	-36.07419
360	3187500	-1.724971E-04	-38.22562
370	3109375	-5.124774E-04	-28.76776
380	3031250	-7.387481E-04	-25.59132
390	2953125	-8.151961E-04	-24.73601
400	2875000	-7.352004E-04	-25.63314
410	2796875	-5.213754E-04	-28.61824
420	2718750	-2.200017E-04	-36.11273
430	2640625	1.08617E-04	-42.2433
440	2562500	4.019169E-04	-30.87853
450	2484375	6.067186E-04	-27.30151
460	2406250	6.886459E-04	-26.20133
470	2328125	6.376656E-04	-26.86939
480	2250000	4.689152E-04	-29.53937
490	2171875	2.188475E-04	-36.15842
500	2093750	-6.239946E-05	-47.05763

Table 2.7

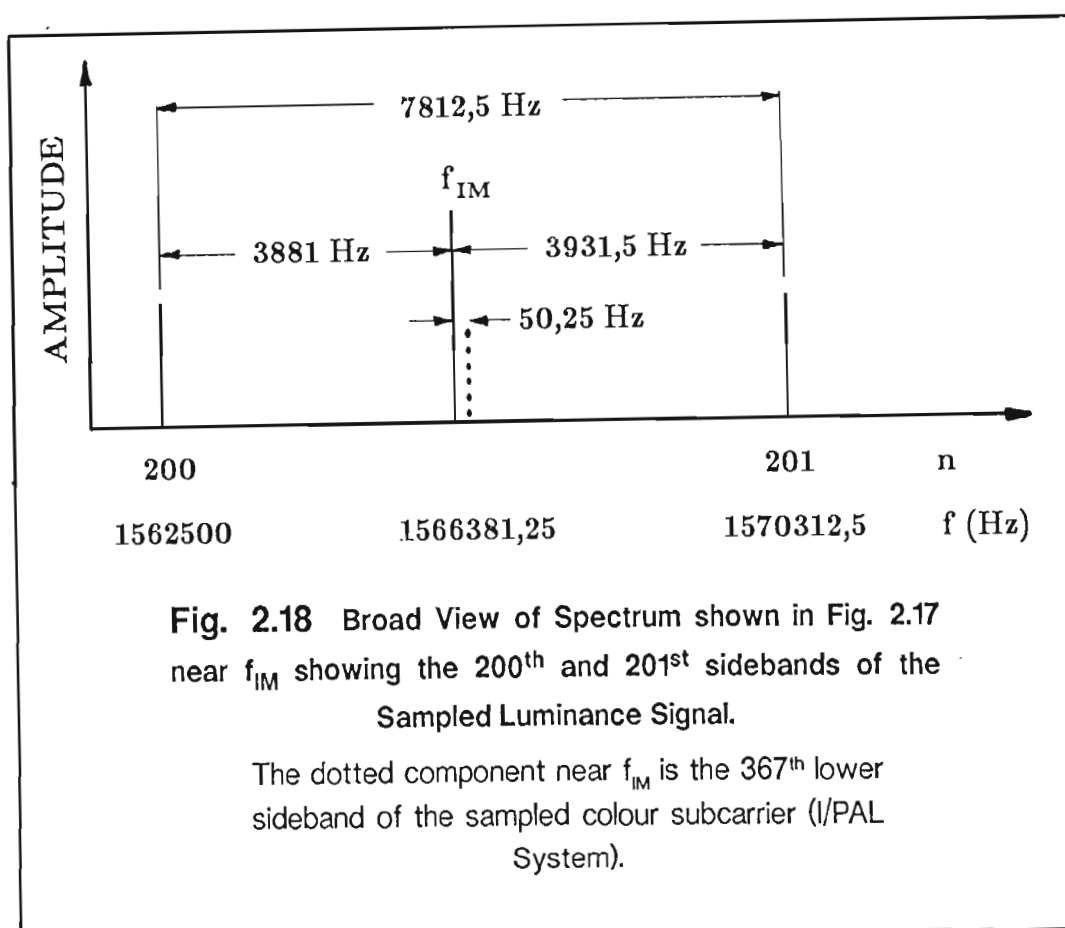
Calculated amplitudes of every tenth sideband produced by the alternate line sampling of a 1 Volt Sound carrier signal at frequency f_{SC} are shown to the left. The dB values are relative to a reference of R_3 Volts or 0.0140625 Volts which is the sampled carrier amplitude.

510	2015625	-3.208701E-04	-32.83467
520	1937500	-5.089712E-04	-28.82738
530	1859375	-5.940843E-04	-27.48429
540	1781250	-5.640809E-04	-27.93442
550	1703125	-4.288219E-04	-30.31571
560	1625000	-2.175215E-04	-36.21121
570	1546875	2.740068E-05	-54.20603
580	1468750	2.587074E-04	-34.70508
590	1390625	4.33337E-04	-30.22474
600	1312500	5.203227E-04	-28.6358
610	1234375	5.061812E-04	-28.87513
620	1156250	3.968661E-04	-30.98837
630	1078125	2.160244E-04	-36.2712
640	1000000	-3.55857E-11	-171.9358
650	921875	-2.093767E-04	-36.54268
660	843750	-3.728131E-04	-31.53143
670	765625	-4.608516E-04	-29.69003
680	687500	-4.591084E-04	-29.72295
690	609375	-3.70535E-04	-31.58467
700	531250	-2.143575E-04	-36.33848

SIDEBAND NUMBER	SIDEBAND FREQUENCY (Hz)	SIDEBAND AMPLITUDE (Volts)	SIDEBAND AMPLITUDE (dB)
562	1609375	-1.697266E-04	-38.36625
563	1601563	-1.45438E-04	-39.7077
564	1593750	-1.209522E-04	-41.30898
565	1585938	-9.631645E-05	-43.28724
566	1578125	-7.158116E-05	-45.86528
567	1570313	-4.679369E-05	-49.55751
568	1562500	-2.200127E-05	-56.11229
569	1554688	2.745794E-06	-74.1879
570	1546875	2.740068E-05	-54.20603
571	1539063	5.191689E-05	-48.65508
572	1531250	7.624519E-05	-45.317

respectively. Fig. 2.18 shows a broad view of the sideband components on either side of the I.M. component. Similar spectra occur in the M/NTSC System but with components spaced at the line frequency of 15625 Hz.

From Fig. 2.18 it is seen that two sideband components of the sampled luminance signal, viz. the 200th and 201st half-line frequency components, are situated closest on either side of the I.M. carrier f_{IM} whose amplitude is to be measured. The 367th lower sideband component of the colour subcarrier is very small due to the 2 MHz low pass filter prior to the mixer discussed in Section 3.2 of Chapter 3, and in Appendix F.



2.5.4 I.M. Measurement using the I.M. Analyser

The equipment configuration shown in block diagram form in Fig. 2.19 was used to measure intermodulation distortion with the I.M. analyser, which effectively replaces the spectrum analyser in the 3TT. A colour bar signal or similar waveform with modulation providing line sync pulses is essential for these measurements. The procedure is very simple, requiring only the correct signals to be connected to the test transmitter and demodulator before I.M. levels can be read from the digital display directly in dBp.

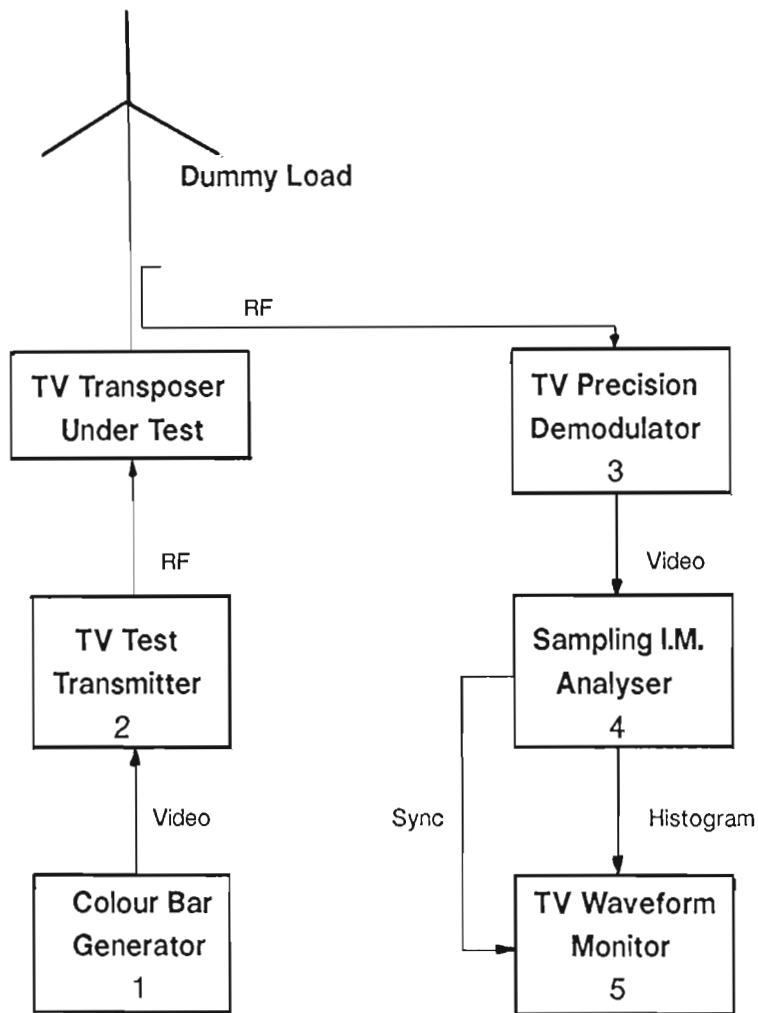


Fig. 2.19 Block Diagram for I.M. Measurement
Using the Sampling I.M. Analyser

Equipment Required:

- | | | |
|----|----------------------|---|
| 1. | Colour Bar Generator | Tektronix 141A or
Rohde & Schwarz SPF2 |
| 2. | TV Test Transmitter | Rohde & Schwarz SBUF |
| 3. | TV Demodulator | Tektronix 1450-3 or
Rohde & Schwarz AMF2 |
| 4. | I.M. Analyser | |
| 5. | Oscilloscope | Rohde & Schwarz OKF or
Tektronix 1480 |

CHAPTER 3

System Design Considerations for a Sampling Type Television Intermodulation Distortion Analyser

3.1 PRACTICAL PROBLEMS ASSOCIATED WITH THE ORIGINAL SAMPLING CONCEPT

3.1.1 Introduction

The main practical difficulty associated with the original I.M. analyser, briefly described in Section 2.5 of Chapter 2, was to ensure that all six channels had identical gains. Feedback amplifiers using operational amplifiers were an obvious solution for the lower frequencies, but gain stability at 1,57 MHz for System I/PAL was another problem. Other more subtle problems arose as the project progressed. These had first to be identified and then solved to achieve a working I.M. analyser. Some of the more important of these are briefly discussed in what follows.

3.1.2 The Need for a Wide Initial Bandwidth

A broadband band pass filter was initially specified as part of the original I.M. analyser's selective input circuit. A tuned circuit working quality factor Q_w of 10 gave a filter bandwidth of

$$\begin{aligned}
 BW &= \frac{f_{IM}}{Q_w} \text{ Hz} \\
 &= 156,7 \text{ kHz}
 \end{aligned} \tag{3.1}$$

allowing many unwanted line harmonics through. This system was potentially noisy, and Q_w was chosen as 50 to reduce the bandwidth to 31kHz, giving an estimated filter rise time of the order of 32 μs from

$$\tau_r \approx \frac{1}{BW} \text{ seconds} \tag{3.2}$$

Unfortunately this slow rise time of the single tuned amplifier was an important factor overlooked in the initial stages of the design.

The first instrument, breadboarded on 'superstrip', gave measurements which in some instances agreed with the three tone test and in others did not. When the measurement conditions were analysed it became clear that there was agreement only when a complete line was modulated with a single colour equivalent to the three tone test signal. Then the analyser input filter circuit had available almost 55 μs , or nearly twice the rise time, in which to respond if sampling occurred near the end of the line.

An analysis of the transient response of the tuned amplifier with Q_w of 50 showed its theoretical rise time to be 22,3 μs [20 to 24]. This was far too long to allow any significant response to an intermodulation signal within a 6,4 μs colour bar. An even shorter rise time is required for sampling to be feasible within the 2,25 μs colour burst.

To allow the analyser to respond to nearly 100% within 6,4 μs necessitated a rise time of approximately 0,5 μs . Unfortunately this required a system bandwidth of the order of 2 MHz, which allowed the 4,43361875 MHz colour subcarrier to pass through the system. Sampling of this subcarrier caused large false readings. The reasons for this effect, and the solution to the problem, are discussed in Appendix F.

3.1.3 Identical Low Pass Filters

The need of seven “identical” low pass filters presented an interesting problem. One possible solution was to make use of switched capacitor filters [60] which, according to manufacture’s specifications, should be closely matched in performance when operated from the same clock signal. Tests conducted on these clocked switched capacitor band pass filters using the MF10 chip showed close matching of pass band responses. The clocking process itself, however, introduced a considerable amount of noise in the output signal. This necessitated additional filtering and careful power supply bypassing to reduce the output noise to an acceptable level. A further complication arose through the noise picked up at the output due to radiation from fast rise time clock signals. Because of these problems clocked switched capacitor filters were eventually abandoned.

3.1.4 Sampling Pulse Timing Tolerances

From the theory presented in Section 2.5 of Chapter 2 it is evident that the gain of each channel is directly proportional to the width of the associated sampling pulse τ_{sa} . For high system accuracy it is essential both to maintain a constant sampling pulse width τ_{sa} and to position the sampling pulse accurately within the colour bar. Pulse position is especially critical when sampling within the narrow colour burst.

Originally, six channels were envisaged, with each corresponding to a colour bar. A $4\ \mu s$ pulse width was proposed which appears to allow a timing tolerance of $\pm 1,2\ \mu s$ in the sampling pulse position within the $6,4\ \mu s$ colour bar width. Tests soon showed, however, that sampling within the first $0,4\ \mu s$ of the colour bar caused an increase in noise for reasons explained in Appendix F. A more realistic timing tolerance of $\pm 0,5\ \mu s$ corresponds to a worst case tolerance of 7,8% which includes all changes in component values due to temperature and manufacturing tolerances, etc.

An instrument accuracy of $0,5\ dBp$ represents 5,93% error, which is determined mainly by the widths of the $4\ \mu s$ pulses. Timing components with 1% tolerances would yield a worst case pulse width error of $\pm 2\%$ for a single timer, or a 4%

worst case pulse width spread if all six timer chips were identical. When temperature effects [89 to 91] and chip performance differences [85 to 88] are included, the resulting tolerance problem would necessitate making each timer circuit individually adjustable, with a consequent increase in production costs [59].

Following a request by the SABC for a seventh channel to allow intermodulation to be monitored within the colour burst, a sample pulse width of $1,8 \mu s$ was proposed to accommodate the minimum colour burst pulse width of $2 \mu s$. This clearly eased the timing problem of sampling within each colour bar, but sampling within $0,2 \mu s$ of the beginning of the colour burst caused noise problems (see Appendix F). Thus a worst case timing tolerance of only $\pm 0,1 \mu s$ in $2 \mu s$, or 5%, was permissible [22].

3.1.5 Phase Alternation of Chrominance "V"

In the PAL TV system [14 to 16, 18, 19] the chrominance signal consists of U and V components made up of the red, blue and green colour signals and the colour subcarrier. The V component changes phase by 180° as each line begins. Intermodulation signals will consequently also change phase every line, and contributions to the mixer output in the same channel (or colour bar) on consecutive lines are therefore unlikely to be additive.

The solution to the errors produced by the swinging "V" component, proposed by A.D. Broadhurst during tests on the I.M. analyser at the Bluff TV Transmitter in Durban, was simply to sample every alternate line when the phases would be the same. A divide-by-two counter driven by the line sync pulses was used to gate the mixer local oscillator signal so that mixing only occurred on alternate lines.

This problem does not arise in the NTSC System. Indeed, alternate line sampling **MUST NOT** be performed when using NTSC colour bars because of the interference that will result. This problem is also considered in Appendix F.

3.1.6 Applicability to all TV Systems

The main difficulty here lies in the different line frequency specifications that apply to the various TV systems [13 to 16]. Horizontal line frequency f_H is 15625 *Hz* for Systems I/PAL and B+G/PAL, and 15734,28 *Hz* for NTSC [13]. Thus the I.M. analyser requires a timing pulse generator capable of adjusting, preferably automatically, to these different line rates.

Another important aspect of the new I.M. analyser design is the down-conversion of the intermodulation frequency to 200 *Hz*. The mixer was followed by a low pass filter with a 500 *Hz* cut-off frequency, creating a -3 *dB* "window" extending to 500 *Hz* corner frequencies on either side of the local oscillator frequency f_{LO} . All signals falling within this window will contribute to the measured intermodulation signal amplitude. Table 3.1 examines the frequency spectra of some TV systems and gives the intermodulation frequency f_{IM} , the two window corner frequencies, the line frequency f_H , the nearest harmonic number of the line frequency to the window, the nearest harmonic frequency and the frequency of this nearest harmonic to the frequency window. Because of the alternate line sampling necessary in the PAL TV systems, harmonics of the half-line frequency $1/2f_H$, or $f_{1/2H}$, must be considered.

The frequencies given in the last column of Table 3.1 show that the intermodulation frequency alone lies within the frequency window, and that the nearest harmonic is a minimum of 2713 *Hz* from this window for all the television systems listed. Adequate rejection of all the adjacent line frequency components may be achieved using an 8th-order active low pass filter with a cut off frequency of approximately 500 *Hz*.

Table 3.1

The intermodulation frequency, the two corner frequencies,
the line frequency, the nearest harmonic number,
the frequency to the window,
and the frequency of the nearest harmonic to the window.

All frequencies are given in *Hz*

TV System	I.M. Frequency f_{IM}	Window Limits		f_H	Harmonic		Freq. to Window Δf
		$f_{IM}-300$	$f_{IM}+700$		No. N_H^*	Freq. $N_H f_H^*$	
B/PAL	1066381,25	1066081	1067081	15625	136*	1062500	3581
G/PAL	1066381,25	1066081	1067081	15625	136*	1062500	3581
I/PAL	1565981,25#	1565681	1566681	15625	200*	1562500	3181
M/PAL	924388,51	924088	925088	15750	117*	921375	2713
M/NTSC	920455,00	920155	921155	15750	59	929250	8095

NOTES:

Due to the 400 *Hz* offset in sound carrier during broadcasting.

* These are harmonic numbers of the half-line frequency $f_{1/2H}$ due to alternate line sampling.

3.2 A PROPOSED TIME DIVISION MULTIPLEXED INTERMODULATION DISTORTION ANALYSER

3.2.1 Introduction

To avoid the problem of constructing seven "identical" channels, a time division multiplexed system [30], shown in simplified block diagram form in Fig. 3.1, was proposed by the author [8, 9]. In this scheme, the same single channel is used in time sequence for the colour burst and each of the six colour bars. The fact that all signals are not being processed continuously makes it necessary to store the measured values while the remaining channels are being sampled.

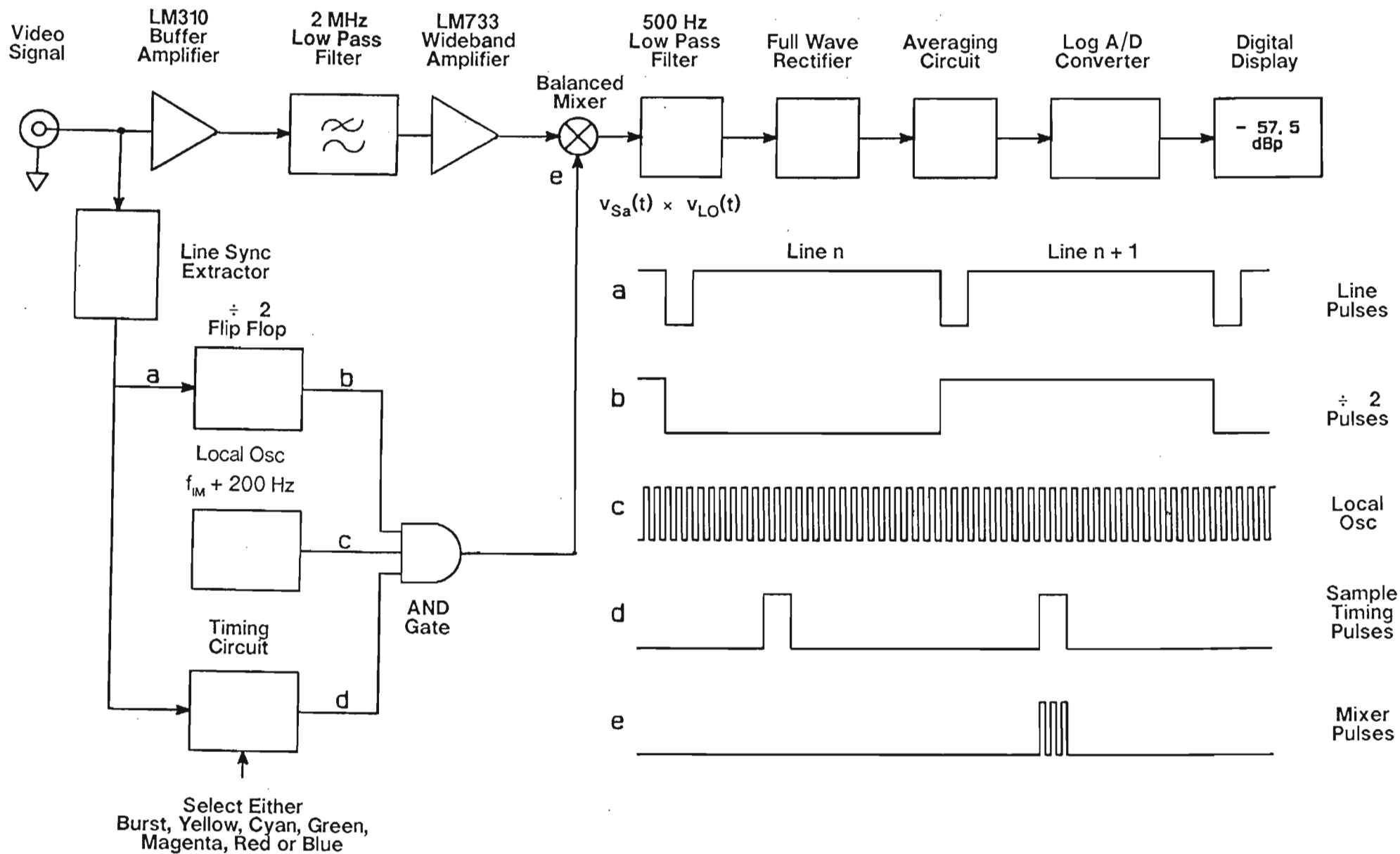


Fig. 3.1 Block Diagram of Multiplexed System

A brief description of the operation of the measurement system follows.

3.2.2 Intermodulation Signal Down-Conversion

To limit the system noise a narrow overall bandwidth was essential. It was thus necessary to down-convert the I.M. frequency and follow the mixer with a low cut-off, low pass filter. 500 *Hz* was chosen as a reasonable compromise for the cut-off frequency f_c , giving an overall system rise time of approximately 2 *ms*. Each colour bar, and the colour burst, was therefore sampled continuously for some 20 *ms* to allow the filter output time to settle.

The I.M. signal was thus down-converted to 200 *Hz* as a convenient value, requiring a local oscillator signal at a frequency of

$$\begin{aligned} f_{LO} &= f_{IM} - 200 \text{ Hz} \\ &= 1566181 \text{ Hz} \end{aligned} \quad (3.3)$$

This choice was unknowingly an excellent one for the following reason. For transmitter I.M. testing in the RSA the video signal is produced by an SBUF TV Test Transmitter with a sound carrier of 6000000 *Hz*. The local oscillator frequency f_{LO} is then 200 *Hz* below f_{IM} . When the transmitter is "on the air" the sound carrier is set at 5999600 *Hz* making f_{LO} 200 *Hz* above f_{IM} . Our choice of local oscillator frequency allows both these sound carrier frequencies to be automatically accommodated.

3.2.3 Active Low Pass Filters

After considering a number of possible configurations [61 to 75] and their sensitivities to component tolerances [76 to 82], an active Sallen and Key circuit [68] with gain was selected and designed with a maximally flat (Butterworth) response. The design was later modified empirically to suit the limited range of close tolerance (1%) components available. A very low ripple, Chebyshev-like response resulted. It was then found that, although analysis was simple, the final empirically chosen component values could not be synthesized using any of the standard techniques to give this particular response.

The practical “500 Hz” low pass filter system consists of four identical active 2nd order low pass Sallen and Key Butterworth filters in cascade. Each 2-pole has a cut-off frequency near 660 Hz giving an overall 3 dB cut-off frequency of 460 Hz and a roll-off rate of 48 dB/octave. Two high pass filters, one at 1,3 Hz and the other at 13 Hz remove any dc offsets.

3.2.4 Intermodulation Signal Amplitude Detection

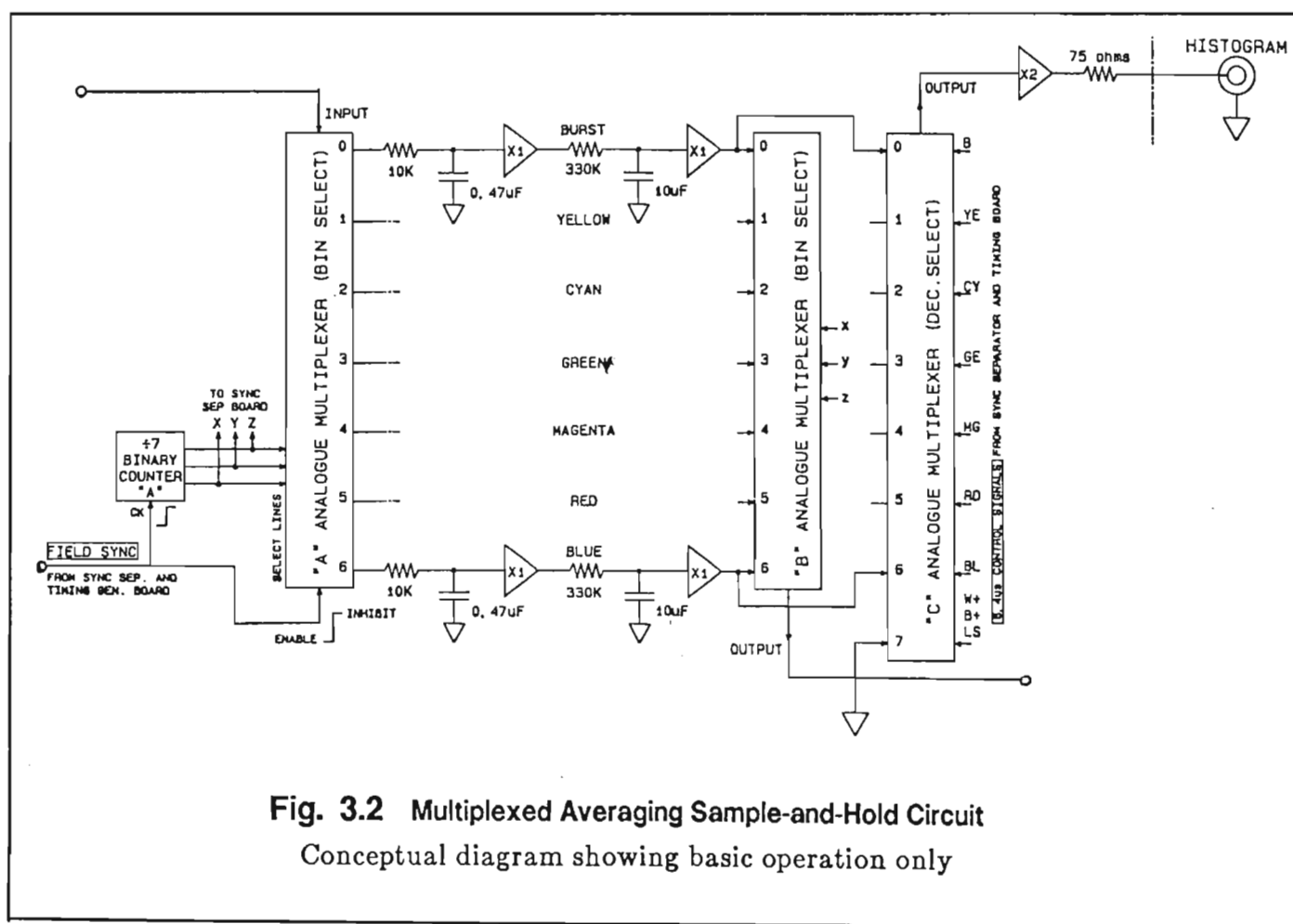
Peak detectors respond to high energy noise pulses superimposed on the desired signal, and are thus subject to considerable error in a noisy environment when used for amplitude detection. The detectors of the original design were therefore replaced by precision full-wave rectifiers with averaging filters [83, 84]. In the multiplexed instrument, a single such precision rectifier circuit suffices to produce a clean rectified signal, with a large 400 Hz ripple component, at its output.

The sudden reappearance of video information at the end of each field sync period produces an overshoot in the 400 Hz precision rectifier output signal amplitude. An inhibit pulse of 5 ms duration, synchronised to the field sync pulse and applied to multiplexer “A”, removes this transient from the multiplexer output.

The average value of the precision rectifier output signal, with its amplitude proportional to the 1,57 MHz intermodulation signal level, is then stored in seven, multiplexed, averaging sample-and-hold circuits developed by the writer and shown in Fig. 3.2. Each circuit consists of two cascaded low pass filters (or averaging circuits) having differing time constants. The output (right hand) filter circuit has a constant R-C time constant of 3,3 s. This reduces the 400 Hz ripple in the dc output to a low level. It also determines the response time of the I.M. distortion analyser.

Each of the seven inputs is selected sequentially for connection to multiplexer “A” input for a 15 ms period. The selected (left hand) filter circuit will then have a low valued input R-C time constant of 4,7 ms, enabling it to respond quickly to signal amplitude changes. When the circuit is deselected the multiplexer “A” output resistance becomes very high compared to 10 k Ω , and the left hand filter

behaves like a sample-and-hold circuit with a long discharge time constant. By holding the average output voltage (\pm some ripple amplitude) the left hand filter circuit presents the long time constant averaging circuit with an almost constant amplitude input signal. 400 Hz ripple amplitude at the output is very low, and that at 50 Hz is reduced significantly by removing the zero amplitude transient signal from the input corresponding to the loss of video during field sync. It also ensures a slightly larger dc output amplitude.



The above averaging sample-and-hold circuit, believed to be unique, gives relatively noise free dc voltages at the inputs of two further analogue multiplexers. Individual outputs may be selected via a front panel push-button switch for connection to the analogue-to-digital converter to display the particular I.M. level. A second output de-multiplexer scanned at ten times line frequency continuously connects each of the seven active outputs (the other

three are connected to ground) sequentially to the oscilloscope display to produce a histogram of the I.M. levels in all colour bars.

Calibration of the detected signal level is achieved via a variable gain control connected in the precision rectifier circuit and situated on the front panel.

3.2.5 Analogue-to-Digital Conversion

A tracking analogue-to-digital (ADC) converter is used to measure the dc voltage from the selected channel. A 9-bit up/down counter is connected to a 9-bit digital-to-analogue (DAC) converter consisting of an 8-bit DAC converter chip plus an external BJT switch for the ninth bit, operating in the inverse mode to minimise the “ON” voltage. The output of the DAC is a dc voltage which is then compared with the input voltage and the comparator output controls the up/down mode of the counter.

3.2.6 Logarithmic Digital dBp Display

A digital display of the measured I.M. level was suggested to make the instrument easier to read and interpret. A particular colour bar, or the colour burst, can be manually selected from the front panel for connection to the digital display. The counter used in the ADC addressed an EPROM which was used purely as a “look up” table for converting the linear digital data produced by the ADC into logarithmic form. The stored data in the EPROM was a BCD representation of the I.M. level reading in dB_p , or dB (peak) relative to peak sync power, which was used to drive the front panel seven segment display. A simple computer programme was written by the author to generate the EPROM data.

3.3 SYSTEM DESIGN PHILOSOPHY

3.3.1 Optimum Noise Performance

For the optimisation of noise performance [95 to 104], high gain was desirable before the mixer. Unfortunately two factors worked against this.

Firstly, two circuits required connection to the video input. For correct matching, and to avoid a 6 dB loss, a unity gain buffer was necessary on one circuit. An LM310 wideband voltage follower was selected for this application. These buffer amplifiers unfortunately contribute to the system noise without increasing the voltage gain.

Secondly, the video input included a wide range of component frequencies from the half-line frequency $f_{1/2H}$ up to approximately 6 MHz. Linear operation of the amplifier before the mixer was essential to avoid false I.M.s from being generated within the analyser. Care was thus taken to avoid saturation of the LM733 video amplifier by overdriving the stage with too large a signal. Low frequency luminance content in the video input signal was therefore reduced by means of a 500 kHz high pass R-C filter at the buffer amplifier input. Spikes remaining on the video signal determined that the maximum allowable gain for the LM733 stage be 20. A safe value of 15 was used to allow for $\pm 10\%$ spreads in expected chip voltage gain.

3.3.2 Selection of a Down-Conversion Mixer

Down-conversion was achieved with analogue CMOS switches in a balanced configuration which was chosen in preference to a diode ring mixer because of its lower distortion specification [42, 88]. The low mark-to-space (M/S) ratio of the sampling pulses caused considerable attenuation in the mixer, so high gain was required within the low pass 500 Hz filter section. Sensitivity considerations [76 to 82] limited the gain of the filters to 10. In practice 7.8 was a convenient value with the close tolerance components easily available.

3.3.3 Choice of a Pulse Timing Generator

The timing tolerance problems of individual circuits can be overcome either through the use of low tolerance, costly components or by separate adjustment. An alternative approach proposed by the author was to use a form of simple state machine for generating the timing pulses. The state machine had to be synchronised with the TV line sync pulses, and this suggested the use of a phase locked loop (PLL).

Investigation of the colour bar signal showed each bar to be $6.4 \mu s$ wide, although this is not stated in the colour bar specifications. A divide-by-ten counter operating in a PLL with the voltage controlled oscillator running at ten times the line frequency f_H formed the basis of the state machine. The specification and design of this unit is discussed in detail in Chapter 4. The heart of the multiplexing system is the proportional timing pulse generator which is required to schedule sampling of the seven channels.

3.3.4 A Temperature Compensation Technique

A most important aspect of the timing circuit was the temperature stability of both the sampling pulse width and position within the colour burst or bar being sampled. In Appendix E a simple theory of temperature compensation for timer chips has been developed. This allows combinations of resistors and capacitors having different temperature coefficients to be used in such a way that the combined effect of the chip and external timing components has zero temperature coefficient. Results obtained for timers designed using this theory have been excellent.

3.4 MULTIPLEXED SYSTEM GAIN ESTIMATION

It is unlikely that a broadcasting authority would require an intermodulation measurement exceeding -40 dBp . This level was therefore selected as the maximum level at which the instrument would operate, and 2.4 Volts DC was chosen as a suitable input voltage to the analogue-to-digital converter (ADC)

corresponding to this level. A more realistic level of -50 dBp is used for the calculations which corresponds to $0,759 \text{ Volts}$ input to the ADC. The overall system voltage gain required to produce this DC reference output voltage of 759 mV was estimated as follows.

Broadcast Reference Level of 0 dBp :

This level corresponds to peak sync power, and is the maximum carrier amplitude that occurs within the sync pulses. When demodulated to a video signal, the peak sync level would be $1,25 \text{ Volts}$ in the South African I/PAL System.

Analyser Reference Level of -50 dBp :

$$\begin{aligned} -50 \text{ dBp} &= 2 \times 1,25 \times 10^{-50/20} \\ &= 7,91 \text{ mV peak} \end{aligned} \quad (3.4)$$

Note that the factor "2" is included to compensate for the loss in the demodulator vestigial sideband filter.

To achieve the 759 mV peak output required:

$$\text{Gain} = 95,95 \quad (3.5)$$

Initial Gain Estimates For Each Stage:

$$\text{Gain of LM310 Buffer Amp} = 1 \quad (3.6)$$

$$\text{Gain of passive } 2 \text{ MHz LPF} = 0,5 \quad (3.7)$$

$$\text{Gain of LM733 Wide Band Amp} = 15 \quad (3.8)$$

$$\text{Gain of } 500 \text{ Hz low pass filter} = 7,83^4 \quad (3.9)$$

(because

$$\text{Gain of each active 2-pole LPF} = 7,83) \quad (3.10)$$

$$\text{Gain of full wave rectifier (variable)} = X \text{ (say)} \quad (3.11)$$

$$\text{Gain of averaging circuit} = 2/\pi \quad (3.12)$$

Gain of analogue switch mixer:

Four significant signals are applied to the mixer:

- 1 Intermodulation distortion signal at ω_{IM} is assumed to be a sinewave of unknown amplitude. For simplicity assume that:

$$v_{IM}(t) = V_{IM} \cos(\omega_{IM}t) \quad (3.13)$$

- 2 Local oscillator signal at ω_{LO} multiplies the input signal to the mixer by +1 or -1, which may be represented as the following Fourier series [26 to 34]:

$$v_{LO}(t) = \frac{4}{\pi} \left[\sum_{n=1,3,5 \text{ etc.}}^{\infty} \frac{1}{n} \cos(n \omega_{LO}t) \right] \quad (3.14)$$

- 3 The effective sampling waveform $v_{sa}(t)$ consists of $1.8 \mu s$ timing pulses with a mark-space ratio of R_3 and unit amplitude. The Fourier series representation can be written in the familiar form:

$$v_{sa}(t) = R_3 + 2R_3 \sum_{n=1}^{\infty} \text{sinc}(n \pi R_3) \cos n \omega_{sa} t \quad (3.15)$$

with

$$R_3 = \frac{1.8}{128} \quad (3.16)$$

and

$$\text{sinc}(x) = \frac{\sin(x)}{x} \quad (3.17)$$

and

$$\begin{aligned} \omega_{sa} &= \frac{1}{2} \omega_H \\ &= \omega_{1/2H} \end{aligned} \quad (3.18)$$

or half the line frequency.

- 4 An effective field pulse waveform, synchronised to the field sync pulses, which has a mark-space ratio of R_4 and unit amplitude. The "space" coincides with the loss of video information within the field sync pulse region. The Fourier series is of similar form to that of the previous pulse waveform, and is given by:

$$v_F(t) = R_4 + 2R_4 \sum_{n=1}^{\infty} \text{sinc}(n\pi R_4) \cos n\omega_F t \quad (3.19)$$

with

$$R_4 = 0,9296 \quad (3.20)$$

It has been shown in Section 2.5 of Chapter 2 that this waveform may be ignored, the penalty being a 0,36 dB error [see Appendix F, Section F.2] which may be compensated for in the calibration process.

When the input signal $v_{IM}(t)$ is multiplied by the two switching functions $v_{LO}(t)$ and $v_{sa}(t)$ a multitude of frequency components is produced at the output of the mixer:

$$\begin{aligned} v_{mix}(t) = & V_{IM} \cos \omega_{IM} t \left[\frac{4}{\pi} \sum_{n=1,3,5 \text{ etc}}^{\infty} \frac{1}{n} \cos(n\omega_{LO} t) \right] \\ & \times \left[R_3 + 2R_3 \sum_{n=1}^{\infty} \text{sinc}(n\pi R_3) \cos n\omega_{sa} t \right] \end{aligned} \quad (3.21)$$

The only component which will pass through the 500 Hz low pass filter is the difference frequency $\omega_{LO} - \omega_{IM}$ (or $\omega_{IMD} = 2\pi \cdot 200 \text{ rad/s}$ with $n=0$) which is given by

$$\begin{aligned} v_{miximd} &= \frac{2}{\pi} R_3 [V_{IM} \cos(\omega_{LO} - \omega_{IM})t] \\ &= 0,0089525 [V_{IM} \cos(\omega_{LO} - \omega_{IM})t] \end{aligned} \quad (3.22)$$

The mixer gain of 0,0089525, or attenuation of 40,96 dB which must be made up in the other stages. Using the values defined in equations (3.6) to (3.12), and noting that four filters (each with a voltage gain of 7,83) are cascaded, the overall gain is estimated as:

$$\begin{aligned} A_v &= 1 \times \frac{1}{2} \times 15 \times 7,83^4 \times \frac{2}{\pi} \times 0,0089525 \\ &= 160,67 \end{aligned} \quad (3.23)$$

The gain required at calibration is 151,71. Hence the variable rectifier gain X is:

$$\begin{aligned} X &= \frac{95,95}{160,67} \\ &= 0,60 \end{aligned} \quad (3.24)$$

3.5 THEORETICAL RELATIONSHIP BETWEEN I.M. MEASUREMENT ERROR SYSTEM RISE TIME AND SAMPLING PULSE DELAY

If a system is assumed to have a single pole, due to an R-C time constant, which determines the rise time τ_r , then the growth of I.M. signal voltage can be expressed as a function of time by the following familiar expression:

$$v_{IM} = V_{max} [1 - \exp(-\frac{t}{\tau_r})] \quad (3.25)$$

The average value of the voltage, sampled from time t_1 to time t_2 , is given by:

$$V_{Ave} = \frac{1}{t_2 - t_1} \int_{t_1}^{t_2} V_{max} [1 - \exp(-\frac{t}{\tau_r})] dt \quad (3.26)$$

where

$$t_2 - t_1 = \tau_w \quad (3.27)$$

which is the pulse width. Hence

$$V_{Ave} = \frac{V_{Max}}{\tau_w} [\tau_w + \tau_r \exp(-\frac{t_2}{\tau_r}) - \tau_r \exp(-\frac{t_1}{\tau_r})] \quad (3.28)$$

The rise time τ_r is related to the system time constant τ as follows:

$$\tau_r = 2.2 \tau \quad (3.29)$$

A computer program was written to evaluate the function in equation (3.28) for selected delay and rise times, and to determine the error in assuming the average voltage V_{Ave} to be equal to the maximum value V_{Max} . The errors are expressed as a percentage, as well as in dBs, and are presented overleaf in Table 3.2 for a range of system rise times. Although the rise time may be estimated from the chrominance bandwidth alone, the measurement system bandwidth of 1.5 MHz will cause a significant increase in the system rise time. A value of 0.7 μs is a reasonable estimate for the complete measurement system for I/PAL signals.

Two facts become immediately clear from the figures in Table 3.2:

Table 3.2

Sample Average Value in % and System Error in dB
versus
Sample Delay Time

Sample Delay μs	Rise Time $\tau_r = 0,5 \mu s$		Rise Time $\tau_r = 0,7 \mu s$		Rise Time $\tau_r = 0,9 \mu s$	
	Ave. Value %	Error dB	Ave. Value %	Error dB	Ave. Value %	Error dB
.1	77.8789	-2.171605	68.86456	-3.240085	61.3132	-4.248922
.2	81.88876	-1.735513	73.00938	-2.732428	65.38153	-3.690899
.3	85.17178	-1.394086	76.60243	-2.31515	69.02203	-3.220245
.4	87.85968	-1.124208	79.71716	-1.968964	72.2797	-2.819674
.5	90.06034	-.9093281	82.41725	-1.679638	75.19479	-2.476246
.6	91.8621	-.7372727	84.75791	-1.436395	77.80331	-2.180039
.7	93.33725	-.5988999	86.78696	-1.230911	80.13754	-1.92328
.8	94.545	-.4872284	88.54591	-1.05663	82.22629	-1.699787
.9	95.53382	-.3968569	90.0707	-.9083294	84.09538	-1.504557
1	96.34341	-.3235604	91.39251	-.7817881	85.76792	-1.333502
1.1	97.00623	-.2640071	92.53836	-.6735641	87.26458	-1.18324
1.2	97.54891	-.2155514	93.53167	-.5808263	88.60384	-1.05095
1.3	97.99322	-.1760794	94.39274	-.5012278	89.80227	-.9342534
1.4	98.35699	-.1438955	95.1392	-.4328109	90.87468	-.831143
1.5	98.65482	-.1176343	95.78628	-.3739348	91.8343	-.739902
1.6	98.89865	-.0961923	96.34721	-.3232165	92.69301	-.6590605
1.7	99.0983	-7.867665E-02	96.83348	-.2794891	93.46142	-.5873531
1.8	99.26175	-6.436136E-02	97.25501	-.2417601	94.14902	-.523684
1.9	99.39557	-5.265983E-02	97.62043	-.2091857	94.76431	-.467104
2	99.50514	-4.309038E-02	97.93721	-.1810456	95.31491	-.4167841
2.1	99.59484	-3.526358E-02	98.21181	-.1567263	95.80759	-.3720018
2.2	99.66828	-2.886057E-02	98.44986	-.1356986	96.24847	-.3321242
2.3	99.72841	-2.362186E-02	98.65622	-.1175114	96.64298	-.2965942
2.4	99.77764	-1.933568E-02	98.83511	-.1017752	96.996	-.264923
2.5	99.81795	-1.582738E-02	98.99018	-8.815759E-02	97.31191	-.2366802
2.6	99.85095	-1.295644E-02	99.12461	-7.637078E-02	97.59459	-.2114855
2.7	99.87797	-1.060667E-02	99.24114	-6.616512E-02	97.84754	-.1890011
2.8	99.90009	-8.682503E-03	99.34216	-.057328	98.0739	-.1689312
2.9	99.9182	-7.108267E-03	99.42973	-4.967457E-02	98.27645	-.151011
3	99.93303	-5.819026E-03	99.50564	-4.304527E-02	98.45769	-.1350064

- 1 Measurements within the colour burst will typically be subject to an error of 2,7 dB, assuming a measurement delay of 0,2 μs . The error sensitivity to a change in delay time is approximately 5 dB/ μs so that a change in timing of only 0,1 μs will produce a change in reading of 0,5 dBp.
- 2 Measurements within the colour bars will typically be subject to an error of about 0,8 dB, assuming a measurement delay of 1 μs . The error sensitivity to a change in delay time is approximately 1 dB/ μs so that a change in timing of 0,1 μs will produce a change in reading of 0,1 dBp. If the delay is increased to 3 μs the error reduces dramatically to less than 0,05 dB, and the error sensitivity to 0,05 dB/ μs .

The original breadboarded prototype had two sampling 1,8 μs monostables. One was triggered by the VCO output and timed to sample within the colour burst, while the second was triggered by the trailing edge of the first, causing sampling within the colour bars to occur some 2,9 μs after the commencement of each bar. This circuit was later simplified to make use of a single monostable pulse generator for sampling. This system was implemented in the final prototype as it was believed that sampling was sufficiently stable to accommodate this error by a calibration adjustment. Although this is true, the error was overlooked as development progressed and was omitted from the calibration calculations. Limitations in the absolute accuracy of our own calibration facilities to ± 1 dB effectively concealed the error during measurements, and it remained unnoticed until it was revealed in the more accurate measurements performed at the Swiss Posts, Telephones and Telegraphs Institute. With adequate calibration equipment available this problem should not have arisen.

3.6 CRYSTAL REFERENCE OSCILLATOR

A MEASURE/CALIBRATION switch on the front panel operates 3 solid state analogue switches to connect the instrument input to either

1. The video signal, or
2. An external 1,566381 *MHz* calibration signal, or
3. An internal 1,566381 *MHz* calibration signal

An internal crystal controlled oscillator is provided to calibrate the equipment. A switch on the rear panel marked INT/EXT CAL, is normally switched to INT. In this mode it connects the output of the reference oscillator to the input bandpass filter when the front panel MEASURE/CALIBRATE switch is switched to CALIBRATE. The dc supply to the crystal oscillator is turned off when this switch is in the MEASURE position.

CALIBRATION:

The frequency of the reference oscillator is f_{IM} or 1,566381 *MHz* and the output is a square wave whose amplitude at f_{IM} corresponds to -50 dBp. This level is adjusted by a potentiometer by first calibrating the unit on EXT CAL using an accurately calibrated signal generator producing -32 dBm or 5,59 mV rms into 50 Ω . The unit is then switched to INT CAL and if the reading is not -50.0 dBp, the potentiometer is adjusted to give this reading. A more accurate calibration results if the dc output of the ADC is measured with a digital voltmeter and set to 759 mV.

CHAPTER 4

Proportional Timing Pulse Generator Operation and Detailed Circuit Design

4.1 OPERATION OF THE PHASE LOCK LOOP BASED SAMPLE TIMING PULSE GENERATOR

4.1.1 Introduction

A phase lock loop (PLL) operating at ten times the line frequency was used to generate the $1.8 \mu\text{s}$ sampling pulses coinciding with the colour burst and each of the six colour bars. The basic theory of the PLL [45 to 58] is presented briefly in Appendix C. Also, root locus diagrams are used in a fairly detailed consideration of second order linear feedback systems and their stability [106]. These diagrams help explain the transient behaviour of the PLL, when lock is lost, which is largely dependent on the choice of low pass filter configuration. A Type 1 Second Order system was chosen incorporating the passive lag-lead filter of Fig. C.3 (a). Since τ_2 and τ_3 can be set independently via R_2 and R_1 it follows that ζ and ω_n can be chosen to give the desired dynamic response.

Successful operation of the proposed PLL sample pulse timer for the multiplexed I.M. analyser requires the implementation of a true phase lock system to ensure that the sample pulse positions are fixed relative to the TV horizontal line sync pulses under all ambient conditions. Only one PLL chip, the CMOS CD4046, has the required capability at present. This chip has two phase detectors. Phase Detector I is a simple exclusive-or gate, while Phase Comparator II (PC-II) is a more sophisticated tri-state digital circuit with memory. The behaviour of both comparators under various signal conditions

is considered in some detail in Appendix C, where it is shown that a PLL using PC-II is alone capable of meeting the system performance requirements. Appendix D describes the measurement of the CD4046 VCO capture and lock ranges and gain under selected operating conditions to facilitate the PLL system design.

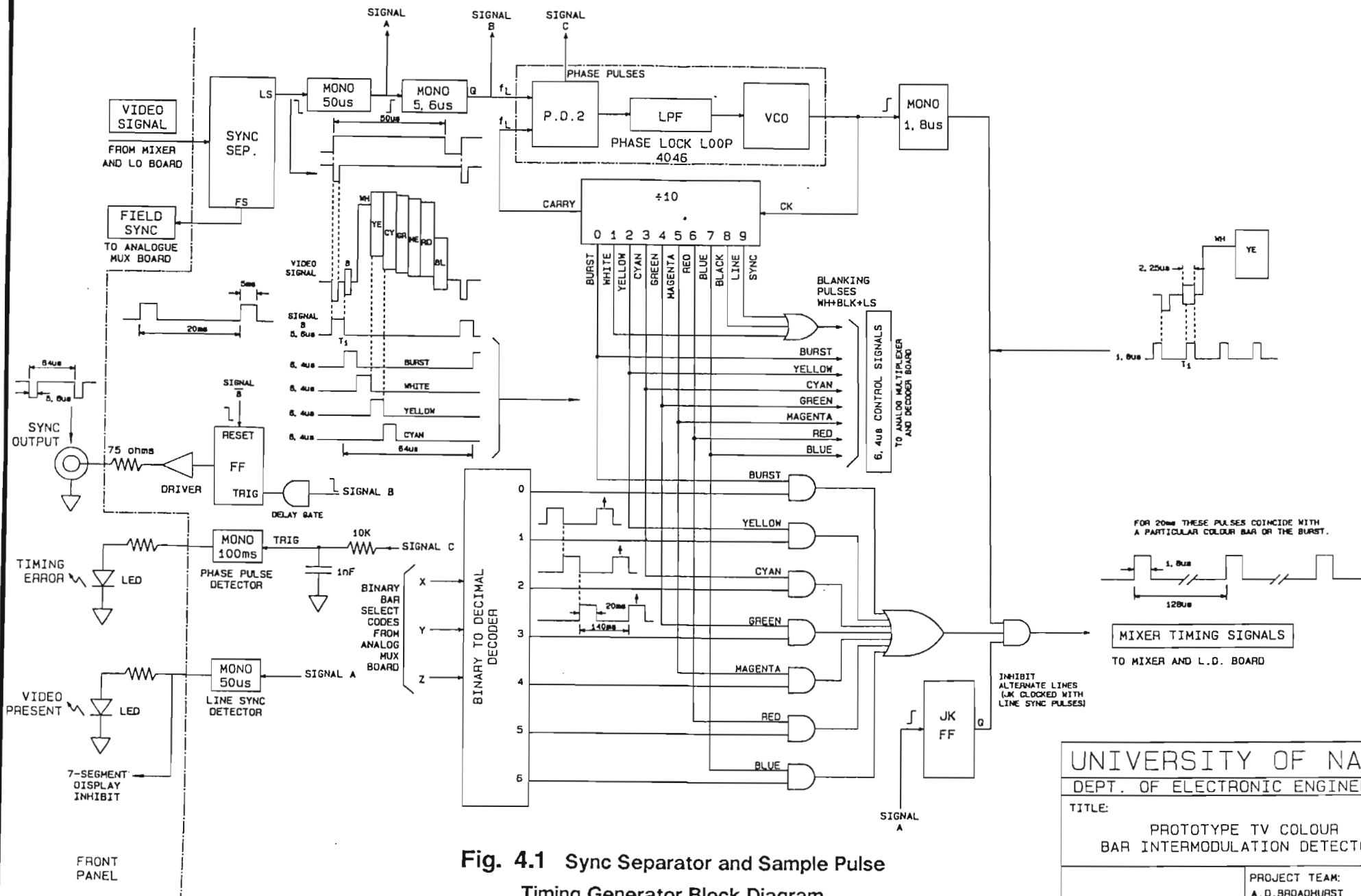
VCO phase jitter and spectral content caused by the ramping of the voltage on the loop low pass filter's capacitor, is considered later in this chapter.

4.1.2 Operation of the Phase Lock Loop Based Sample Timing Pulse Generator

A block diagram of the proposed PLL-based pulse generator is presented in Fig. 4.1 overleaf. The video input signal is applied to the sync separator which produces both line and field sync pulses at its output. Figs. G.3 and G.4 in Appendix G show the SABC Specification for the field and line synchronising pulses used in the 625 line System I/PAL Transmissions in South Africa. Line sync pulse leading edge at output "LS" triggers an edge triggered non-retriggerable $50\ \mu\text{s}$ monostable, which then runs continuously at line frequency f_H even during the field blanking periods when the equalising and broad pulses occur.

Signal "A" triggers the $5,6\ \mu\text{s}$ monostable at the leading edge of the line sync pulses, with a small propagation delay. Signal "B" is a positive going pulse of duration $5,6\ \mu\text{s}$ with its trailing edge about $450\ \text{ns}$ inside the $2,25\ \mu\text{s}$ colour burst. This repetitive pulse is used as external input by a CMOS type CD4046 phase lock loop having a divide-by-10 counter in its feedback loop. The VCO output signal thus has a frequency of $10 f_H$ or $156250\ \text{Hz}$ and a period of $6,4\ \mu\text{s}$. The divide-by-10 counter has an internal binary-to-decimal decoder with outputs 0 through to 9 sequentially producing pulses $6,4\ \mu\text{s}$ wide. The leading edges of these $6,4\ \mu\text{s}$ pulses fall conveniently within the burst and colour bars.

The VCO output signal rising edge triggers a $1,8\ \mu\text{s}$ monostable to produce timing pulses which coincide with the back $1,8\ \mu\text{s}$ of the colour burst pulse, and begin approximately $1,1\ \mu\text{s}$ after the leading edges of each of the six $6,4\ \mu\text{s}$ colour bars, and are used to gate the mixer local oscillator on and off during the colour



UNIVERSITY OF NATAL	
DEPT. OF ELECTRONIC ENGINEERING	
TITLE:	
PROTOTYPE TV COLOUR BAR INTERMODULATION DETECTOR.	
PROJECT TEAM:	
A. D. BROADHURST	
P. F. BOUNER	
G. VATH	
DRAWN: P. J. FACOLINE	
DATE: 26 AUGUST 1985	

bar periods. For a measurement to be performed it is necessary to select each of the colour bars, and the burst, for a continuous period of 20 *ms* in the following sequence:

burst → yellow → cyan → green → magenta → red → blue → burst

the process being repeated every $7 \times 20 \text{ ms}$ or 140 *ms*.

Binary signals X, Y and Z from a divide-by-seven counter in the analogue multiplexer section produce decimal output signals numbered 0 through to 6, of 20 *ms* duration and repetition period of 140 *ms*, as shown on the timing diagram inserts in Fig. 4.1. These signals are gated with the 6,4 μs signals from the phase lock loop divide-by-10 counter. Each two input AND gate produces positive pulses of 6,4 μs duration every 64 μs which are only present for 20 *ms* and absent throughout the 120 *ms* idle period.

At the final 3-input AND gate the 6,4 μs and 1,8 μs pulses combine for 20 *ms* periods to produce 1,8 μs pulses corresponding in position to either the burst or one of the 6 colour bars. The third input of this final AND gate is an output signal from a J-K flip flop, clocked at the line frequency, which inhibits alternate lines for measurements in the PAL System.

4.1.3 Phase Lock Loop Synchronisation

An examination of the video waveform diagrams in Figs. G.3 and G.4 of Appendix G reveals that negative-going edges exist at regular intervals of one line period, or 64 μs for System I/PAL, at all times throughout the sync pulse train. These edges are identified by the “^” symbols below them in the figures mentioned. The synchronising signal for M/NTSC differs mainly in the number of equalising pulses.

Negative-going edges do occur in the first half of some line periods within the field sync and equaliser pulse sequence, but never during the latter half of any line period. This is not true of the positive-going edges. This led to the realisation by the writer that a very effective drive signal was available for the PLL if these negative-going edges, spaced at 64 μs intervals, could be utilised. The negative-going leading edges of the sync pulses at the output of comparator IC01 at pin 7 were therefore applied to the trigger input of a non-retriggerable

50 μs monostable IC16 [85 to 87]. The pulse period of 50 μs was chosen as it lay between a half-line period and 64 μs . This effectively prevents the monostable from being triggered in the middle of a line once synchronisation to the 64 μs negative edges has been established.

This synchronisation process is automatic and requires only one normal line period for completion. The leading edge of IC16 output pulse in turn triggers a 5,6 μs monostable IC02 at pin 4, and its output signal will therefore have a steady 64 μs repetition period with no breaks during the equalisation and field synchronisation periods. As a result, the PLL circuit never goes out of lock under normal operating conditions. This makes the design of the PLL low pass filter much simpler. A further consequence is that the histogram display may be made free of observable jitter by triggering the monitor externally from the 5,6 μs pulse output at IC02 pin 6.

4.2 PHASE LOCK LOOP SYSTEM DESIGN

4.2.1 Initial Parameter Estimates

Various approaches to the design of feedback systems in general, and PLLs in particular, can be obtained from the many texts available [45 to 57]. Reasonable initial design assumptions must be made and system parameter starting values selected before the design can be systematically performed. Previously derived equations for system natural resonant frequency and damping factor, for a Type 1 second order PLL using the lag-lead filter, were used and additional design equations for acquisition time, 3 dB bandwidth and noise bandwidth are quoted from texts by Gardner [47] and Rohde [54].

The system natural resonant frequency ω_n directly influences many performance parameters as is evident from the equations that follow.

Acquisition time τ_{acq} :

$$\tau_{acq} = \frac{4(\Delta f)^2}{BW_n^3} \text{ seconds} \quad (4.1)$$

where the noise bandwidth BW_n is

$$BW_n = \frac{\omega_n}{2} \left[\zeta + \frac{1}{4\zeta} \right] \text{ rad/s} \quad (4.2)$$

Taking a worst case situation in which the free-running frequency f_o is assumed to be zero, the required Δf is 156 250 Hz. Table 4.1 shows some selected values of noise bandwidth BW_n and their corresponding acquisition times.

Table 4.1
Acquisition Time vs System Noise Bandwidth

BW_n	1 000	3 000	10 000	<i>rad/s</i>
τ_{acq}	97,66	3,6169	0,0977	<i>secs</i>

Clearly the noise bandwidth of the system should be of the order of 10 000 *rad/s* for a reasonable acquisition time under the conditions described.

Frazier and Page [46] have shown that acquisition is optimised for a damping factor of

$$0,5 \leq \zeta \leq 0,85 \quad (4.3)$$

Maximum loop gain, which corresponds to a large VCO timing resistor R_4 , gives high damping values and slows the acquisition performance of the PLL. Because the loop is arranged never to lose lock, rapid acquisition is relatively unimportant, but a value of 0,7 was chosen as a useful starting value for ζ for the prototype. Hence it will be assumed that

$$\zeta = 0,7 \quad (4.4)$$

Thus

$$\zeta + \frac{1}{4\zeta} = 1,057 \quad (4.5)$$

and, assuming a noise bandwidth BW_n of 10 000 *rad/s*, the system natural frequency is

$$\begin{aligned} \omega_n &= 1,892 BW_n \text{ rad/s} \\ &= 18919 \text{ rad/s} \end{aligned} \quad (4.6)$$

based on the acquisition time requirements. The damping factor ζ also determines the overshoot during input transients, while ω_n governs the settling time τ_s of the output phase to within some acceptably close proximity of the input phase. As an initial estimate, settling time may be taken as

$$\tau_s = \frac{5}{\omega_n} \text{ secs} \quad (4.7)$$

For

$$\begin{aligned} \tau_s &= 1 \text{ ms} \\ \omega_n &= \frac{5}{10^{-3}} \\ &= 5000 \text{ rad/s} \end{aligned}$$

which gives a noise bandwidth of

$$BW_n = 2642,9 \text{ Hz} \quad (4.8)$$

If this value of noise bandwidth of 2642,9 *Hz* is used instead of 18919 *Hz*, acquisition time will be increased by a factor of 7,158³ or 366,84 times, which is unacceptable. Two alternatives are available to the designer. These are:

- 1 Increase the system natural resonant frequency. This will affect a number of parameters adversely, including the noise bandwidth and system 3 *dB* bandwidth.
- 2 Raise the free-running VCO frequency f_o by including a finite-valued timing resistor R_4 , thereby reducing Δf and decreasing τ_{acq} considerably.

The latter of the two choices was adopted as it made the choice of ω_n far more flexible.

The measured maximum and minimum loop gains for the chips tested were:

$$\frac{K_o K_d}{N} = 8333,33 \text{ min} \quad (4.9)$$

and

$$\frac{K_o K_d}{N} = 34218,4 \text{ max} \quad (4.10)$$

These gain variations are sufficient to cause considerable changes in the values of both ω_n and ζ , as will be evident from Table 4.4 later.

The system -3 dB bandwidth BW_{3dB} can be derived from the system transfer function $STF(j\omega)$ under steady state conditions, and the following equation results:

$$BW_{3dB} = \frac{\omega_n}{2\pi} (a + \sqrt{a^2 + 1}) \text{ Hz} \quad (4.11)$$

where

$$a = 2\zeta^2 + 1 - b(4\zeta - b) \quad (4.12)$$

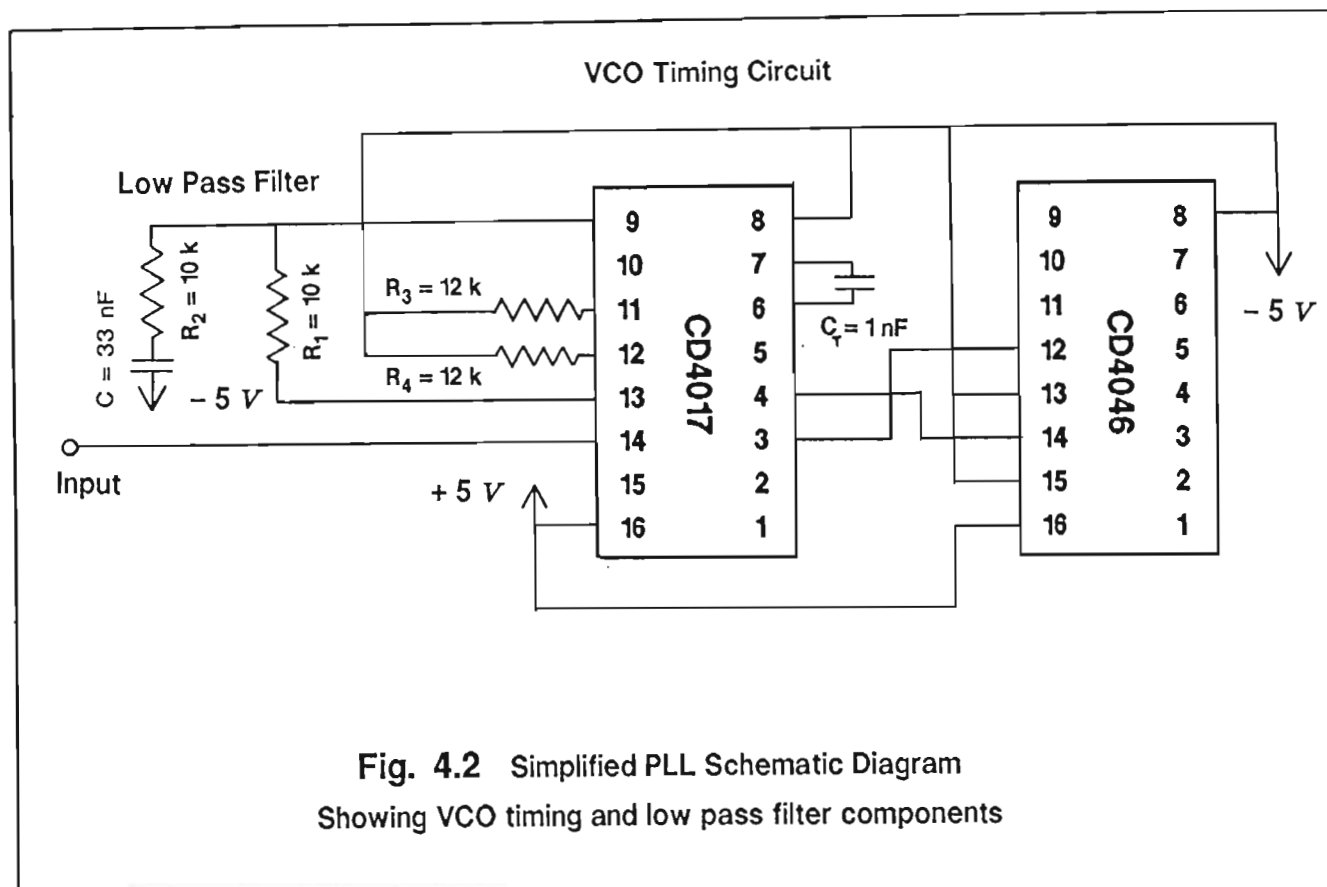
and

$$b = \frac{\omega_n}{K} \quad (4.13)$$

This bandwidth is again largely dependent on the value chosen for ω_n , being typically of the same order of magnitude as ω_n . To achieve a large attenuation in signals at the input frequency of 156250 Hz the bandwidth should be approximately $0,1 \times 156250 \text{ Hz}$, or $2486,8 \text{ rad/s}$. Hence 2500 rad/s is a convenient choice for ω_n .

4.2.2 Choice of VCO Timing Component Values

A simplified schematic diagram showing only the PLL section of the timing pulse generator is found in Fig. 4.2 in which the CD4046 CMOS chip VCO timing components and low pass filter elements are illustrated.



The inclusion of VCO timing resistor R_4 of Fig. 4.2 provides a frequency offset f_{MIN} which reduces the capture range of the PLL and decreases the loop gain K . The lower frequency limit f_{MIN} is determined by R_4 and C_T , and this is also the free running frequency f_o of the VCO when Phase Comparator II is used, ie.

$$f_o = f_{\text{MIN}} \quad (4.14)$$

Diminution of loop gain also decreases both the system damping and the natural resonant frequency. In fact in some instances the CD4046 VCO would not oscillate unless a value of R_4 less than 10 $M\Omega$ were used.

For this design the VCO oscillation frequency limits must span the desired centre frequency of 156250 Hz, or ten times the TV line frequency f_H . Table 4.2 gives selected timing component values for two of many possible PLL designs. Values were chosen with the aid of the manufacturer's curves reproduced in Figs. 4.3 (a) and (b).

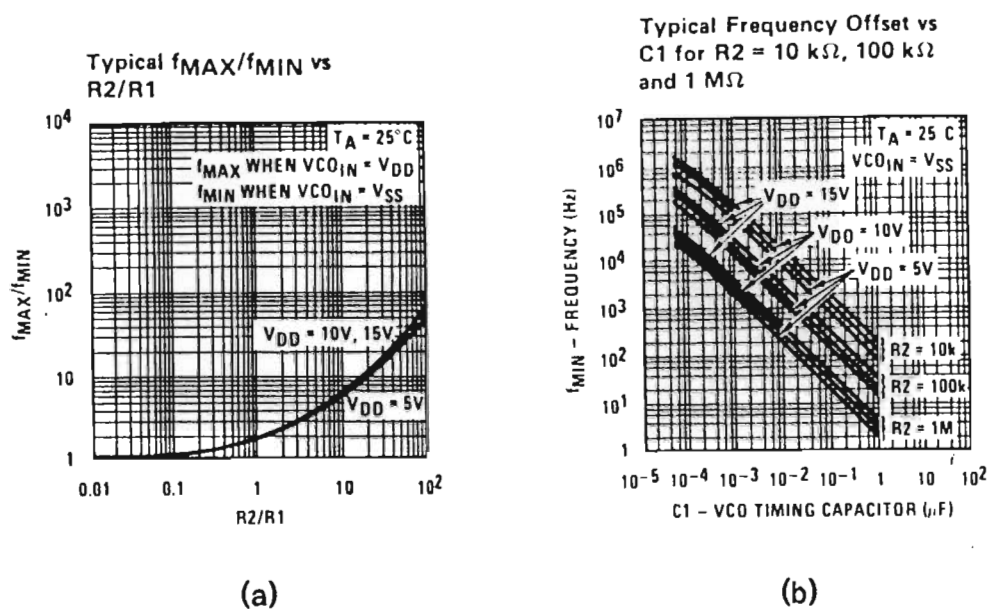


Fig. 4.3 CD4046 CMOS PLL Circuit Design Curves
 (a)VCO Frequency Ratio vs Timing Resistance Ratio
 (b)VCO Frequency Offset vs Timing Capacitor C_T

Table 4.2

Selected Component Values for PLL VCO Circuit Designs.
 Two frequency ratios of 2:1 and 3,5:1 were used.
 Frequency range includes $10 \times f_H = 156250\text{ Hz}$

$f_{MAX}:f_{MIN}$	2:1	Units
$R_4:R_3$	1:1	
$f_{MIN} = f_0$	110	kHz
f_{MAX}	220	kHz
$f_{MAX}:f_{MIN}$	3,5:1	Units
$R_4:R_3$	4:1	
$f_{MIN} = f_0$	80	kHz
f_{MAX}	280	kHz

The chosen frequency ratios of 2,0 and 3,5 corresponded, from Fig. 4.3 (a) data, with VCO timing resistor ratios of 4:1 and 1:1 for which two alternative designs were performed. The resistor value combinations were based on the E24 series of standard values. From Fig. 4.3 (b) the capacitance value required for C_T to give the desired value for f_{MIN} was found. Table 4.3 lists combinations of R_3 , R_4 and C_T values for both designs.

Table 4.3
Combinations of Values for R_3 , R_4 and C_T
for two PLL VCO circuit designs with specified resistor ratios

R_3 ($k\Omega$)	VCO TIMING COMPONENTS		$R_4:R_3$
	R_4 ($k\Omega$)	C_T (pF)	
12	12	1000	1:1
100	100	150	1:1
24	100	200	4,17:1
13	51	400	3,92:1
2,4	10	1100	4,17:1

The design with $R_3 = R_4 = 12\text{ k}\Omega$ and $C_T = 1\text{ nF}$, was used for the prototype. Reducing $C_T = 560\text{ pF}$ would also allow all CD4046E chips tested to meet the required frequency range specifications. As the CD4046E is a low gain chip, however, its use should be avoided.

4.2.3 Selection of Low Pass Filter Components

Filter components were chosen to give the desired values of ζ and ω_n with the lowest loop gain value of 4166,67. Table 4.4 shows the system natural resonant frequency ω_n and the damping factor ζ for the PLL using the filter component values indicated. Equations (C.35) and (C.36) in Appendix C were used for these calculations.

Table 4.4**Passive lag-lead filter designs and system parameters**

Noise bandwidth and acquisition time limits calculated

for $R_4:R_3 = 4:1$ and $R_4:R_3 = 1:1$

Filter	A	B	C	D	E	Units
R_1	10	10	10	10	10	$k\Omega$
R_2	10	3,3	2,2	0,91	0,1	$k\Omega$
C	33	100	100	100	100	nF
τ_2	330	330	220	91	10	μs
τ_3	660	1330	1220	1091	1010	μs
Minimum Loop Gain $K = 8333,33$						
ω_n	3553,3	2503,1	2613,5	2763,7	2872,4	rad/s
ζ	0,800	0,563	0,444	0,292	0,316	
BW_n	1491,1	1260,4	1315,9	1587,7	1590,1	Hz
τ_{acq}	7,015	$\Delta f = 76250 \text{ Hz for } R_4:R_3 = 4:1$				μs
		11,614	10,206	5,811	5,785	
τ_{acq}	2,581	$\Delta f = 46250 \text{ Hz for } R_4:R_3 = 1:1$				μs
		4,273	3,755	2,138	2,128	
Maximum Loop Gain $K = 34218,4$						
ω_n	7200,4	5072,3	5296,0	5600,4	5820,6	rad/s
ζ	1,293	0,911	0,660	0,337	0,114	
BW_n	5352,1	3006,4	2750,7	3022,0	6703,4	Hz
τ_{acq}	0,152	$\Delta f = 76250 \text{ Hz for } R_4:R_3 = 4:1$				μs
		0,856	1,117	0,843	0,677	
τ_{acq}	0,056	$\Delta f = 46250 \text{ Hz for } R_4:R_3 = 1:1$				μs
		0,315	0,411	0,310	0,028	

Filter A was used for the prototype timer. The lower calculated values are to be expected because the final resistance ratio was chosen at 1:1. This gives a lower loop gain and an expected acquisition time of approximately 56 *ms* from Table 4.4 which is acceptable.

4.2.4 Measured VCO Transient Performance

The practical performance of the PLL with some extreme values of ζ chosen from Table 4.4 is represented in Figs. 4.4 to 4.7. For the first three tests the non-retriggerable 50 μ s monostable IC16 was removed from the circuit to enable the PLL to lose lock at the end of each field. Overshoot and acquisition time can be determined from the waveforms shown, and these waveforms compare favourably to curves in Figure 4 given by Nash [52] with ζ values corresponding to those calculated for the filters tested. That PLL transient performance deteriorates very rapidly for values of damping factor $\zeta < 0.5$ is evident from the LPF output waveform (or VCO input waveform) in Figs. 4.4 through to 4.6.

For Fig. 4.7 the retriggerable 50 μ s monostable IC16 was reconnected to prevent loss of lock during the field sync region. The filter outputs were almost constant apart from some small spikes that correspond to the slight adjustments in timing made within the chip to correct small phase errors. All five filters performed in much the same way as those represented in Fig. 4.7, but the outputs filters D and E were more noisy than the first three and they are therefore not recommended for use in the sample timer.

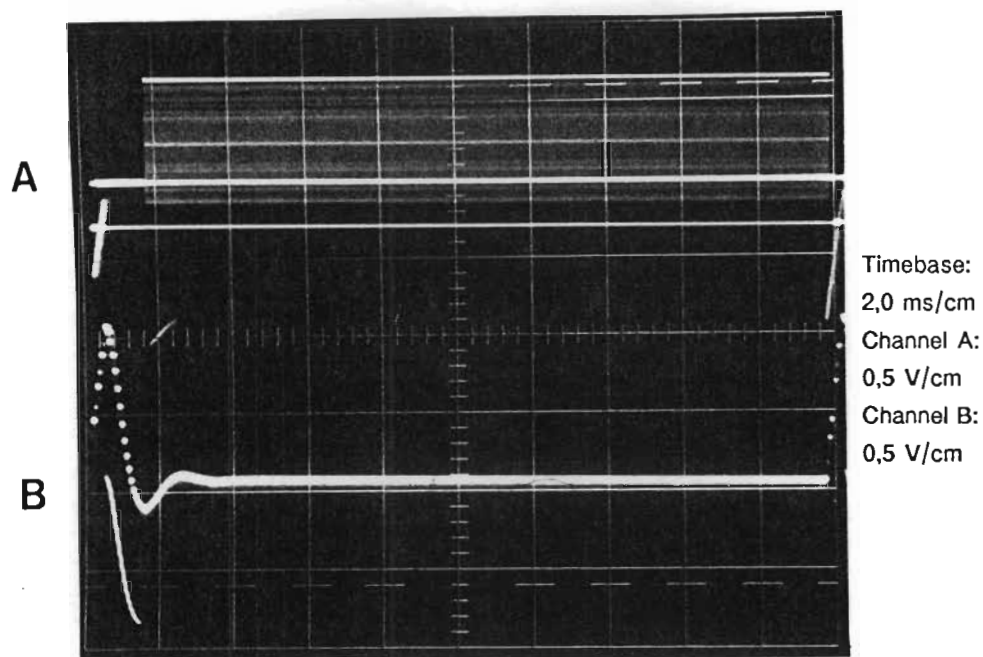


Fig. 4.4 Transient performance of low pass filter A
VCO Input voltage with IC16 disabled to allow loss of lock

Calculated $\zeta = 0,8$ Estimated $\zeta = 0,6$

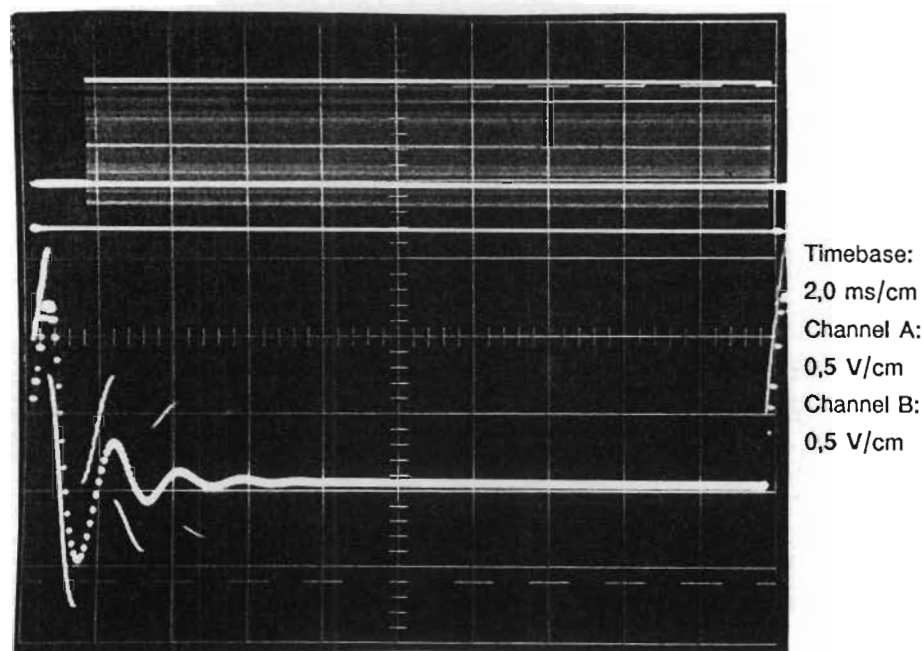


Fig. 4.5 Transient performance of low pass filter C
VCO Input voltage with IC16 disabled to allow loss of lock

Calculated $\zeta = 0,44$ Estimated $\zeta = 0,3$

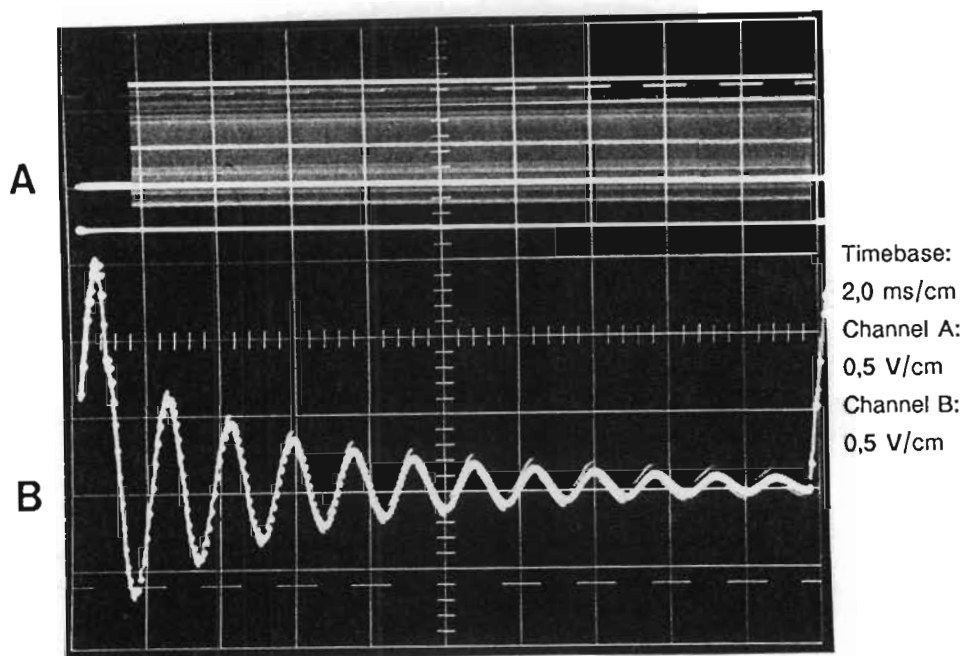


Fig. 4.6 Transient performance of low pass filter E
VCO Input voltage with IC16 disabled to allow loss of lock

Calculated $\zeta = 0,114$ Estimated $\zeta = 0,1$

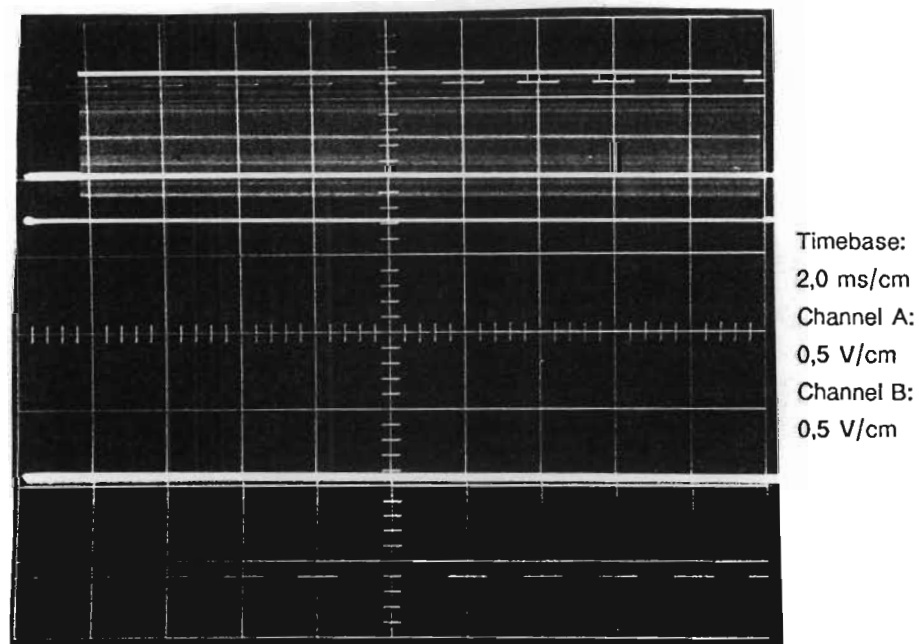
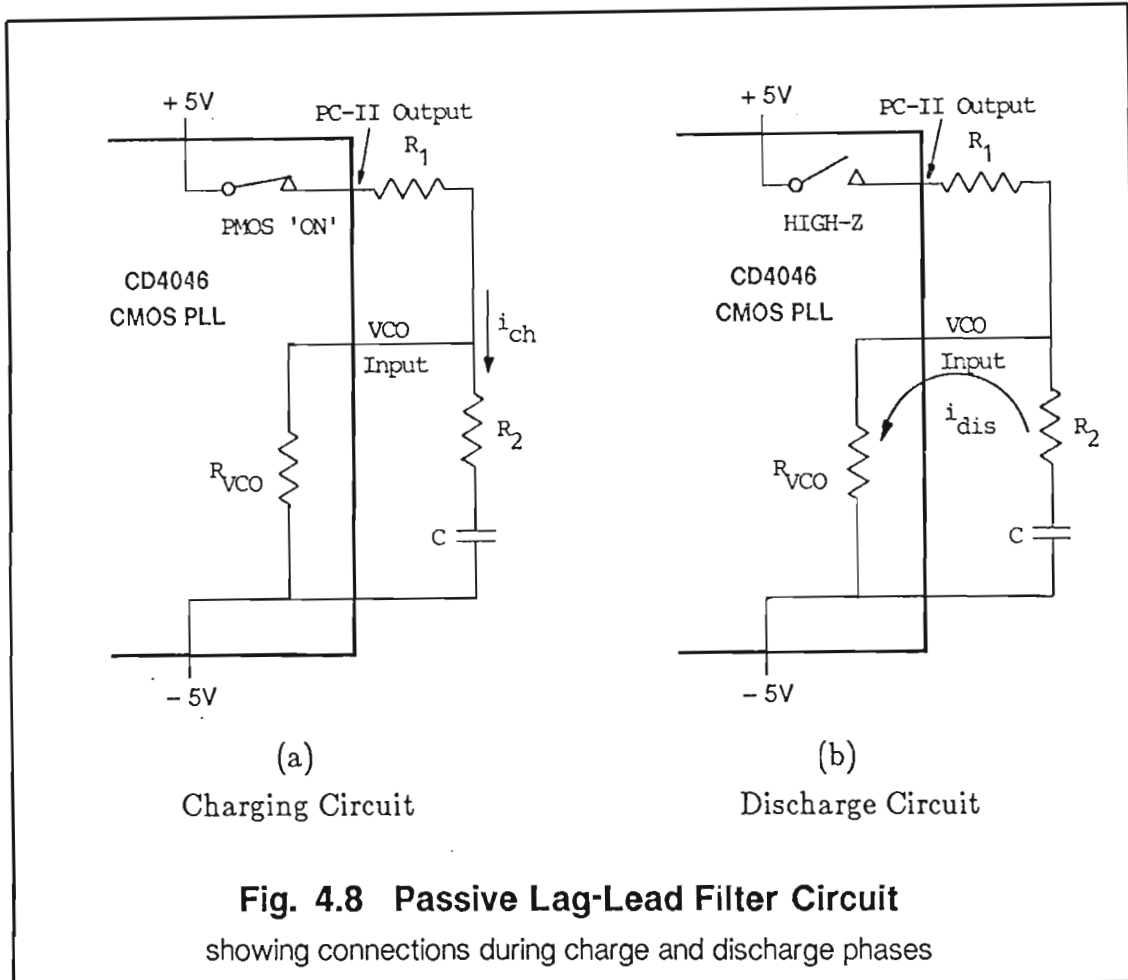


Fig. 4.7 Transient performance of low pass filter A, B and C
VCO Input voltage with IC16 reconnected to prevent loss of lock

4.2.5 PLL VCO Phase/Timing Error Estimates

Fig. 4.8 (a) shows the charging circuit for the filter capacitor C with PC-II in its active ON state, and Fig. 4.8 (b) indicates the discharge path for C . The VCO input resistance R_{VCO} is very large compared to R_2 and is thus disregarded in performing the charge calculations, and R_2 is ignored for the discharge calculations.



A detailed analysis of the behaviour of lag-lead low pass filter A is presented in order to estimate the change in the VCO input voltage, or filter output voltage, with the consequent frequency jitter and phase error during normal locked operation. With filter component values of

$$R_1 = 10 \text{ k}\Omega$$

$$R_2 = 10 \text{ k}\Omega$$

$$C = 33 \text{ nF}$$

the filter charging time constant is

$$\tau = 0,66 \text{ ms} \quad (4.15)$$

assuming zero internal resistance for the comparator output. This time constant is very long compared to the line repetition period of $64 \mu\text{s}$. The discharge characteristic of the filter capacitor C is therefore almost linear. Fig. 4.9 (a) shows the expected VCO input waveform as the capacitor C discharges during each line period. The initial transient voltage step has been ignored for simplicity. Fig. 4.9 (b) shows the squarewave VCO output signal, which is frequency modulated by the ramp input voltage in Fig. 4.9 (a).

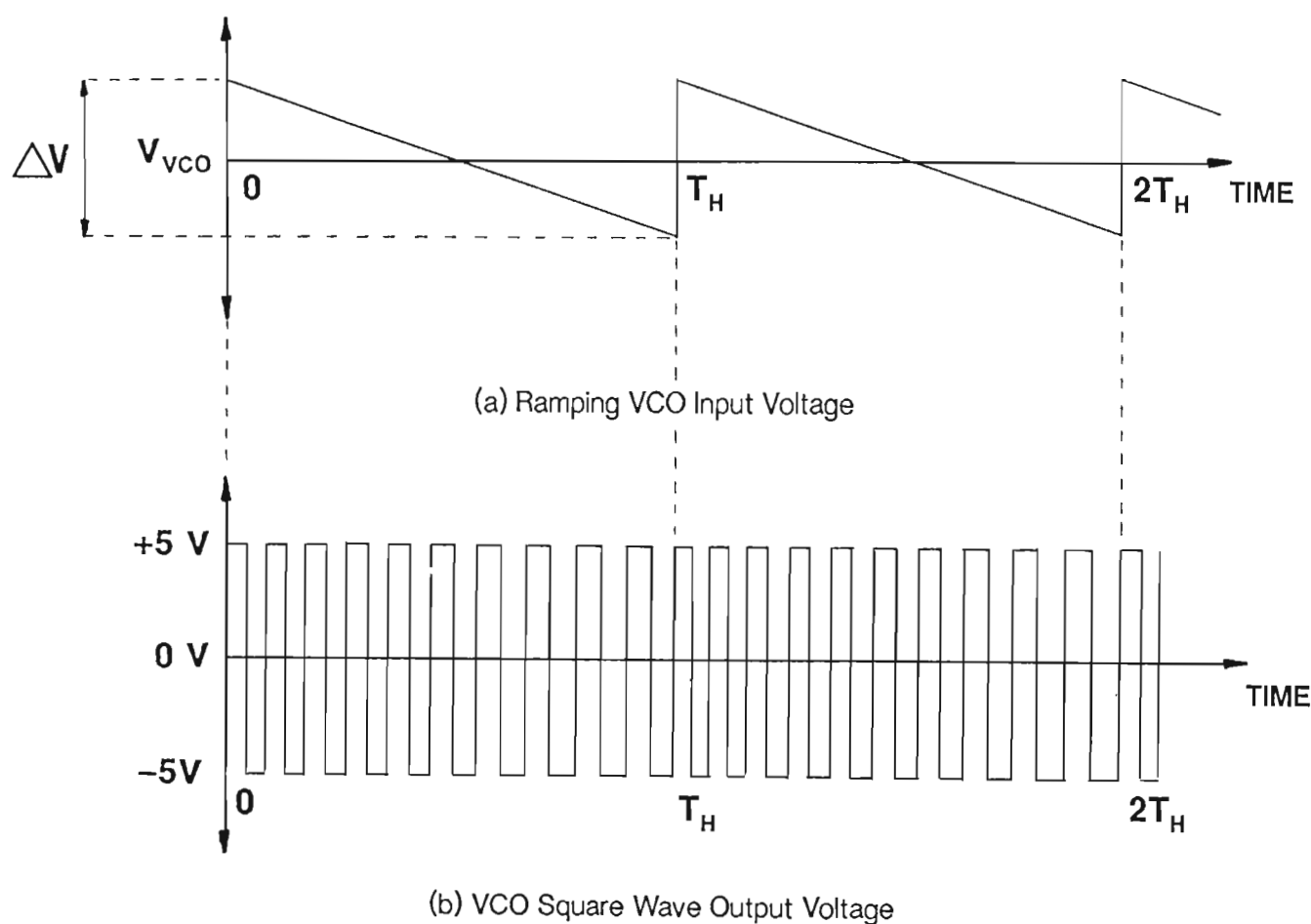


Fig. 4.9 VCO Input and Output Waveforms

With the VCO centre frequency at

$$\omega_o = 2\pi \times 156250 \text{ rad/s} \quad (4.16)$$

and

$$K_o = 70162 \text{ rad/Vs} \quad (4.17)$$

average from Table D.2 in Appendix D. A VCO input voltage of approximately 4 V is required [see Fig. D.3 in Appendix D] to produce the desired ω_o if the CD4046E chip is excluded. During the discharge period t_{dis} given by

$$\begin{aligned} t_{dis} &= T_H \\ &= 64 \mu s \end{aligned} \quad (4.18)$$

Discharge current i_{dis} is given by

$$i_{dis} = \frac{V_C}{R_{vco}} \quad (4.19)$$

where R_{vco} is the manufacturer's specified VCO input resistance of 100 M Ω . During normal operation, humidity and other deposits on the printed circuit board surface will reduce this figure to a lower value, possibly closer to 10 M Ω . Hence a high estimate for i_{dis} with V_C at 4 V is:

$$i_{dis} = 400 \text{ nA} \quad (4.20)$$

The change in charge ΔQ on the capacitor C is

$$\begin{aligned} \Delta Q &= C \Delta V \\ &= i_{dis} T_H \\ &= 25,6 \text{ pC} \end{aligned} \quad (4.21)$$

giving

$$\Delta V = 775,8 \mu V \quad (4.22)$$

Lost charge must be replaced at the end of each video input line. If the supply voltage V is 10 V and the initial voltage V_C on capacitor C is 4 V a charging current i_{ch} given by

$$\begin{aligned} i_{ch} &= \frac{V - V_C}{R_1 + R_2} \\ &= 0,300 \text{ mA} \end{aligned} \quad (4.23)$$

will flow into capacitor C via R_1 and R_2 in series. It will take a time of t_{ch} seconds to replace the charge lost from C during each line period, where

$$\begin{aligned} t_{ch} &= \frac{C \Delta V}{i_{ch}} \\ &= 85,33 \text{ ns} \end{aligned} \quad (4.24)$$

which is 0,133% of one line period T_H . A high estimate for the total change in VCO frequency during the linear ramping portion of the VCO input signal, which is most of the line period, is:

$$\begin{aligned} \Delta \omega &= \Delta V K_o \\ &= 54,43 \text{ rad/s} \end{aligned}$$

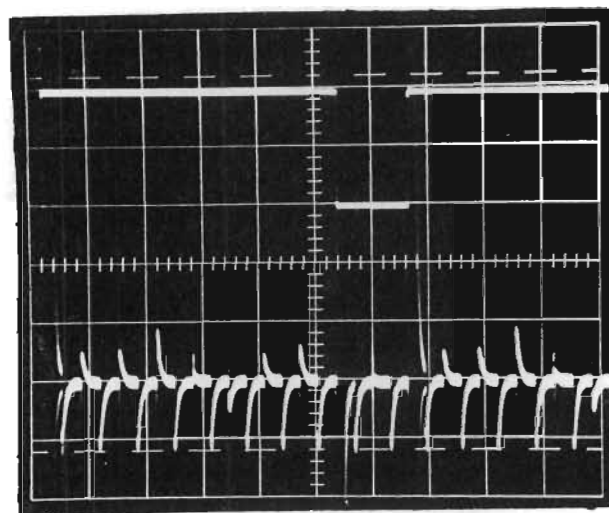
or

$$\Delta f = 8,663 \text{ Hz} \quad (4.25)$$

Fig. 4.10 (a) overleaf shows a typical VCO input waveform measured with a filter capacitance C of 100 nF. Noise spikes coinciding with the VCO output waveform transitions are visible, superimposed on the VCO input ramp. Much of this noise is due to radiation from the divide-by-ten counter chip. When the two traces are compared, and noting that the graticule is not quite aligned with the horizontal trace, there is little discernible slope in VCO input voltage on the oscilloscope display outside of the line sync region. Hence R_{VCO} is very large indeed. With C reduced to 10 nF and reduced sweep speed in Fig. 4.10 (b) large transients are seen to occur at each transition of the input line sync pulse. These large spikes at the end of each line adjust the charge on the loop filter capacitor.

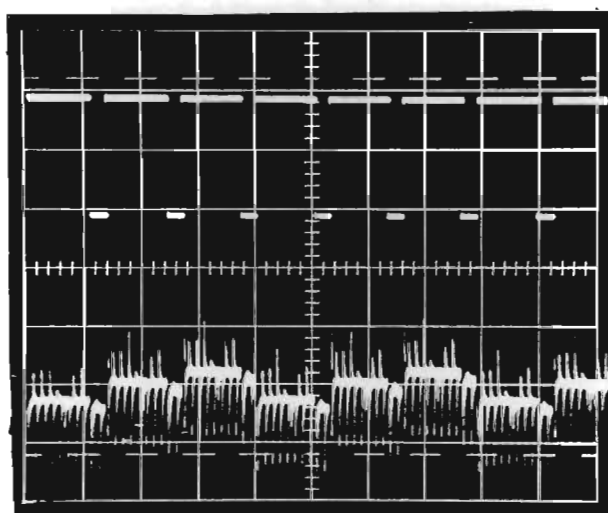
Although ramping of the VCO input signal must be present, it represents a component of very small amplitude which is not easily measured. Fig. 4.9 (a) shows the theoretical VCO input waveform, ignoring the initial pulses at the commencement of each line due to charging current flowing through R_2 . The instantaneous VCO frequency can thus be expressed as the linear time function

$$\omega_{vco} = \left[\omega_o + \frac{1}{2} \Delta \omega - (\Delta \omega / T_H) t \right]_{0 \leq t < T_H} \quad (4.26)$$



Timebase:
 $10 \mu\text{s/cm}$
 Channel A:
 5 V/cm
 Channel B:
 2 mV/cm

(a) Filter capacitor C with a value of 100 nF
 Very little ramping of the VCO voltage is evident.



Timebase:
 $50 \mu\text{s/cm}$
 Channel A:
 5 V/cm
 Channel B:
 2 mV/cm

(b) Filter capacitor C with a value of 10 nF
 Noise at $\frac{1}{3} \omega_H$ is seen with the lower C value.
 The origin of this noise is not clear.

Fig. 4.10 Measured VCO Input Waveforms

Noise spikes coincide with VCO square wave edges as explained in the text.

For the time interval $0 < t < T_H$ the instantaneous VCO phase is given by:

$$\begin{aligned}\theta_{vco} &= \int_0^{T_H} \omega dt \\ &= \omega_o t + \frac{1}{2} \Delta \omega t - \frac{1}{2} (\Delta \omega / T_H) t^2 + \text{Con}\end{aligned}\quad (4.27)$$

The phase error between the instantaneous VCO signal and the desired, or reference frequency signal ω_o at ten times the line frequency or 156250 Hz, is given by:

$$\begin{aligned}\theta_e &= \theta_{vco} - \theta_o \\ &= \frac{1}{2} \Delta \omega t - \frac{1}{2} (\Delta \omega / T_H) t^2 + \text{Con}\end{aligned}\quad (4.28)$$

Due to PLL action, the phase error between ω_{vco} and ω_o is zero at time $t=0$, ignoring the time delay through the $\div N$ counter. Hence the integration constant

$$\text{Con} = 0 \quad (4.29)$$

and

$$\theta_{vco} = \omega_o t + \frac{1}{2} \Delta \omega t - \frac{1}{2} (\Delta \omega / T_H) t^2 \quad (4.30)$$

Clearly:

$$\theta_e = 0 \quad \text{for } t = 0 \quad (4.31)$$

Maximum phase error $\theta_{e \max}$ is determined by differentiating equation (4.28) and equating the result to zero. This gives the time at which maximum error occurs as

$$t_{\max} = \frac{1}{2} T_H \quad (4.32)$$

where

$$T_H = 64 \mu s \quad (4.33)$$

This is because $\omega_{vco} > \omega_o$ at the commencement of each line, so the phase θ_{vco} advances initially. As ω_{vco} decreases the rate at which θ_{vco} advances is reduced, reaching zero when

$$\omega_{vco} = \omega_o \quad (4.34)$$

This occurs at the line centre at time

$$t = 1/2 T_H \quad (4.35)$$

Thereafter θ_{vco} is retarded relative to θ_o and co-incidence occurs at time

$$t = T_H \quad (4.36)$$

Substitution of equation (4.32) into (4.38) gives:

$$\theta_{e\max} = 1/8 \Delta\omega T_H \quad (4.37)$$

With

$$\Delta\omega = 54,43 \text{ rad/s}$$

we have

$$\begin{aligned} \theta_{e\max} &= 4,3544 \times 10^{-4} \text{ rad} \\ &= 0,02495^\circ \end{aligned} \quad (4.38)$$

This maximum phase error corresponds to the back end of the CYAN colour bar, where a timing tolerance of $\pm 500 \text{ ns}$ is acceptable. The maximum phase error calculated above corresponds to a maximum sample timing error t_{\max} which is calculated as follows. At ω_{vco} a phase of $2\pi \text{ rad}$ corresponds to a period of $6,4 \mu\text{s}$. Thus the maximum timing error is

$$\begin{aligned} t_{\max} &= \frac{\theta_{e\max}}{2\pi} \times 6,4 \mu\text{s} \\ &= 0,4435 \text{ ns} \end{aligned} \quad (4.39)$$

Hence no timing problems are expected. With R_{vco} at $100 \text{ M}\Omega$ these errors will be further reduced.

4.2.6 Frequency Spectrum of the Ramp Modulated VCO Output Signal

All sampling timing pulses produced by the PLL will be subject to timing error or phase jitter because of the ramping of the VCO input signal illustrated previously in Fig. 4.9.

The spectrum of the unmodulated VCO output squarewave has only the odd harmonics of ω_{vco} where

$$\omega_{\text{VCO}} = \frac{2\pi}{T_{\text{VCO}}} \quad (4.40)$$

and

$$\begin{aligned} T_{\text{VCO}} &= 6,4 \mu s \\ &= 0,1 T_H \end{aligned} \quad (4.41)$$

Due to closed loop action, the VCO squarewave is always phase-coincident with the input video line sync pulses. Thus the frequency modulated VCO wave is a periodic waveform with a repetition period of T_H or $64 \mu s$. A Fourier series representation of the VCO output is therefore possible, and an evaluation of the coefficients was attempted using the direct approach described by Lathi [26] as follows.

The linear ramp input voltage can be expressed in terms of "t" as the function:

$$v(t) = V_{\text{VCO}} + \frac{\Delta V}{2} - \frac{2\Delta V}{T_H} t \quad (4.42)$$

Hence the instantaneous frequency of the VCO output is

$$\omega(t) = K_{\text{VCO}} \left[V_{\text{VCO}} + \frac{\Delta V}{2} - \frac{2\Delta V}{T_H} t \right] \quad (4.43)$$

The instantaneous phase of the VCO output is therefore

$$\theta(t) = \int \omega(t) dt \quad (4.44)$$

$$\begin{aligned} &= K_{\text{VCO}} V_{\text{VCO}} t + \frac{1}{2} K_{\text{VCO}} \Delta V t - (K_{\text{VCO}} \Delta V / T_H) t^2 \\ &= \omega_{\text{VCO}} t - \psi(t) \end{aligned} \quad (4.45)$$

where

$$\begin{aligned} \psi(t) &= \frac{1}{2} \Delta \omega t - (\Delta \omega / T_H) t^2 \\ &\text{for } 0 \leq t \leq T_H \end{aligned} \quad (4.46)$$

The phase function $\psi(t)$ is periodic, so that

$$\psi(t) = \psi(t \pm nT_H) \quad (4.47)$$

and the frequency modulated signal may therefore be represented by

$$\phi_{FM}(t) = A \exp\{j\psi(t)\} \exp\{j\omega_{VCO}(t)\} \quad (4.48)$$

Phase function $\psi(t)$ is also periodic, and can be expressed as the Fourier series

$$\exp\{j\psi(t)\} = \sum_{n=-\infty}^{\infty} \alpha_n \exp\{jn\omega_H t\} \quad (4.49)$$

and

$$\begin{aligned} \alpha_n &= \frac{1}{T_H} \int_0^{T_H} \exp\{j\psi(t)\} \exp\{-jn\omega_H t\} dt \\ &= \frac{1}{T_H} \int_0^{T_H} \exp\{1/2j\Delta\omega t - (\Delta\omega/T_H)t^2\} dt \end{aligned} \quad (4.50)$$

This integral is of the form

$$\int_0^{T_H} \exp[\alpha t] \exp[-\beta t^2] dt \quad (4.51)$$

which becomes an infinite series in powers of "t" and cannot be evaluated in closed form. Burdic [26] has considered this problem in relation to radar systems and states that integrals of the form in equation (4.51) are known as Fresnel Integrals for which tables of solutions are available. Because of their complexity and non-availability there was little advantage in pursuing the theory further, so the spectrum of the VCO fundamental frequency at $10 \times f_H$ (or 156250 Hz) was measured and is presented for interest in Fig. 4.11 that follows. Complex sidebands caused by the ramping of the VCO input voltage, and other jitter components due to superimposed noise, are clearly visible.

One such important source of phase jitter not considered thus far is the external video waveform generator. If the line frequency is produced via a PLL controlled frequency synthesizer, jitter is unavoidable, and care must be taken to ensure that the generator specifications are compatible with the timer stability requirements. The colour bar generator used for this test may have contributed to the jitter, and therefore to the sidebands in Fig. 4.11.

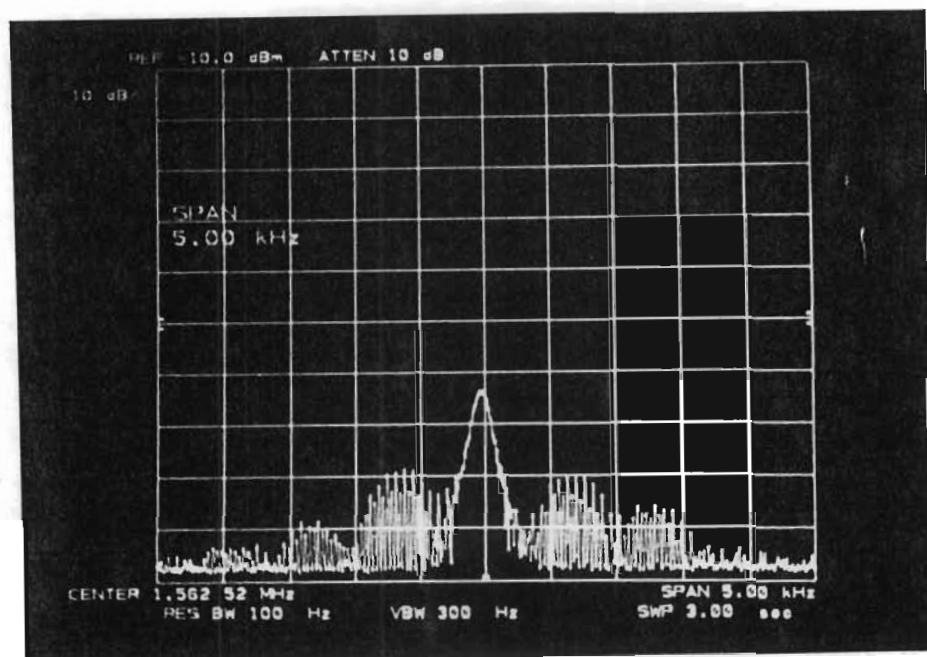


Fig. 4.11 Measured VCO Frequency Spectrum
Showing the sidebands produced by ramping
and other sources of phase jitter such as noise.

4.3 PLL STATUS INDICATION CIRCUITS

4.3.1 Introduction

The LM556 dual timer chip was chosen for the status monostables because of its capability of either sourcing or sinking a high output current of up to 200 mA. Although the CD4046 chip has a “phase pulses” output which can be used to indicate whether the loop is locked or not, the output current capability is too low for the 20 mA LED current requirement. By contrast, an LED presents a very light load to the LM556.

A detailed circuit schematic diagram of the phase lock loop based sample timing circuit is shown overleaf in Fig. 4.12. All circuitry associated with the PLL timer is illustrated. This comprises the line and field sync separators, PLL status circuits, alternate line inhibit flip flop, line sync driver for external histogram display synchronisation, and sample pulse width and delay pulse monostables and sample pulse gating. The following circuit descriptions refer to Fig. 4.12.

4.3.2 PLL Status: Video Present

The negative going edge of the 50 μ s pulses from pin 10 of IC16 are used to trigger one of the monostables at pin 8. These pulses occur regularly every 64 μ s. The period of the monostable was also chosen as 50 μ s and the output signal from pin 9 drives a green VIDEO PRESENT LED on the front panel. Should the video signal be removed for any reason no line sync pulses are produced. The monostable output from pin 9 remains low preventing the LED from turning on. Otherwise the LED is on for 50 μ s out of every 64 μ s and is thus almost at full brightness.

4.3.3 PLL Status: Locked or Unlocked

The other monostable in IC04 is triggered at pin 6 by phase pulses from pin 1 of the PLL IC03. If the PLL is locked and operating correctly these pulses are of small amplitude and very narrow, and cannot trigger the monostable because of integrating network R7 and C78. However, if the PLL cannot lock these pulses become broader and larger in amplitude, and are thus capable of triggering the monostable which has a period of 100 ms set by R12 and C10. The output from pin 5 of IC04 then turns on a red LED marked TIMING ERROR on the front panel.

4.3.4 LM556 Dual Monostable Status Timer

The timing capacitor C is normally discharged, and commences charging only when the timer chip has been triggered. The charging of C is described by the equation:

$$\begin{aligned} v_C &= V_{DD}(1 - e^{-t/RC}) \\ &= \frac{2}{3} V_{DD} \end{aligned} \quad (4.52)$$

When this two thirds supply potential is reached the internal comparator triggers the control flip flop to discharge C. The total charging time τ_{ch} is thus given by:

$$\frac{2}{3} = 1 - \exp(-\tau_{ch}/RC)$$

Hence

$$\tau_{ch} = 1.0986 RC \quad (4.53)$$

Table 4.6 summarises the designs for the two timer circuits.

Table 4.6
Component Values for Status Indicator Timer Circuits

Required Pulse Width	Timing		Calculated Pulse Width
	Resistor	Capacitor	
50 <i>ms</i>	47 <i>kΩ</i>	1,0 <i>nF</i>	51,7 <i>ms</i>
100 <i>ms</i>	56 <i>kΩ</i>	1,5 <i>μF</i>	92,4 <i>ms</i>

4.3.5 Synchronisation of Histogram Display

A negative going 5,6 μs wide synchronising pulse of approximately 4 V peak was required for the 75 Ω sync input to the OKF waveform monitor used to display the hystogram. These pulses were to be available from a BNC socket on the front panel of the instrument. It was initially decided to design an amplifier with a 75 Ω output impedance to avoid reflections, but this meant that an 8 V pulse amplitude at 53,3 mA would have to be generated. A LM555 timer chip (IC15) was found to provide a simple pulse “amplifier” when used as a power flip flop.

IC15 is connected to +5 V and -5 V supplies. The output from pin 3 is connected to the front panel via a 75 Ω resistor to effect a 75 Ω source resistance. The internal flip-flop of IC15 is reset at pin 4 by the falling edge of the 5,6 μs pulse produced by IC02 at pin 7 (NOT QA). This causes the output at pin 3 of IC15 to go low to -5 V.

5,6 μs later the LM555 timer is set at pin 2, via one gate delay in IC11, from the falling edge of the QA output of IC02 at pin 6. The LM555 is thus used as an R-S flip flop with high output drive capabilities.

4.4 TIMER CIRCUIT STABILITY

4.4.1 Introduction

A complete circuit schematic diagram of the prototype phase lock loop pulse timing generator was shown in Fig. 4.12. Instability of the timer circuit can arise from two main sources.

Firstly, there is the problem of spurious triggering due to noise pulses present at the phase lock loop (PLL) input. These pulses may be due to a common earth conductor carrying large current pulses. Radiation from a fast switch, magnetic induction, and capacitive coupling in close proximity high impedance circuits may also cause noise induction. Noise occasionally caused antiphase locking of the CD4046 PLL in the breadboarded prototype, despite the use of Phase Comparator II. Electromagnetic compatibility of adjacent circuits and printed circuit boards was thus a primary consideration in the mechanical design of the instrument [95, 103 and 104]. By careful screening and routing of critical cables, using logic devices with adequate but not excessive switching speed, and low pass filtering of the external PLL input, the unit was made to operate successfully.

Secondly, the positions of the sampling pulses within the colour bars may alter significantly during operation due to temperature changes and component ageing. No such problem arises due to the CD4046 PLL chip itself when Phase Comparator II is used. This comparator is a digital, memory-based LOGIC type which maintains zero phase shift between the two comparator input signals under "lock" conditions.

Critical circuits in the timer are the sync pulse separator, the $5,6 \mu s$ monostable for adjusting pulse position, and the $1,8 \mu s$ monostable which determines the sampling pulse width. Each circuit will be considered separately.

4.4.2 Sync Separator Timing Stability

The line sync pulse rise time is specified in Fig. G.5 of Appendix G as:

$$\begin{aligned}\tau_r &= 0,2 \pm 0,1 \mu s \\ &= 200 ns \pm 100 ns\end{aligned}\quad (4.54)$$

The negative-going line sync pulse signal amplitude is 300 mV peak. Rise time is defined as the time taken for the pulse potential to rise from 10% to 90% of the final level, or 0,24 V, and in the limits represents a voltage rate-of-rise range from 0,8 V/ μs to 2,4 V/ μs .

An LM311 comparator was employed to separate the line sync pulses from the video input signal. Tobey et al [107] have shown that the drift in offset voltage for a bipolar differential input stage of an operational amplifier type comparator is given by:

$$\frac{\partial V_{os}}{\partial T} = \frac{V_{os}}{\Delta T} \quad (4.55)$$

which corresponds to a drift of 3,3 $\mu V/^{\circ}C$ per millivolt of offset at room temperature. With a worst case specification of

$$V_{os} = 10 mV \quad (4.56)$$

for the LM311, thermal drift will be a maximum of 33 $\mu V/^{\circ}C$ or 1,65 mV for a temperature increase from 0 $^{\circ}C$ to 50 $^{\circ}C$. This will cause a change in sync pulse output timing of $1,65/240 \times 300 ns$ in the worst case, or 2,063 ns which is negligible.

A germanium diode clamp was used as a DC restorer at the sync separator input. This prevents the comparator input potential from going more negative than about -150 mV (measured) at room temperature.

The variation in the clamping voltage with temperature is -2 mV/ $^{\circ}C$ so that, over the temperature range from 0 $^{\circ}C$ to 50 $^{\circ}C$, the clamping potential will vary by 100 mV from -200 mV to -100 mV respectively. This represents a worst case change in timing of some $100/240 \times 300 ns$ or 125 ns. The timing pulse will thus advance by an amount of $\Delta T = 0,125 \mu s$ as the circuit cools from 50 $^{\circ}C$ to 0 $^{\circ}C$.

4.4.3 Design Philosophy for Temperature Stable CMOS Monostable Pulse Generators

If the PLL is synchronised to either the leading or trailing edge of the line sync pulse on the input video waveform, sampling cannot coincide simultaneously with the colour bars and the colour burst pulse. When the PLL input pulses are delayed by approximately $5,6 \mu\text{s}$ the leading edges of the VCO pulses, which are at $10 f_H$, can be positioned correctly for all the desired sampling positions.

Clearly the required delay pulse width may vary from one TV System to another. Adjustment may thus be necessary between systems and also to accommodate tolerances within one TV System. Once set, the width of this delay pulse must not alter appreciably with temperature variations or component ageing.

A detailed general analysis of the temperature stability of monostable timer circuits is presented in Appendix E. The objective of this analysis is to develop a simple method for designing temperature stable pulse timer circuits. These may have more than one resistor and capacitor with differing temperature coefficients in the external time constant circuit, and the design technique presented in Appendix E is simple to apply, and may be original.

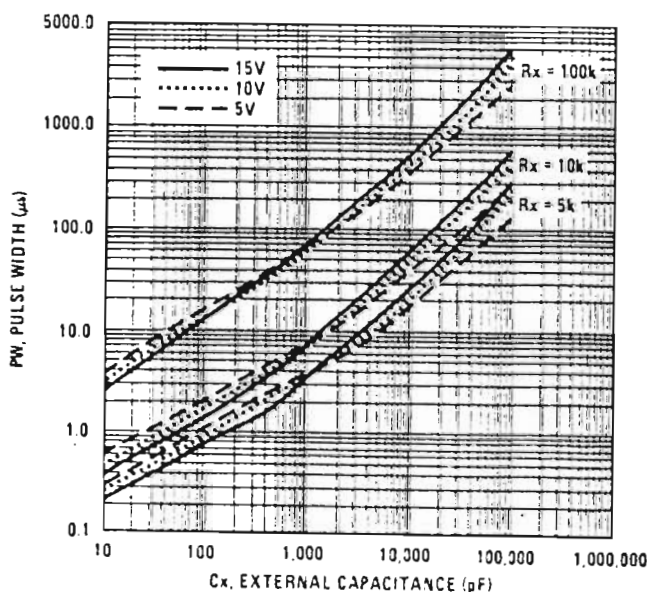
Numerical characterisation of the manufacturer's published "pulse width vs temperature" curves was achieved through the application of a least squares curve fitting technique [92]. A programme written in BASIC performs this operation, and outputs the coefficients of the fitted polynomial representing the pulse width temperature coefficients. Values of resistance and capacitance are assumed to vary linearly with temperature, and the effective value of temperature coefficient of resistance α_r , or capacitance α_c , for series or parallel combinations of components are derived. Since a wide range of temperature coefficients is available in small ceramic capacitors, the design procedure is aimed at finding the value of α_c that would achieve temperature compensation of the timing circuit. Practical values available for C_1 and C_2 are limited to the E12 series within the range manufactured with each particular T.C. value [89 to 91]. A careful choice of resistance values provides considerable scope for compensation.

Timer circuits designed for the I.M. analyser can employ either the CMOS CD4528 or CD4538 monostable timer chips [87, 88]. The CD4538 is the preferred device because of the following improved performance characteristics over the CD45285:

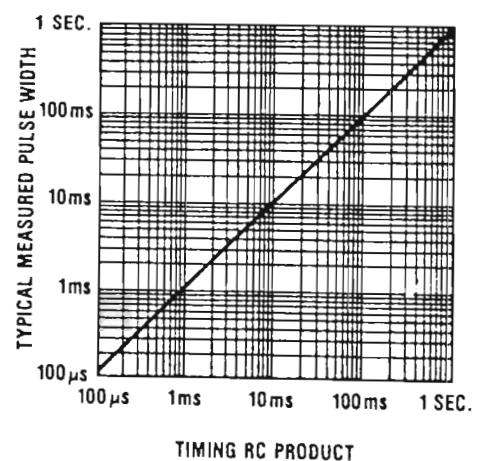
- 1 $\pm 1\%$ pulse width variation typical between chips.
- 2 High output drive capability (TTL compatible)
- 3 Pulse width $PW = K_{pw} \tau = RC$ (ie. $K_{pw} = 1$)
- 4 Wide pulse width range from $1 \mu s$ to ∞ [NEC chips only]

The CD4538 monostable can have problems when used to produce narrow pulses of the order of microseconds. Chips from some manufacturers, notably Motorola, have large effective internal timing capacitances making circuit design difficult. These internal capacitances were measured by operating selected CD4538 timer chips with an external $18 k\Omega$ timing resistor but no external timing capacitor. Pulses widths of 0.7 to $2.3 \mu s$ were produced, corresponding to effective internal capacitances of 38 to $127 pF$. This reveals the lack of true interchangeability of devices from different manufacturers in this application.

Figs. 5 and 14 published in the National CMOS Data Book [88] for the CD4528 and CD4538 monostable chips respectively show the relationship between pulse width and R-C time constant. These curves are reproduced in Figs. 4.13 (a) and (b) respectively.



(a) Data for a CMOS CD4528 monostable



(b) Data for a CMOS CD4538 monostable

Fig. 4.13 Monostable Pulse Width Design Data

External Time Constant vs Output Pulse Width

4.4.4 Monostable Pulse Circuit Designs

4.4.4.1 Choice of Timing Resistors

Temperature compensation of the monostable circuits was required over the temperature range of 0°C to 50°C. A timing circuit configuration was chosen, consisting of two parallel resistors (because failure of the trimpot will not leave the circuit open) and two parallel capacitors. Considering the resistors first [90, 91], choose

$$R_1 = 18 \text{ k}\Omega \text{ metal film}$$

$$\alpha_{r1} = +220 \text{ ppm/K}$$

and

$$R_2 = 50 \text{ k}\Omega \text{ cermet trimpot}$$

$$\alpha_{r2} = +150 \text{ ppm/K}$$

At a temperature of 0°C:

Set R_2 to 22,500 $\text{k}\Omega$ (near centre), giving a parallel equivalent resistance at 0°C of:

$$R = 10 \text{ k}\Omega$$

At a temperature of 50°C:

$$R_1 + \Delta R_1 = 18,198 \text{ k}\Omega$$

$$R_2 + \Delta R_2 = 22,68875 \text{ k}\Omega$$

whence

$$R + \Delta R = 10,09444 \text{ k}\Omega$$

The effective temperature coefficient for the resistor combination is:

$$\alpha_r = \frac{\Delta R}{R \Delta T}$$

$$= 188,83 \text{ ppm/K}$$

4.4.4.2 5,6 μs Delay Pulse Monostable Designs

From the published data reproduced in Fig. 4.13 (a) for a CMOS CD4528 the slope K_{pw} for a 10 $k\Omega$ timing resistor is estimated at:

$$K_{pw} = 0,7$$

Hence

$$\begin{aligned} C &= 800 \text{ pF} \\ &= C_1 + C_2 \end{aligned}$$

Equation (E.13) from Appendix E gives:

$$\alpha_c = -192,665 \text{ ppm/K}$$

Two ceramic capacitors are chosen to make up the required timing capacitance of 800 pF having T.C.s that must of necessity encompass the desired α_c of $-192,665 \text{ ppm/K}$. Again suitable T.C.s are -150 ppm/K and -220 ppm/K for C_1 and C_2 respectively. Rearranging equation (E.21) we have:

$$C_1 + C_2 = \frac{-0,0015C_1 - 0,0022C_2}{-0,000192665}$$

Solving:

$$\begin{aligned} C_1 &= 312,4 \text{ pF} & (\text{T.C.} = -150 \text{ ppm/K}) \\ C_2 &= 487,6 \text{ pF} & (\text{T.C.} = -220 \text{ ppm/K}) \end{aligned}$$

A similar procedure for a CMOS CD4538 using the published data reproduced in Fig. 4.13 (b) gives the slope K_{pw} as:

$$\begin{aligned} K_{pw} &= 0,7 \\ C &= 560 \text{ pF} \\ &= C_1 + C_2 \end{aligned}$$

Equation (E.13) yields:

$$\alpha_c = -173,157 \text{ ppm/K}$$

Suitable T.C.s in this case are -150 ppm/K and -220 ppm/K for C_1 and C_2 respectively. Hence equation (E.21) becomes:

$$C_1 + C_2 = \frac{-0,00015C_1 - 0,00022C_2}{-0,000173157}$$

Solving:

$$\begin{aligned} C_1 &= 374,7 \text{ pF} & (\alpha_{c1} = -150 \text{ ppm/K}) \\ C_2 &= 185,3 \text{ pF} & (\alpha_{c2} = -220 \text{ ppm/K}) \end{aligned}$$

4.4.4.3 1,8 μs Sample Pulse Monostable Designs

A single metal film resistor of $18\text{ k}\Omega$ and α_r of 150 ppm/K was chosen for this fixed width pulse timer. A 2% tolerance would be acceptable as the stability is more important than the absolute timing accuracy.

Fig. 4.13 (a) for the CMOS CD4528 chip gives the slope K_{pw} for a $18\text{ k}\Omega$ timing resistor as:

$$\begin{aligned} K_{pw} &= 1,6 \\ C &= 62,5\text{ pF} \\ &= C_1 + C_2 \\ \alpha_r &= 150\text{ ppm/K} \end{aligned}$$

Equation (E.13) yields:

$$\alpha_c = -154,49\text{ ppm/K}$$

Suitable T.C.s in this case are -75 ppm/K and -220 ppm/K for C_1 and C_2 respectively. Hence:

$$\begin{aligned} C_1 &= 58,5\text{ pF} \quad (\alpha_{c1} = -75\text{ ppm/K}) \\ C_2 &= 4,0\text{ pF} \quad (\alpha_{c2} = -220\text{ ppm/K}) \end{aligned}$$

For the CMOS CD4538 slope K_{pw} for a $18\text{ k}\Omega$ timing resistor is estimated at:

$$\begin{aligned} K_{pw} &= 1,0 \\ C &= 100\text{ pF} \\ \alpha_r &= 150\text{ ppm/K} \end{aligned}$$

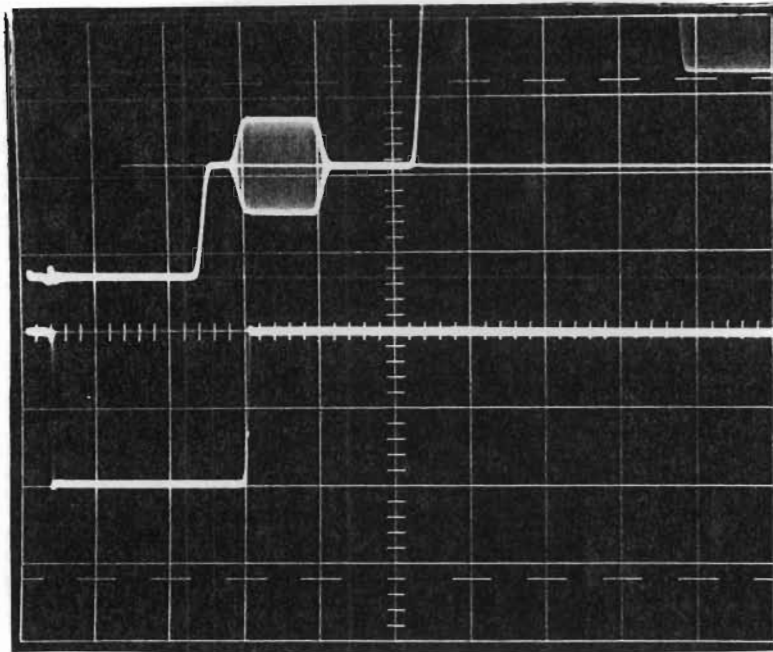
Equation (E.13) yields:

$$\alpha_c = -134,95\text{ ppm/K}$$

Suitable T.C.s in this case are -75 ppm and -150 ppm for C_1 and C_2 respectively. Hence:

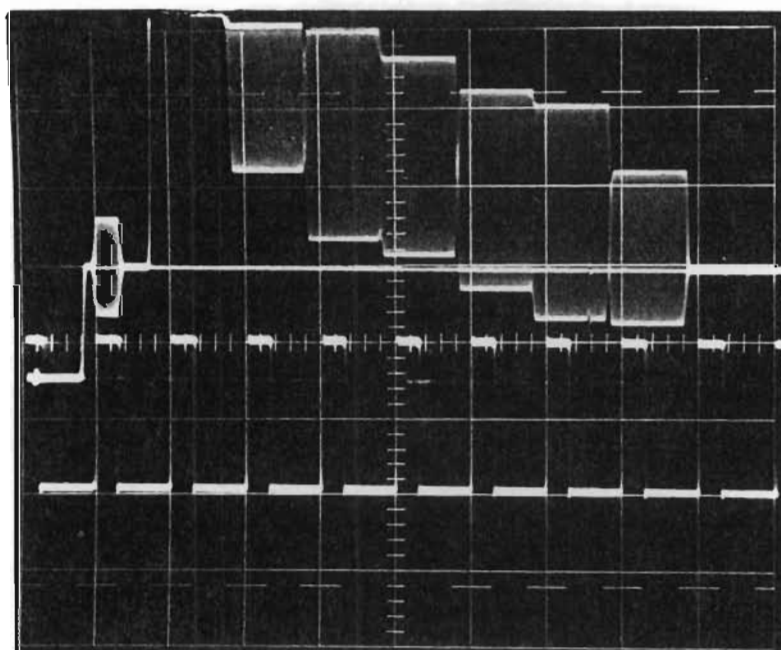
$$\begin{aligned} C_1 &= 20,0\text{ pF} \quad (\alpha_{c1} = -75\text{ ppm/K}) \\ C_2 &= 80,0\text{ pF} \quad (\alpha_{c2} = -150\text{ ppm/K}) \end{aligned}$$

The positions of the $5,6\text{ }\mu s$ delay pulse and $1,8\text{ }\mu s$ sampling pulse relative to a colour bar video signal are illustrated in the waveforms in Figs. 4.14 and 4.15 respectively.



Timebase:
2,0 $\mu\text{s}/\text{cm}$
Channel A:
0,2 V/cm
Channel B:
5,0 V/cm

Fig. 4.14 The 5,6 μs Monostable Delay Pulse
Trailing edge position relative to the colour burst
Channel A displays the colour bar video input waveform



Timebase:
2,0 $\mu\text{s}/\text{cm}$
Channel A:
0,2 V/cm
Channel B:
5,0 V/cm

Fig. 4.15 The 1,8 μs Monostable Sampling Pulse
Sampling pulse positions within a colour bar waveform
Channel A displays the colour bar video input waveform

CHAPTER 5

Timing Generator Calibration I.M. Analyser Tests, Applications and Error vs System Rise Time

5.1 TIMING GENERATOR CALIBRATION

5.1.1 INTRODUCTION

All the circuit boards in the I.M. analyser prototype were checked and adjusted individually before testing the complete unit. A simple test rig was built for the prototype I.M. analyser using a 64-way Eurocard DIN 41612 female A + C connector. Supplies were connected as required, and signals applied to the appropriate terminals for test purposes. The connections were changed for each Eurocard to cater for the different functions to be checked.

The calibration of the sync separator and timing generator is described with reference to the circuit schematic diagram in Fig. 4.12 of Chapter 4.

5.1.2 TEST AND CALIBRATION PROCEDURE

1. Refer to the circuit diagram in Fig. 4.3. +5 V and -5 V power supplies were connected to the board using a 64-way Eurocard DIN 41612 female A + C connector.
2. The video output signal from a TV PAL Colour Bar Pattern Generator was connected to the VIDEO INPUT BNC terminal P4-1. Using a BNC T-piece a 75 Ω termination was arranged for this signal. The test pattern selected

was a 100-0-75-0 colour bar.

3. Composite sync pulses of approximately 5 V amplitude were monitored at pin 7 of IC01. Their presence with the correct format confirmed that the sync separator circuit was operational.
4. The positive line pulses at pin 10 of IC16 were then checked for the correct duration illustrated in Fig. 5.1. The PLL would lose lock during the equalisation pulses in the video waveform if these pulses were too short. R_{23} could be selected to achieve the required timing if necessary.

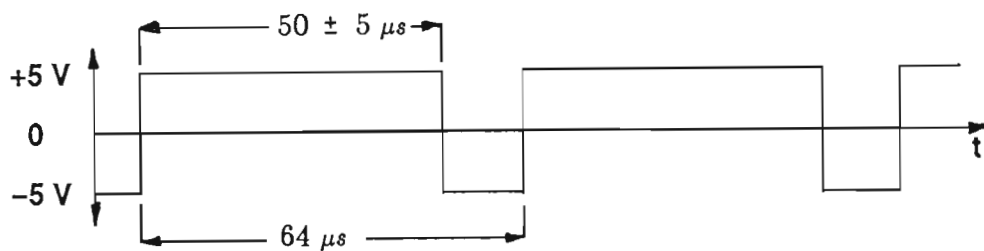


Fig. 5.1 Pulses at Pin 10 of IC16

5. The negative line pulses observed at pin 7 of IC02 confirmed the operation of the 'A' half of Monostable IC02. Their width was adjusted by means of VAR1 to give $5.6 \mu s$, as shown in Fig. 5.2. This was only an initial adjustment which would later require final setting to fine limits, as it determines the position of the sampling pulses relative to the colour burst.

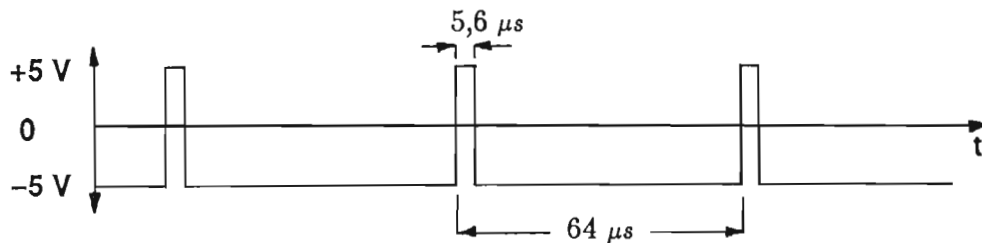


Fig. 5.2 Pulses at Pin 7 of IC02

6. The line sync output pulses at pin 217 (17c) of connector P4 were then monitored. Their amplitude was 10V peak to peak, as illustrated in Fig. 5.3, confirming the correct operation of IC15. These pulses are used to provide

external synchronisation for the histogram display.

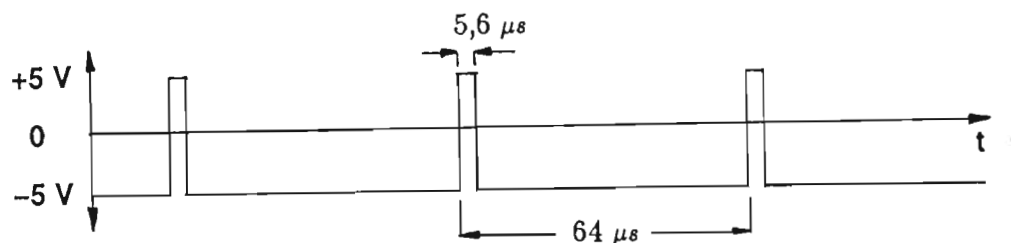


Fig. 5.3 Pulses at Pin 217 of Connector P4

7. Field sync pulses present at pin 228 (28c) of connector P4 would confirm the operation of the 'B' half of Monostable IC02. The expected waveform is shown in Fig. 5.4.

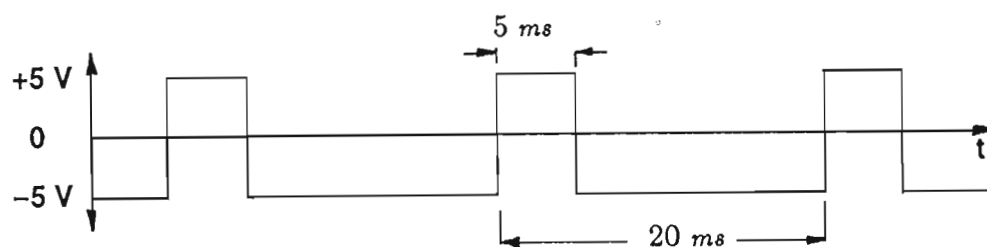


Fig. 5.4 Pulses at Pin 228 of Connector P4

8. The frequency of the pulses at pin 4 of IC03 (PLL) were then checked. The correct frequency of this square wave, shown in Fig. 5.5, is $10 \times$ line frequency f_H , or 156250 Hz.

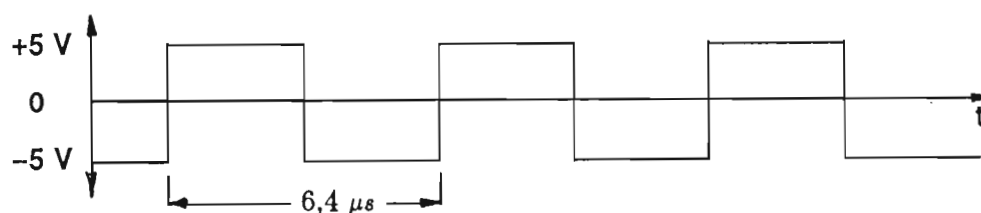


Fig. 5.5 Pulses at Pin 4 of IC03

9. The frequency of the pulses at pin 3 of IC03 (PLL) was then compared with the horizontal line frequency. Again a square wave was expected, as illustrated in Fig. 5.6, the correct frequency being equal to f_H or 15625 kHz.

The correct frequency and waveform confirmed the operation of the divide-by-ten counter IC05, which is within the closed PLL feedback loop.

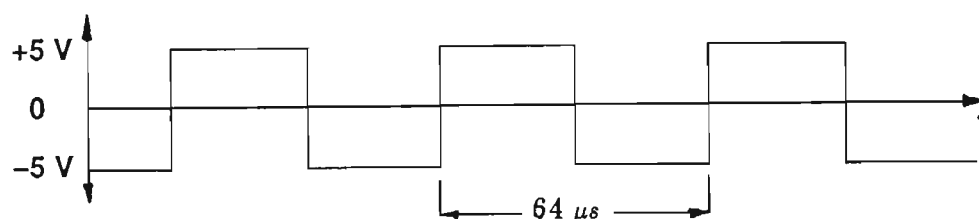


Fig. 5.6 Pulses at Pin 3 of IC03

10. The duration of the pulses at pin 12 of 3-input AND gate IC11 was then measured. This positive going pulse is illustrated in Fig. 5.7 and was expected to have a duration of $1,8 \mu s$, $\pm 0,1 \mu s$. The width of these pulses is determined by the R-C timing components associated with IC06, and selection of R16 would effect any necessary change in pulse width.

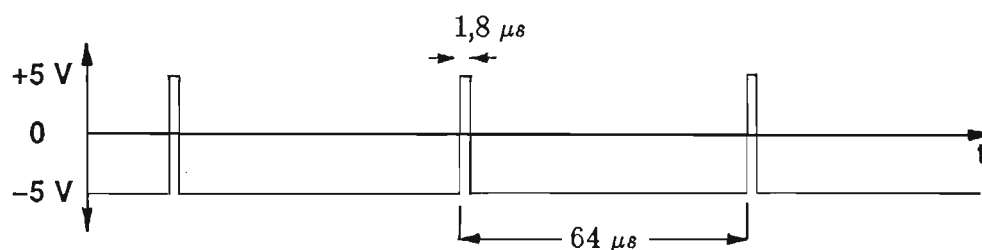


Fig. 5.7 Pulses at Pin 12 of IC11

11. Observation of a square wave form of half the line frequency at pin 13 of IC11, as shown in Fig. 5.8, confirmed the operation of the JK Flip Flop IC07. This Flip Flop is clocked by the line pulses produced by IC16 and provides the alternate line gating pulse required for use with PAL TV Systems.

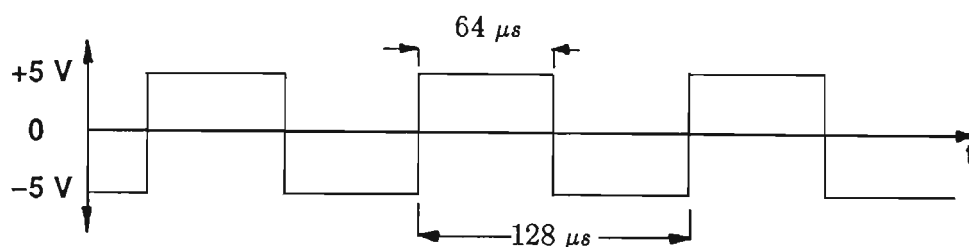


Fig. 5.8 Pulses at Pin 13 of IC11

12. The $1,8 \mu s$ mixer timing signals were monitored at pin 227 (27c) of connector P4 using a dual trace oscilloscope. Simultaneously the other trace was used to display the colour bar video test signal applied to the board. The trailing edge of the $1,8 \mu s$ pulse was then aligned with the trailing edge of the colour burst using VAR1 as shown in Fig. 5.9. Note the $1,8 \mu s$ pulse coincides with the burst pulse because of the pull-down resistors R20, R21, and R22, which set the Colour Bar Select Code to 000.

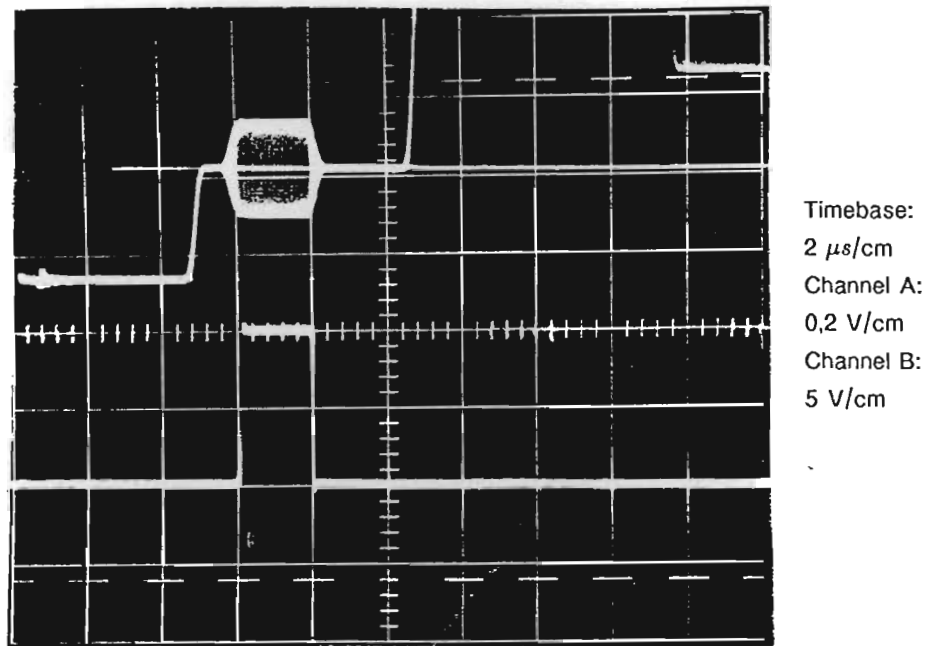


Fig. 5.9 Correct Position of Sampling Pulse Within the colour burst pulse

13. As a final check, the pins 230, 231 and 232 were connected to $+5 V$ according to the binary codes 000 to 111, with 232 the LSB and 230 the MSB, to move the $1,8 \mu s$ pulse at pin 227 to each colour bar position. The sampling pulse actually occurs at about the second quarter of the colour bar width, as illustrated in Fig. 5.10.

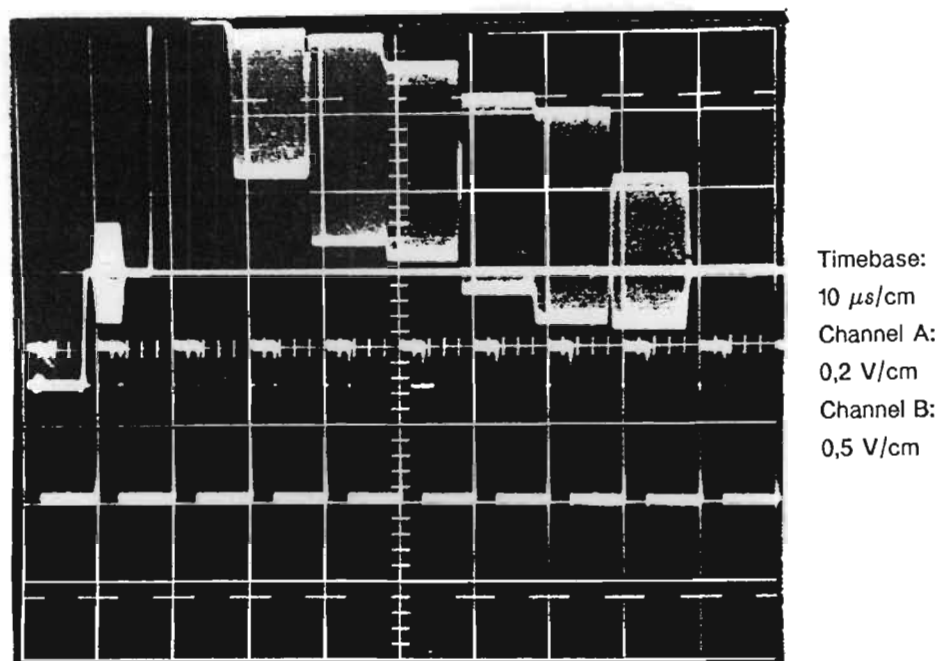


Fig. 5.10 Correct Position of Sampling Pulses Within each colour bar

14. A temporary short was connected across R9, i.e. a $10\text{ k}\Omega$ resistor associated with the LPF of the PLL IC03 caused the PLL to become unstable and lose lock. The waveform monitored at pin 219 (19c) of connector P4 should be short negative going pulses which occur every $100\text{ ms} \pm 25\text{ ms}$, as illustrated in Fig. 5.11, to indicate that the PLL has lost lock. One half of monostable IC04 was therefore operational.

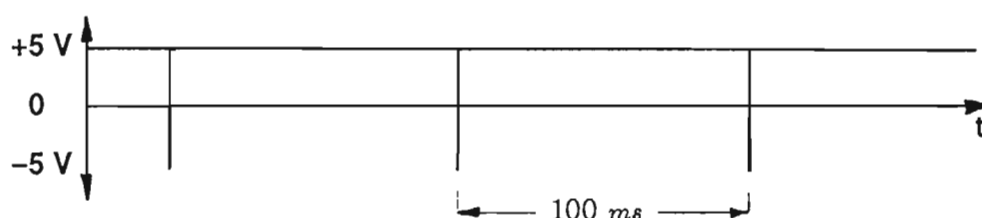


Fig. 5.11 Pulses at Pin 219 of Connector P4

15. The temporary short circuit was then removed. This should cause the pulses at Pin 219 to cease and the output remain low at -5 V .
16. The waveform at pin 218 (18c) of connector P4 was then monitored. Positive pulses of $50\text{ }\mu\text{s} \pm 10\text{ }\mu\text{s}$ should be observed indicating the presence of a video signal. This would confirm the operation of the other half of monostable IC04.

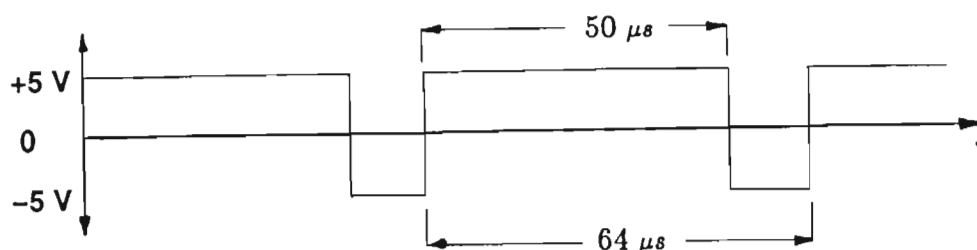


Fig. 5.12 Pulses at Pin 218 of Connector P4

17. Removal of the video input signal from BNC plug P4-1 should cause the pulses at Pins 218 and 219 of connector P4 to cease and the voltage to remain low at -5 V .

5.2 COMPARATIVE TESTS PERFORMED AT 25°C

I.M. ANALYSER vs THREE TONE TEST

5.2.1 Introduction

Comparative tests were performed by technical staff of both the SABC and Barlows Communications, at the Barlows factory in Pineside Road, Pinetown. The objective was to compare the I.M. values obtained with the SABC three tone test set and those measured by the I.M. distortion analyser. For each colour the three tone levels of the three tone test generator, measured at the RF output of the SBUF transmitter on a spectrum analyser (S.A.), were adjusted in accordance with the colour being measured. Results obtained during these tests, and submitted to the SABC by Mr. Freemantle, their Transmitter Manager for Natal, are tabled in this chapter in modified form with kind permission of the SABC [12].

Table 5.1 lists the three tone test levels corresponding to each of the six colour bars. The peak sync reference level was set to 0 db as reference on the spectrum analyser before the other levels are adjusted. The video filter was switched OFF for this calibration procedure.

Table 5.1
Three Tone Test Reference Levels
Corresponding to 100/0/75/0 Colour Bar
Relative to Peak Sync as Reference (0 dBp)

Carrier Level Colour	Vision (dBp)	Colour (dBp)	Sound (dBp)
Yellow	-8,23	-20,53	-10
Cyan	-6,64	-17,54	-10
Green	-5,79	-18,13	-10
Magenta	-4,63	-18,13	-10
Red	-3,95	-17,54	-10
Blue	-2,95	-20,53	-10

5.2.2 Preliminary Checks and Precautions

Before performing the actual tests it was necessary to check the carrier frequencies to ensure that f_{IM} would lie within the pass band of the I.M. analyser. Thus the vision carrier frequency f_v , and the sound and colour subcarrier frequencies f_s and f_{sc} respectively were measured with a frequency counter. These were chosen to correspond to the IF frequency of the SBUF Test Transmitter.

RESULTS:

$$f_v = 38,899 \text{ MHz}$$

$$f_s = 6,0000 \text{ MHz}$$

$$f_{sc} = 4,43361875 \text{ Mhz}$$

The corresponding I.M. frequency f_{IM} is

$$\begin{aligned} f_{IM} &= f_s - f_{sc} \\ &= 1,56638125 \text{ MHz} \end{aligned}$$

It was necessary to ensure that the I.M. analyser was correctly calibrated. This was checked using an external calibration signal of 1,5664 MHz and 5,59 mV. A reading of 50 dBp was expected for this input.

The modulator/demodulator was then to be calibrated so that a carrier modulated to 20 % residual carrier by a 1 V peak-to-peak signal gave a 1 V peak-to-peak video output. The AGC operation should be set to "back porch" and not to "sync tip". This prevents a stretching of the positive (0,7 V) going portion of the video signal in the event of sync crushing which would occur if set to peak sync AGC.

It was important that the RF level into the demodulator was kept within the optimum range for linear operation, viz. -69 dBm to -3 dBm with no input attenuation. Linearity was also dependent on the setting of the gain control potentiometer on the SBUF vision sound/modulator. This control must remain in the fully CCW "-6 db max linear" position at all times. The vision/sound ratio of the SBUF vision/sound modulator was 10 dB.

For instrument protection, the initial setting for the spectrum analyser input attenuator was at a minimum of -10 dB.

5.2.3 Comparison Test Procedure

The test procedure will be described with reference to cyan. The other colours require different carrier and subcarrier levels as defined in Table 5.1. Intermodulation distortion was introduced by overdriving a low power (1 Watt) amplifier used for common amplification, and distortion was measured to the nearest 0,5 dB.

- 1 The IF output of the three tone test generator was fed into the IF input of the SBUF test transmitter.
- 2 The three tone levels of the three tone test generator were adjusted in accordance with the requirements for the particular colour being measured [see Table 5.1]. For Cyan (100/0/75/0 colour bar) the following signal levels were set:

At f_v	=	38,899 MHz :	-6,64 dBp	
At $f_v - f_s$	=	32,899 MHz :	-17,54 dBp	(lower sideband)
At $f_v - f_{sc}$	=	34,465 Mhz :	-10,00 dBp	

- 3 The SBUF vision/sound modulator was driven with 100/0/75/0 colour bars and the IF output of the vision/sound modulator was fed via an attenuator into the IF input of the SBUF test transmitter.
- 4 The 0-80 dB variable attenuator was then adjusted so that peak sync level was 6,64 dB greater than the level of f_v in step 2 above. For this setting it was necessary to ensure that the video filter was in the 'off' position.
- 5 A series of tests were made at different drive levels into the non-linear amplifier. These levels were adjusted by means of the attenuators on the SBUF test transmitter.

In the case of the I.M. analyser, the SBUF test transmitter was fed from the colour bar modulated vision/sound modulator. The I.M. analyser was fed with the demodulated output of the non-linear amplifier, and I.M. distortion measurements were read from the digital display on the I.M. analyser front panel.

In the case of the 'three tone test', The SBUF test transmitter was fed from the Three Tone Test generator, which was found not to have sufficient range in levels to achieve the equivalence of certain colours in the 100/0/75/0 colour bar signal. Where required, the RF generator was used to provide the greater range in levels. The measurement was recorded from the spectrum analyser display.

The results of these tests, and others to examine the temperature stability of the I.M. distortion analyser, are presented in the tables that follow.

5.2.4 Results of the Comparative Tests Performed at 25°C

Tests were performed colour by colour to facilitate the setting up of the carrier levels for the three tone tests. The results are presented for each colour, with increasing input levels applied to the non-linear amplifier, on the following two pages in Table 5.2.

Table 5.2
Results of Comparative Tests
Three Tone Test vs I.M. Analyser
 Temperature = 25°C

Colour	Input to 1 W Amp (dBp)	I.M. Analyser (dBp)	3TT Results (dBp)	Error (dB)
Burst	0	-44	-42	-2,0
	-2	-47	-45,5	-2,5
	-4	-52	-50	-2,0
	-6	-58	-56	-2,0
	-8	-63,5	-61,5	-2,0
	-10	-68,5	-66	-2,5
Yellow	0	-43,5	-43	-0,5
	-2	-50	-49	-1,0
	-4	-56,5	-55,5	-1,0
	-6	-61,5	-60,5	-1,0
	-8	-66	-65	-1,0
	-10	-70	-69	-1,0
Cyan	0	-41,5	-40,5	-1,0
	-2	-47,5	-47	-0,5
	-4	-53,5	-53,3	-0,2
	-6	-59	-58,5	-0,5
	-8	-63,5	-63	-0,5
	-10	-67	-67	0
Green	0	-45	-44	-1,0
	-2	-52	-50,5	-1,5
	-4	-57,5	-56	-1,5
	-6	-62	-60,5	-1,5
	-8	-66	-65	-1,0
	-10	-70	-68,5	-1,5

Table 5.2 contd.
Results of Comparative Tests
Three Tone Test vs I.M. Analyser
 Temperature = 25°C

Colour	Input to 1 W Amp (dBp)	I.M. Analyser (dBp)	3TT Results (dBp)	Error (dB)
Magenta	0	-44	-44	0
	-2	-50	-50	0
	-4	-56	-56	0
	-6	-61	-61	0
	-8	-65	-65	0
	-10	-68,5	-68	-0,5
Red	0	-41,5	-41,5	0
	-2	-47,5	-47,5	0
	-4	-53,5	-54	-0,5
	-6	-59	-58	-1,0
	-8	-63,5	-63	-0,5
	-10	-67	-66,5	-0,5
Blue	0	-41	-40,5	-0,5
	-2	-45	-45,5	0,5
	-4	-51	-51	0
	-6	-57,5	-57,5	0
	-8	-62	-62	0
	-10	-66	-66	0

5.3 COMPARATIVE TESTS PERFORMED AT 0°C & 25°C & 50°C I.M. ANALYSER vs THREE TONE TEST

5.3.1 Test Procedure

Because of the long time required to perform each three tone test it was decided to perform tests at the temperature specification extremes of 0°C and 50°C with one colour only. As cyan is the closest equivalent to the standard three tone test (see Table 5.3 for a comparison) this colour bar was used for the comparisons made at the temperature limits mentioned above. Carrier levels were, however, set according to the colour bar requirement for cyan as detailed in Table 5.1.

A series of tests was first performed with the chamber temperature at 0°C and different input levels applied to the non-linear amplifier. The chamber temperature was then raised to 50°C and the test sequence repeated for the same input levels, which also corresponded to the levels used at 25°C. The procedure outlined was adopted for reasons of convenience in using the test chamber.

5.3.2 Test Results

Other measurements performed at 25 °C are included in the tables to give results over the full operating temperature range. To facilitate comparisons, however, it was considered best to rearrange the results so that measurements performed at the same input level and differing temperatures are presented together in the same table. Tables 5.4 through to 5.9 present the data measured in this format.

Table 5.3
Comparison Between Test Settings For
Cyan Colour Bar and Standard Three Tone Test
 All values relative to peak sync power (0 dBp)

Carrier Level	Cyan (dBp)	3TT (dBp)
VISION	-6,64	-6,0
COLOUR	-17,54	-17,0
SOUND	-10,0	-10,0

Table 5.4
Results of Comparative Tests
Three Tone Test vs I.M. Analyser
 Temperature = 0°C
 All values relative to peak sync power (0 dBp)

Colour	Input to 1 W Amp (dBp)	I.M. Analyser (dBp)	3TT Results (dBp)	Error (dB)
Cyan	0	**	-32	N/A
	-2	-38,5	-38	-0,5
	-4	-44,5	-44,5	0
	-6	-50	-50	0
	-8	-54,5	-55	0,5
	-10	-58	-58	0
	-12	-60	-62++	2,0

Notes:

**** Out of range for the I.M. Analyser**

++ Considerable noise present; probably high

Table 5.5

Results of Comparative Tests
Three Tone Test vs I.M. Analyser
 Temperature = 50°C
 All values relative to peak sync power (0 dBp)

Colour	Input to 1 W Amp (dBp)	I.M. Analyser (dBp)	3TT Results (dBp)	Error (dB)
Cyan	0	-39	-40	1,0
	-2	-39	-40	1,0
	-4	-45,5	-46	0,5
	-6	-50	-51	1,0
	-8	-55	-55,5	0,5
	-10	-59	-58	-1,0
	-12	-62	-62,5	0,5

Table 5.6

Temperature Tests on I.M. Analyser
 Input to N/L Amplifier at -6 dB
 relative to peak sync power (0 dBp)
 Test signal: 100/0/75/0 Colour Bar

I.M. Distortion Analyser Reading at Test Chamber Temperature:				
Colour	0°C (dBp)	25°C (dBp)	50°C (dBp)	Change (dB)
Burst	-64	-64	-64	0
Yellow	-67	-67	-67	0
Cyan	-62	-62,5	-62	0,5
Green	-61	-62	-62	1,0
Magenta	-60	-60,5	-60	0,5
Red	-58,5	-59	-59	0,5
Blue	-60	-60,5	-60,5	0,5

Table 5.7

Temperature Tests on I.M. Analyser
 Input to N/L Amplifier at -4 dB
 relative to peak sync power (0 dBp)
 Test signal: 100/0/75/0 Colour Bar

I.M. Distortion Analyser Reading at Test Chamber Temperature:				
Colour	0°C (dBp)	25°C (dBp)	50°C (dBp)	Change (dB)
Burst	-59	-59	-59	0
Yellow	-63,5	-63,5	-62,5	1,0
Cyan	-58	-58	-57,5	0,5
Green	-57,5	-57,5	-57,5	0
Magenta	-56	-56	-56	0
Red	-54	-54,5	-54,5	0,5
Blue	-55,5	-56	-56	0,5

Table 5.8

Temperature Tests on I.M. Analyser
 Input to N/L Amplifier at -2 dB
 relative to peak sync power (0 dBp)
 Test signal: 100/0/75/0 Colour Bar

I.M. Distortion Analyser Reading At Test Chamber Temperature:				
Colour	0°C (dBp)	25°C (dBp)	50°C (dBp)	Change (dB)
Burst	-52,5	-53	-52,5	0,5
Yellow	-58,5	-58,5	-58,5	0
Cyan	-53	-53	-53	0
Green	-52	-52,5	-52,5	0,5
Magenta	-50,5	-50,5	-50,5	0
Red	-48,5	-48,5	-48,5	0
Blue	-49,5	-50	-50	0,5

Table 5.9

Temperature Tests on I.M. Analyser

Input to N/L Amplifier at -0 dB relative to peak sync power (0 dBp)

Test signal: 100/0/75/0 Colour Bar

	I.M. Distortion Analyser Reading At Test Chamber Temperature:			
Colour	0°C (dBp)	25°C (dBp)	50°C (dBp)	Change (dB)
Burst	-47	-47,5	-47	0,5
Yellow	-53	-53	-52	1,0
Cyan	-47	-47,5	-47,5	0,5
Green	-46	-46,5	-46,5	0,5
Magenta	-44	-44	-44,5	0,5
Red	-42	-42,5	-42,5	0,5
Blue	-43,5	-43,5	-44	0,5

5.3.3 Test Equipment Requirements

Table 5.10 below lists the equipment required to perform the above three tone test comparison at the three temperatures used:

Table 5.10

Test Equipment Used to Perform Comparative Tests

Vision/Sound Modulator	Rohde and Schwarz
Test Transposer	Rohde and Schwarz SBUF
Colour Bar Generator	Tektronix
Variable Attenuator	Rohde and Schwarz 0 – 80 dB
Wideband Amplifier	Hewlett-Packard
1 Watt RF Amplifier	Rohde and Schwarz
2 x 20 dB Attenuators	
Demodulator	Tektronix 1450
3 Tone Test Generator	SABC
Waveform Monitor	Rohde and Schwarz OKF
Spectrum Analyser	Hewlett-Packard 141T
RF Generator	Hewlett-Packard

5.4 ACCEPTANCE TESTS PERFORMED BY THE SWISS INSTITUTE FOR POSTS, TELEPHONES AND TELEGRAPHS

5.4.1 Introduction

A report on tests performed by the Swiss Posts, Telephones and Telegraphs (PT&T) Institute was submitted to the Inventions Development Corporation and selected results are presented in this section [17].

5.4.2 Test Procedures

Low frequency (video) comparative measurements were performed using the I.M. analyser and a spectrum analyser as reference.

In the high frequency comparative measurements, the I.M. analyser reading was compared with values obtained from two spectrum analysers: one analogue and one digital. A third wobulation technique was also used, but details were not given. These three measurements were averaged to provide reference values. Table 5.12 gives the results of comparative tests at an I.M. level of -58 dBp, and Table 5.13 records their results for the six colour bars.

Table 5.11
Precision of Measured Intermodulation Levels

Apparatus	Type	Band	I.M. max (dBp)	Error (dB)
I.M. Analyser		LF	-61	$\pm 0,7^+$
S.A.	TR 4172	LF	-57,5	$\pm 0,7^+$
S.A.	TR 4172	HF	-58,1	$\pm 0,5$
S.A.	7 L 13	HF	-58	$\pm 1,0$
Wobulator	SWOF 3/Z	HF	-57	$\pm 1,0$

Notes:

$+$ Includes errors due to AMF 2 precision demodulator

S.A. Spectrum analyser as specified


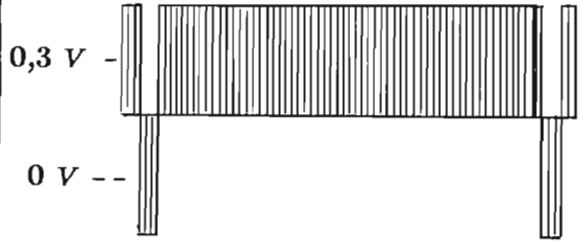
Table 5.12
Colour Bar Comparative Measurements

Colour	Analyser Reading (dBp)	Reference Reading (dBp)	Analyser Error (dB)
Yellow	-58,5	-55,7	-2,8
Cyan	-53,5	-51,0	-2,5
Green	-53,5	-50,0	-3,5
Magenta	-51,5	-48,7	-2,8
Red	-50,0	-47,0	-3,0
Blue	-51,0	-48,5	-2,5

5.4.3 Colour Burst Measurements

Two video waveforms, shown in Table 5.13, were used to test the performance of the I.M. analyser over the full line width.

Table 5.13
Comparison Between Colour Burst and Bar Measurements

Video Line Signal	I.M. Measured Within:	
	Bar	Burst
	-56,0	-59,0
	-56,0	-56,0

5.4.4 I.M. Analyser Frequency Bandwidth

By varying the sound intercarrier frequency until a 0,5 *dB* change in I.M. analyser reading was observed, the 0,5 *dB* bandwidth of the analyser was measured. Relative to the centre frequency of 1,066381 *MHz* a total deviation of -200 *Hz* to +60 *Hz* was possible. This exceeded the expected carrier frequency tolerance of ± 55 *Hz* [see Appendix G, Section G.2.2].

5.4.5 Internal Reference Oscillator Check

Both the frequency and absolute level of the internal calibration oscillator were measured, with the results following in Table 5.14.

Table 5.14
Reference Oscillator Frequency and Level

Parameter	Value	Error	Units
Frequency:	1 006 378	-3,0	<i>Hz</i>
Level:	-50,3	-0,3	<i>dBp</i>

5.5 PRACTICAL DISTORTION MEASUREMENTS ON TV TRANSPOSERS USING THE I.M. ANALYSER

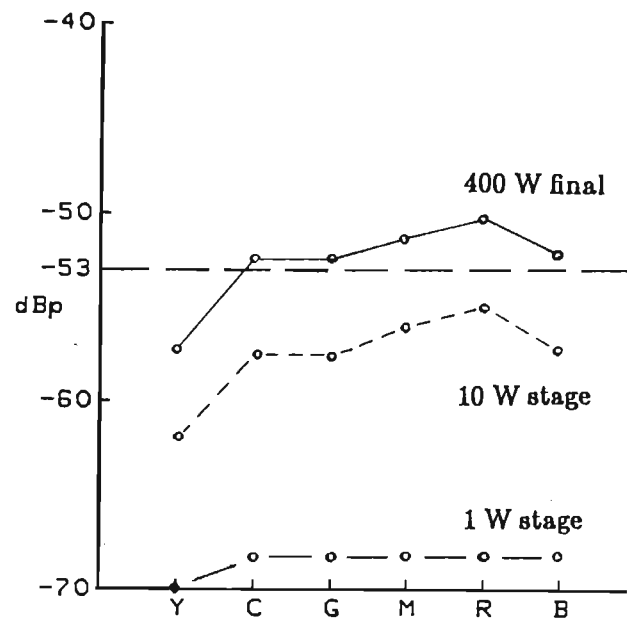
Extensive tests have been performed by SABC technical staff using the I.M. analyser on TV transmitters both with, and without, pre-correctors. Some selected results are presented in Fig. 5.13 overleaf.

Fig. 5.13(a) shows the results of measurements on a 400 *Watt* UHF tetrode transposer without pre-correction. The variation of final distortion figures from one colour bar to another is almost precisely that predicted for the TH382 by the third order terms in Table B.9 of Appendix B. This performance would be expected of any under-run tetrode power stage.

Fig. 5.13(b) shows the range of I.M. distortion pre-corrector adjustment on a 1000 *Watt* UHF TV transposer. The broken curve corresponding to the minimum influence of the pre-corrector follows the P_{tot} values in Table B.10 closely, and a significant 5th order distortion component is therefore evident. The pre-corrector coped well with the Yellow, Cyan and Green colour bars but had a 7 *dB* variation over the Magenta, Red and Blue colour bars indicating inadequate design in this latter region.

Fig. 5.13(c) illustrates the range of I.M. distortion pre-corrector adjustment on a 1000 *Watt* VHF TV transposer. In this case pre-corrector performance is quite unpredictable. The pre-corrector was clearly designed to optimise distortion in the Cyan region, as measured by the 3TT. Design is totally inadequate in the Magenta, Red and Blue colour bar regions where the transposer could not meet the required -53 *dBp* specification.

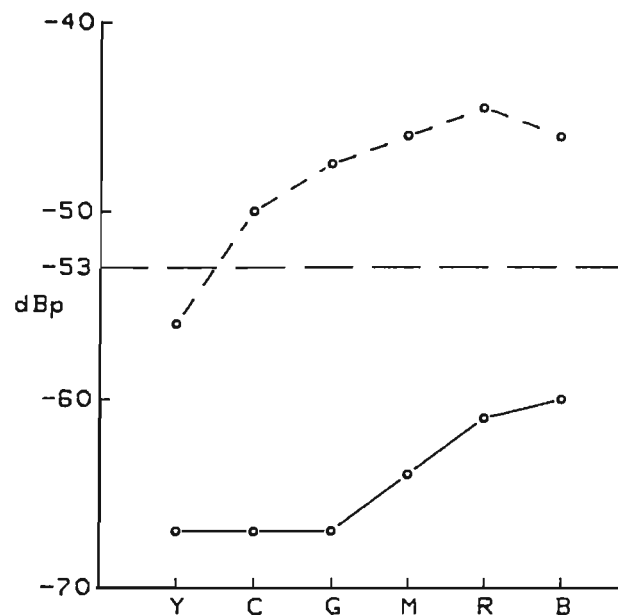
Further applications of the I.M. analyser are discussed in a paper by Broadhurst et al [9].



Colour Bars

(a)

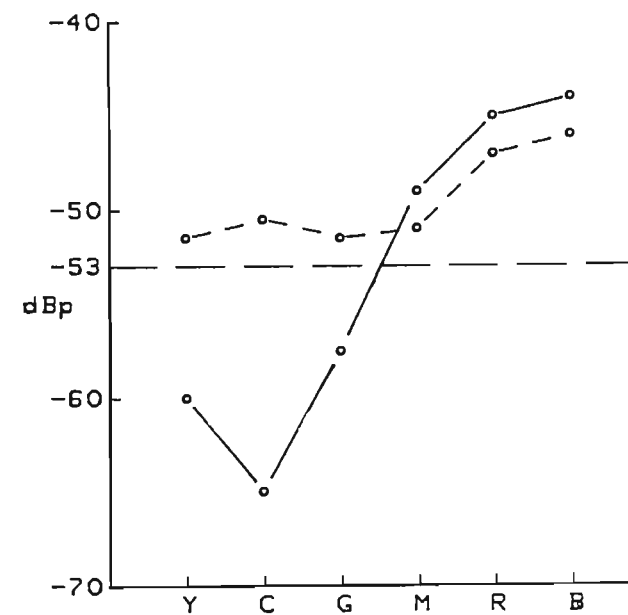
I.M. Distortion in a 400 *Watt* UHF Tetrode TV Transposer measured with the I.M. analyser. No pre-corrector present.



Colour Bars

(b)

Range of I.M. Distortion pre-corrector adjustment on a 1000 *Watt* UHF Tetrode Transposer.



Colour Bars

(c)

Range of I.M. Distortion pre-corrector adjustment on a 1000 *Watt* VHF Tetrode Transposer.

Fig. 5.13 I.M. Distortion Analyser Measurements on TV transposers with, and without, pre-correctors.

CHAPTER 6

CONCLUSIONS

6.1 BARLOWS COMMUNICATIONS TEST RESULTS.

In the comparative tests performed at 25°C, the results obtained from the sampling I.M. analyser were in close agreement with those obtained from the three tone test (3TT). A maximum difference of $\pm 2,5$ dB was noted which corresponded to readings within the colour burst taken at 25°C (see Table 5.2).

The 3TT results, however, were consistently low by about 2,5 dBp, when compared to the sampling I.M. analyser measurements, implying a possible calibration error for the 3TT. Otherwise a 0,5 dB difference was typical and acceptable.

Temperature tests produced a maximum reading difference of 1 dB for the Yellow colour bar over the test temperature range of 0°C to 50°C, which is wider than the actual specification. The 3TT appears to have produced readings consistently low by some 0,5 dB in most of these recorded results. The results were very satisfying when one considers that a first prototype was the subject of these tests.

6.2 SWISS PT&T INSTITUTE TEST RESULTS.

Reported results of tests performed on the analyser by the Swiss PT&T show consistent differences between the I.M. analyser readings and their reference measurements. This is illustrated in Fig. 6.2. Part of the reading difference was due to a calibration error through an oversight on our part. The peak video level is 1,1 V for B+G/PAL signals, and not 1,25 V. An error of -1,11 dB in the instrument readings was the result. The consistent difference between the I.M.

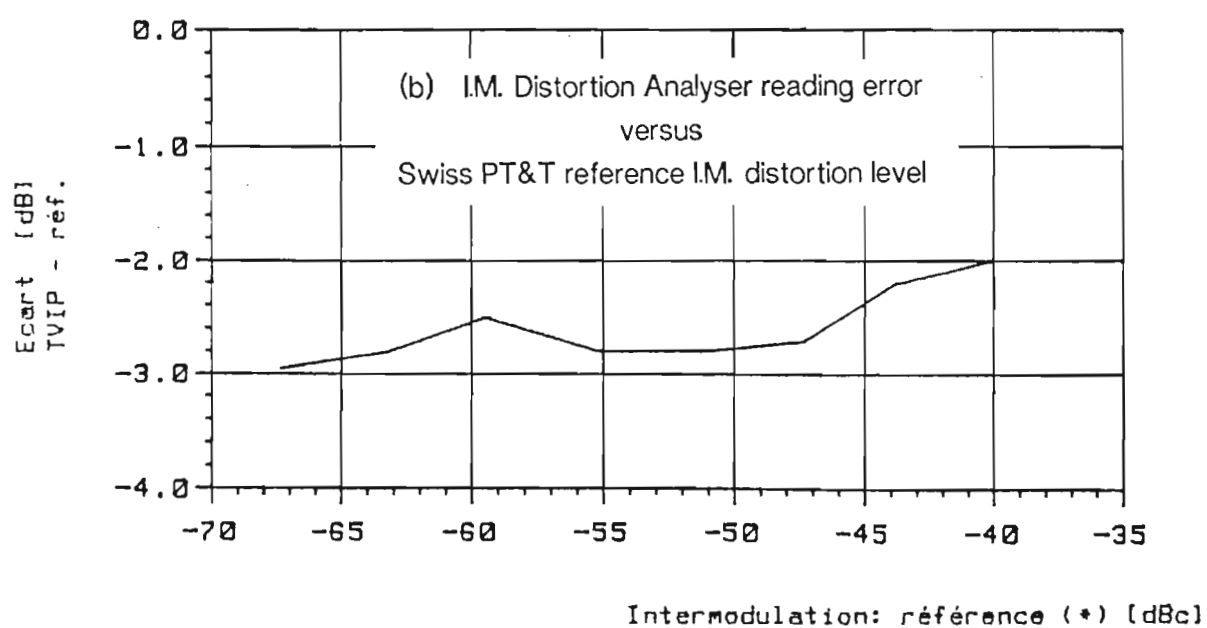
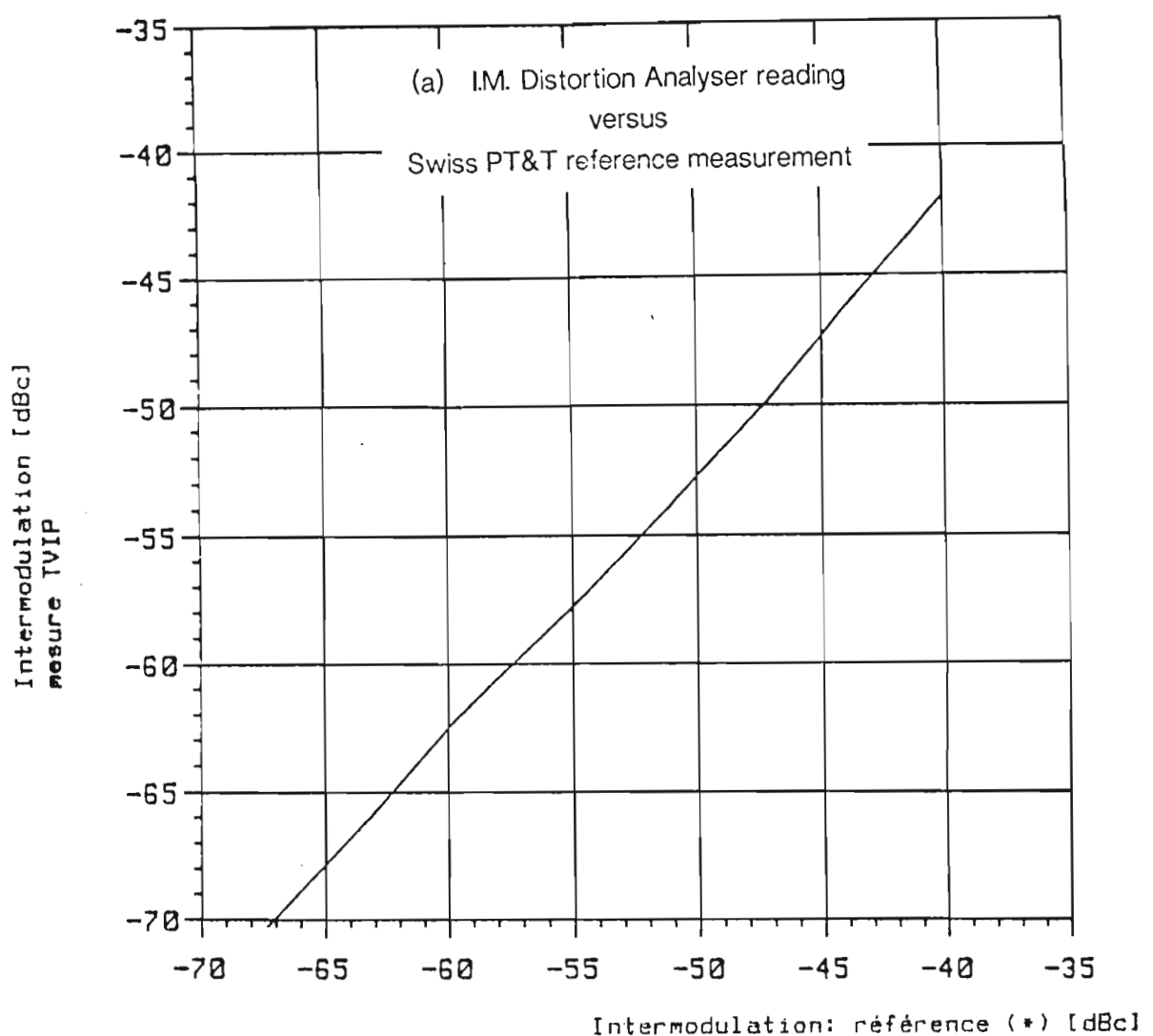


Fig. 6.2 Swiss PT&T Comparative Intermodulation
Distortion Measurements

analyser and the Swiss reference measurements was thereby reduced from approximately -3 dB to -2 dB . Considering that our only available reference oscillator had an absolute signal level accuracy of $\pm 1\text{ dB}$ such a result was not unexpected.

It is believed that the Swiss PT&T standards would be met with proper calibration of the analyser. This would necessitate access to a calibration facility such as that of the Swiss PT&T, which is not economically feasible.

6.3 ERRORS DUE TO SYSTEM RISE TIME.

The observed 2,0 to 2,5 dB error in measurements within the colour burst in Table 5.2, and 3 dB error in Table 5.13, of Chapter 5 confirm the averaging problem that results from a system rise time that is longer than the sampling delay time within the I.M. signal region. The averaging sample-and-hold circuit could be designed to have a 3 dB gain to compensate for this unavoidable loss.

6.4 STABILITY OF SAMPLING DELAY TIME.

Sampling is not timed to occur at the beginning of each bar or the colour burst, but is delayed to avoid the differentiated luminance spikes that are present within these regions. The actual delay time is most significant within the narrow colour burst pulse, where sampling typically takes place between 0,1 and 0,4 μs after the burst pulse commences. A 0,125 μs change in sampling delay can cause a change in I.M. analyser reading of 0,625 dB which is unacceptable. The same change in delay within a colour bar results in a small reading error of only 0,125 dB . Sampling pulse delay changes of the order of 125 ns have not been observed in the temperature tests, however, as will be evident from the constancy of the I.M. readings within the colour burst over the full operating temperature range as recorded in Tables 5.6 and 5.7 in Chapter 5. A high degree of temperature stability in sample timing has thus been achieved.

6.5 APPLICATIONS OF THE SAMPLING I.M. ANALYSER.

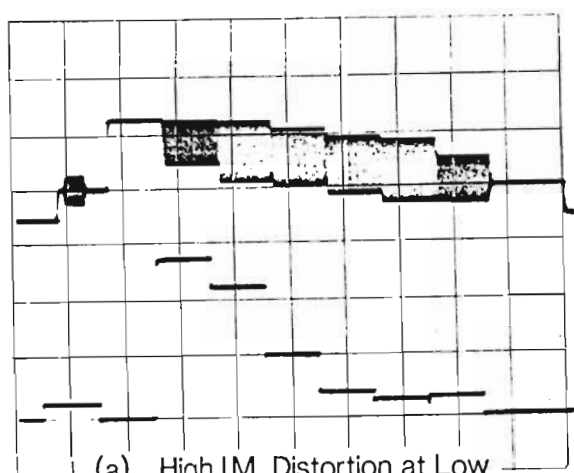
By using a standard colour bar signal, or one modified so that the BLUE luminance level may be adjusted to "blacker than black", an amplifier under test is exercised over its whole dynamic range by means of the varying luminance levels. Rapid adjustment of both power tube operating conditions and pre-corrector settings is then possible using the analyser.

Television transmitter amplifier characterisation and pre-corrector adjustment are facilitated through the histogram form of simultaneous display of measured I.M. levels corresponding to the colour burst and the six colours. A series of histograms, simulating pre-corrector adjustor settings, is shown overleaf in Fig. 6.1. As adjustments are made so the I.M. distortion levels change within each colour bar, giving a clear indication of either improved or worsened system performance.

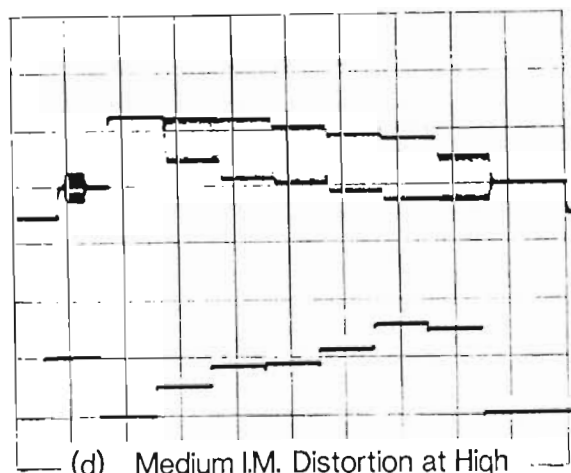
Other tests performed by the SABC using the I.M. analyser have revealed wider applications for the instrument. Transmitter parameters such as differential gain, differential phase, vision/sound cross modulation, and sync pulse crushing are all proportional to the polynomial coefficient ratio K_3/K_1 (or G_3/G_1). Some of these results were presented at the Washington IEEE Conference on Broadcasting in September 1987 [9]. It was shown that K_3 , and hence each transmitter parameter above, can be optimised by minimising all seven I.M. levels. Table 6.1 lists the actual I.M. readings that should be minimised to optimise a particular transmitter parameter.

Table 6.1
Parameter Optimisation using the I.M. Analyser

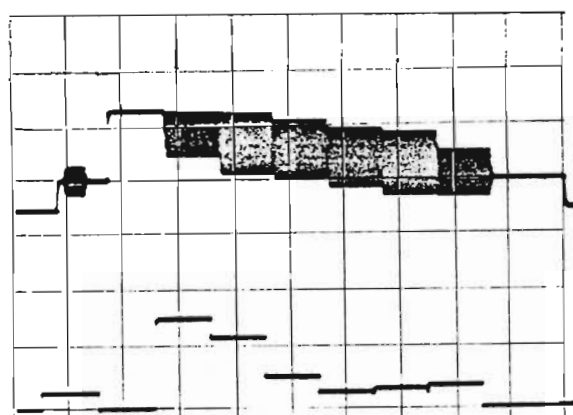
TRANSMITTER PARAMETER	COLOUR BAR FOR BEST MINIMISATION
Vision Sound X-mod Differential Gain Differential Phase	Burst, Blacker than black Blue, Red and Magenta Blacker than black



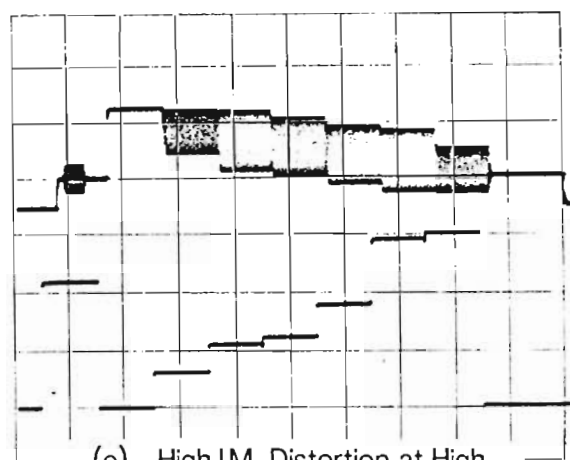
(a) High I.M. Distortion at Low Video Modulation Levels
Affects Yellow and Cyan mainly



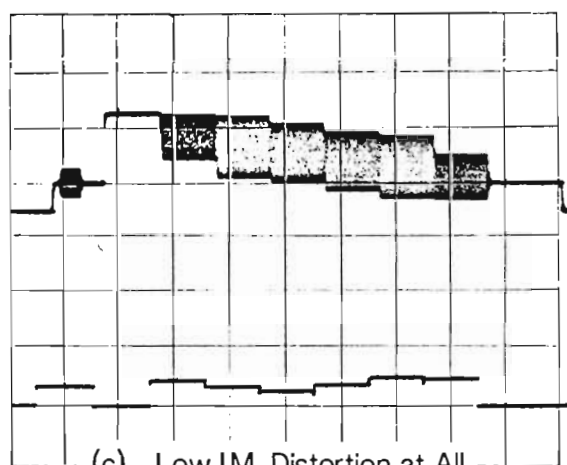
(d) Medium I.M. Distortion at High Video Modulation Levels
Affects Burst, Red and Blue mainly



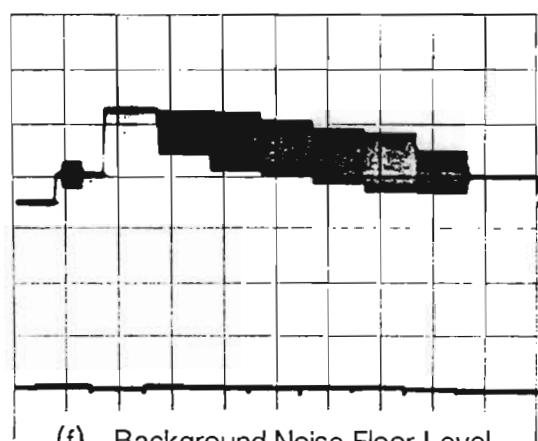
(b) Medium I.M. Distortion at Low Video Modulation Levels
Affects Yellow and Cyan mainly



(e) High I.M. Distortion at High Video Modulation Levels
Affects Burst, Red and Blue mainly



(c) Low I.M. Distortion at All Video Modulation Levels



(f) Background Noise Floor Level of the I.M. Distortion Analyser

Fig. 6.1 Histogram Display Series

Simulation of the Adjustment of a Television Transmitter

Distortion Pre-Corrector using the I.M. Analyser

Settling Time, which is also the Measurement Time,
is approximately three seconds.

The development of a unique instrument, for measuring intermodulation product distortion in common amplifier television transmitters, has been presented in this thesis. The success of the I.M. analyser prototype, based on the original sampling concept of A.D. Broadhurst [1], was largely influenced by the adoption of a time division multiplexed measurement system and the stable, proportional, sample pulse timer proposed by the author. The objective behind the prototype development was to demonstrate the feasibility of measuring I.M. distortion quickly and accurately over the whole dynamic range of the transmitter characteristic using the new sampling technique. This has been achieved, but improvements are possible in both system noise performance and accuracy.

A 6 dB improvement in gain is possible from each of the following modifications to the design, viz.

- (a) Use of a four-switch mixer arrangement which doubles the output voltage fed to the 500 Hz filter, and
- (b) Adoption of a singly-terminated passive 2 MHz low pass filter to reduce the level of the colour subcarrier entering the mixer.

Both design alterations mentioned above are simple to implement but they were not done as there appears to be little interest in the measurement of very low levels of I.M. distortion, say below -70 dBp. Such levels would have little if any observable effect on the picture quality of a television transmission.

A complete redesign of the instrument along entirely digital lines is feasible using the high speed ADCs available today. This avenue was not pursued for two main reasons. Firstly, the unattended operation of transposers in Japan and other countries has led to a tremendous reduction in test equipment requirements, in terms of numbers of instruments, for broadcasting companies. Expensive test gear such as spectrum analysers are thus no longer a serious financial burden. In discussing the design of modern UHF Transmitting Facilities, George and Hiatt [105] have concluded that the spectrum analyser is an adequate test instrument for all distortion measurements. This is true when one considers the lack of definitive specifications in many countries requiring, say, better resolution or lower measurement thresholds than can be provided by a good spectrum analyser. Secondly, the advent of high definition television has tolled the death knell of both the NTSC and PAL Television Systems. In these circumstances, further development of the I.M. Analyser has little to commend it.

APPENDIX A

Intermodulation Distortion Analyser Functioning and Specifications

A.1 INTRODUCTION

The brochure that follows gives a colourful description of the basic functioning of the Intermodulation Distortion Analyser.

Results of measurements performed on selected pre-correctors with the analyser, using a colour bar test signal, are also presented. They reveal serious pre-corrector design limitations. As pre-corrector performance is normally tested by means of the three tone test, most designs have been optimised for these particular carrier levels. This is evident from the low distortion levels measured within the Cyan colour bar, which has chrominance and luminance levels corresponding most closely to those of the three tone test.

Pre-corrector performance characteristics usually deteriorate within the Red and Blue colour bars which correspond to regions having high vision carrier amplitudes. The worst distortion figures are obtained in the colour burst and, where such a signal is provided, in a bar having a negative luminance level, which is the so-called 'blacker-than-black' modulation. Pre-corrector design will not be advanced to the point where intermodulation distortion is within acceptable limits over the full range of video luminance levels until testing is compulsory over this range. The I.M. Analyser provides a simple method of performing such tests.

Detailed specifications of distortion analyser performance are also supplied, together with details of a colour bar cum staircase waveform generator (with a blacker-than-black modulation option) designed by our team.

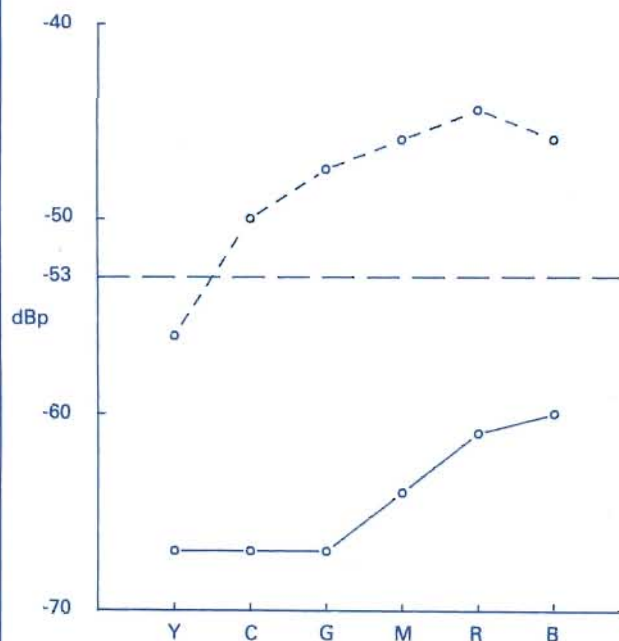
measure television in-band
INTERMODULATION DISTORTION
WITHOUT A SPECTRUM ANALYSER



- **simplest, fastest way ever of measuring intermodulation distortion**
- **representative of actual programme conditions**
- **best way of setting up intermodulation distortion precorrectors over whole operating range**
- **0.5dB accuracy and resolution. - 40dBp to -70dBp range**
- **analogue and digital readouts**

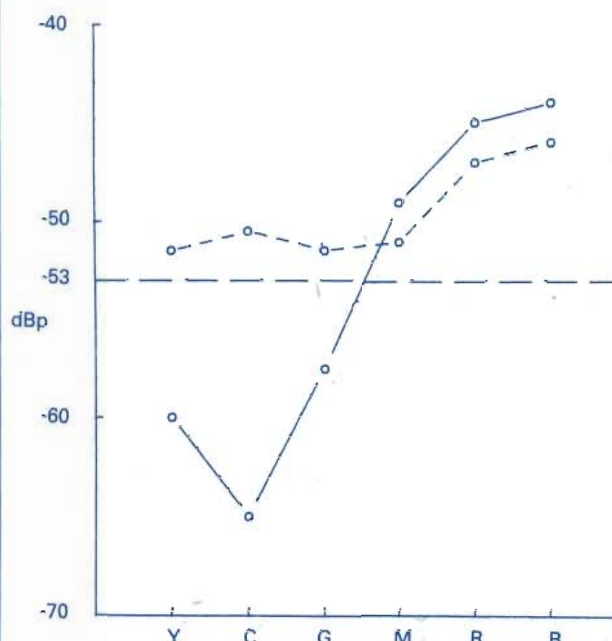
• **LRAL, R/G PAL and M-NTSC options**

RESULTS



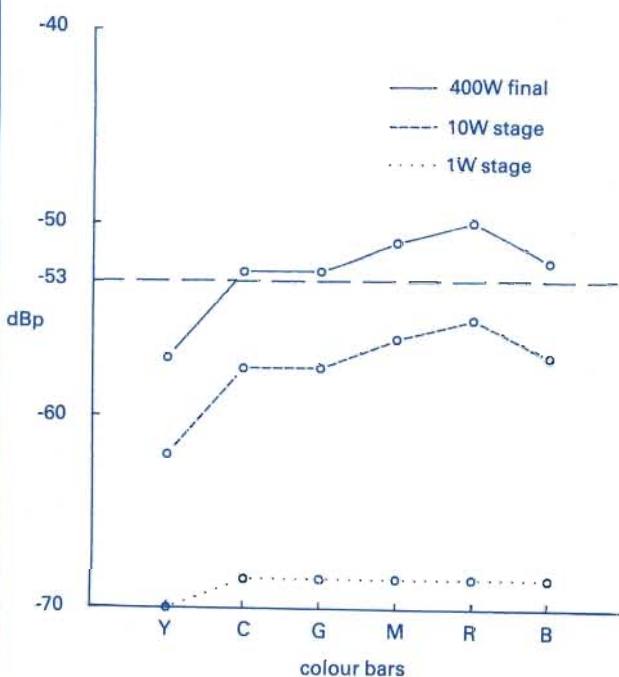
100/0/75/0 colour bar intermodulation product amplitude relative to peak sync power level.

Range of adjustment of a properly working 1kW UHF tetrode intermodulation precorrector



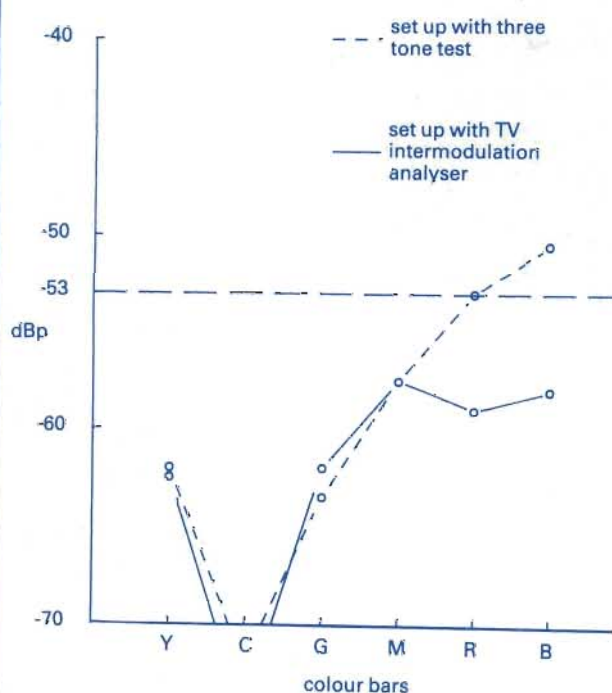
100/0/75/0 colour bar intermodulation product amplitude relative to peak sync power level.

Range of adjustment of faulty 1kW VHF tetrode intermodulation precorrector



100/0/75/0 colour bar intermodulation product amplitude relative to peak sync power level.

A larger than normal increase in IP level in the 10W stage of a 400W UHF tetrode output transposer



100/0/75/0 colour bar intermodulation product amplitude relative to peak sync power level.

Setting up a 5kW VHF tetrode IP precorrector with the three tone test and the TV intermodulation distortion analyser

APPENDIX B

Theory of Intermodulation Distortion in Television Transposers due to Non-Linear Common Amplification

B.1 INTRODUCTION

The theory of non-linear intermodulation distortion in common amplification television transmitters has been investigated by a number of researchers [36, 37, 39, 40, 41]. In general, the transfer characteristic of a television transmitter amplifier is represented by the infinite power series:

$$v_{\text{out}} = \sum_{r=0}^{\infty} K_r v_{\text{in}}^r \quad (\text{B.1})$$

Expansion of equation (B.1) yields terms representing both linear and non-linear operation.

Shelswell and others [4, 5, 7] have shown that the most visible intermodulation distortion is due to the third order term G_3 in the transmitter transfer function. Shelswell has therefore claimed that the non-linear transfer function may be simplified to the following terms with little error:

$$v_{\text{out}} = K_1 v_{\text{in}} + K_3 v_{\text{in}}^3 \quad (\text{B.2})$$

In order to determine whether the above third order assumption is valid or not, a practical power tetrode, the Thomson CSF TH382, was modelled in terms of the modified version of equation (B.1) shown in (B.3), which related the distortion components of the anode current i_A , and hence output power into a 50 Ω load, to the grid input voltage v_{in} via conductance coefficients G_r as follows:

$$i_A = \sum_{r=0}^{\infty} G_r v_{in}^r \quad (B.3)$$

The coefficients G_r (for $r = 0$ to 5) were evaluated by computer. Third and fifth order distortion power levels were then predicted for each colour bar, and conclusions drawn from their relative magnitudes. These predictions and conclusions from the major part of this Appendix.

B.2 I.M. DISTORTION THEORY

If the phase relationships are ignored, the three tone test input signal voltage may be expressed as:

$$v_{in} = V_v \cos(\omega_v t) + V_{sc} \cos(\omega_{sc} t) + V_s \cos(\omega_s t) \quad (B.4)$$

where

$$\begin{aligned} \omega_v &= 2\pi f_v t \\ \omega_{sc} &= 2\pi(f_v + f_{sc})t \\ \omega_s &= 2\pi(f_v + f_s)t \end{aligned} \quad (B.5)$$

Applying this input signal to the amplifier represented in equation (B.3) the distortion terms may be determined by analysis. The more significant terms are enumerated in what follows.

Linear anode current components:

$$\begin{aligned} i_{A1} &= G_1 [V_v \cos(\omega_v t) + V_{sc} \cos(\omega_{sc} t) + V_s \cos(\omega_s t)] \\ &= G_1 V_v \cos(\omega_v t) + G_1 V_{sc} \cos(\omega_{sc} t) + G_1 V_s \cos(\omega_s t) \end{aligned} \quad (B.6)$$

Second order anode current components:

$$i_{A2} = G_2 [V_v \cos(\omega_v t) + V_{sc} \cos(\omega_{sc} t) + V_s \cos(\omega_s t)]^2 \quad (B.7)$$

The squared terms produce second harmonics, and dc terms which shift the amplifier operating point (or bias value of anode current). Harmonics and other products result in "sum" and "difference" frequencies outside the band of interest.

Third order anode current components:

Intermodulation products of the form $(\omega_v \pm \omega_{sc} \pm \omega_s)$ are produced by the third order term, together with other components that also lie within the frequency window:

$$\begin{aligned}
 i_{A3} &= G_3 [V_v \cos(\omega_v t) + V_{sc} \cos(\omega_{sc} t) + V_s \cos(\omega_s t)]^3 \\
 &= G_3 [V_v^3 \cos^3(\omega_v t) + V_{sc}^3 \cos^3(\omega_{sc} t) + V_s^3 \cos^3(\omega_s t)] + \\
 &\quad + 3G_3 [V_v^2 V_{sc} \cos^2(\omega_v t) \cos(\omega_{sc} t) + V_v^2 V_s \cos^2(\omega_v t) \cos(\omega_s t) \\
 &\quad + V_{sc}^2 V_v \cos^2(\omega_{sc} t) \cos(\omega_v t) + V_{sc}^2 V_s \cos^2(\omega_{sc} t) \cos(\omega_s t) \\
 &\quad + V_s^2 V_{sc} \cos^2(\omega_s t) \cos(\omega_{sc} t) + V_s^2 V_v \cos^2(\omega_s t) \cos(\omega_v t)] \\
 &\quad + 6G_3 [V_v \cos(\omega_v t) V_{sc} \cos(\omega_{sc} t) V_s \cos(\omega_s t)] \quad (B.8)
 \end{aligned}$$

Table B.1 lists the frequencies and amplitudes of anode current components due to the third order term:

Table B.1
Third Order Mixer Output Current
Symbolic Frequencies and Amplitudes

Frequency	Anode Current Component Amplitudes
f_v	$G_3 V_v [V_v^2 + 2V_{sc}^2 + 2V_s^2]$
f_{sc}	$G_3 V_{sc} [2V_v^2 + V_{sc}^2 + 2V_s^2]$
f_s	$G_3 V_s [2V_v^2 + 2V_{sc}^2 + V_s^2]$
$2f_v - f_{sc}$	$3/4 G_3 V_v^2 V_{sc}$
$2f_v - f_s$	$3/4 G_3 V_v^2 V_s$
$2f_{sc} - f_v$	$3/4 G_3 V_{sc}^2 V_v$
$2f_{sc} - f_s$	$3/4 G_3 V_{sc}^2 V_s$
$2f_s - f_v$	$3/4 G_3 V_s^2 V_v$
$2f_s - f_{sc}$	$3/4 G_3 V_s^2 V_{sc}$
$f_v \pm f_{sc} \pm f_s$	$3/2 G_3 V_v V_{sc} V_s$

Fourth order anode current components:

$$\begin{aligned}
 i_{A4} &= G_4 [V_v \cos(\omega_v t) + V_{sc} \cos(\omega_{sc} t) + V_s \cos(\omega_s t)]^4 \\
 &= 12 G_4 [V_v \cos^2(\omega_v t) V_{sc} \cos(\omega_{sc} t) V_s \cos(\omega_s t) \\
 &\quad + V_v \cos(\omega_v t) V_{sc} \cos^2(\omega_{sc} t) V_s \cos(\omega_s t) \\
 &\quad + V_v \cos(\omega_v t) V_{sc} \cos(\omega_{sc} t) V_s \cos^2(\omega_s t)] + \dots \quad (B.9)
 \end{aligned}$$

The second harmonics and frequency difference terms are all out-of-band, and are thus ignored.

Fifth order anode current components:

Intermodulation products of the form $(\omega_v \pm \omega_{sc} \pm \omega_s)$ are produced at the mixer output. All other components are out-of-band, thus the relevant output voltage components are:

$$\begin{aligned}
 i_{A5} &= G_5 [V_v \cos \omega_v t + V_{sc} \cos(\omega_{sc} t) + V_s \cos(\omega_s t)]^5 \\
 &= 20 G_5 [V_v \cos^3(\omega_v t) V_{sc} \cos(\omega_{sc} t) V_s \cos(\omega_s t) \\
 &\quad + V_v \cos(\omega_v t) V_{sc} \cos^3(\omega_{sc} t) V_s \cos(\omega_s t) \\
 &\quad + V_v \cos(\omega_v t) V_{sc} \cos(\omega_{sc} t) V_s \cos^3(\omega_s t)] + \dots \quad (B.10)
 \end{aligned}$$

Since

$$\cos^3(\omega t) = \frac{1}{4} \cos(\omega t) - \frac{1}{4} \cos(3\omega t)$$

it follows that

$$\begin{aligned}
 i_{A5} &= 20/16 G_5 [V_v^3 V_{sc} V_s + V_v V_{sc}^3 V_s + V_v V_{sc} V_s^3] \\
 &\quad \times \cos(\omega_v \pm \omega_{sc} \pm \omega_s)t \quad (B.11)
 \end{aligned}$$

B.3 PREDICTION OF I.M. DISTORTION FOR A THOMSON CSF TYPE TH382 POWER TETRODE

B.3.1 Constant Current and Mutual Characteristics

Constant current characteristics of a typical power tetrode, the Thomson CSF TH382, used for common amplification of the vision and sound signal at a peak sync power level of 5.25 kW into 50 Ω , are shown in Fig. B.1 overleaf. Assuming

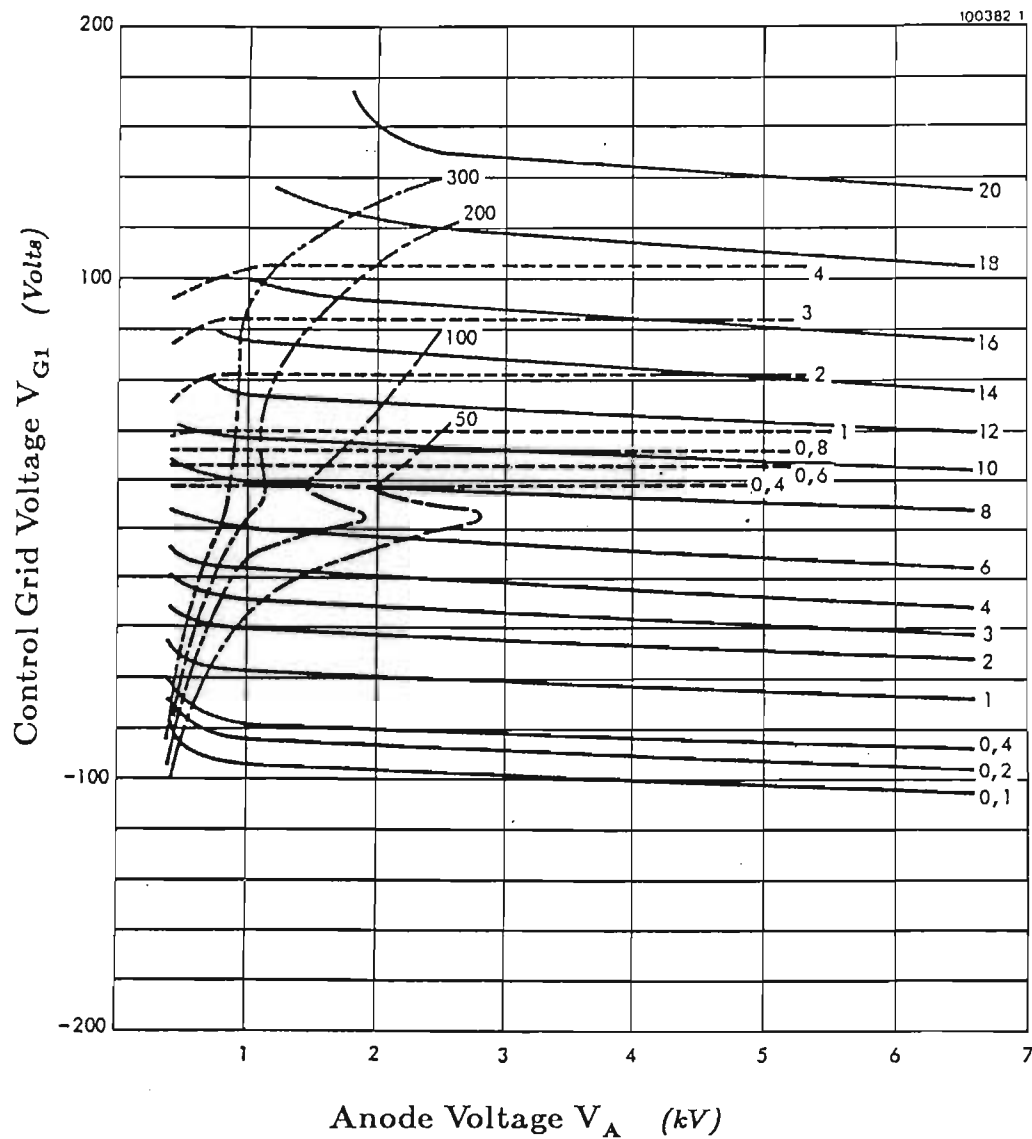


Fig. B.1 Thomson CSF TH382 Power Tetrode
Anode Characteristic
Screen Grid Voltage $V_{G2} = 600$ Volts

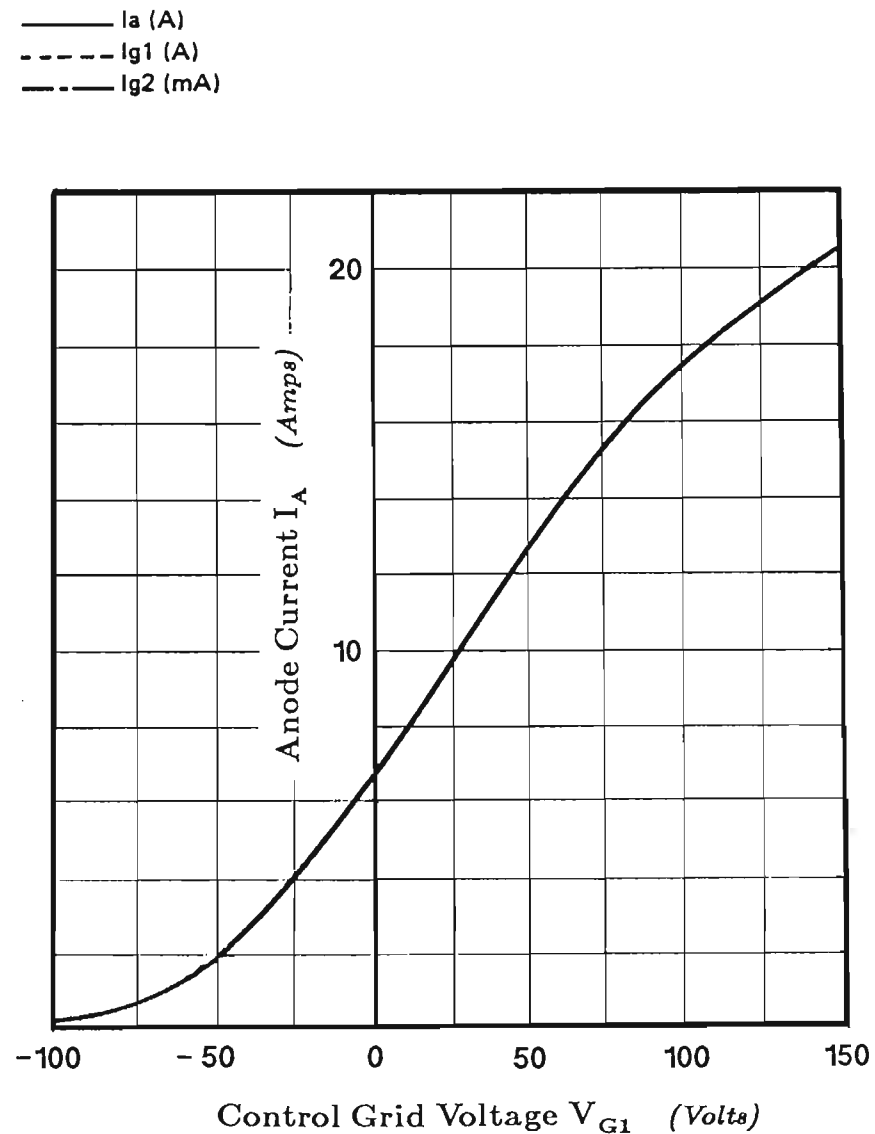


Fig. B.2 Thomson CSF TH382 Power Tetrode
Mutual Characteristic
Anode Voltage $V_A = 5500$ Volts

an anode voltage of 5,5 kV, the intercepts on these constant current curves with the vertical line at 5,5 kV define the mutual transfer characteristic which is plotted on Fig. B.2 on the same page.

B.3.2 Transfer Characteristic Modelling

Table B.2 lists selected data pairs for the TH382 power tetrode mutual characteristic taken from Fig. B.3.

Table B.2

TH382 Power Tetrode Transfer Characteristic

Data pairs taken from Fig. B.3

Anode Voltage $V_A = 5,5 \text{ kV}$

Screen Grid Voltage = 600 V

I_A	0,1	0,2	0,4	1	2	3	4	5	<i>Amps</i>
V_G	-162,5	-144,5	-125,5	-108,5	-92,5	-75,5	-57	-37,5	<i>Volts</i>
I_A	6	7	8	9	10	11	12	13	<i>Amps</i>
V_G	-8,5	1	10	18	27	34,5	43	51,5	<i>Volts</i>
I_A	14	15	16	17	18	19	20	20,98	<i>Amps</i>
V_G	60	68,5	80	92,5	108	122,5	140	157	<i>Volts</i>

For a modulated TV carrier wave, peak sync corresponds to 100% of carrier amplitude, the "black" level to 76% and "white" level to 20%. With the anode current designated as I_A , current values corresponding to various power levels may be determined as follows.

Two TH382 power tetrodes are assumed to be used in a "linear" Class B push-pull amplifier stage with an efficiency of 70%. For the specified 5,25 kW peak sync power delivered to the 50 Ω load, 7,5 kW must be produced by the tetrodes at their anodes. This is the reference power, which means a peak anode current of

$$I_{A\ 100\%} = \sqrt{\frac{7500}{50}} \times \sqrt{2} \text{ A} \quad (\text{B.12})$$

$$= 17,32 \text{ A rms} \quad (\text{B.13})$$

and

$$I_{Ap\ 20\%} = 3,464\ A\ peak \quad (B.14)$$

From the data in Table B.2:

$$I_{Ap\ 100\%} = 17,32\ A\ peak \quad \rightarrow \quad V_{Gp\ 100\%} = +97,0\ V \quad (B.15)$$

and

$$I_{Ap\ 20\%} = 3,46\ A\ peak \quad \rightarrow \quad V_{Gp\ 20\%} = -33,0\ V \quad (B.16)$$

The upper 80% of the vision carrier sine wave covers the grid voltage range from $-33\ V$ to $+97\ V$ which is a total of $120\ V$. For a linear grid drive signal, the maximum vision carrier amplitude of 100% is therefore $162,5\ V$. This gives the lower grid potential as $-65,5\ V$ which, together with its corresponding current of $1,1\ A$ is taken as "zero" and corresponds to the dc bias point for tetrode. By assuming typical push-pull operation with current sharing at low levels (Class AB), the amplifier mutual (or transfer) characteristic is "linearised" so that the effective "cross-over" point corresponds to $-65,5\ Volts$ and $0,0\ Amps$.

Table B.3 shows the mutual characteristic of Fig. B.2 with origin shifted to $-65,5\ V$. All data pairs have $+65,5\ V$ added to their voltage value so that the $10\ A$, $27\ V$ pair becomes the $10\ A$, $92,5\ V$ pair in Table B.3. Each tetrode sees one half of the applied grid drive voltage, and the characteristic is mirrored about the shifted "zero" to represent Class B operation. A peak drive voltage of $162,5\ V$ is required to achieve a peak anode current of $17,32\ A$ in each tetrode.

Table B.3

Symmetrical TH382 Power Tetrode Transfer Characteristic

65,5 V added to voltage values in Table B.2

Negative data is mirror image of positive half

Anode Voltage $V_A = 5,5\ kV$

Screen Grid Voltage = $600\ V$

I_A	-17,32	-16	-14	-12	-10	-8	-6	-4	-2	<i>Amps</i>
V_G	-162,5	-144,5	-125,5	-108,5	-92,5	-75,5	-57	-37,5	-15,5	<i>Volts</i>
I_A	0									<i>Amps</i>
V_G	0									<i>Volts</i>
I_A	2	4	6	8	10	12	14	16	17,32	<i>Amps</i>
V_G	15,5	37,5	57	75,5	92,5	108,5	125,5	144,5	162,5	<i>Volts</i>

The "least squares" technique described in Section E.6 of Appendix E was used to fit a polynomial to the data in Table B.3 and evaluate the coefficients G_3 and G_5 . The values obtained were:

$$G_3 = 1,123521 \times 10^{-6} S \quad (B.17)$$

and

$$G_5 = -3,600811 \times 10^{-11} S \quad (B.18)$$

For a three tone test the sound carrier is set at -10 dBp or 31,62% of peak sync amplitude, which is 51,38 V. The unmodulated vision carrier amplitude (which defines the luminance level) and the chrominance modulation amplitude within each colour bar are given in Tables B.4 and B.5 respectively. Table B.6 contains the modulation index "m" for the chrominance signal within each bar, and the corresponding sideband amplitudes as a percentage of peak sync signal. These sideband amplitudes are the product of "m" and the unmodulated vision carrier amplitude within that bar. Since the vision carrier is used in the definition of the modulation index, sideband amplitudes are simply half the chrominance modulation amplitude.

Table B.4

Peak Vision Carrier Amplitude (Unmodulated)
Expressed as a percentage of peak sync amplitude
with 100% = 162,5 Volts
Input signal is a 100-0-75-0 colour bar

Colour	V_V = Peak Vision Carrier Amplitude (Unmodulated)	V_G (Volts)
Yellow	$\frac{1}{2} (57,6 - 20)\% + 20\% = 38,80\%$	63,05
Cyan	$\frac{1}{2} (73,12 - 20)\% + 20\% = 46,56\%$	75,66
Green	$\frac{1}{2} (76,16 - 27,2)\% + 27,2\% = 51,68\%$	83,98
Magenta	$\frac{1}{2} (83,44 - 33,84)\% + 33,84\% = 58,64\%$	95,29
Red	$\frac{1}{2} (90 - 36,72)\% + 36,72\% = 63,36\%$	102,96
Blue	$\frac{1}{2} (90 - 52)\% + 52\% = 71,00\%$	115,38
Burst	$\frac{1}{2} (88 - 64)\% + 64\% = 76,00\%$	123,50

Table B.5Peak chrominance modulation amplitude in (*Volts*) andPercentage of peak sync with 100% = 125,6 *Volts*

Input signal is a 100–0–75–0 colour bar

Colour	V_{SCM} = Chrominance Modulation %	(Volts)
Yellow	$\frac{1}{2} (57,6 - 20)\% = 18,80\%$	30,55
Cyan	$\frac{1}{2} (73,12 - 20)\% = 26,56\%$	41,54
Green	$\frac{1}{2} (76,16 - 27,2)\% = 24,48\%$	39,78
Magenta	$\frac{1}{2} (83,44 - 33,84)\% = 24,80\%$	50,64
Red	$\frac{1}{2} (90 - 36,72)\% = 26,64\%$	43,29
Blue	$\frac{1}{2} (90 - 52)\% = 19,00\%$	30,88
Burst	$\frac{1}{2} (88 - 64)\% = 12,00\%$	19,50

Table B.6Peak chrominance sideband amplitude V_{SC} in *Volts* andPercentage of peak sync with 100% = 162,5 *Volts*

and Modulation Index "m"

Input signal is a 100–0–75–0 colour bar

Colour	m	V_{SC} %	V_{SC} (<i>Volts</i>)
Yellow	0,4845361	9,40	15,28
Cyan	0,5489691	13,28	21,58
Green	0,4736842	12,24	19,89
Magenta	0,4229195	12,40	20,15
Red	0,4204545	13,32	21,65
Blue	0,2676056	9,50	9,75
Burst	0,1578947	6,00	7,54

B.4 I.M. DISTORTION POWER AMPLITUDES

Having modelled the transfer characteristic for the TH382 tetrode, and determined the coefficients G_3 and G_5 , signal voltages were calculated for each colour bar. These signal voltages are listed in Table B.7 below.

Table B.7
Peak grid drive video signal component amplitudes
Peak Sync Power = 7,5 kW into 50 Ω or 0 dBp

Colour	Signal Voltages (Volts)		
	V_v	V_{sc}	V_s
Yellow	63,05	15,28	51,35
Cyan	75,66	21,58	51,35
Green	83,98	19,89	51,35
Magenta	95,29	20,15	51,35
Red	102,96	21,65	51,35
Blue	115,38	15,44	51,35
Burst	123,50	9,75	51,35

The voltages in Table B.7 above were used to calculate the the third and fifth order anode current distortion components shown in Table B.8 overleaf using the equations summarised below:

3rd Order Component Amplitude:

$$I_{3rd} = 1,5 G_3 [V_v V_{sc} V_s] \text{ Amps} \quad (\text{B.19})$$

peak, and hence, for a 50 Ω load

$$P_{3rd} = 25(I_{3rd})^2 \text{ Watts} \quad (\text{B.20})$$

5th Order Component Amplitude:

$$A_{5th} = 1,25 G_5 [V_v^3 V_{sc} V_s + V_v V_{sc}^3 V_s + V_v V_{sc} V_s^3] \text{ Amps} \quad (\text{B.21})$$

peak, and hence, for a 50 Ω load

$$P_{5th} = 25(I_{5th})^2 \text{ Watts} \quad (B.22)$$

Total Power:

$$P_{tot} = P_{3rd} + P_{5th} \text{ Watts} \quad (B.23)$$

Reference Power:

$$P_{ref} = 7500 \text{ Watts} \quad (B.24)$$

Power Ratio:

$$PR = 10 \log [P_{nth}/P_{ref}] \text{ dBp} \quad (B.25)$$

Table B.8

Power Developed in a 50 Ohm Load
by Anode Current Components at Harmonics of f_{IM}
Expressed both in *mW* and *dBp*

Peak Sync Power = 7,5 kW into 50 Ω or 0 dBp

Polynomial Coeffs: $G_3 = 1,123521 \times 10^{-6} S$ $G_5 = -3,600811 \times 10^{-11} S$

Colour	P_{3rd}		P_{5th}		P_{tot}	
	(<i>mW</i>)	(<i>dBp</i>)	(<i>mW</i>)	(<i>dBp</i>)	(<i>mW</i>)	(<i>dBp</i>)
Yellow	34,30	-53,40	5,81	-61,11	40,11	-52,72
Cyan	98,59	-48,81	27,74	-54,32	126,33	-47,74
Green	103,19	-48,61	37,90	-52,96	141,08	-47,26
Magenta	135,35	-47,40	72,36	-50,16	208,71	-45,56
Red	183,68	-46,11	124,60	-47,80	308,28	-43,86
Blue	117,32	-48,06	111,00	-48,30	228,32	-45,17
Burst	53,63	-51,46	62,63	-50,78	116,25	-48,10

Distortion values in Table B.8 are also expressed in *dB* relative to Cyan as reference in Table B.9 to show how the colour bars vary from the three tone test values that correspond closely to Cyan.

Table B.9

Peak Distortion Powers for each Colour Bar
 Expressed relative to Cyan as reference at 0 dB
 Peak Sync Power = 7,5 kW into 50 Ω

Colour	Distortion Powers Relative to Cyan (dB)		
	P _{3rd}	P _{5th}	P _{tot}
Yellow	-4,59	-12,30	-4,98
Cyan	0,00	0,00	0,00
Green	0,20	-4,15	0,48
Magenta	1,41	-1,35	2,18
Red	2,70	1,01	3,88
Blue	0,75	0,51	2,57
Burst	-2,65	-1,97	-0,36

Table B.10 records the calculated third and fifth order distortion levels, the "total" power as the sum of the two, and the error made in equation (B.2) by neglecting the fifth order power contribution.

Table B.10

Third Order, Fifth Order and Total Distortion Power
 and the Error in the Third Order Approximation
 due to neglecting the Fifth Order Contribution

Distortion Colour	P _{3rd} (dBp)	P _{5th} (dBp)	P _{tot} (dBp)	Error (dB)
Yellow	-53,40	-61,11	-52,72	-0,68
Cyan	-48,81	-54,32	-47,74	-1,07
Green	-48,61	-52,96	-47,26	-1,35
Magenta	-47,40	-50,16	-45,56	-1,84
Red	-46,11	-47,80	-43,86	-2,25
Blue	-48,06	-48,30	-45,17	-2,89
Burst	-51,46	-50,78	-48,10	-3,36

If all the signal levels are reduced by 25% to 75% of those values required to produce 7,5 kW peak sync power, the reduced distortion levels recorded in Table B.11 result.

Table B.11

Third Order, Fifth Order and Total Distortion Power
at reduced signal level of 75% or 121,9 V
Peak Sync Power is reduced to 4,219 kW
and the Error in the Third Order Approximation
due to neglecting the Fifth Order Contribution

Distortion Colour	P_{3rd} (dBp)	P_{5th} (dBp)	P_{tot} (dBp)	Error (dB)
Yellow	-59,64	-72,35	-59,41	-0,23
Cyan	-55,06	-65,56	-54,69	-0,37
Green	-54,86	-64,20	-54,38	-0,48
Magenta	-53,65	-61,40	-52,98	-0,67
Red	-52,36	-59,04	-51,51	-0,85
Blue	-54,30	-59,54	-53,16	-1,14
Burst	-57,70	-62,03	-56,34	-1,36

B.5 CONCLUSIONS

Third Order Approximation: From both Tables B.10 and B.11 it is clear that the third order approximation to the polynomial in equation (B.2) is not valid for the TH382 tetrode when operating at the two specified output power levels.

Three Tone Test (3TT) Results: Cyan corresponds closely to the signal amplitude combination used for the 3TT. From Table B.7 the third and fifth order distortion components of -48,81 and -54,32 dBp respectively show that the SABC requirement for I.M. distortion levels to be below -53 dBp is only met by the fifth order component. Their combined distortion power of -47,74 dBp,

however, is well above the limit. Distortion limits are exceeded in all the remaining test regions, with Red as the worst case at $-43,86 \text{ dBp}$ and Yellow the best at $-52,72 \text{ dBp}$. A standard 3TT therefore does not produce results which are definitive of the actual amplifier I.M. distortion performance as the poor performance within the Magenta, Red and Blue colour bars is not revealed.

No general conclusion can be reached with regard to the third order approximation in equation (B.2) for modelling power devices, however, as the polynomial coefficients G_r are both device and power level dependent. Mutual characteristic data used in this simulation was read from curves, and small errors could lead to significant changes in the values of polynomial coefficients G_3 and G_5 . If these predictions are representative of device performance then it is evident that the TH382 tetrode cannot be used successfully in a common amplification stage without the inclusion of a pre-corrector, unless the power level is reduced considerably. In Table B.11, Magenta and Red both fail to make the -53 dBp distortion limit.

APPENDIX C

Phase Lock Loop Theory and CMOS CD4046 Phase Lock Loop Phase Comparator Circuits: Detailed Analysis of Operation

C.1 PHASE LOCK LOOP THEORY

C.1.1 Introduction to Phase Lock Loop Theory

A Block Diagram of a PLL, which includes a divide-by-N counter in the feedback path (with $N=10$ in this application), is shown in Fig. C.1 overleaf.

The input signal applied to the phase detector is a digital pulse waveform, which may be represented by its Fourier series as

$$v_i(t) = V_i \sin(\omega_i t) + \text{harmonics of } \omega_i \quad (\text{C.1})$$

If the counter output signal is a square wave, it may similarly be represented as

$$v_k(t) = V_k \sin(\omega_k t) + \text{ODD harmonics of } \omega_k \quad (\text{C.2})$$

Assuming the phase detector to be a simple linear multiplier, the product of these two waveforms will produce "sum" and "difference" frequencies at the phase detector output. Those components due to the harmonics will be removed by the low pass filter if the cut-off frequency $\omega_c \ll \omega_i$. Hence we need only consider the fundamentals of both the input and counter output waveforms to describe the operation of the loop. The input signal fundamental frequency component may be represented by

$$v_i(t) = V_i \sin(\omega_i t)$$

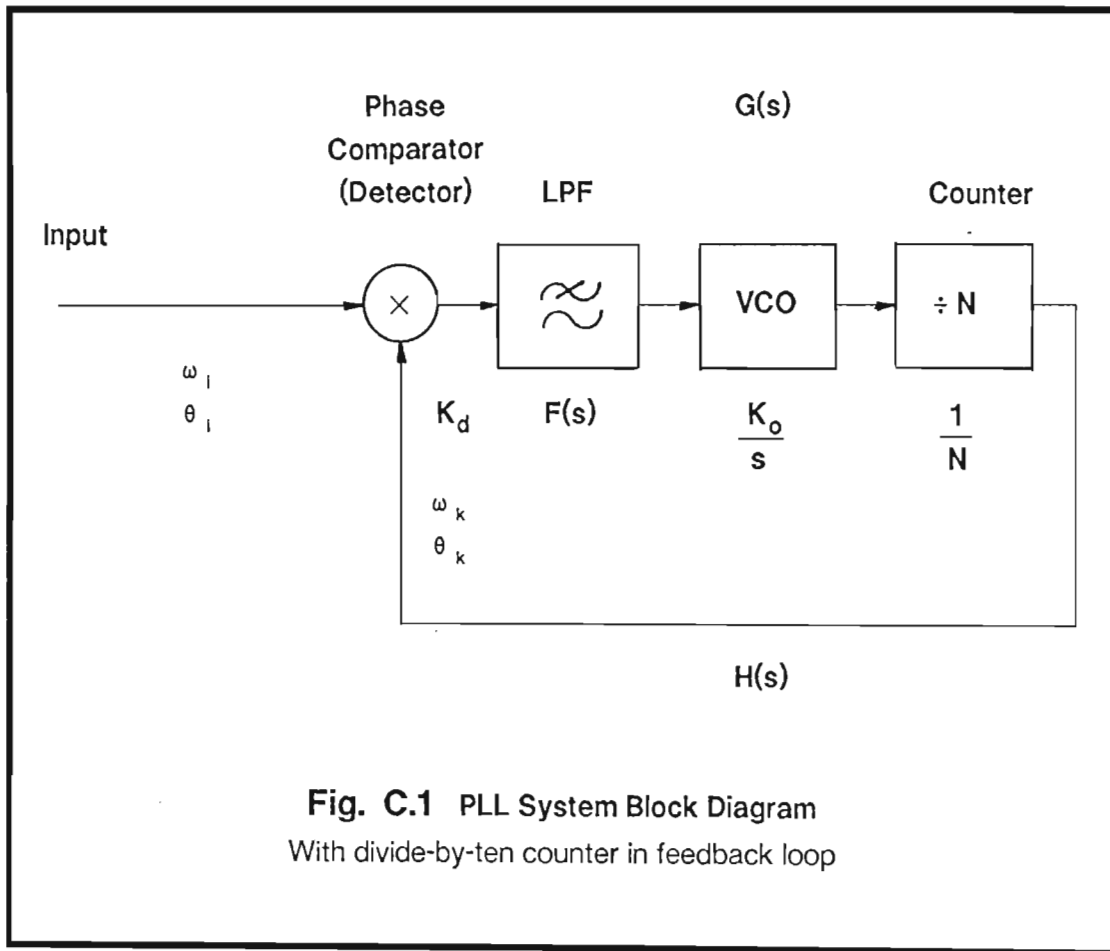
which is in phase with the input rectangular pulses, while the counter output fundamental is

$$v_k(t) = V_k \sin(\omega_k t)$$

which is in phase with the counter output pulses. The counter output fundamental frequency is

$$\omega_k = \frac{\omega_o}{N} \quad (C.3)$$

where ω_o is the VCO frequency.



For an unlocked loop:

$$\omega_k \neq \omega_i \quad (C.4)$$

When the phase detector is a linear multiplier, the detector output signal will be

$$v_d(t) = KV_i V_k \sin \omega_i t \sin \omega_k t \quad (C.5)$$

where K is a constant. It follows that

$$\begin{aligned} v_d(t) &= 0,5 KV_i V_k \cos(\omega_i - \omega_k)t + \text{components removed by LPF} \\ &= K_d \cos(\omega_i - \omega_k)t \end{aligned} \quad (C.6)$$

where K_d is the phase comparator gain. K_d is a constant only when $v_i(t)$ and $v_k(t)$ are amplitude limited before application to the phase detector. In this design both signals are LOGIC level signals and thus have constant amplitudes determined by the supply voltages V_{DD} and V_{SS} and designated V_L . Hence only the phase or frequency differences will matter. The external input signal and counter output fundamental components may also be written respectively in terms of instantaneous phase θ_i as

$$v_i(t) = V_L \sin \theta_i$$

and

$$v_k(t) = V_L \sin \theta_k$$

Both above signals are in phase with their respective pulse waveforms. Note that θ_x actually represents the time function $\theta_x(t)$.

Define Phase Error θ_e

$$\theta_e = \theta_i - \theta_k \quad (C.7)$$

where θ_e is the phase angle between the counter output signal $v_k(t)$ and the external input signal $v_i(t)$ waveforms once lock occurs. In equation (C.45), it is shown that for either phase comparator in the CD4046 CMOS PLL chip the relationship between input phase difference and output voltage is linear, so that

$$v_d(t) = K_d \theta_e \quad (C.8)$$

In the filter pass band, the low pass transfer function $F(s)$ becomes

$$F(s) = 1 \quad (C.9)$$

so that the filter output from equations (C.6) and (C.9) is

$$v_f(t) = K_d \cos(\omega_i - \omega_k)t$$

This low beat frequency may drive ω_k towards ω_i in order to achieve lock. After lock is achieved the counter output frequency is identical to the input frequency, ie.

$$\omega_k = \omega_i \quad (C.10)$$

C.1.2 Derivation of the Phase Lock Loop System Transfer Function STF(s)

During transient conditions the deviation $\Delta\omega$ of the VCO output frequency from its free running value ω_f is given by

$$\begin{aligned}\Delta\omega &= \omega_o - \omega_f \\ &= K_o v_f(t)\end{aligned}\tag{C.11}$$

where K_o is the VCO gain factor relating the change in output frequency to the change in input voltage.

Since instantaneous frequency is defined as the rate of change of phase we may write

$$\frac{\partial \theta_o}{\partial t} = \omega_o$$

The rate of change of VCO phase is also given by

$$\frac{\partial \theta_o}{\partial t} = K_o v_f(t)\tag{C.12}$$

Taking Laplace Transforms of both sides of equation (C.12), and assuming zero initial conditions to obtain the transfer function, we get:

$$s \theta_o(s) = K_o V_f(s)\tag{C.13}$$

The gain of the VCO can thus be expressed in the frequency domain as the ratio

$$\frac{\theta_o(s)}{V_f(s)} = \frac{K_o}{s}\tag{C.14}$$

The counter output frequency can be obtained by dividing the VCO output frequency by N , which gives:

$$\begin{aligned}\frac{s \theta_o(s)}{N} &= \frac{K_o V_f(s)}{N} \\ &= s \theta_k(s)\end{aligned}\tag{C.15}$$

It is clear from the block diagram of Fig. C.1, and basic feedback theory, that the System Transfer Function $STF(s)$ can be expressed as:

$$\begin{aligned}
 STF(s) &= \frac{\theta_k(s)}{\theta_i(s)} \\
 &= \frac{\text{forward gain}}{1 + \text{loop gain}} \\
 &= \frac{G(s)}{1 + G(s)H(s)} \tag{C.16}
 \end{aligned}$$

In this configuration

$$\begin{aligned}
 G(s) &= \frac{K_o K_d F(s)}{Ns} \\
 &= \frac{K}{s}
 \end{aligned}$$

and

$$H(s) = 1$$

so that

$$STF(s) = \frac{K_o K_d F(s)/N}{s + K_o K_d F(s)/N} \tag{C.17}$$

The System Error Function $SEF(s)$ is given by:

$$\begin{aligned}
 SEF(s) &= \frac{\theta_e(s)}{\theta_i(s)} \\
 &= \frac{1}{1 + \text{loop gain}} \\
 &= \frac{1}{1 + G(s)H(s)} \tag{C.18}
 \end{aligned}$$

The expressions in equations (C.17) and (C.18) find application in an examination of the stability of PLL feedback systems and the determination of the final phase error of these systems under transient input signal conditions respectively.

C.2 PHASE LOCK LOOP FEEDBACK SYSTEM STABILITY CONSIDERATIONS

C.2.1 A System Analysis Problem

Analysis of the digital PLL, using the CMOS CD4046 chip with passive lag-lead filter and PC-II, a digital $\div N$ counter and passive lag-lead filter within the feedback loop, has been performed by Rohde [54]. His analysis follows other typical linear PLL analyses [47, 48] in which the sampling phase comparator PC-II treated as a linear multiplier. Observed closed loop transient behaviour of the PLL approaches closely to that predicted by the linear theory.

System transient behaviour may best be predicted from root locus diagrams which necessitate an analysis of the system to determine its transfer function $STF(s)$ in the frequency domain. A root locus plot for varying loop gain makes rapid assessment of system transient behaviour possible because system damping decreases as the complex poles of $STF(s)$ approach closer to the $j(\omega)$ axis.

When estimating the maximum phase, or timing, error of the sample timing circuit a time domain approach to the filter analysis is helpful. In this regard it is important to note that the PLL system operates under open loop conditions for most of the time with PC-II output in its high impedance, or open circuit, state.

C.2.2 The Root Locus Approach

System stability is considered briefly in this section using the "root locus" approach which provides a pictorial explanation of system transient behaviour. The relationship between loop gain (or return ratio) and the system pole positions, which determine system damping and hence ringing and overshoot, are clearly shown for different low pass filter configurations within the feedback loop.

The **TYPE** of a closed loop system refers to the number of poles of the loop gain function $G(s)H(s)$ located at the s-plane origin, while the **ORDER** refers to the highest degree of the characteristic equation (CE) given by

$$1 + G(s)H(s) = 0 \quad (C.19)$$

The roots of this CE, corresponding to the poles of the system transfer function, vary with the loop gain factor K where

$$K = \frac{K_o K_d F(0)}{N} \quad (C.20)$$

and $F(0)$ is the dc response defined for four different filters in Figs. C.2 (a) through to C.5 (a) that follow. K_o and hence K varies with the choice of filter, VCO timing component values and make of chip. As K varies so the roots of the CE move along loci that may easily be plotted using techniques described by Kuo [49], Luyben [106] and Nash [52]. Each root locus plot begins at a pole with $K = 0$ and ends at a zero with $K = \infty$. The loci move towards zeros and away from poles as loop gain K increases. A point on the root locus diagram at which two loci meet, corresponding to a pair of identical real roots, is called the "centre of gravity". Locus diagrams for the four filters considered are presented in Figs. C.2 (b) through to C.5 (b) together with an explanation of their main features.

A second order system was used for the design, it being adequate for the task in hand and producing a CE of the following form:

$$s^2 + 2\zeta\omega_n s + \omega_n^2 = 0 \quad (C.21)$$

Closed loop performance depends markedly on the low pass filter used. By comparing coefficients of the CEs with those of the general expression in equation (C.21) the system damping factor ζ and the natural resonant frequency ω_n may be determined for these various filter configurations and are included in the analyses that follow. Some important parameter inter-relationships for complex conjugate pairs of roots have previously been established in Chapter 2, section 2.3.

C.2.3 Type 1 Second Order Systems using a Passive R-C Low Pass Filter

The single break frequency ω_1 of this simple R-C filter causes the system ω_n and ζ to be interdependent, which is a serious disadvantage to the designer.

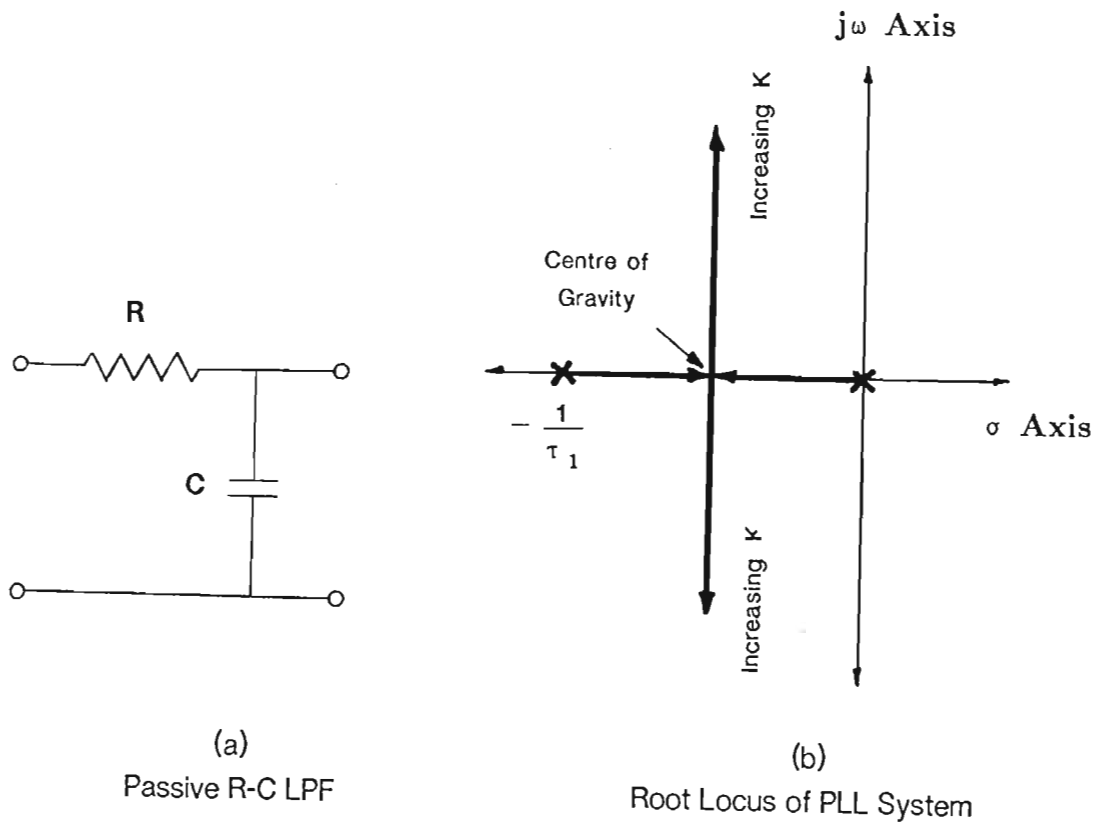


Fig. C.2 Type 1 Second Order System

The R-C filter transfer function is

$$F(s) = \frac{1}{s\tau_1 + 1} \quad (\text{C.22})$$

with

$$\tau_1 = RC \text{ seconds} \quad (\text{C.23})$$

At $s=0$,

$$F(0) = 1$$

giving a loop gain K of

$$K = \frac{K_o K_d}{N}$$

The System CE when using the passive filter of Fig. C.2 (a) is

$$1 + \frac{K}{s(s\tau_1 + 1)} = 0$$

Hence

$$s^2 + 1/\tau_1 s + K/\tau_1 = 0 \quad (\text{C.24})$$

with poles at

$$s = \frac{-1/\tau_1 \pm \sqrt{(1/\tau_1)^2 - 4K/\tau_1}}{2} \quad (\text{C.25})$$

The centre of gravity lies on the real axis at the point where the roots have identical values and the root locus splits into two paths giving complex conjugate roots. Thus the centre of gravity occurs at

$$s = -\frac{1}{2\tau_1}$$

for a loop gain within the pass band of

$$K = \frac{1}{4\tau_1}$$

For higher values of K the roots become complex and occur in conjugate pairs. The root locus is shown in Fig. C.2 (b).

Hence the system natural resonant frequency is

$$\omega_n = \sqrt{\frac{K}{\tau_1}} \text{ rad/s} \quad (\text{C.26})$$

and the damping factor is

$$\zeta = \frac{1}{2\sqrt{K\tau_1}} \quad (\text{C.27})$$

C.2.4 Type 1 Second Order Systems using a Passive Lag-Lead Low pass Filter

The introduction of a zero via R_2 in Fig. C.3 (a) that follows gives the filter two break frequencies ω_2 and ω_3 which allow the system ω_n and ζ to be determined independently.

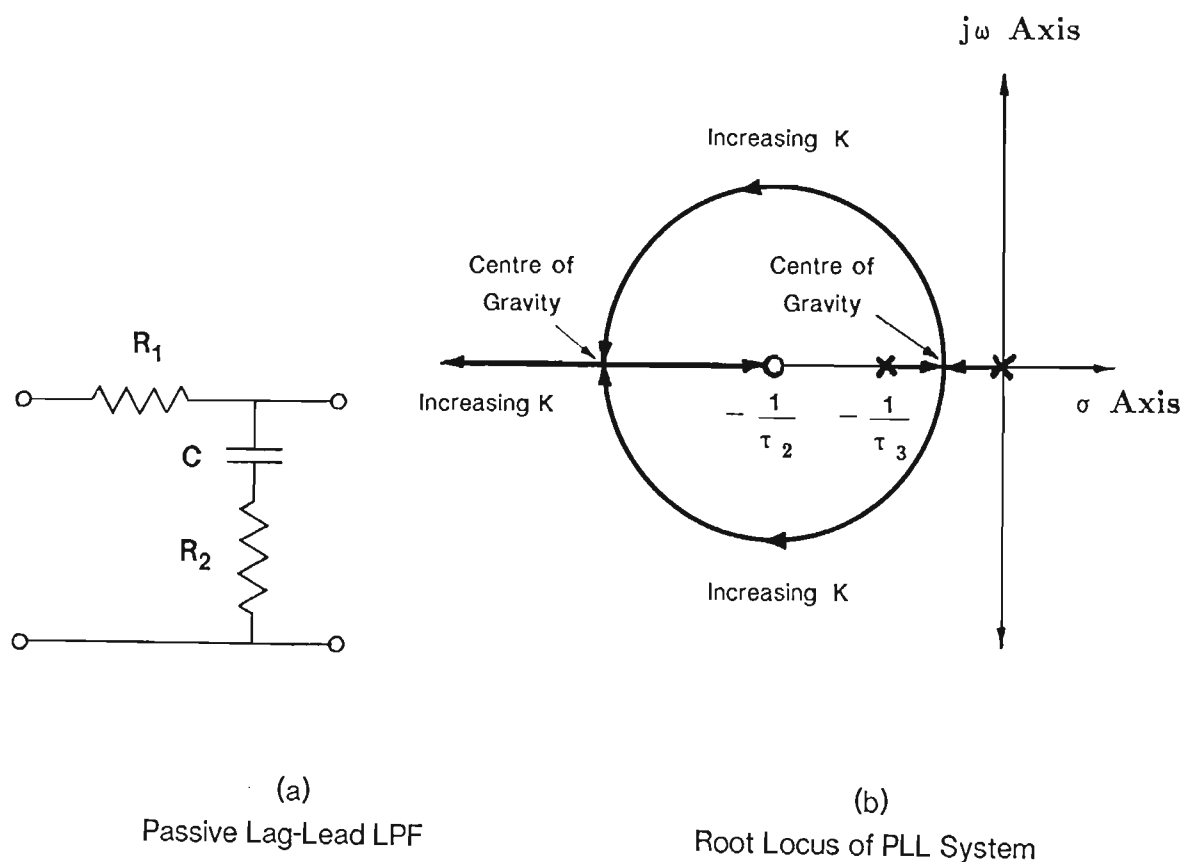


Fig. C.3 Type 1 Second Order System

The lag-lead filter transfer function is

$$F(s) = \frac{s\tau_2 + 1}{s\tau_3 + 1} \quad (\text{C.28})$$

with

$$\tau_2 = CR_2 \text{ seconds} \quad (\text{C.29})$$

$$\tau_3 = C(R_1 + R_2) \text{ seconds} \quad (\text{C.30})$$

At $s=0$,

$$F(0) = 1$$

giving a loop gain within the pass band of

$$K = \frac{K_o K_d}{N} \quad (C.31)$$

A Type 1 Second Order system was chosen incorporating the passive lag-lead filter of Fig. C.3 (a). Since τ_2 and τ_3 can be set independently via R_2 and R_1 it follows that ζ and ω_n can be chosen to give the desired response.

C.3 CMOS CD4046 PHASE LOCK LOOP

The two phase comparators within the CD4046 CMOS PLL chip are usually shown together on a single logic diagram [58]. In this appendix their circuits will be presented separately to facilitate explanation of their operation.

It is important to note that, in these comparators, **POSITIVE LOGIC** is used with the logic levels defined by the logic supply voltages as follows:

$$\begin{aligned} V_{DD} &= +5 \text{ V} \\ &= \text{LOGIC "1"} \end{aligned} \quad (C.32)$$

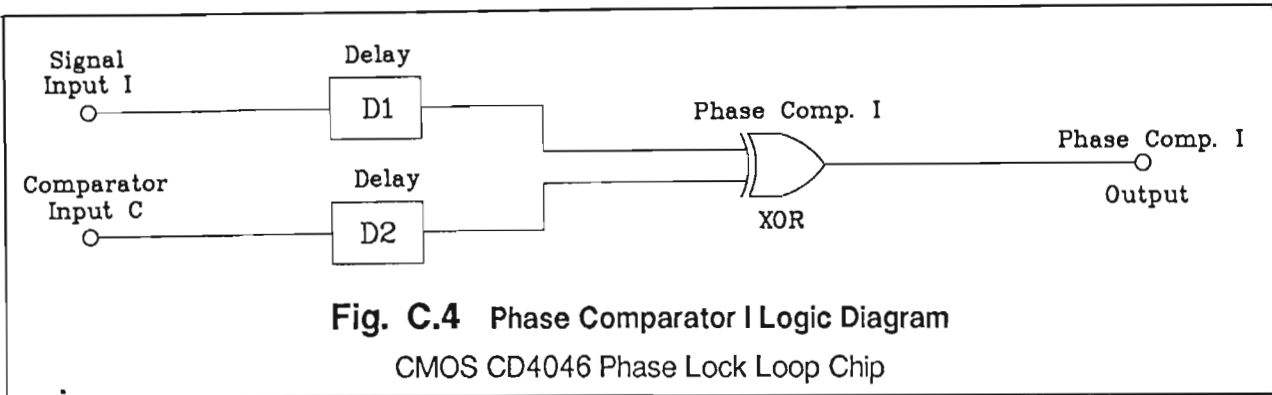
$$\begin{aligned} V_{SS} &= -5 \text{ V} \\ &= \text{LOGIC "0"} \end{aligned} \quad (C.33)$$

The signal "ground" is at zero volts, which is the supply centre connection.

C.4 CMOS CD4046 PHASE COMPARATOR I

C.4.1 Basic Operation

Phase Comparator I is a simple EXCLUSIVE-OR (XOR) gate, as is evident from the logic diagram of Fig. C.4 overleaf. Time delays D1 and D2 in the two input connections will not be considered here as they have little effect on this comparator.



The output of Phase Comparator I goes HIGH (to V_{DD}) when either input goes HIGH (but not both together), and goes LOW (to V_{SS}) when both inputs are HIGH or both inputs are LOW. When no external input signal is present the detector output follows the free running VCO output which has an even mark-to-space ratio. Average output potential under these conditions is midway between V_{SS} and V_{DD} , or zero volts, which determines the VCO free running frequency ω_f .

The output waveforms of Phase Comparator I are derived for the locked loop condition in the two timing diagrams which follow in Figs. C.5 and C.6. The comparator signals for these diagrams are defined as follows:

$I(t)$ = External input signal

$C(t)$ = Input from counter output

$O(t)$ = Comparator output signal
= $v_o(t)$

Each signal is a LOGIC level signal and swings between the limits set by the logic supply voltages specified above.

C.4.2 Phase Difference Operation

Typical operation is represented by the one set of phase comparator input and output waveforms presented on the following timing diagram, ie. Fig. C.5. Input signals have identical frequencies and a phase error (or difference) θ_e as shown. The diagram, based on exclusive-OR (XOR) logic, is self explanatory.

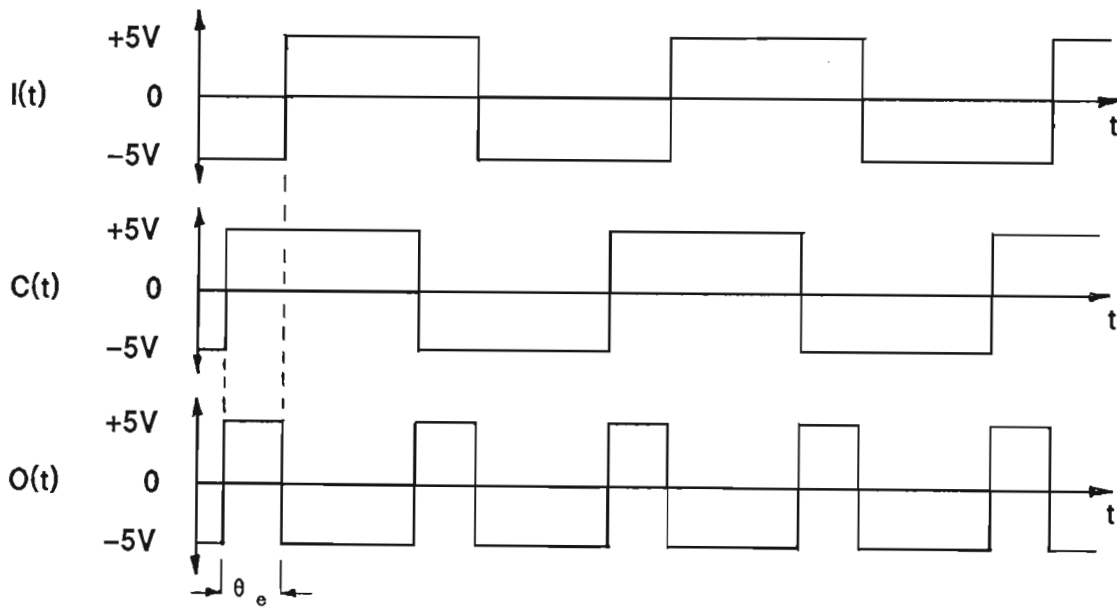


Fig. C.5 Phase Comparator I Timing Diagram

For an input phase error of θ_e

Mean output voltage v_d :

$$\begin{aligned}
 v_d &= V_{SS} + \int_0^{\theta_e} (V_{DD} - V_{SS}) dt \\
 &= \frac{\theta_e}{\pi} (V_{DD} - V_{SS}) + V_{SS}
 \end{aligned} \tag{C.34}$$

For

$$\begin{aligned}
 \theta &= 0 \\
 v_d &= V_{SS} \\
 &= -5 \text{ V}
 \end{aligned} \tag{C.35}$$

and with

$$\begin{aligned}
 \theta &= \pi \\
 v_d &= V_{DD} \\
 &= +5 \text{ V}
 \end{aligned} \tag{C.36}$$

Clearly a linear relationship exists between the phase detector mean output voltage v_d and the input phase angle error θ_e which can be expressed as:

$$v_d = K_{d1} \theta_e \quad (C.37)$$

C.4.3 Frequency Locked – not Phase Locked

The phase angle error θ_e between the external input and counter output signals under locked conditions varies with the frequency of the input signal. When the input frequency matches the free-running VCO frequency ω_f angle θ_e is 90 degrees. As the input frequency rises so the comparator mark-to-space ratio increases, thus raising the VCO control voltage in order to maintain lock. Thus θ_e increases as the frequency rises.

Alternatively, θ_e changes under locked conditions when the input frequency remains constant but the VCO free-running frequency ω_f alters for any reason, such as timing component value variations with change in ambient temperature.

In either case, the phase integrity of the sampling system is destroyed. *Such a system is frequency locked and not phase locked, and in this case “phase lock loop” is a misnomer. Consequently Phase Comparator I cannot be used in this timer application.*

C.4.4 The Problem of Harmonic Locking

Another serious problem with Phase Comparator I is its inability to distinguish between inputs harmonically related to the free-running frequency ω_f . This is illustrated in Fig. C.6, which shows the phase detector output waveform under harmonic locking conditions. Harmonic relation to other VCO frequencies would require some phase shift between the signals for locking to occur.

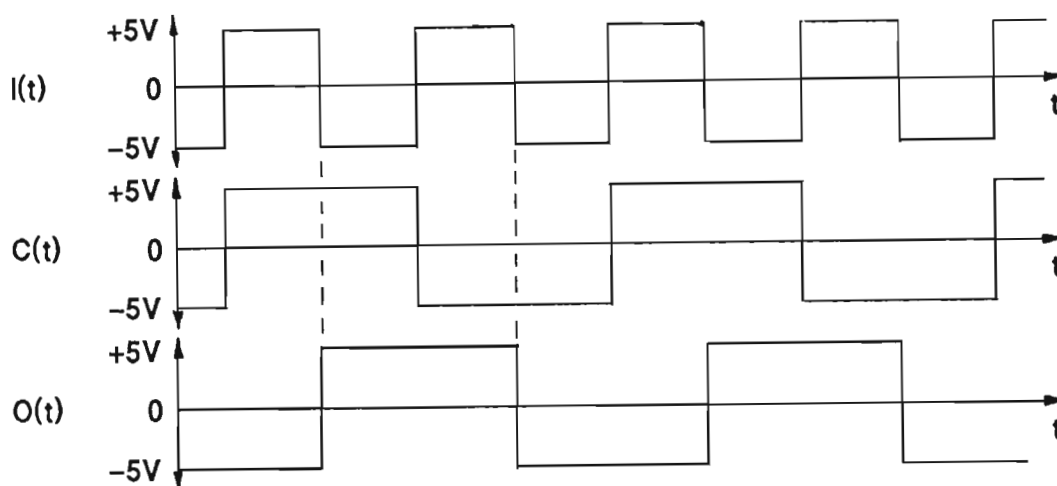


Fig. C.6 Harmonic Locking of Phase Comparator I

Input $I(t)$ is a harmonic of VCO free running frequency f_i

Such a situation could not be tolerated in the proposed timing generator because of the numerous harmonics present in both the signal input and counter output signals.

C.5 CMOS CD4046 PHASE COMPARATOR II

C.5.1 Basic Operation of Phase Comparator II

This comparator is a digital memory circuit, and the output only changes state on positive going signal transitions on either input. The memory consists of the control gate and four R-S FLIP-FLOPS shown in Fig. C.7 [58]. A tri-state output stage is driven by the memory to provide three possible comparator output states:

- (a) Output high at V_{DD} → **PMOS FET ON**
- (b) Output low at V_{SS} → **NMOS FET ON**
- (c) Output open circuit → **Both FETs OFF**

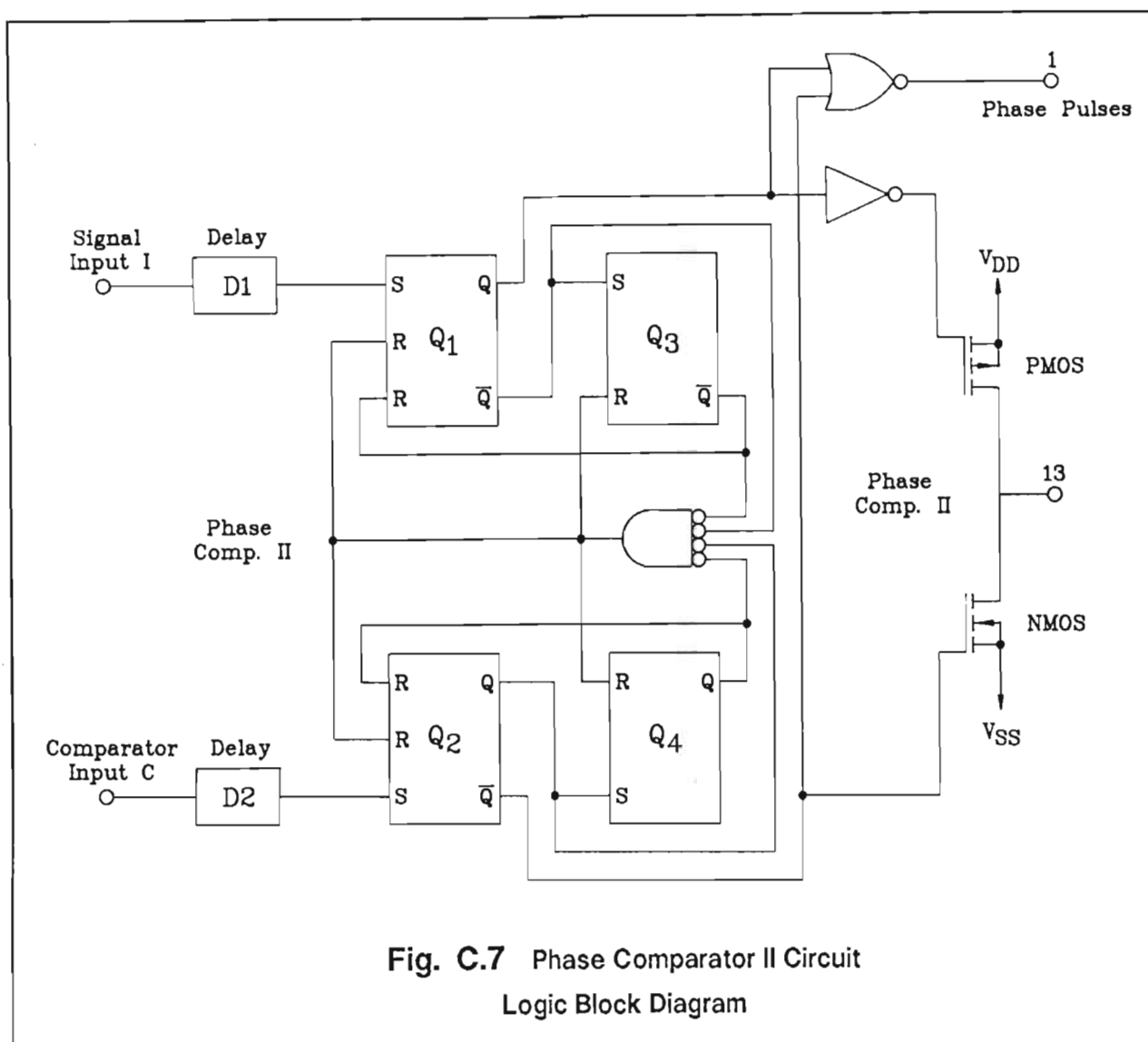


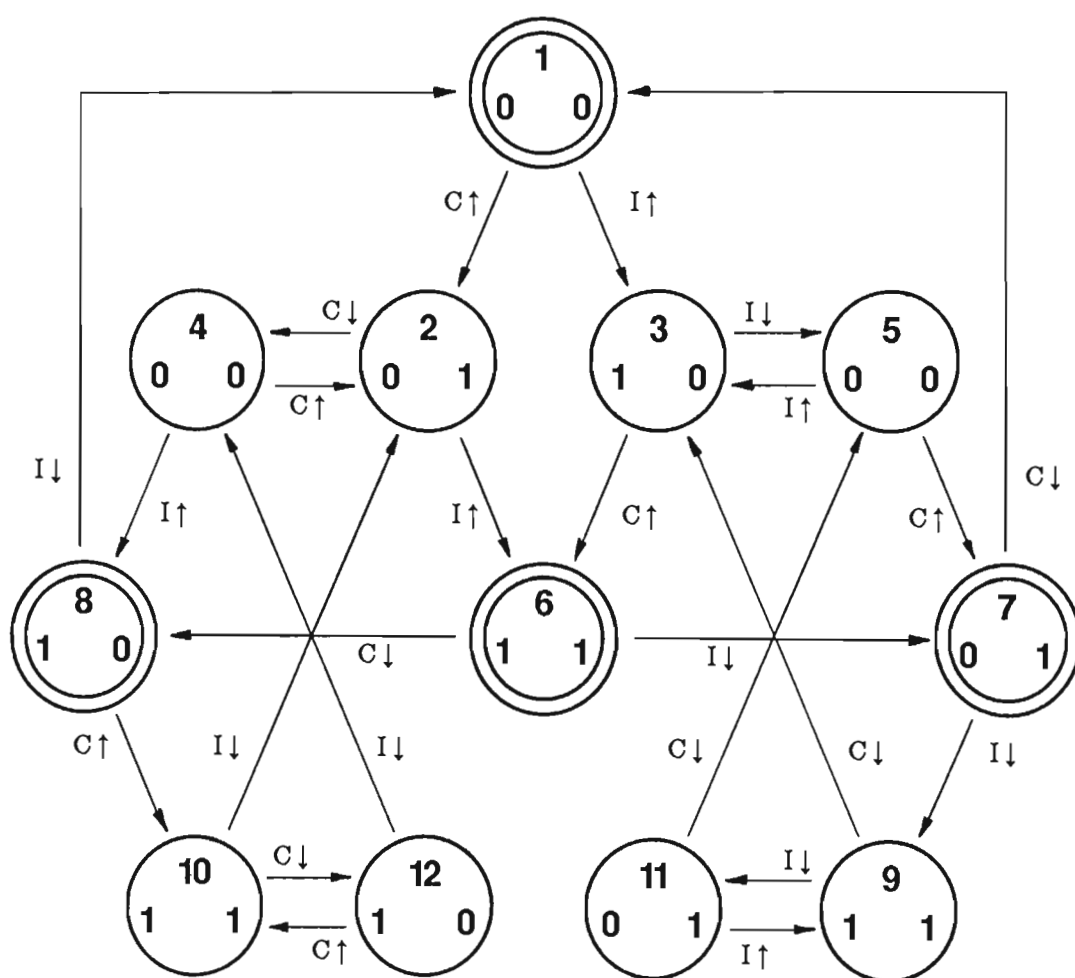
Fig. C.7 Phase Comparator II Circuit
Logic Block Diagram

The behaviour of Phase Comparator II can be represented in simple form by the State Diagram in Fig. C.8. A detailed picture of its operation, however, can only be seen from the Flip-flop State Transition Diagram in Fig. C.9. Note that the AND gate providing the delayed reset "DR" to all four flip-flops provides one gate delay, which is essential for stable operation. As inputs, the AND gate has the inverted outputs of the flip-flops which are again inverted at the AND gate input. This means that delayed RESET DR is given by:

$$DR = \overline{Q_1 \cdot Q_2 \cdot Q_3 \cdot Q_4} \quad (C.38)$$

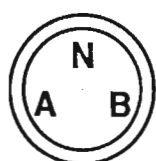
A RESET results in a high impedance state with both MOS devices OFF.

The path traced by the operation of this phase comparator can be determined by noting the sequence of LOGIC level changes of the two inputs $I(t)$ and $C(t)$. For convenience it will be assumed that the initial state corresponds to state number 1. From state 1 a $C \uparrow$ transition would take operation to state 2 while an $I \uparrow$ transition would lead to state 3. State 1 cannot be left when either $C \downarrow$ or $I \downarrow$ transitions occur.



NMOS "ON"

PMOS "ON"

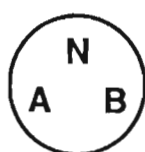


"High Z" State

N = State Number

A = State of External Input

B = State of Counter Output



Mosfet "ON"

State Transitions

 $\uparrow = -5V \text{ to } +5V$ $\downarrow = +5V \text{ to } -5V$

I = Transition at External Input

C = Transition at Counter Output

Output Condition:

High "Z"

NMOS FET "ON"

PMOS FET "ON"

Phase Pulses "HIGH"

Phase Pulses "LOW"

State Numbers:

1,6,7 and 8

2,4,10 and 12

3,5,9 and 11

1,6,7 and 8

2,3,4,5,9,10,11 and 12

Fig. C.8 Flip Flop State Diagram for CD4046 PLL

Indicating state sequence for specified input transisions

PRESENT STATE											NEXT STATE												
Input Levels		State Number	Flip-Flop States				Ouput State			Input Change		Input Levels		State Number	Flip-Flop States				Reset	Ouput State			State Change
I	C		Q1	Q2	Q3	Q4	P	N	H	I	C	I	C		Q1	Q2	Q3	Q4		DR	P	N	
0	0	1	0	0	1	1	0	0	1		↑	0	1	2	0	1	1	1	0	0	1	0	1 → 2
0	0	1	0	0	1	1	0	0	1	↑		1	0	3	1	0	1	0	0	1	0	0	1 → 3
0	1	2	0	1	1	1	0	1	0		↓	0	0	4	0	1	1	1	0	0	1	0	2 → 4
0	1	2	0	1	1	1	0	1	0	↑		1	1		1	1	1	1	1				Unstable
												1	1		0	0	0	0	0				Unstable
												1	1	6	0	0	1	1	0	0	0	1	2 → 6
1	0	3	1	0	1	1	1	0	0	↓		0	0	5	1	0	1	1	0	1	0	0	3 → 5
1	0	3	1	0	1	1	1	0	0		↑	1	1		1	1	1	1	1				Unstable
												1	1		0	0	0	0	0				Unstable
												1	1	6	0	0	1	1	0	0	0	1	3 → 6
0	0	4	0	1	1	1	0	1	0	↑		1	0		1	1	1	1	1				Unstable
												1	0		0	0	0	0	0				Unstable
												1	0	8	0	0	1	1	0	0	0	1	4 → 8
0	0	4	0	1	1	1	0	1	0		↑	0	1	2	0	1	1	1	0	0	1	0	4 → 2
0	0	5	1	0	1	1	1	0	0		↑	0	1		1	1	1	1	1				Unstable
												0	1		0	0	0	0	0				Unstable
												0	1	7	0	0	1	1	0	0	0	1	5 → 7
0	0	5	1	0	1	1	1	0	0	↑		1	0	3	1	0	1	1	0	1	0	0	5 → 3
1	1	6	0	0	1	1	0	0	1	↓		1	1	7	0	0	1	1	0	0	0	1	6 → 7
1	1	6	0	0	1	1	0	0	1		↓	1	0	8	0	0	1	1	0	0	0	1	6 → 8
0	1	7	0	0	1	1	0	0	1	↑		1	1	9	1	0	1	1	0	1	0	0	7 → 9
0	1	7	0	0	1	1	0	0	1		↓	0	0	1	0	0	1	1	0	0	0	1	7 → 1
1	0	8	0	0	1	1	0	0	1		↑	1	1	10	0	1	1	1	0	0	1	0	8 → 10
1	0	8	0	0	1	1	0	0	1	↓		0	0	1	0	0	1	1	0	0	0	1	8 → 1
1	1	9	1	0	1	1	1	0	0		↓	1	0	3	1	0	1	1	0	1	0	0	9 → 3
1	1	9	1	0	1	1	1	0	0		↓	0	1	11	1	0	1	1	0	1	0	0	9 → 11
1	1	10	0	1	1	1	0	1	0		↓	1	0	12	0	1	1	1	0	0	1	0	10 → 12
1	1	10	0	1	1	1	0	1	0	↓		0	1	2	0	1	1	1	0	0	1	0	10 → 2
0	1	11	1	0	1	1	1	0	0		↓	0	0	5	1	0	1	1	0	1	0	0	11 → 5
0	1	11	1	0	1	1	1	0	0	↑		1	1	9	1	0	1	1	0	1	0	0	11 → 9
1	0	12	0	1	1	1	0	1	0	↓		0	0	4	0	1	1	1	0	0	1	0	12 → 4
1	0	12	0	1	1	1	0	1	0		↑	1	1	10	0	1	1	1	0	0	1	0	12 → 10

Fig. C.9 Flip Flop State Transition Diagram

Showing the edge-triggering of the Flip Flops
under specified input logic transition conditions

Paths should be traced for all possible starting points corresponding to each state number in turn to ensure that the comparator is self-starting and not prone to latching up in some initial state. Whatever the initial starting point, the comparator should quickly settle to tracing an identical path for the same input signal conditions. No such detailed analysis is attempted here.

It is important to note the time delays built into the comparator input connections. Delay D_1 in input $I(t)$ is longer than D_2 in input $C(t)$ by some two inverter propagation times.

C.5.2 Phase Difference Operation

Operation of Phase Comparator II under different error conditions is illustrated with the timing diagrams in Figs. C.10 through to C.13. Again we define the comparator input signals as:

$I(t)$ = External signal input waveform

$C(t)$ = Input waveform from counter output

$O(t)$ = Output waveform

Inputs of the same frequency but differing in phase are now applied to the comparator, and the comparator flip flop state path traced is determined for the waveforms given in Figs. C.10 through to C.13 that follow.

$$i_{ch} = \frac{V_{DD} - V_C}{R_1 + R_2} \quad (C.40)$$

and V_C is the initial voltage on capacitor C . Each contribution to the charge on C is therefore a linear function of θ_e as long as the resulting change in capacitor voltage V_C is small.

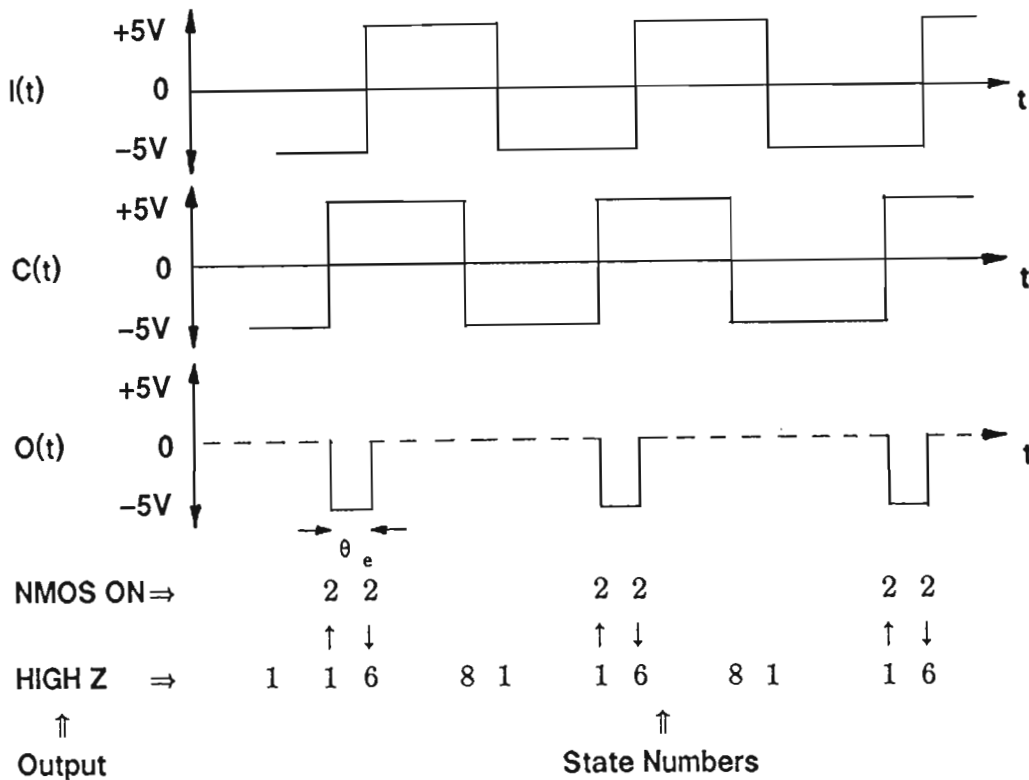


Fig. C.11 Phase Comparator II State Transition Diagram

Input wave lags counter output wave in phase by θ_e .

"Zero" on $O(t)$ corresponds to the "High Z" state.

In Fig. C.11 the NMOS device is ON for a short period corresponding to the phase difference θ_e . This will decrease the voltage stored on the timing capacitor, decreasing the VCO frequency and thus retarding the phase of the counter output pulses $C(t)$. Note that conduction for the NMOS device commences when $C(t)$ goes high, and ceases when $I(t)$ goes high. The output $O(t)$ will have the same form for $0 \leq \theta_e \leq 2\pi \text{ rad.}$

Again the mean output voltage can be determined from the average charge contributed to the filter capacitor in one cycle. Thus

Mean charge ΔQ added to capacitor C:

$$\Delta Q = \int_0^{\theta_e} i_{ch} dt \quad (C.41)$$

where

$$i_{ch} = \frac{V_{ss} - V_C}{R_1 + R_2} \quad (C.42)$$

and V_C is the initial voltage on capacitor C. Each contribution to the charge on C is therefore a linear function of θ_e as long as the resulting change in capacitor voltage V_C is small.

Introduction of the delays D1 and D2 would have no effect on the above explanations provided that their difference represents a phase angle smaller than θ_e .

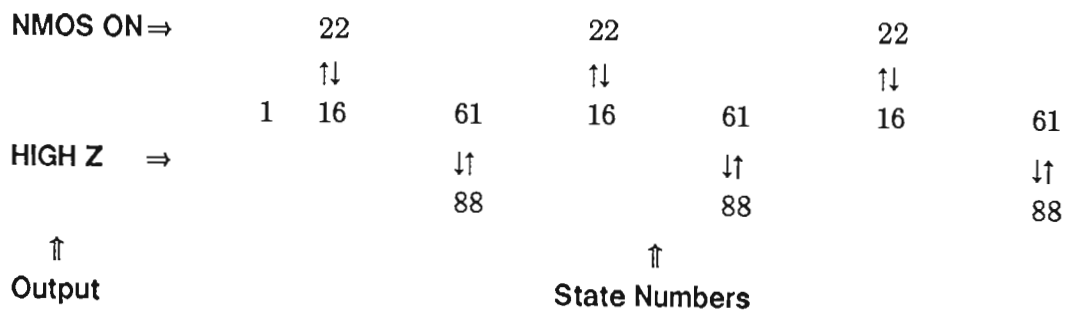
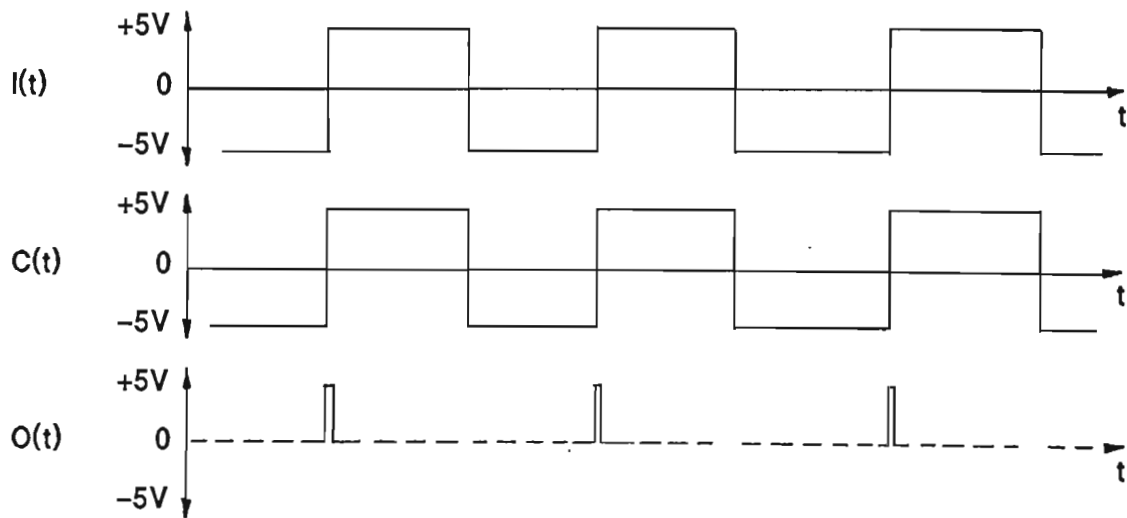


Fig. C.12 Phase Comparator II State Transition Diagram

Zero initial phase error between input and counter output waves with

$$\theta_e = 0^\circ$$

Input $I(t)$ marginally behind counter output $C(t)$ and $D1 > D2$

The state followed in the case of Fig. C.12 would be unpredictable if the wave zero crossings were exactly co-incident at the phase comparator inputs and time delays $D1$ and $D2$ did not exist. In Fig. C.12 the marginal time retardation is due to the fact that the external input $I(t)$ is delayed relative to the counter output $C(t)$ because time delay $D1 > D2$. The NMOS device thus turns ON for only a brief period so that the output state remains **HIGH Z** virtually all the time. The phase comparator is thus in a **HOLD** state. Whatever charge was on the loop filter capacitor will theoretically remain there indefinitely, and the VCO frequency will remain unchanged. In practice this capacitor charge must leak away slowly as described in Section 4.2.5 of Chapter 4, and be replaced periodically by the NMOS device.

If wave $I(t)$ were marginally ahead of $C(t)$, states 3 and 7 would replace 2 and 8 respectively and the output $O(t)$ would remain unchanged. Delays $D1$ and $D2$ are thus of little real consequence.

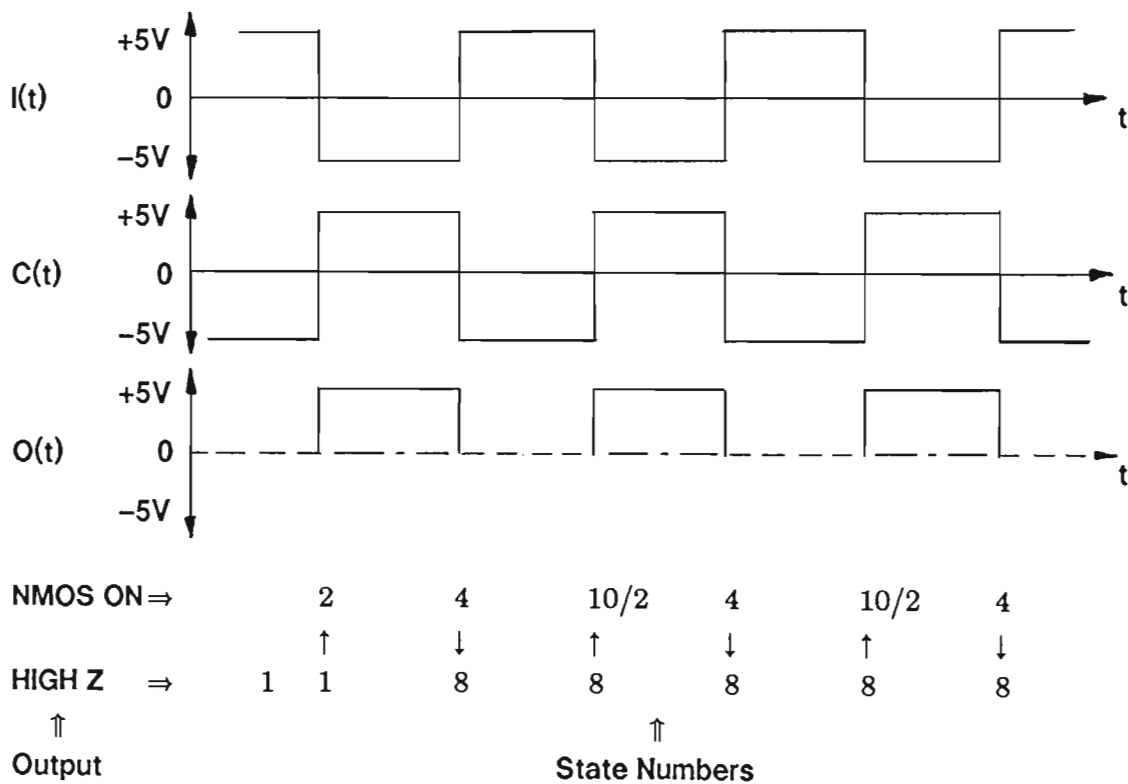


Fig. C.13 Phase Comparator II State Transition Diagram

Initially the input and counter output waves are in antiphase with

$$\theta_e = 180^\circ$$

Input $I(t)$ transitions behind counter output $C(t)$ and $D1 > D2$

Again the state path traced in Fig. C.13 would be unpredictable if the phase comparator input wave zero crossings were exactly in anti-phase and time delays D1 and D2 did not exist. The NMOS device remains ON for each alternate half cycle. This will charge the loop filter capacitor and raise the VCO frequency, driving the loop towards lock. With no external influences such as induced noise pulses it is not possible for the loop to lock in the anti-phase state.

The actual state path traced depends only on the relative timing of the two phase comparator input waveforms. If wave I(t) were marginally ahead of C(t) then states 3, 5 and 7 would replace 2, 4 and 8 respectively. The PMOS device would then be ON for alternate half-cycles, driving the VCO toward lock by reducing its frequency.

C.5.3 Frequency Difference Operation

Signals of differing frequencies are applied to the comparator inputs, and the flip flop state path is traced in Fig. C.14 that follows. A particular condition will be considered, corresponding to a harmonic relationship between the two input frequencies. The result is then generalised for all input conditions with differing input frequencies.

In Fig. C.14 the path traced during operation causes the PMOS device to remain ON almost continuously, charging the LPF capacitor C and thereby increasing the VCO frequency ω_o . Clearly lock is impossible until the VCO frequency rises to that of the external input.

If the inputs in Fig. C.14 are swapped then the state path traced would show the NMOS device to remain ON almost continuously, discharging the LPF capacitor C and thereby decreasing the VCO frequency ω_o . Lock is again impossible until the VCO frequency drops to that of the external input.

Being able to distinguish between differing input frequencies is one of two characteristics of Phase Comparator II vital for this particular timer application. Together the two characteristics result in a loop which is both frequency locked and phase locked.

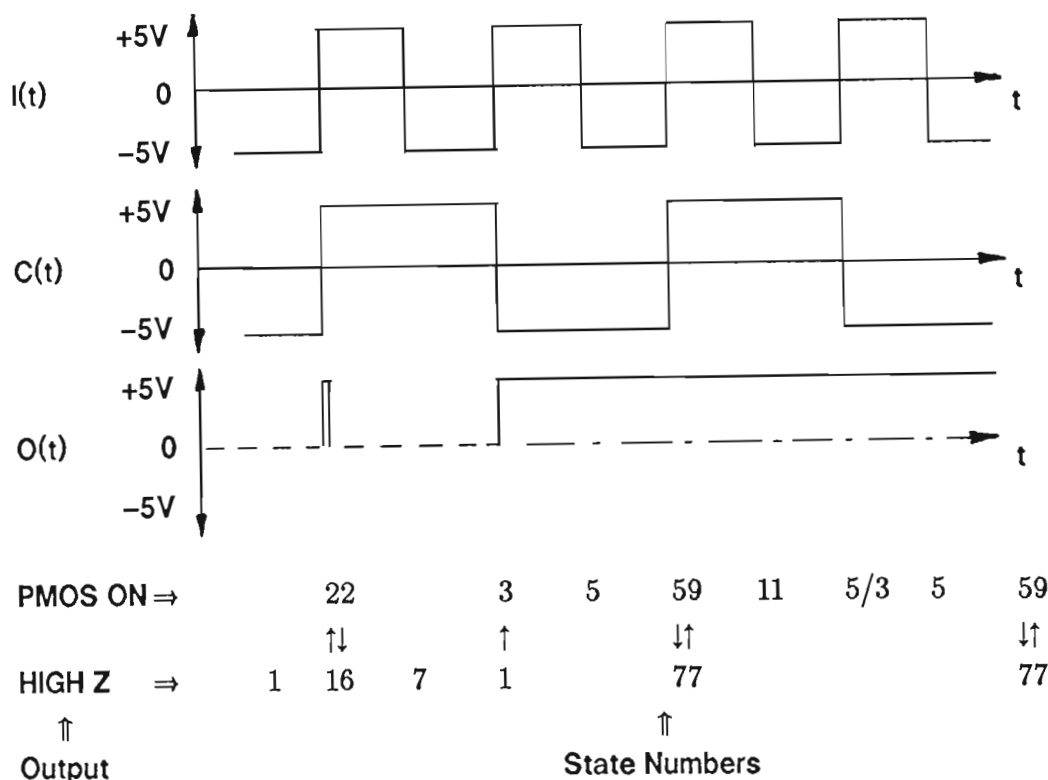


Fig. C.14 Phase Comparator II State Transition Diagram

Zero initial phase error with $\theta_e = 0^\circ$

Input $I(t)$ a harmonic of counter output $C(t)$ and $D1 > D2$

"Zero" on $O(t)$ corresponds to the "High Z" state.

C.6 PHASE COMPARATOR GAIN K_d

A change in phase angle of $\Delta\theta_i$ in the input signal $v_i(t)$ thus causes a change in phase detector output $\Delta v_d(t)$ which initially alters the duty cycle of $v_d(t)$. The voltage on the filter capacitor then changes to adjust the VCO frequency ω_o , and hence ω_n , until ω_o is equal to ω_i once more. At this point $v_i(t)$ and $v_n(t)$ are in phase and the output of the VCO becomes an open circuit (the "HIGH Z" state). The filter capacitor voltage cannot change until either θ_i or θ_n (or ω_i or ω_n) changes for some reason. Effectively this comparator produces an output voltage $v_d(t)$ which is proportional to the initial phase difference θ_e between $v_i(t)$ and $v_n(t)$.

Define Phase Error θ_e

$$\theta_e = \theta_i - \theta_o \quad (C.43)$$

It follows that for Phase Comparator II we have the linear relationship between the phase error θ_e and the phase detector output v_{d2} given by

$$v_{d2} = K_{d2} \theta_e \quad (C.44)$$

where K_{d2} is the Gain Factor for Phase Comparator II, which is constant dependent on the VCO component values.

C.7 OBSERVATIONS AND CONCLUSIONS

Linear transfer function: Both phase comparators have a linear relationship between output voltage v_{d1} and input phase error θ_e so that for both comparators in general:

$$v_d = K_d \theta_e \quad (C.45)$$

where K_d is a constant which is comparator dependent.

Sensitivity to external noise: The loop was very sensitive to stray pulses induced in the comparator input leads through radiation. False triggering, when using the bread-boarded analyser, led to some serious synchronisation problems. On rare occasions it was noticed that lock even occurred under anti-phase conditions. Once the radiation problem had been recognised and cured,

no further occurrences of anti-phase lock were noted. False triggering due to radiation is thus believed to have been the cause.

Phase Comparator II, in achieving both frequency and phase lock, was clearly ideal for application to the sampling pulse timer in the intermodulation product distortion analyser when using a colour bar type video input signal.

APPENDIX D

Measurement of Performance Parameters for the CMOS CD4046 Phase Lock Loop Chip

D.1 INTRODUCTION

The major parameters of interest are the comparator and VCO gains, the frequency range of the VCO, and the loop capture and lock ranges. These parameters were measured using the simple techniques described by Gardner [47].

D.2 PHASE COMPARATOR II GAIN FACTOR K_{d2}

A transfer characteristic for Phase Comparator II is shown in Fig. D.1 overleaf. The output of this phase detector is a LOGIC level signal varying between limits determined by the supply voltages, which are:

$$\begin{aligned} V_{CC} &= +5 \text{ V} \\ &= \text{LOGIC "1"} \end{aligned} \quad (\text{D.1})$$

and

$$\begin{aligned} V_{SS} &= -5 \text{ V} \\ &= \text{LOGIC "0"} \end{aligned} \quad (\text{D.2})$$

Ideally a change in output potential of 10 *Volts* corresponds to a change in input phase of 2π radians. Hence

$$\begin{aligned}
 K_{d2} &= \frac{10}{2\pi} \text{ V/rad} \\
 &= 1,59155 \text{ V/rad}
 \end{aligned}
 \tag{D.3}$$

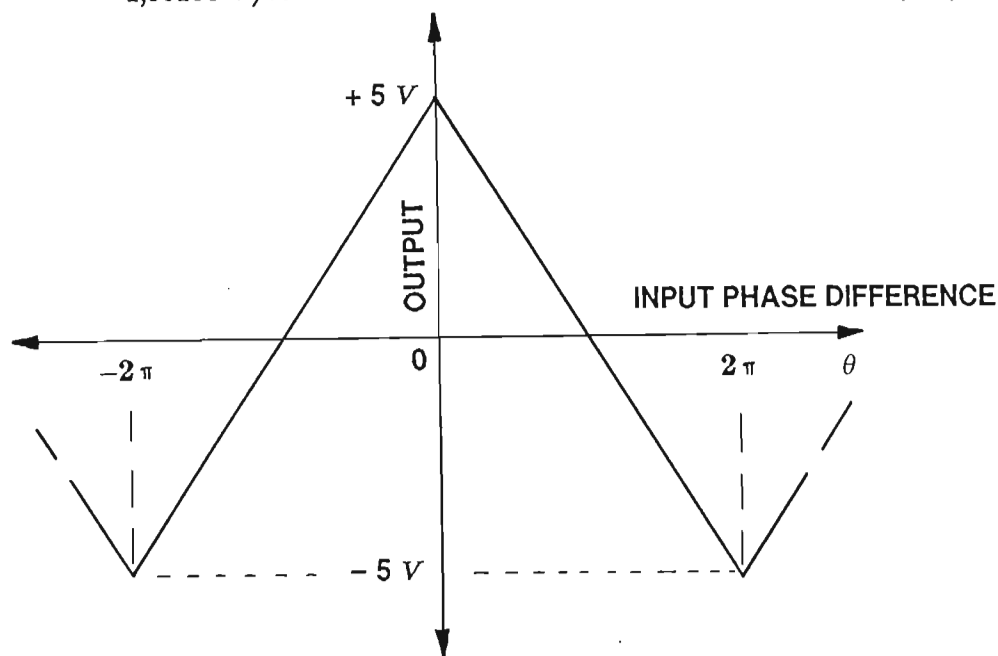
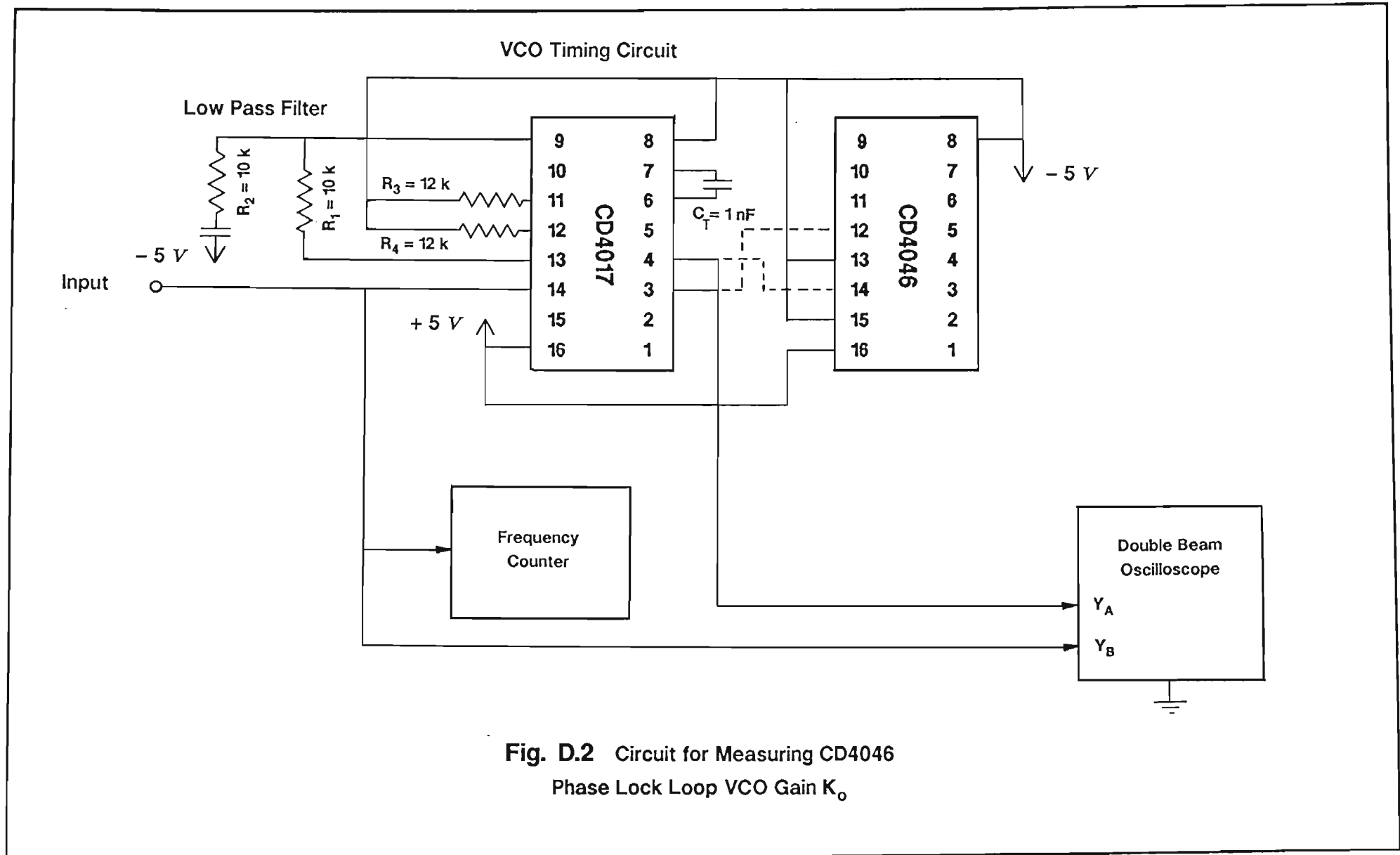


Fig. D.1 Transfer Characteristic for Phase Comparator II

D.3 VCO GAIN FACTOR K_o

Gardner [47] has described the basic technique for measuring PLL performance parameters. For the tests performed, the CD4046 PLL chip was connected as shown in Fig. D.2 overleaf. The VCO input (or control) voltage, measured relative to the negative rail or V_{SS} , was varied from zero to +10 V in 1 V steps and the corresponding VCO output frequency monitored with a frequency counter. The input voltage limits corresponded in potential to V_{SS} and V_{DD} respectively and were adjusted to within 50 mV of the required 1 Volt step values. Measured frequencies rounded to the nearest kilohertz are listed in Tables D.1, D.3 and D.5.

Two designs, selected from a number that were investigated, had timing resistor ratios $R_4:R_3$ of 1:1 and 4:1 respectively. In the tables that follow these same ratios have been used, together with a few others. VCO gain factor K_o (in



rad/Vs) corresponds to the slope of the appropriate "VCO Frequency vs Input Voltage" curves in Figs. D.3 and D.4 for the two designs respectively. The effective loop gain within the filter pass band is given by:

$$K = \frac{K_o K_d F(0)}{N} \quad (\text{D.4})$$

with

$$F(0) = 1 \quad (\text{D.5})$$

$$N = 10 \quad (\text{D.6})$$

A few chips from different manufacturers were tested and spreads of approximately 25% were observed in measured values. These values were unlikely to include any worst case values.

Table D.1

PLL VCO Frequency f_o vs Control Voltage V_{in}

Design (a) with $R_4:R_3 = 1:1$

PLL VCO Component Values of:

$$R_3 = 12 \text{ k}\Omega \quad R_4 = 12 \text{ k}\Omega \quad C_T = 1 \text{ nF}$$

V_{in} (Volts)	CD4046E (kHz)	CD4046BF (kHz)	HEF4046BP (kHz)
0	103	131	128
1	104	131	129
2	108	135	131
3	117	146	144
4	126	156	159
5	135	167	176
6	143	177	190
7	152	187	205
8	158	197	220
9	159	206	224
10	159	207	224

Table D.2

Mean Values of VCO Gain K_o and Loop Gain
determined from the curves in Fig. D.3 (Table D.1)

Design with $R_4:R_3 = 1:1$

	CD4046E	CD4046BF	HEF4046BP
VCO Gain: K_o (rad/Vs)	52360	64926	93201
Loop Gain: K	16667	20667	29667

Table D.2 has the rounded values of VCO and Loop gains for design (a) with $R_4:R_3 = 1:1$ determined from the results in Table D.1 over the linear range, which represents input voltages between 2 and 8 Volts. Table D.4 records the corresponding linear range values of mean VCO and loop gains determined from the results for the design with $R_4:R_3 = 4:1$ given in Table D.3

Table D.3

PLL VCO Frequency vs Control Voltage

Design with $R_4:R_3 = 4:1$

PLL VCO Component Values of:

$R_3 = 12\text{ k}\Omega$ $R_4 = 51\text{ k}\Omega$ $C_T = 560\text{ pF}$

V_{in} (Volts)	CD4046E (kHz)	CD4046BF (kHz)	HEF4046BP (kHz)
0	60	73	68
1	60	73	68
2	74	85	73
3	96	113	101
4	118	139	135
5	139	164	167
6	160	187	199
7	179	211	231
8	198	232	261
9	208	253	286
10	208	256	288

Table D.4

Mean Values of VCO Gain and Loop Gain
determined from the curves in Fig. D.4 (Table D.3)

Design with $R_4:R_3 = 4:1$

	CD4046E	CD4046BF	HEF4046BP
VCO Gain: K_o (rad/Vs)	129852	153938	196873
Loop Gain: K	41332	49000	62667

It was also decided to measure the effect of changing timing resistor R_4 on the operating range of the VCO, as this also affects the VCO gain factor K_o . A CD4046E chip was used for all these tests, and the results of these measurements are presented in Table D.5 and plotted in Fig. D.5. Table D.6 gives the corresponding VCO and Loop gains for the three different resistor combinations. These results are representative of what could be expected of CD4046 PLL chips in general.

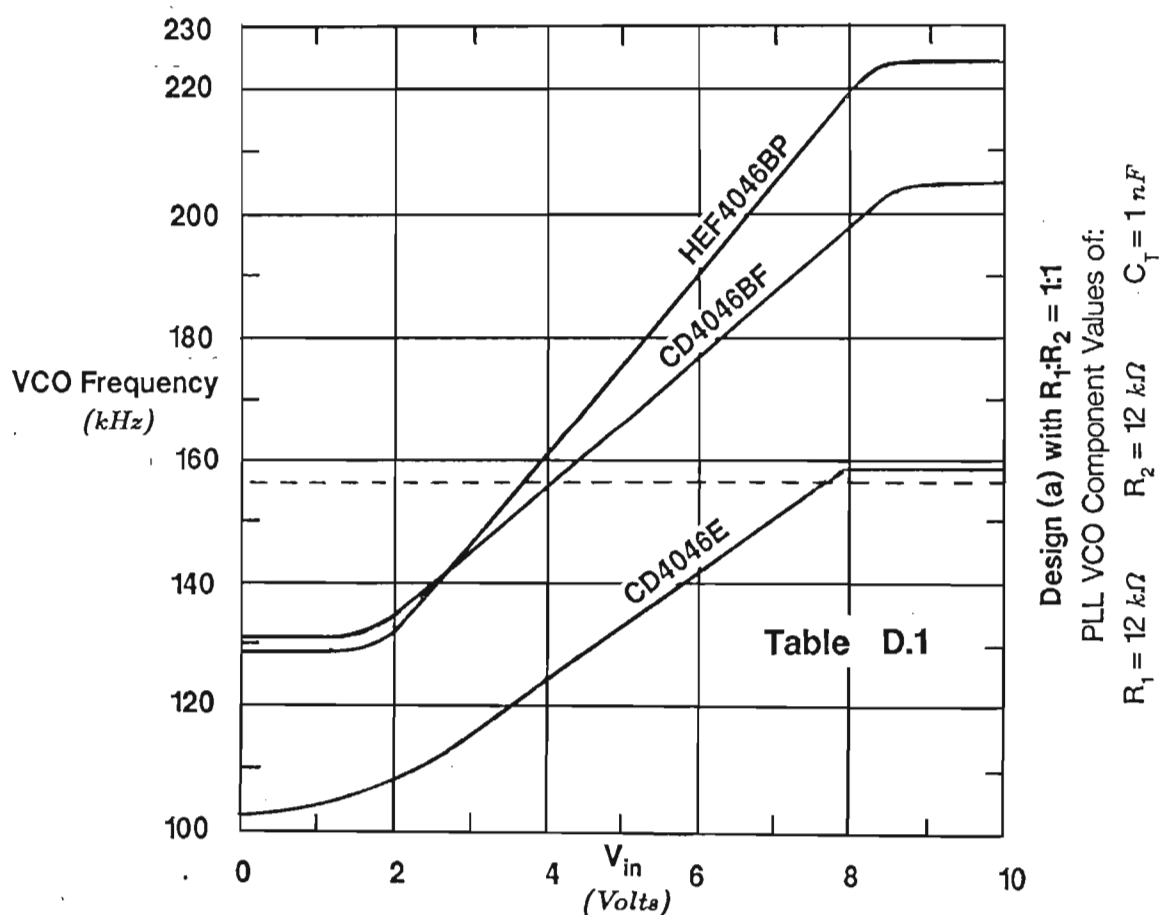


Fig. D.3 VCO Transfer Characteristics
 Graphs of the data in Table D.1 for Design (a)

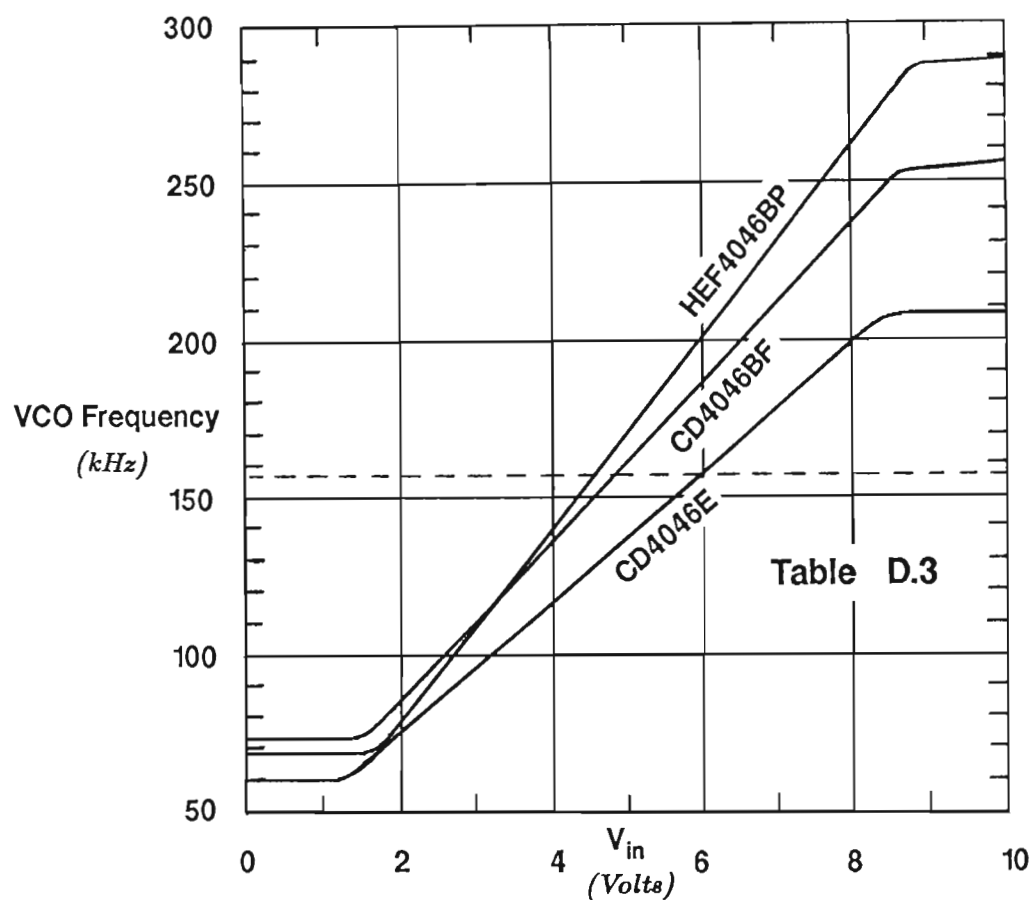


Fig. D.4 VCO Transfer Characteristics
 Graphs of the data in Table D.3 for Design (b)

Design (b) with $R_1 R_2 = 1:4$
 PLL VCO Component Values of:
 $R_1 = 12\text{ k}\Omega$ $R_2 = 51\text{ k}\Omega$ $C_T = 560\text{ pF}$

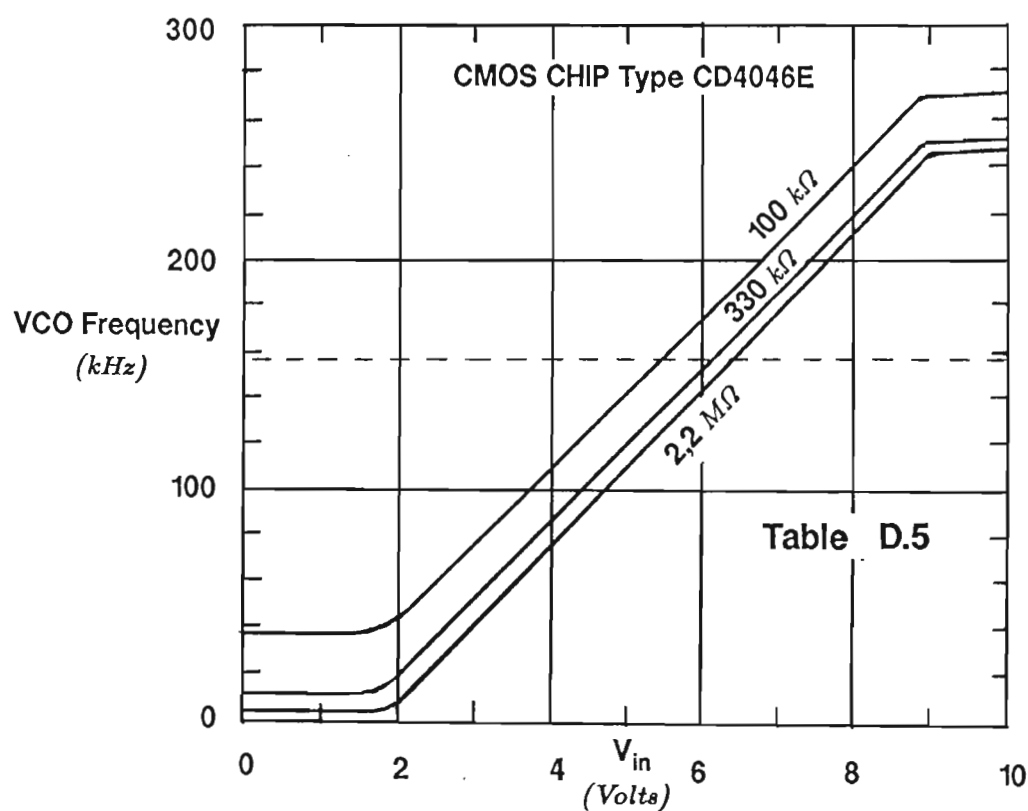


Fig. D.5 VCO Transfer Characteristics
 Graphs of the data in Table D.5 with R_2 as parameter

$R_1 = 12\text{ k}\Omega$, $C_T = 560\text{ pF}$
 R_2 as a Parameter

Table D.5
PLL VCO Frequency vs Control Voltage
CMOS CHIP Type CD4046E
 $R_3 = 12\text{ k}\Omega$, $C_T = 560\text{ pF}$
 R_4 as a Parameter

V_{in} (Volts)	VCO Output f_o (kHz) with R_4 as Parameter		
	100 k Ω (kHz)	330 k Ω (kHz)	2,2 M Ω (kHz)
0	38	12	2
1	38	12	2
2	43	19	9
3	74	50	40
4	108	85	75
5	140	119	111
6	174	154	146
7	207	188	180
8	239	220	214
9	265	249	242
10	269	252	246

Table D.6
Mean Values of VCO Gain K_o and Loop Gain
determined from the curves in Fig. D.5 (Table D.5)

	100 k Ω	330 k Ω	2,2 M Ω
VCO Gain: K_o (rad/Vs)	205000	210000	215000
Loop Gain: K	65254	66845	68437

D.4 PLL CAPTURE AND LOCK RANGE

The circuit arrangement of Fig. D.6 was used to measure the capture and lock ranges of the CD4046 PLL. Tests were performed both with a divide-by-ten counter included, and without the counter, in the feedback loop.

The input frequency was initially adjusted to ensure lock which was confirmed by observing no relative movement (ie. zero relative frequency) in the dual trace oscilloscope display produced by the signals at the two phase comparator inputs (pins 14 and 3 of the CD4046). The frequency of the input signal at pin 14 was then gradually increased until lock was lost to determine the upper lock limit f_{Lmax} . Then the frequency was slowly decreased until lock was achieved once more. This frequency corresponded to the upper limit of the capture range f_{Cmax} . With lock re-established the input frequency was reduced until lock was lost to determine the lower lock limit f_{Lmin} . Then the frequency was slowly increased until lock was again achieved, at which point the frequency corresponded to the lower capture limit f_{Cmin} . Phase Comparator II was used throughout these tests.

Lock range: f_L

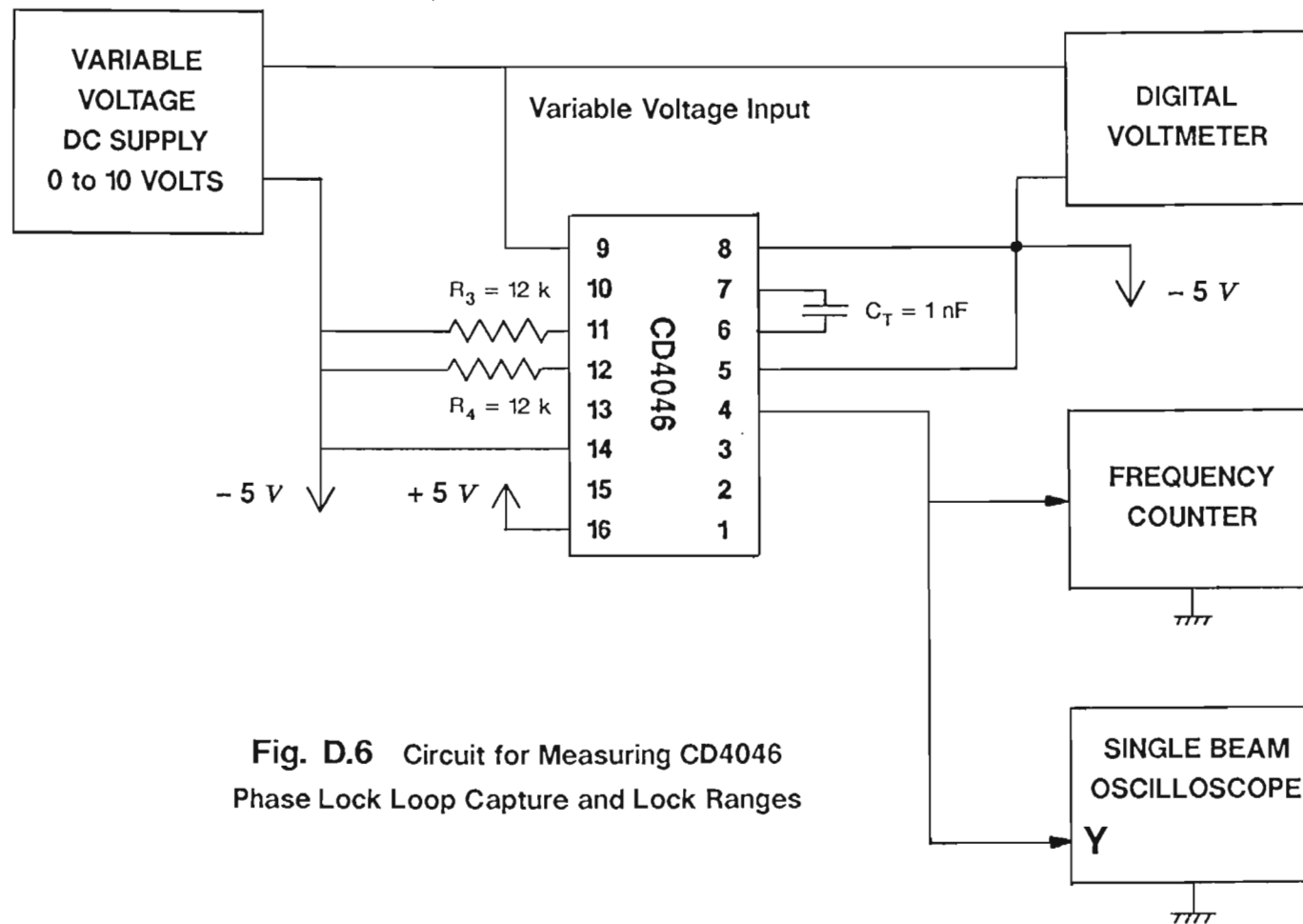
$$f_L = 1/2 (f_{Lmax} - f_{Lmin}) \quad (D.7)$$

Capture range: f_C

$$f_C = 1/2 (f_{Cmax} - f_{Cmin}) \quad (D.8)$$

Note that the factor $1/2$ comes in because the lock and capture range are usually defined as frequency excursions from the free running value f_o which is assumed to correspond to the centre of the useful operating frequency range. This definition is retained, although f_o corresponds to the minimum frequency in this case.

It was thus determined empirically that, for Phase Detector II, both the Capture Range and the Lock Range of the PLL correspond to the full operating range of the VCO. Results are presented in Tables D.7 and D.8 later.



Measured VCO operating range: f_{OR}

$$f_{OR} = f_{MAX} - f_{MIN} \quad (D.9)$$

Measured lock range: f_L

$$f_L = 1/2(f_{MAX} - f_{MIN}) \quad (D.10)$$

Measured capture range: f_C

$$f_C = 1/2(f_{MAX} - f_{MIN}) \quad (D.11)$$

Measured capture and lock ranges for the chips used, and presented in Table D.7 that follows, could have been taken from the ranges in VCO frequency that are to be seen in the data of Tables D.1 and D.3.

Table D.7

Lock and Capture Ranges for CD4046 PLL
 Values Measured without Divide-by-Ten Counter
 Lock Range f_L = Capture Range f_C

	CD4046E (kHz)	CD4046BF (kHz)	HEF4046BP (kHz)
Table D.1 (kHz) $R_4:R_3 = 1:1$	56	76	96
Table D.3 (kHz) $R_4:R_3 = 4:1$	148	183	220

The divide-by-ten counter can have no effect on the internal gain factors of the VCO and phase detector, but clearly the overall loop gain factor A_1 is reduced by a factor of $1/N$, as shown previously in equation (D.4). This will affect loop transient performance and has been accounted for in the analyses above.

In the pass band, filter transfer function is given by:

$$F(0) = 1 \quad (D.12)$$

Rey [53] has shown that the values for the lock and capture range correspond to the loop gain factor:

$$\omega_{\text{capture}} = \omega_{\text{lock}} \quad (\text{D.13})$$

$$= K \text{ rad/s} \quad (\text{D.14})$$

The introduction of a divide-by-ten counter will reduce both f_{MAX} and f_{MIN} by a factor of ten, thus decreasing the capture and lock range accordingly. Capture and lock range measurements were performed on the PLL configuration including the divide-by-ten counter and recorded in Table D.8. These results show that previous range values determined from data in Tables D.1, D.3 and D.5 apply with minor errors to the new configuration if they are simply divided by ten.

Table D.8

Lock and Capture Ranges for CD4046 PLL

Rounded Values measured with Divide-by-Ten Counter

Lock Range f_L = Capture Range f_c

	CD4046E (kHz)	CD4046BF (kHz)	HEF4046BP (kHz)
Table D.1 (kHz) $R_4:R_3 = 1:1$	5,6	7,6	9,6
Table D.3 (kHz) $R_4:R_3 = 4:1$	14,8	18,3	22,0

D.5 MEASUREMENT OF PHASE SHIFT ERROR WHEN USING PHASE COMPARATOR II

A dual beam (Philips) oscilloscope was used for these measurements as it does not have the synchronisation limitations of a dual trace instrument (ie. "chopped" or "alternate" mode). It was thus possible to confirm that, over the entire lock range, the two input signals to the comparator at pins 14 and 3 were always in phase, within the measurement limits of the oscilloscope.

D.6 SUMMARY AND OBSERVATIONS

All Measurements were Simple: Few problems were experienced in performing the measurements described above, and the values obtained confirmed damping ratios and natural frequencies observed during dynamic performance tests.

Not all CD4046 Chips have like Performance: There are some serious reservations to be expressed about chips from different manufacturers having type number CD4046. It is evident from the results that the VCO in the CD4046E chip has a limited frequency range when compared to those of the other two chips tested. Although the three chips originally tested all covered the required frequency range, recent tests on a new batch of CD4046E chips have revealed that some do not cope under worst case conditions. Hence use of the CD4046E should be avoided. It should be noted, however, that the objective of the tests was to ensure good performance of a single prototype instrument, so this avenue of investigation was not pursued.

Open Loop Gain K: Gain ranges from a minimum of 16667 to a maximum of 215000. As the high value corresponds to a large ratio of $R_4:R_3$ and 1:1 was used in the prototype, the lower gain value of 16667 will give theoretical results closer to those measured in practice.

Identical Capture and Lock Ranges: These results are not expected from the theory. Again, the loop gain appears to be much larger than that predicted, making the two ranges equal.

APPENDIX E

Temperature Compensation Theory for CMOS Monostable Pulse Generators

E.1 INTRODUCTION

In order to achieve the proposed accuracy of 0,5 *dB* it was essential to provide compensation for the effects of temperature changes on timer pulse widths. This appendix presents an approach to the systematic design of timer circuits with this particular problem in mind.

Two CMOS dual monostable timer chips are available for use in this instrument, viz. types CD4528 and CD4538 with the latter version preferred for reasons given in Chapter 3. For both timer chips, the pulse width is determined by an R-C network connected externally to the chip. A variable resistor is often included as part of this network to facilitate pulse width adjustment. Two capacitors may then be necessary to achieve the required time constant with the desired temperature coefficient.

E.2 TIMER CIRCUIT DESIGN PROCEDURE

Suppose that the external R-C timing circuit consists of two resistors and two capacitors. The design process is begun by finding the equivalent T.C. for the pair of resistors. This equivalent α_r is then used together with the chip T.C.s α_{pw} and β_{pw} to find the temperature coefficient α_c required for the capacitor combination in order to achieve temperature compensation. As a limited range of specific T.C. values is available for the capacitors [see Table E.2], a pair of

equations derived in what follows must be solved simultaneously to determine both the capacitor values and their corresponding T.C.s.

The method can be extended to networks comprising more than two resistors and two capacitors by combining like components in pairs until the effective T.C. for the complete network is known. The reason for using this technique, which may be original, is that the theory soon becomes unwieldy when more than two like components having differing temperature coefficients are used as part of a timing circuit. This technique gives an "exact" equivalent T.C. provided that all component T.C.s are constant over the temperature range.

E.3 TEMPERATURE COMPENSATION THEORY

E.3.1 Temperature Behaviour of R-C Components

Resistors and capacitors will be assumed to have a linear element value versus temperature characteristic over the temperature range ΔT specified below:

Temperature range ΔT :

$$\begin{aligned} T_1 &= \text{lower temperature limit in } ^\circ\text{C} \\ T_2 &= \text{upper temperature limit in } ^\circ\text{C} \\ \Delta T &= T_2 - T_1 \end{aligned} \tag{E.1}$$

At lower temperature T_1 :

$$\begin{aligned} R &= \text{value of } R \text{ at temperature } T_1 \\ C &= \text{value of } C \text{ at temperature } T_1 \\ \tau_1 &= RC \end{aligned} \tag{E.2}$$

At upper temperature T_2 :

$$\begin{aligned} R + \Delta R &= \text{value of } R \text{ at temperature } T_2 \\ C + \Delta C &= \text{value of } C \text{ at temperature } T_2 \end{aligned}$$

where

$$\Delta R = \alpha_r R \Delta T$$

$$\Delta C = \alpha_c C \Delta T$$

Hence

$$\begin{aligned} \tau_2 &= (R + \Delta R)(C + \Delta C) \\ &= RC(1 + \alpha_r \Delta T)(1 + \alpha_c \Delta T) \\ &= \tau_1(1 + \alpha_r \Delta T + \alpha_c \Delta T + \alpha_r \alpha_c \Delta T^2) \end{aligned} \quad (E.3)$$

E.3.2 Pulse Width vs Temperature Performance: CMOS Dual Monostable Chips

Because of the non-linear pulse width versus temperature characteristic which is typical for a timer chip, the pulse width temperature performance should be represented by a suitable polynomial of the form shown in equation (E.4). A "least squares" curve fitting technique was then used to approximate such a polynomial to the characteristic published by the manufacturer.

$$PW_2 = PW_1(a_0 + a_1 \Delta T + a_2 \Delta T^2 + a_3 \Delta T^3 + \dots + a_n \Delta T^n) \quad (E.4)$$

Coefficients for the polynomial were calculated by a computer programme which performed the curve fitting. It was noted that the coefficients of the third and higher degree terms were of little significance for those chips modelled, being at least three orders smaller than the second degree terms. Thus for the analysis that follows, a second order temperature variation has been assumed having the following form:

$$PW_2 = PW_1(1 + \alpha_{pw} \Delta T + \beta_{pw} \Delta T^2) \quad (E.5)$$

At Lower Temperature T_1 :

$$\begin{aligned} PW_1 &= \text{pulse width at temperature } T_1 \\ &= K_{pw1} \tau_1 \end{aligned} \quad (E.6)$$

At Upper Temperature T_2 :

$$\begin{aligned}
 PW_2 &= \text{pulse width at temperature } T_2 \\
 &= PW_1 + \Delta PW_1 \\
 &= K_{pw2} \tau_2
 \end{aligned} \tag{E.7}$$

where

$$K_{pw2} = K_{pw1} (1 + \alpha_{pw} \Delta T + \beta_{pw} \Delta T^2) \tag{E.8}$$

if

$$\begin{aligned}
 \tau_2 &= \tau_1 \\
 &= \tau
 \end{aligned} \tag{E.9}$$

Time constant τ is constant in these chip considerations, and variations in pulse width are assumed to be caused by changes in chip parameters alone.

E.3.3 Pulse Width Temperature Compensation

Temperature compensation is achieved when zero change in pulse width ΔPW_1 occurs due to both the timer chip and its associated R-C timing circuit over the desired temperature range ΔT , ie. when

$$K_{pw1} \tau_1 = K_{pw2} \tau_2 \tag{E.10}$$

with

$$\tau_2 \neq \tau_1$$

Combining equations E.3 and E.4 to account for both timer chip and R-C timing component T.C.s, we get:

$$\begin{aligned}
 K_{pw1} \tau_1 &= K_{pw1} \tau_1 [1 + \alpha_{pw} \Delta T + \beta_{pw} \Delta T^2] \\
 &\quad \times (1 + \alpha_r \Delta T + \alpha_c \Delta T + \alpha_r \alpha_c \Delta T^2)
 \end{aligned} \tag{E.11}$$

which means that

$$\begin{aligned}
 1 &= (1 + \alpha_r \Delta T + \alpha_c \Delta T + \alpha_r \alpha_c \Delta T^2)(1 + \alpha_{pw} \Delta T + \beta_{pw} \Delta T^2) \\
 &= 1 + (\alpha_r + \alpha_c + \alpha_{pw}) \Delta T \\
 &\quad + (\alpha_r \alpha_c + \alpha_{pw} \alpha_r + \alpha_{pw} \alpha_c + \beta_{pw}) \Delta T^2 \\
 &\quad + (\alpha_r \beta_{pw} + \alpha_c \beta_{pw} + \alpha_r \alpha_c \alpha_{pw}) \Delta T^3 \\
 &\quad + \alpha_r \alpha_c \alpha_{pw} \Delta T^4 + \alpha_r \alpha_c \beta_{pw} \Delta T^4
 \end{aligned} \tag{E.12}$$

This condition allows the capacitor T.C. value α_c which is required for temperature compensation to be expressed in terms of the other T.C.s as:

$$\alpha_c = - \frac{\alpha_r + \alpha_{pw} + (\alpha_r \alpha_{pw} + \beta_{pw}) \Delta T + \alpha_r \beta_{pw} \Delta T^2}{1 + (\alpha_r + \alpha_{pw}) \Delta T + (\alpha_r \alpha_{pw} + \beta_{pw}) \Delta T^2 + \alpha_r \beta_{pw} \Delta T^3} \quad (\text{E.13})$$

If both second and third order temperature coefficient products, and products involving β_{pw} , are neglected, equation (E.13) reduces to:

$$\alpha_c = - (\alpha_r + \alpha_{pw}) \quad (\text{E.14})$$

This result is also achieved through a simple linear analysis.

E.4 EFFECTIVE TEMPERATURE COEFFICIENT FOR TWO LIKE ELEMENTS

E.4.1 Two Resistors in Series

A simple R-C timing circuit with two series resistors R_1 and R_2 and a single ideal capacitor C (with zero T.C.) is assumed. The effective timing resistance R is given by the following expressions:

At temperature T_1 :

$$R = R_1 + R_2$$

At temperature T_2 :

$$\begin{aligned} R + \Delta R &= R_1 + \Delta R_1 + R_2 + \Delta R_2 \\ &= R_1 (1 + \alpha_{r1} \Delta T) + R_2 (1 + \alpha_{r2} \Delta T) \end{aligned}$$

Also

$$R + \Delta R = (R_1 + R_2) (1 + \alpha_r \Delta T)$$

The change in resistance ΔR is therefore:

$$\Delta R = R_1 \alpha_{r1} \Delta T + R_2 \alpha_{r2} \Delta T$$

Also

$$\Delta R = (R_1 + R_2) \alpha_r \Delta T$$

Thus

$$\alpha_r = \frac{R_1 \alpha_{r1} + R_2 \alpha_{r2}}{R_1 + R_2} \quad (\text{E.15})$$

E.4.2 Two Resistors in Parallel

A simple R-C timing circuit with two parallel resistors R_1 and R_2 and a single ideal capacitor C (with zero T.C.) is assumed. The effective timing resistance R is given by the following expressions:

At temperature T_1 :

$$R = \frac{R_1 R_2}{R_1 + R_2}$$

At temperature T_2 :

$$R + \Delta R = \frac{(R_1 + \Delta R_1)(R_2 + \Delta R_2)}{(R_1 + \Delta R_1 + R_2 + \Delta R_2)}$$

Also

$$R + \Delta R = R (1 + \alpha_r \Delta T)$$

The change in total resistance ΔR is therefore:

$$\Delta R = \frac{(R_1 + \Delta R_1)(R_2 + \Delta R_2)}{(R_1 + \Delta R_1 + R_2 + \Delta R_2)} - \frac{R_1 R_2}{R_1 + R_2}$$

Also

$$\Delta R = R \alpha_r \Delta T$$

Thus

$$\alpha_r = \frac{R_1 \alpha_{r2} + R_2 \alpha_{r1} + (R_1 + R_2) \alpha_{r1} \alpha_{r2} \Delta T}{R_1 + R_2 + R_1 \alpha_{r1} \Delta T + R_2 \alpha_{r2} \Delta T} \quad (\text{E.16})$$

E.4.3 Linearisation of a Thermistor

Burke [93] has shown how a thermistor, with the general resistance equation

$$R_{th} = a e^{-bT} \quad (E.17)$$

may be approximately linearised with the aid of a single parallel resistor R . The effective total parallel resistance R_T will then be:

$$R_T = \frac{R_{th} R}{R_{th} + R}$$

Let

$$R_1 = \text{thermistor resistance at temperature } T_1$$

$$R_2 = \text{thermistor resistance at temperature } T_2$$

$$R_3 = \text{thermistor resistance at temperature } T_3$$

where R_2 is the value at the mean temperature T_2 , given by:

$$T_2 = \frac{1}{2}(T_1 + T_3)$$

and the total change in temperature is

$$\Delta T = T_3 - T_1$$

Connect a fixed resistor of zero T.C. (or low T.C. relative to the thermistor T.C.) in parallel with the thermistor such that:

$$\frac{1}{2} \Delta R_T = \frac{R R_2}{R + R_2} - \frac{R R_3}{R + R_3}$$

and

$$\frac{1}{2} \Delta R_T = \frac{R R_1}{R + R_1} - \frac{R R_2}{R + R_2}$$

Solving simultaneously for R gives the parallel resistance required to "linearise" the thermistor over the temperature range ΔT :

$$R = \frac{R_1 R_3 + R_2 R_3 - 2 R_1 R_2}{R_1 + R_3 - 2 R_2} \quad (E.18)$$

The change in parallel resistance ΔR_T over the whole temperature range ΔT is given by:

$$\begin{aligned}
\Delta R_T &= \frac{2R^2(R_2 - R_3)}{(R + R_2)(R + R_3)} \\
&= \frac{2R^2(R_1 - R_2)}{(R + R_1)(R + R_2)}
\end{aligned} \tag{E.19}$$

This results in an effective T.C. of:

$$\alpha_r = \frac{\Delta R_T}{R_T \Delta T} \tag{E.20}$$

Thermistors having either positive or negative T.C.s may be used to achieve nearly-linear resistors having relatively large T.C. values [93].

Burke's linearisation technique can be extended for improved accuracy by modelling the parallel thermistor/resistor combination R_T with a second order polynomial. Application of the least squares curve fitting technique allows a determination of both α_r and β_r for the combination. This near-linear component can then be used in a design with some modification to the theory presented.

E.4.4 Two Capacitors in Parallel

A simple R-C timing circuit with two parallel capacitors C_1 and C_2 and a single ideal resistor R having zero T.C. is assumed. The analysis in this case is analogous to that for the two series resistors, and leads to:

$$\alpha_c = \frac{C_1 \alpha_{c1} + C_2 \alpha_{c2}}{C_1 + C_2} \tag{E.21}$$

E.4.5 Two Capacitors in Series

A simple R-C timing circuit with two series capacitors C_1 and C_2 and a single ideal resistor R having zero T.C. is assumed. The analysis in this case is analogous to that for the two parallel resistors, and leads to:

$$\alpha_c = \frac{C_1 \alpha_{c2} + C_2 \alpha_{c1} + (C_1 + C_2) \alpha_{c1} \alpha_{c2} \Delta T}{C_1 + C_2 + C_1 \alpha_{c1} \Delta T + C_2 \alpha_{c2} \Delta T} \quad (\text{E.22})$$

E.5 PASSIVE COMPONENT T.C. SPECIFICATIONS

Some typical temperature coefficients for various component materials are listed in Table E.1 [89 to 91]. Table E.2 illustrates the very useful range of temperature coefficients available from PHILIPS [91] in small ceramic capacitors.

Table E.1
Some Typical Component Temperature Coefficients

Component Type	Material Type	T.C. (ppm/K)
Resistors	Metal film (Ni/Cr)	+220
	Metal Film	+150
	Cracked Carbon	-200 (low R) to -1000 (high R)
	Cermet	+150
Capacitors	Mica	+70
	Polystyrene	-150
	Metallised Polyester	+400
	Metallised Polycarbonate	+150
	Metallised Polypropylene	-400
	Ceramic	zero (low ϵ) to -1500 (high ϵ)

Evidently a combination of polystyrene capacitor and cermet or metal film resistor would lead to an R-C circuit with zero temperature coefficient of time constant α_{rc} . If a particular time constant temperature coefficient were required, this could be achieved by making use of the available, standard range of ceramic capacitor temperature coefficients listed in Table E.2.

Table E.2
CERAMIC Miniature Plate Capacitor Temperature Coefficients

Capacitance Range (pF)	Temp. Coeff. (ppm/K)	Colour Code
0,56 to 47	+100	red/violet
1,8 to 120	zero	black
3,9 to 120	-75	red
3,9 to 150	-150	orange
3,9 to 150	-220	yellow
4,7 to 180	-330	green
6,8 to 220	-470	blue
3,9 to 330	-750	violet
18,0 to 560	-1500	orange/orange

E.6 POLYNOMIAL CURVE FITTING

E.6.1 The Least Squares Technique

It is desired to fit "n" data pairs x_i, y_i , for $i=1$ to n , to the polynomial:

$$f(x) = a_0 + a_1x + a_2x^2 + a_3x^3 + \dots + a_mx^m \quad (\text{E.23})$$

Sokolnikoff and Sokolnikoff [92] have shown that, to use the least squares approach, the equations in (E.24) must be generated to solve for the polynomial coefficients. Solving these equations simultaneously then gives the required coefficients.

A computer programme was written both to generate the set of simultaneous equations in (E.24) that follow, from the input data pairs, and to solve them. The programme output consists of the required polynomial coefficients as well as the calculated values of y_i for an input x_i so that the quality of the curve fit may be assessed.

$$\begin{aligned}
na_0 + a_1 \sum_{i=1}^n x_i + a_2 \sum_{i=1}^n x_i^2 + \dots + a_2 \sum_{i=1}^n x_i^m &= \sum_{i=1}^n y_i \\
a_0 \sum_{i=1}^n x_i + a_1 \sum_{i=1}^n x_i^2 + a_2 \sum_{i=1}^n x_i^3 + \dots + a_2 \sum_{i=1}^n x_i^{m+1} &= \sum_{i=1}^n x_i y_i \\
a_0 \sum_{i=1}^n x_i^2 + a_1 \sum_{i=1}^n x_i^3 + a_2 \sum_{i=1}^n x_i^4 + \dots + a_2 \sum_{i=1}^n x_i^{m+2} &= \sum_{i=1}^n x_i^2 y_i \\
&\vdots \\
&\vdots \\
&\vdots \\
a_0 \sum_{i=1}^n x_i^m + a_1 \sum_{i=1}^n x_i^{m+1} + a_2 \sum_{i=1}^n x_i^{m+2} + \dots + a_2 \sum_{i=1}^n x_i^{m+n} &= \sum_{i=1}^n x_i^m y_i
\end{aligned} \tag{E.24}$$

E.6.2 Application to CD4528 and CD4538 CMOS Monostable Timer Chips

The pulse width temperature performance of the CMOS CD4528 and CD4538 chips can be found from the graphs of “Normalised Pulse Width vs Temperature” supplied by the manufacturer [88]. Given the temperature data for a particular chip, a least squares curve fit is then used to determine the first and second order temperature coefficients.

The data in Tables E.3 and E.4 were obtained from the manufacturer’s published graphs [88], Fig. 4 for the CD4528 chip, and Fig. 12 for the CD4538, chip, respectively. The National CD4538 chips are unique in that they produce a pulse width having a zero temperature coefficient at an ambient temperature of 35°C when operated from a 10 V supply. So called equivalent chips from other sources differ considerably in their temperature performance.

Table E.3

Output of Least Squares Polynomial Fitting Programme
 Input Data is Pulse Width (Y) versus Temperature (X)
 for a CD4528 CMOS Monostable Timer Chip
 Error information allows the fit to be assessed.

X INPUT	Y INPUT	CALCULATED Y	ERROR %
-40	.908	.9671862	6.518307
-10	.955	.9550595	6.235083E-03
20	.99	.9898809	-.0120293
50	1.025	1.025119	1.161854E-02
80	1.063	1.062941	-5.595996E-03
110	1.095	1.095012	1.088669E-03

POLYNOMIAL COEFFICIENTS:

K 0	.9671862
K 1	1.169973E-03
K 2	-3.325621E-06
K 3	8.899224E-08
K 4	-5.40127E-10

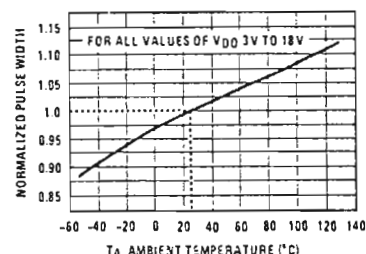


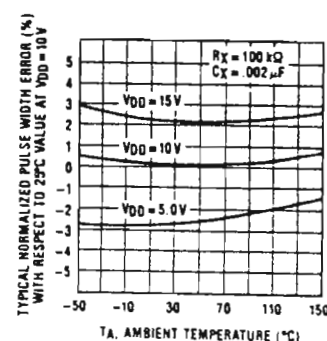
Table E.4

Output of Least Squares Polynomial Fitting Programme
 Input Data is Pulse Width (Y) versus Temperature (X)
 for a CD4538 CMOS Monostable Timer Chip
 Error information allows the fit to be assessed.

X INPUT	Y INPUT	CALCULATED Y	ERROR %
-50	1.005	1.001727	-.3256608
-10	1.002	1.00199	-9.874622E-04
30	1.0015	1.00152	1.97591E-03
70	1.002	1.00198	-1.974925E-03
110	1.0035	1.00351	9.859862E-04
150	1.008	1.007998	-2.010474E-04

POLYNOMIAL COEFFICIENTS:

K 0	1.001727
K 1	-2.002211E-05
K 2	5.71563E-07
K 3	-5.335022E-09
K 4	2.848353E-11



E.7 CONCLUSIONS

Precise measurements of $1,8\ \mu\text{s}$ and $5,6\ \mu\text{s}$ pulse widths are difficult because of the associated oscilloscope trigger problems. Pulse edges have finite slopes, and the actual trigger level varies with ambient temperature. Trigger jitter was also a problem, therefore no detailed records were made of the variation of sampling, and other, critical pulse widths with temperature. No observable change in pulse width occurred over the specified temperature range, so that actual changes were less than 1%.

Performance of the I.M. analyser as a whole was measured with varying temperature on the basis that small changes would be reflected in the readings obtained. Unfortunately no readings were taken of the analogue output voltage during tests performed at Barlows Communications. These values would have increased the precision of the measurements and would also have included such factors as the changing voltage gain of the active filters and full wave rectifier. Our own departmental environmental chamber is too small to accommodate the analyser for such tests.

APPENDIX F

Determination of Noise Levels due to the sampling of Luminance and Chrominance Signals

F.1 INTRODUCTION

Two distinct interference problems arise due to the sampling process performed by the mixer in the I.M. analyser. Their origins, and the solutions proposed by the writer, are considered in this Appendix.

The first problem arises when sampling a video signal with luminance component only. False I.M. readings corresponding to sampling luminance noise of the order of up to 40% of the analyser calibration level, ie. -58 dBp , were observed for an input colour bar video signal with luminance components only and no I.M. distortion present. A simple analysis of the sampling process in Chapter 2 [equation (2.31) and Fig. 2.18] showed that no half-line harmonic components fall within the frequency measurement window defined by the 500 *Hz* low pass filter. These harmonics therefore do not contribute directly to system noise. Interference does arise, however, through modulation by the effective 50 *Hz* field pulse producing sidebands having 50 *Hz* spacing on either side of the 200th and 201st half-line harmonics. Some of these sidebands fall within the window and pass through the 500 *Hz* filter as unwanted interference or noise. The sampling pulse width determines the amplitudes of the half-line harmonics and thus, to a large extent, the noise floor level of the measurement system.

A second, more serious noise problem arises when the colour subcarrier is sampled. In this case a half-line frequency sideband component of considerable amplitude is produced that falls directly within the measurement window [see

equation (2.33) and Fig. 2.18], and this, together with some twenty 50 *Hz* sidebands, contributes enormously to the noise floor level. Again false I.M. readings were obtained, using an input video signal with chrominance components only (and no I.M.), which reached near to the upper limit of the analyser at -40 *dBp* with no I.M. distortion present.

In Chapter 2, Section 2.5, the waveforms applied to the AND gate driving the mixer switch were considered in some detail. Two of these waveforms were responsible for the sample timing and a third represented the loss of video during the field sync period. Their frequency components were described in terms of their mark-to-space ratios R_3 and R_4 and the sinc function [see equations (2.19) to (2.34)], giving the Fourier Series repeated below:

The Sampling Waveform:←

$$v_{sa}(t) = R_3 + 2R_3 \sum_{n=1}^{\infty} \text{sinc}(n\pi R_3) \cos(n\omega_{sa}t) \quad (F1)$$

where

$$R_3 = \frac{1,8}{128} \quad (F2)$$

for the PAL System.

The Field Pulse Waveform:←

$$v_F(t) = R_4 + 2R_4 \sum_{n=1}^{\infty} \text{sinc}(n\pi R_4) \cos(n\omega_F t) \quad (F3)$$

where

$$R_4 = 0,93 \quad (F4)$$

for the I/PAL System, and 0,94 for M/NTSC System.

In Section 2.5 of Chapter 2 the effect of the field pulse waveform in producing 50 *Hz* sidebands on either side of f_{IM} was considered briefly. Clearly every frequency component present at the mixer video input will be similarly modulated by these pulses, producing sidebands with 50 *Hz* spacings.

F.2 NOISE PRODUCED BY THE SAMPLING OF A CONSTANT LUMINANCE SIGNAL V_{Lum}

F.2.1 System I/PAL Luminance Sampling Noise

An expanded view of the half-line harmonics on either side of the f_{IM} frequency in Fig. 2.18 showed the 200th and 201st half-line harmonic components having non-zero amplitudes on either side of f_{IM} . Both harmonics are more than 3800 *Hz* away from f_{IM} , which is well into the stop band of the 500 *Hz* low pass filter, and would be attenuated by at least 140 *dB*.

When the field pulse waveform is included in the analysis, however, the product $V_{\text{Lum}} \times v_{\text{Sa}}(t) \times v_{\text{F}}(t)$ must be expanded to illustrate the sidebands with 50 *Hz* spacing. Figs. F.1 and F.2 reveal the relationships of the sideband frequencies to the local oscillator frequency f_{LO} at 1,566181 *MHz*, which also defines the centre of the measurement window, and f_{IM} the I.M. frequency. The only sidebands with significant amplitudes within the measurement window are, from Fig. F.1, the upper sidebands of the 200th half-line harmonic and, from Fig. F.2, the lower sidebands of the 201st half-line harmonic. These components are represented in equations (F.5) and (F.6) respectively:

Upper sidebands of the 200th half-line harmonic:

$$v_{\text{USB}}(t) = 2V_{\text{Lum}} \mathbf{R}_3 \mathbf{R}_4 \text{sinc}(200 \pi \mathbf{R}_3) \sum_{n=64}^{83} \text{sinc}(n \pi \mathbf{R}_4) \cos(200 \omega_{\text{Sa}} t + n \omega_{\text{F}} t) \quad (\text{F.5})$$

Lower sidebands of the 201st half-line harmonic:

$$v_{\text{LSB}}(t) = 2V_{\text{Lum}} \mathbf{R}_3 \mathbf{R}_4 \text{sinc}(201 \pi \mathbf{R}_3) \sum_{n=73}^{92} \text{sinc}(n \pi \mathbf{R}_4) \cos(201 \omega_{\text{Sa}} t - n \omega_{\text{F}} t) \quad (\text{F.6})$$

Tables F.1 and F.2 contain the non-zero magnitudes and frequencies of the 50 *Hz* sidebands over a somewhat wider frequency range, together with the low pass filter magnitude ratio $H(j\omega)$ applicable to each sideband frequency passing through the measurement window, where

Table F.1

Upper 50 *Hz* Sidebands of the 200th Half-Line Harmonic
of 1 Volt luminance signal sampled every 128 μ s

which overlap the measurement frequency window.

To determine actual sideband amplitudes multiply by V_{Lum} .

The video loss field pulse mark-space ratio is 0,9296.

Four 2nd order low pass filters with $f_c = 660$ *Hz* in cascade.

Sideband Number	Sideband Frequency <i>Hz</i>	Sideband Amplitude $\times V_{Lum}$	Filter Power Ratio $ F(j\omega) ^2$	Normalised Power $\times V_{Lum}^2$ <i>Watts</i>
50	1565000	-1.12582E-05	7.897921E-03	3.953062E-15
51	1565050	7.804638E-06	1.079816E-02	3.5512E-15
53	1565150	-7.510119E-06	2.067497E-02	1.205462E-14
54	1565200	1.042426E-05	2.891424E-02	4.542387E-14
55	1565250	-7.237057E-06	4.065856E-02	4.329102E-14
57	1565350	6.983121E-06	8.102005E-02	1.600494E-13
58	1565400	-9.705347E-06	.1140745	6.128709E-13
59	1565450	6.746383E-06	.1593807	5.780741E-13
61	1565550	-6.525235E-06	.2968216	1.875657E-12
62	1565600	9.079196E-06	.3903704	6.28085E-12
63	1565650	-6.318017E-06	.4966405	4.92284E-12
65	1565750	6.123611E-06	.7159276	9.610001E-12
66	1565800	-8.528941E-06	.8100871	2.386842E-11
67	1565850	5.94089E-06	.8845456	1.380745E-11
69	1565950	-5.768641E-06	.9706498	1.567625E-11
70	1566000	8.041573E-06	.9887824	3.161211E-11
71	1566050	-5.606171E-06	.9969031	1.561739E-11
73	1566150	5.452572E-06	.9999902	1.486498E-11
74	1566200	-7.606893E-06	.9999986	2.893233E-11
75	1566250	5.307155E-06	.9997611	1.407622E-11
77	1566350	-5.169342E-06	.9914571	1.313374E-11
78	1566400	7.216797E-06	.9761884	2.481568E-11
79	1566450	-5.038419E-06	.9470128	1.138336E-11
81	1566550	4.914009E-06	.8299013	8.315623E-12
82	1566600	-6.864758E-06	.7400523	1.290462E-11
83	1566650	4.795659E-06	.6349251	4.63566E-12
85	1566750	-4.682779E-06	.4149337	1.887708E-12
86	1566800	6.545467E-06	.3178537	2.164242E-12
87	1566850	-4.575152E-06	.2366424	5.860926E-13
89	1566950	4.472334E-06	.1237203	1.530806E-13
90	1567000	-6.254557E-06	.0879919	1.514427E-13
91	1567050	4.374029E-06	6.233135E-02	3.716605E-14
93	1567150	-4.279992E-06	.0313655	9.010738E-15
94	1567200	5.988406E-06	2.239513E-02	8.992894E-15
95	1567250	-4.189843E-06	1.609502E-02	2.273781E-15
97	1567350	4.10345E-06	8.507132E-03	6.09305E-16
98	1567400	-5.743982E-06	6.262037E-03	6.468853E-16
99	1567450	4.020603E-06	4.648599E-03	1.746612E-16

Normalised noise power = 2.627938756158474D-10 * V_{lum}^2 Watts

Normalised reference power = 8.690357208251953D-05 Watts

Power ratio = -55.19422555434892 dBp for $V_{lum} = 1$ Volt

Table F.2

Lower 50 Hz Sidebands of the 201st Half-Line Harmonic
of 1 Volt luminance signal sampled every 128 μ s
which overlap the measurement frequency window.
To determine actual sideband amplitudes multiply by V_{Lum} .
The video loss field pulse mark-space ratio is 0,9296.
Four 2nd order low pass filters with $f_c = 660$ Hz in cascade.

Sideband Number	Sideband Frequency Hz	Sideband Amplitude $\times V_{Lum}$	Filter Power Ratio $ F(j\omega) ^2$	Normalised Power $\times V_{Lum}^2$ Watts
57	1567462.5	6.482342E-06	4.32062E-03	3.922166E-16
58	1567412.5	-9.00935E-06	5.807949E-03	1.368997E-15
59	1567362.5	6.262581E-06	7.87359E-03	1.215688E-15
61	1567262.5	-6.057292E-06	1.483619E-02	4.038049E-15
62	1567212.5	8.428102E-06	.0206064	1.508113E-14
63	1567162.5	-5.864935E-06	2.881657E-02	1.428173E-14
65	1567062.5	5.68447E-06	5.717571E-02	5.281693E-14
66	1567012.5	-7.917308E-06	8.074153E-02	2.043238E-13
67	1566962.5	5.514853E-06	.1136882	1.965479E-13
69	1566862.5	-5.354956E-06	.2190123	6.877311E-13
70	1566812.5	7.46489E-06	.295966	2.440622E-12
71	1566762.5	-5.204137E-06	.3893626	2.052939E-12
73	1566662.5	5.061554E-06	.6072395	4.723432E-12
74	1566612.5	-7.061383E-06	.7149046	1.274224E-11
75	1566562.5	4.926564E-06	.809236	7.947099E-12
77	1566462.5	-4.798634E-06	.9369599	1.010758E-11
78	1566412.5	6.69926E-06	.9704006	2.113128E-11
79	1566362.5	-4.6771E-06	.988659	1.069095E-11
81	1566262.5	4.561612E-06	.9995351	1.039448E-11
82	1566212.5	-6.372467E-06	.9999896	2.030375E-11
83	1566162.5	4.451749E-06	.9999988	9.90901E-12
85	1566062.5	-4.346964E-06	.9979248	9.408876E-12
86	1566012.5	6.076073E-06	.991557	1.814894E-11
87	1565962.5	-4.247055E-06	.9764012	8.598098E-12
89	1565862.5	4.151611E-06	.8997606	6.976815E-12
90	1565812.5	-5.806026E-06	.830701	1.163101E-11
91	1565762.5	4.060356E-06	.7410388	4.526683E-12
93	1565662.5	-3.973062E-06	.52441	2.170514E-12
94	1565612.5	5.558961E-06	.4159723	2.673536E-12
95	1565562.5	-3.889379E-06	.3187505	7.684791E-13
97	1565462.5	3.809181E-06	.1729574	2.170258E-13
98	1565412.5	-5.332065E-06	.1241381	2.19064E-13
99	1565362.5	3.732274E-06	8.829466E-02	5.429827E-14
101	1565262.5	-3.658336E-06	4.430367E-02	1.313459E-14
102	1565212.5	5.122964E-06	3.147223E-02	1.299773E-14
103	1565162.5	-3.587318E-06	2.247002E-02	3.248752E-15
105	1565062.5	3.518984E-06	1.169148E-02	8.463367E-16
106	1565012.5	-4.929644E-06	8.533601E-03	8.848421E-16

Normalised noise power = 1.790456251458139D-10 * V_{lum}^2 Watts
Normalised reference power = 8.690357208251953D-05 Watts
Power ratio = -56.86074182596088 dBp for $V_{lum} = 1$ Volt

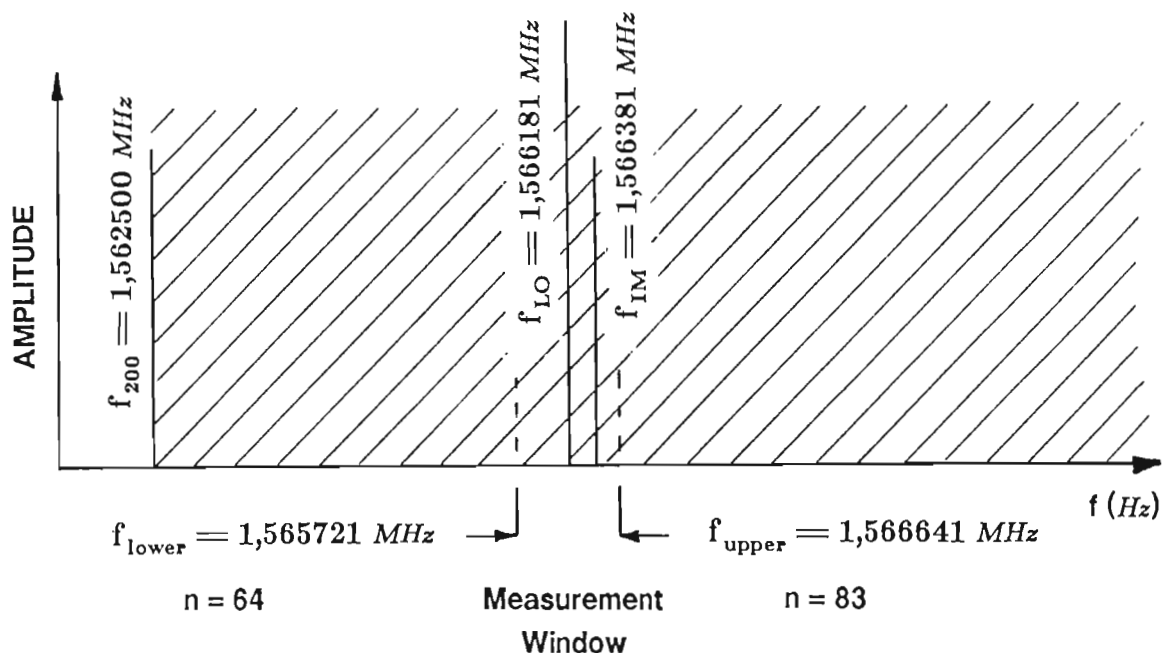


Fig. F.1 Upper 50 Hz sideband noise components (shaded area) associated with the 200th half-line harmonic which overlap the frequency window centred on f_{LO} . The video loss field pulse mark-space ratio is 0,9296.

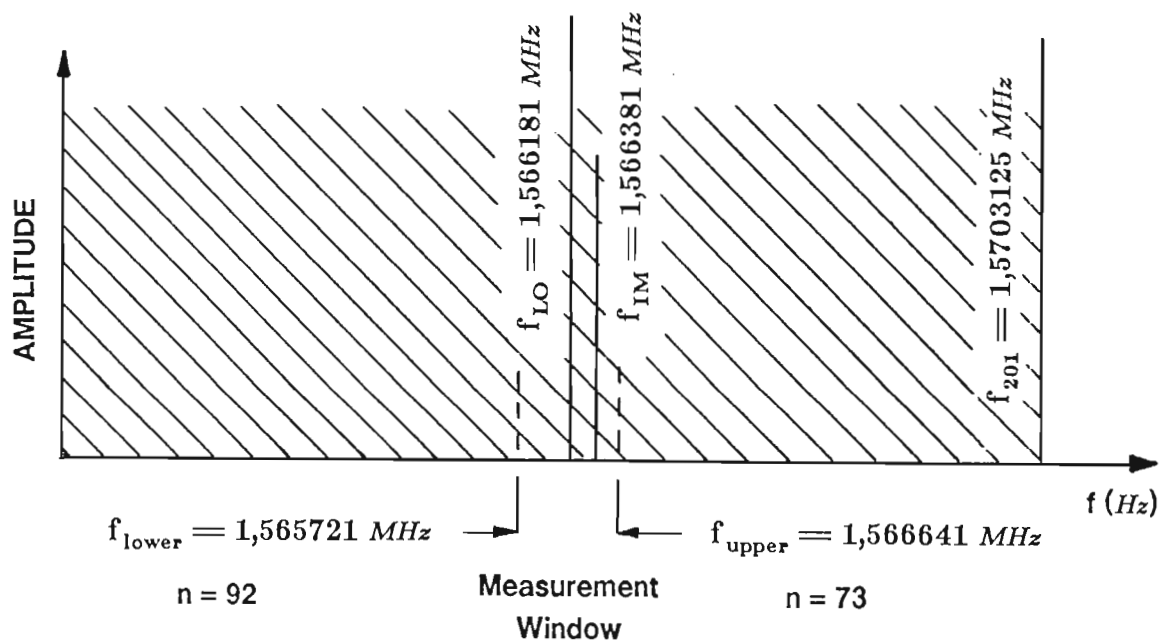


Fig. F.2 Lower 50 Hz sideband noise components (shaded area) associated with the 201st half-line harmonic which overlap the frequency window centred on f_{LO} . The video loss field pulse mark-space ratio is 0,9296.

$$|H(j\omega)| = \left[1 + \left\{ \frac{f}{f_c} \right\}^{2k} \right]^{-L/2} \quad (F.7)$$

Here

$$\begin{aligned} k &= \text{order of the filter} \\ &= 2 \end{aligned} \quad (F.8)$$

and

$$\begin{aligned} L &= \text{number of filters in cascade} \\ &= 4 \end{aligned} \quad (F.9)$$

The last columns in each of Tables F.1 and F.2 contain values of the power developed by each sidebands, normalised for a 1 Ω load resistor and a 1 *Volt* luminance signal. These powers are summed to give the total power in all the sidebands situated within the frequency window. This power must be multiplied by V_{Lum}^2 to determine the actual normalised power associated with each luminance signal level. The total power may then be compared to the reference power produced by the sampled 1,25 *Volt* peak sync (vision carrier signal before demodulation), again normalised for a 1 Ω load. A 1 *Volt* luminance signal is assumed in the following calculations. Calculations at other luminance levels, corresponding to those within the colour bars, can be found in Table F.3 later.

The normalised power sum from Table F.1 is:

$$P_{200} = 0,26279388 \text{ nW} \quad (F.10)$$

The normalised power sum from Table F.2 is:

$$P_{201} = 0,17904488 \text{ nW} \quad (F.11)$$

The combined power sum for both half-line harmonics is:

$$P_{\text{tot}} = 0,44183901 \text{ nW} \quad (F.12)$$

For any luminance level other than 1 *Volt* the total contribution to the normalised noise power will be

$$P_{\text{Lum}} = P_{\text{tot}} \times V_{\text{Lum}}^2 \quad (F.13)$$

This normalised luminance power may be compared to the normalised reference power P_{Ref} produced by the 1,25 *Volt* peak sync pulse:

$$\begin{aligned} P_{Ref} &= 1/2 [V_{Ref} \times R_3 \times R_4]^2 \\ &= 86,903572 \mu W \end{aligned}$$

(F.14)

The power ratio, expressed in *dBp*, is then given by:

$$P\text{-Ratio} = 10 \log \left[\frac{P_{Lum}}{P_{Ref}} \right] \text{ dBp}$$

(F.15)

Table F.3 shows some typical noise levels calculated for luminance levels within the 100-0-75-0 colour bar for System I/PAL.

Table F.3
Noise due to Sampling of Luminance Signals
Within a 100-0-75-0 Colour Bar Input Signal
Normalised Power Sum (NPS) is 0,44183901 *nW*
for a 1 Volt peak Luminance Signal
Noise power is NPS × *V_{Lum}*² *nW*
Normalised reference power is 86,903572 *μW*

Colour	Luminance Level (Volts)	Noise Power (pW)	Noise Power (dBp)
Yellow	0,465	95,53664	-59,59
Cyan	0,368	59,83561	-61,62
Green	0,308	41,91462	-63,17
Magenta	0,217	20,80576	-66,21
Red	0,157	10,89089	-69,02
Blue	0,060	1,590620	-77,37

F.2.2 System M/NTSC Luminance Sampling Noise

Similar problems occur within the NTSC System. A major difference, however, is that alternate line sampling *MUST NOT* be used. For a line frequency of 15734,28 Hz, the 117th harmonic of the half-line frequency is 920454 Hz which is only 1 Hz below the NTSC I.M. frequency of 920455 Hz. Considerable noise would thereby be introduced directly into the frequency window through alternate line sampling.

For System M/NTSC:

$$\omega_{sa} = \omega_H \quad (F.16)$$

Sampling every line produces harmonics with line frequency spacings, and the 58th and 59th harmonics of the line frequency contribute to the noise floor of the histogram in the same way that occurred in the PAL System for the 200th and 201st half-line harmonics. These noise components may be evaluated in the same manner as was used for System I/PAL sidebands.

F.2.3 Luminance Noise Reduction Techniques

Two techniques are available for the reduction of luminance sampling noise.

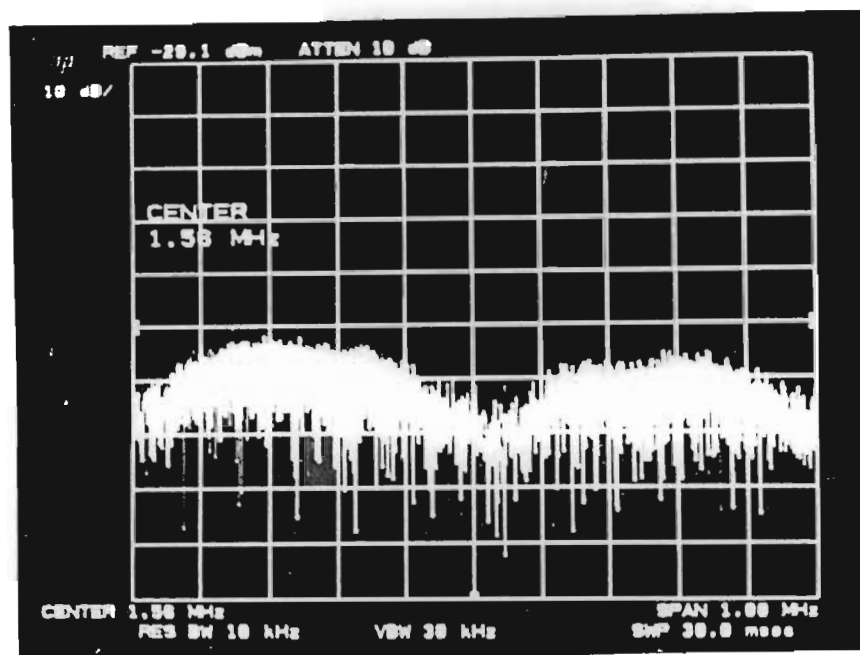
The first reduction method is concerned with the optimisation of the "1,8 μs " sampling pulse width. For the particular sideband at $n = 200$ to have zero amplitude a sample pulse width of

$$\tau_{sa} = 1,92 \mu s \quad (F.17)$$

would be required. Likewise for zero sideband amplitude at $n = 201$ a sampling pulse width of

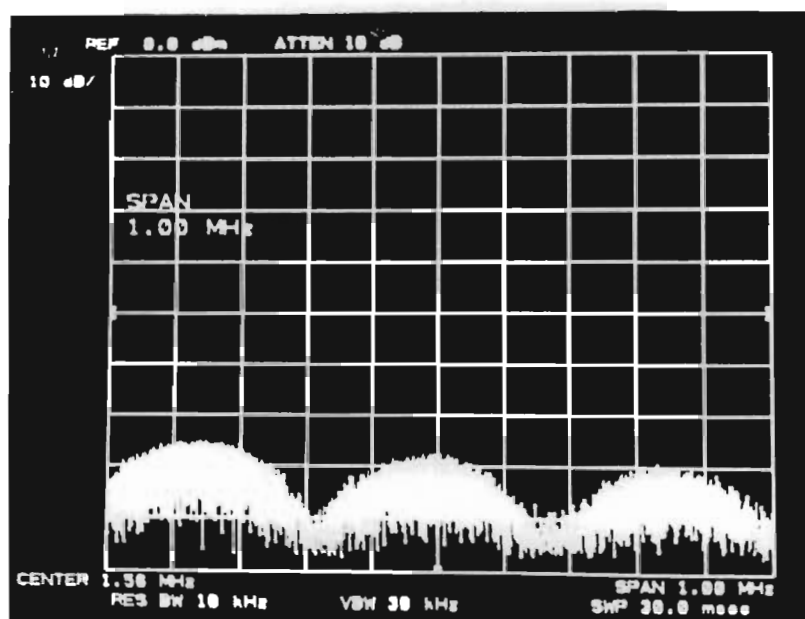
$$\tau_{sa} = 1,91 \mu s \quad (F.18)$$

is necessary. These increased pulse widths could be successfully used for sampling within the colour burst. They are remarkably close to the adopted pulse width of 1,8 μs which was initially chosen to suit the width of the colour burst pulse. Figs. F.3 (a) and (b) overleaf show recorded spectra of half-line harmonics near f_{IM} for the selected, nearly optimal sampling pulse width of 1,8



- (a) Luminance signal sampled every $128 \mu\text{s}$
with a $1.8 \mu\text{s}$ sample pulse width.

This is near to the optimum case at $192 \mu\text{s}$



- (b) Luminance signal sampled every $128 \mu\text{s}$
with a $2.8 \mu\text{s}$ sample pulse width.

This is the worst possible case.

Fig. F.3 Sampled luminance spectra about f_{IM}

Note the different Reference Levels for (a) and (b) above.

μs , together with a worst case pulse width of $2,8 \mu s$ respectively.

The second, preferred technique is to diminish luminance sampling noise by reducing the amplitude of the video signal luminance component itself before it enters the I.M. analyser down-conversion mixer. A simple R-C high pass filter with a 500 kHz cut-off frequency, shown in Fig. F.4 that follows, proved to be very effective in this regard. The sampled luminance component has an effective fundamental frequency of $7812,5 \text{ Hz}$ because of alternate line sampling. Cut-off occurs at 64 times this half-line frequency so that the luminance component is reduced in amplitude by 36 dB. Unfortunately this does not solve the problem completely.

Fig. F.5 shows the transients due to the vertical edges of the luminance waveform that are differentiated by the 500 kHz high pass filter. The amplitudes of the pulses in Fig. F.5 are proportional to the changes in luminance level at the edges that are differentiated but not equal to them because of the finite slopes of these "steps". If sampling overlaps all or part of one of these pulses, the histogram noise floor can be seen to rise. This proved to be helpful when aligning the sampling pulse position within the colour burst, since the optimum pulse position corresponded to the minimum noise floor level.

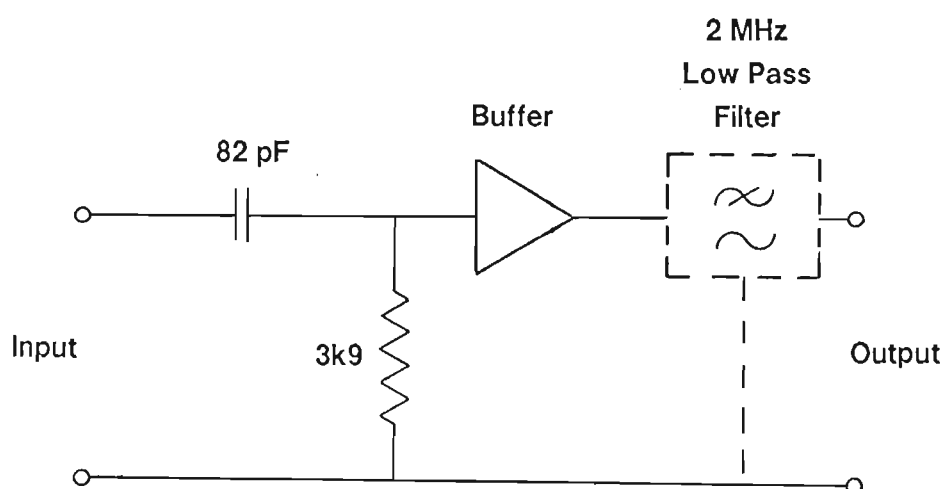


Fig. F.4 500 kHz High Pass Luminance Filter

Used to reduce luminance sampling noise.

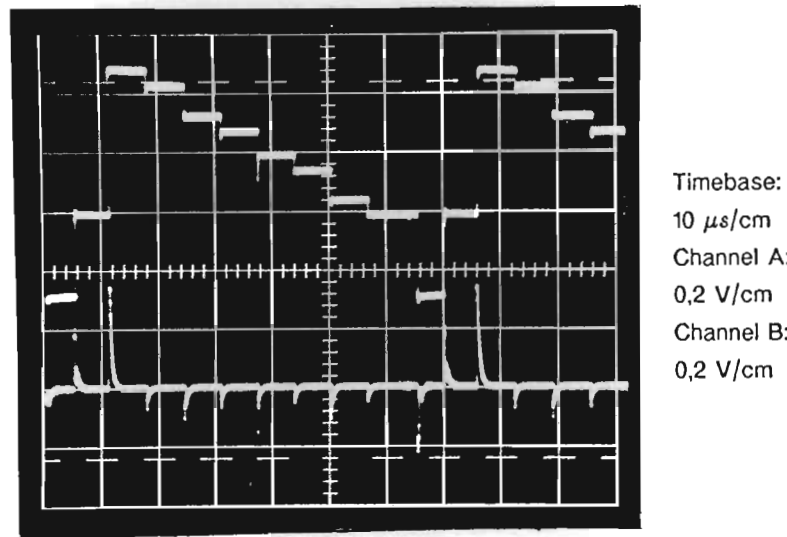


Fig. F.5 Differentiated Luminance Signal Transients

Upper Trace shows Colour Bar Luminance Content

Lower Trace shows 500 kHz High Pass Filter Output

The normalised noise power produced when a complete pulse from the high pass filter output falls within a $1,8 \mu s$ sampling period may be estimated as follows. The instantaneous filter output voltage is given by:

$$v = 0,7 V_{\text{Step}} \exp[-t/\tau] \quad (\text{F.19})$$

where the factor 0,7 (measured) corresponds to the reduction in pulse amplitude due to the finite slope of the luminance transitions. The average pulse voltage, taken over one sampling period of τ_{Sa} or $1,8 \mu s$ is therefore:

$$V_{\text{Ave}} = 0,7 \frac{1}{\tau_{\text{Sa}}} \int_0^{\tau_{\text{Sa}}} [V_{\text{Step}} \exp(-t/\tau)] dt \quad (\text{F.20})$$

$$= 0,7 \frac{\tau}{\tau_{\text{Sa}}} V_{\text{Step}} [1 - \exp(-\tau_{\text{Sa}}/\tau)] \quad (\text{F.21})$$

$$= 0,124 V_{\text{Step}} \quad (\text{F.22})$$

where V_{Step} is the change in luminance level being differentiated.

Table F.4 contains noise powers determined for the differentiated luminance signal, and assumes that the sampled signal overlaps the complete pulse. Clearly this is a worst case assumption.

Sampling within the black-to-white transient is the worst situation possible, and must be avoided if a low noise floor is to be achieved. This would represent an abnormal condition with sampling extending well beyond the end of the colour burst.

Table F.4
Noise due to Sampling of Differentiated Luminance Signals
Within a 100-0-75-0 Colour Bar Input Signal
Normalised Power Sum is 0,44183901 nW
For a 1 Volt peak Luminance Step Signal
Pulse noise power reduction factor is $(0,124 \times V_{\text{Step}})^2$
Normalised reference power is 86,903572 μW

Level Change	Luminance Step (Volts)	Noise Power (pW)	Noise Power (dBp)
Sync-Black	0,300	0,6151877	-81,50
Black-White	0,700	3,3493554	-74,14
White-Yellow	0,235	0,377486	-83,62
Yellow-Cyan	0,097	0,0643145	-91,31
Cyan-Green	0,060	0,0246075	-95,48
Green-Magenta	0,091	0,0566041	-91,86
Magenta-Red	0,060	0,0246075	-95,48
Red-Blue	0,097	0,0643145	-91,31

F.3 NOISE PRODUCED WHEN SAMPLING THE COLOUR SUBCARRIER $V_{\text{Chr}} \cos(\omega_{\text{SC}} t)$

F.3.1 Chrominance Sampling Noise Theory

Combining the sampling waveform with the field gating waveform and the colour subcarrier cosine signal gives the composite mixer output signal as the product $v_{\text{Chr}}(t) \times v_{\text{Sa}}(t) \times v_{\text{F}}(t)$. Analysis then revealed that the colour subcarrier has sideband pairs at half-line frequency spacings of

$$\begin{aligned} n^{\text{th}} \text{sb}[f_{\text{SC}}] &= f_{\text{SC}} \pm (m f_{1/2\text{H}}) \\ &= f_{\text{SC}} \pm (m 7812,5) \text{ Hz} \end{aligned} \quad (\text{F.23})$$

where "m" is an integer. The half-line sideband of the colour subcarrier ω_{SC} nearest to the intermodulation product frequency f_{IM} corresponds to the sideband number "m", where

$$m = \frac{\omega_{\text{SC}} - \omega_{\text{IM}}}{1/2 \omega_{\text{H}}} = 367 \quad (\text{F.24})$$

This corresponds to a frequency of 1566431,25 Hz which is only 50,25 Hz off the desired I.M. frequency f_{IM} at 1566381 Hz.

Each of the half-line frequency sidebands has sidebands with 50 Hz spacings due to the inhibit pulses. These relevant frequency components in mixer output are given by:

$$\begin{aligned} v_{\text{mix}}(t) &= V_{\text{Chr}} \mathbf{R}_3 \mathbf{R}_4 \text{sinc}(367 \pi \mathbf{R}_3) \sum_{n=-26}^{16} \text{sinc}(n \pi \mathbf{R}_4) \\ &\quad \times \cos(\omega_{\text{SC}} - 367 \omega_{\text{Sa}} + n \omega_{\text{F}}) t \end{aligned} \quad (\text{F.25})$$

as the frequency measurement window is centred on f_{LO} . Table F.5 overleaf lists the normalised noise powers associated with those 50 Hz sidebands falling within the window. These noise powers are summed as before to allow the total chrominance noise to be estimated for each colour bar, and the results are presented in Table F.6. The total noise was also calculated using only the 367th half-line frequency sideband and ignoring all 50 Hz sidebands. This gave a

Table F.5

50 Hz Sidebands of the 367th Half-Line Harmonic
of 1 Volt chrominance signal sampled every 128 μ s
which overlap the measurement frequency window.

To determine actual sideband amplitudes multiply by V_{chr} .

The video loss field pulse mark-space ratio is 0,9296.

Four 2nd order low pass filters with $f_c = 660$ Hz in cascade.

Sideband Number	Sideband Frequency Hz	Sideband Amplitude $\times V_{Lum}$ Volts	Filter Power Ratio $ F(j\omega) ^2$	Normalised Power $\times V_{Lum}^2$ Watts
-26	1565131.25	-2.612366E-06	1.823233E-02	1.134285E-15
-25	1565181.25	3.66135E-06	.0254356	4.336472E-15
-24	1565231.25	-4.611952E-06	.0356997	1.355403E-14
-23	1565281.25	5.410771E-06	5.032311E-02	3.707005E-14
-22	1565331.25	-6.006638E-06	7.107096E-02	9.112074E-14
-21	1565381.25	6.3527E-06	.1002292	2.0271E-13
-20	1565431.25	-6.408412E-06	.1405358	4.055501E-13
-19	1565481.25	6.141354E-06	.1948602	7.160516E-13
-18	1565531.25	-5.528828E-06	.2654957	1.077336E-12
-17	1565581.25	4.559054E-06	.3530407	1.295296E-12
-16	1565631.25	-3.23208E-06	.4551508	1.082043E-12
-15	1565681.25	1.560191E-06	.565846	3.896927E-13
-14	1565731.25	4.319401E-07	.6761678	4.265067E-14
-13	1565781.25	-2.707892E-06	.7763765	2.209925E-12
-12	1565831.25	5.220259E-06	.8587928	1.004919E-11
-11	1565881.25	-7.911992E-06	.9197949	2.648034E-11
-10	1565931.25	1.07181E-05	.9600642	5.294273E-11
-9	1565981.25	-1.356763E-05	.9833464	8.900014E-11
-8	1566031.25	1.638593E-05	.9946852	1.328262E-10
-7	1566081.25	-1.909717E-05	.9989469	1.819671E-10
-6	1566131.25	2.162677E-05	.9999341	2.338277E-10
-5	1566181.25	-2.39039E-05	1	2.856983E-10
-4	1566231.25	2.586397E-05	.9999341	3.344284E-10
-3	1566281.25	-2.745076E-05	.9989469	3.759788E-10
-2	1566331.25	2.861837E-05	.9946852	4.051644E-10
-1	1566381.25	-2.933287E-05	.9833464	4.159989E-10
0	1566431.25	-3.905029E-04	.9600642	7.027795E-08
1	1566481.25	-2.933287E-05	.9197949	3.639662E-10
2	1566531.25	2.861837E-05	.8587928	3.020207E-10
3	1566581.25	-2.745076E-05	.7763765	2.271033E-10
4	1566631.25	2.586397E-05	.6761678	1.529218E-10
5	1566681.25	-2.39039E-05	.565846	9.147538E-11
6	1566731.25	2.162677E-05	.4551508	4.844666E-11
7	1566781.25	-1.909717E-05	.3530407	2.272782E-11
8	1566831.25	1.638593E-05	.2654957	9.462962E-12
9	1566881.25	-1.356763E-05	.1948602	3.494812E-12
10	1566931.25	1.07181E-05	.1405358	1.134435E-12
11	1566981.25	-7.911992E-06	.1002292	3.144345E-13
12	1567031.25	5.220259E-06	7.107096E-02	6.882376E-14
13	1567081.25	-2.707892E-06	5.032311E-02	9.284695E-15
14	1567131.25	4.319401E-07	.0356997	1.188902E-16
15	1567181.25	1.560191E-06	.0254356	7.87426E-16
16	1567231.25	-3.23208E-06	1.823233E-02	1.736274E-15

Normalised noise power = 7.405301982092451D-08 * V_{chr}^2 Watts

Normalised reference Power = 1.335080014541745D-04 Watts

Power Ratio = -32.55964424321171 dBp for $V_{chr} = 1$ Volt

power ratio of $-32,79 \text{ dBp}$ for a 1 Volt peak chrominance signal, or $-0,27 \text{ dB}$ error. If R_4 is ignored the error becomes $-0,27 + 0,63 \text{ dB}$, or $0,36 \text{ dB}$. This justifies the decision made in Chapter 2 to ignore v_F when considering the I.M. component as the small error so introduced may be calibrated out.

Table F.6

Noise due to Sampling of Chrominance Signals
 Within a 100-0-75-0 Colour Bar Input Signal
 Normalised Power Sum is 77,503 nW
 for a 1 Volt peak Chrominance Signal
 Normalised reference power is 0,133508 mW

Colour	Chrominance Peak Signal (Volts)	Noise Power (nW)	Noise Power (dBp)
Yellow	0,235	3,401532	-45,14
Cyan	0,332	6,789144	-42,14
Green	0,302	5,617625	-42,96
Magenta	0,310	5,919895	-42,73
Red	0,334	6,871187	-42,09
Blue	0,235	3,401532	-45,14

F.3.2 Chrominance Noise Reduction Techniques

Again two methods are available for reducing the chrominance sampling noise.

Firstly, it is possible to reduce the amplitude of the particular sideband at $n = 367$ to zero by narrowing the sampling pulse width to

$$\tau_{sa} = 348,77 \text{ ns} \quad (\text{F.26})$$

A loss of gain of $14,25 \text{ dB}$ would result from this sampling pulse width, which is far smaller than the $1,8 \mu\text{s}$ pulse width in use in the sampling analyser. This method does not present a practical solution to the problem.

The second preferred solution is obvious once the problem has been identified. This involves removing the colour subcarrier from the video signal, before it reaches the mixer where the sampling is performed, without attenuating the level of the wanted I.M. signal at f_{IM} significantly. A passive low pass Butterworth filter was selected for this purpose because of its maximally flat pass band characteristic, and the cut-off frequency chosen at 2 MHz to pass f_{IM} while attenuating f_{SC} by some 40 dB . This 2 MHz cut off frequency, together with the 500 kHz high pass luminance filter, resulted in a system bandwidth BW of 1.5 MHz which produced a system rise time of approximately BW^{-1} or $0.67\text{ }\mu\text{s}$. Sampling should therefore be timed to occur more than $3.0\text{ }\mu\text{s}$ after the beginning of each I.M. signal measurement region. This could be implemented within each of the six colour bars, but was not possible in the colour burst.

F.3.3 Low Pass Filter Design Options

Two passive Butterworth filter design options were considered. These are the doubly-terminated filter with equal, non-zero resistive source and load terminations, and the singly-terminated filter driven from an ideal voltage source with zero internal resistance and loaded with a resistor at the output.

The major disadvantage of the former filter is the 6 dB pass band loss inherent in the network due to the voltage divider effect of the equal valued source and load resistors. A disadvantage of the singly-terminated network is that ringing is more likely to occur if the filter is incorrectly tuned, and the doubly-terminated option was therefore chosen for the prototype. It should be noted, however, that a 6 dB signal-to-noise improvement is possible in the analyser if the alternative singly-terminated filter is used.

F.3.4 Filter Component Values

It was decided to attenuate the colour subcarrier component at frequency f_{SC} by at least 40 dB . The squared form of the normalised Butterworth transfer function (which is the power transfer function) for an k^{th} order filter is

$$|H(j\omega)|^2 = \frac{1}{1 + \omega^{2k}}$$

$$= 10^{-4} \quad (\text{F.27})$$

for a 40 dB reduction at f_{SC} . The value used for ω in equation (F.27) is the frequency ratio f_{SC}/f_c . Choosing

$$f_c = 2.0 \text{ MHz} \quad (\text{F.28})$$

we find that

$$k = 6 \quad (\text{F.29})$$

A general sixth order passive filter schematic diagram is shown in Fig. F.6. Normalised values for a sixth order low pass filter with Butterworth (maximally flat) response are available from tables, such as those in Kuo [64], and are given in Table F.7.

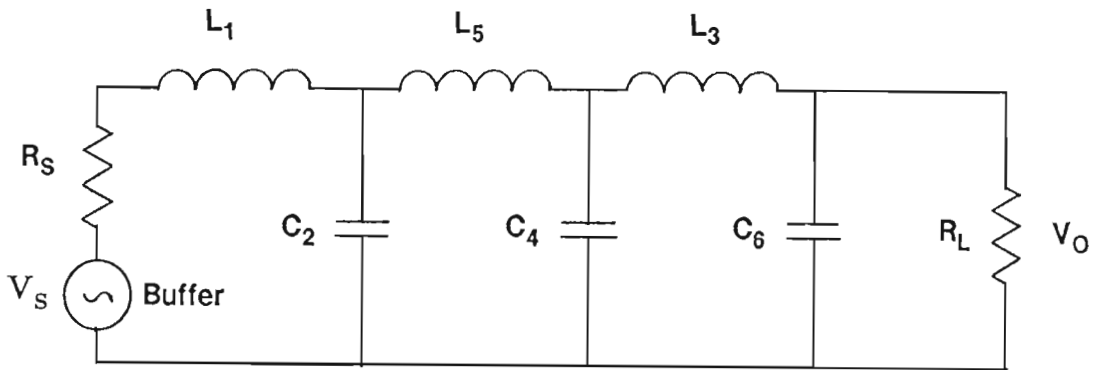


Fig. F.6 Sixth Order Passive Butterworth Filter

$R_S = 0$ and $R_L = 1 \Omega$ for Singly-Terminated

Both R_S and $R_L = 1 \Omega$ for Doubly-Terminated

To scale these values for a termination of R_o and a cut off frequency of ω_c the following factors are required:

Inductor Scaling:

$$L_i = \frac{L_{iN} R_o}{\omega_c} \quad (\text{F.30})$$

Table F.7
Normalised Values for Butterworth Filter
Ideal Elements

$R_s = 0$ and $R_L = 1 \Omega$ for Singly-Terminated
Both R_s and $R_L = 1 \Omega$ for Doubly-Terminated

Normalised Values	Singly-Terminated	Doubly-Terminated
L_{1N}	0,5586 μH	0,5176 μH
C_{2N}	1,7590 F	1,4140 F
L_{3N}	1,5530 μH	1,9320 μH
C_{4N}	1,2020 F	1,9320 F
L_{5N}	0,7579 μH	1,4140 μH
C_{6N}	0,2588 F	0,5176 F

Table F.8
Scaled Ideal Elements Values
Butterworth Low Pass Filter

$R_s = 0$ and $R_L = R_o$ for Singly-Terminated
Both R_s and $R_L = R_o$ for Doubly-Terminated

Normalised Values	Singly-Terminated	Doubly-Terminated
L_1	123,6 μH	3,10 μH
C_2	140,0 pF	1,50 nF
L_3	123,6 μH	11,53 μH
C_4	95,7 pF	2,00 nF
L_5	60,3 μH	8,44 μH
C_6	20,6 pF	0,55 nF

Capacitor Scaling:

$$C_j = \frac{C_{jN}}{R_o \omega_c} \quad (F.31)$$

For

$$R_o = 1000 \Omega \quad (F.32)$$

and

$$\omega_c = 2 \pi 2,0 \text{ Mrad/s} \quad (F.33)$$

the scale factors are:

$$L_i = 7,957747 \times 10^{-5} L_{iN} \quad (F.34)$$

$$C_j = 7,957747 \times 10^{-11} C_{jN} \quad (F.35)$$

The scaled values are summarised in Table F.8.

F.3.5 Response of Passive Butterworth Filter

The behaviour of the filter when connected in the analyser system, which includes a 500 kHz high pass R-C filter, is represented in Fig. F.7. A sweep generator and spectrum analyser were used for the tests. The 1 k Ω terminations were included in the output of the voltage follower LM310 and the input to the video amplifier which made use of an LM733 wideband amplifier chip.

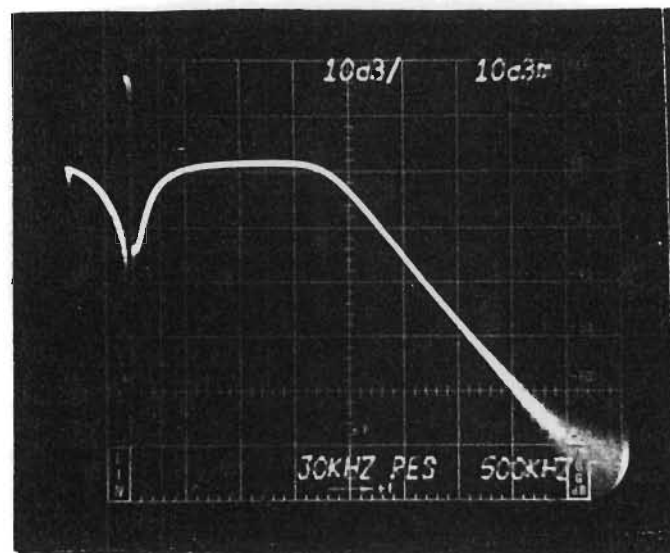


Fig. F.7 Butterworth Filter Frequency Response
Spectrum Analyser Plot from Sweep Generator

F.4 CONCLUSIONS

Luminance Sampling Noise Reduction: The simple high pass R-C filter with a 500 *kHz* cut-off frequency proved very effective in reducing noise introduced by sampling a luminance signal.

Chrominance Sampling Noise Reduction: A more complex 2 *MHz* low pass passive filter also proved adequate to the task of reducing the interference caused by sampling a chrominance signal. I.M. measurements were impossible without this filter, and its inclusion was a major factor in the success of the I.M. analyser. The consequent reduction in system bandwidth had the undesired effect of increasing response time and thereby increasing the error associated with all I.M. distortion measurements.

APPENDIX G

SABC TV Specifications for TV Colour Bar Signals and TV Carrier Frequency Tolerances

G.1 TV COLOUR BAR SPECIFICATIONS

G.1.1 Introduction

Before a specification for the sampling pulse timing generator could be drawn up, the colour bar input signals were carefully investigated. Although the colour bars are subject to rather detailed specifications in almost all respects, a few important exceptions were noted. These will be considered later.

The SABC specifications for one line of each of the 100-0-100-0 composite field colour bar signal and an alternative 100-0-75-0 colour bar signal, which can be applied to the I.M. analyser, are given in Figs. G.1 and G.2 respectively on the next page. Both video signals have a peak white to sync tip amplitude of 1,0 V. Line sync and colour burst pulses are specified in both relative position and absolute amplitude with some precision. Luminance levels and chrominance subcarrier amplitudes are also carefully specified in millivolts.

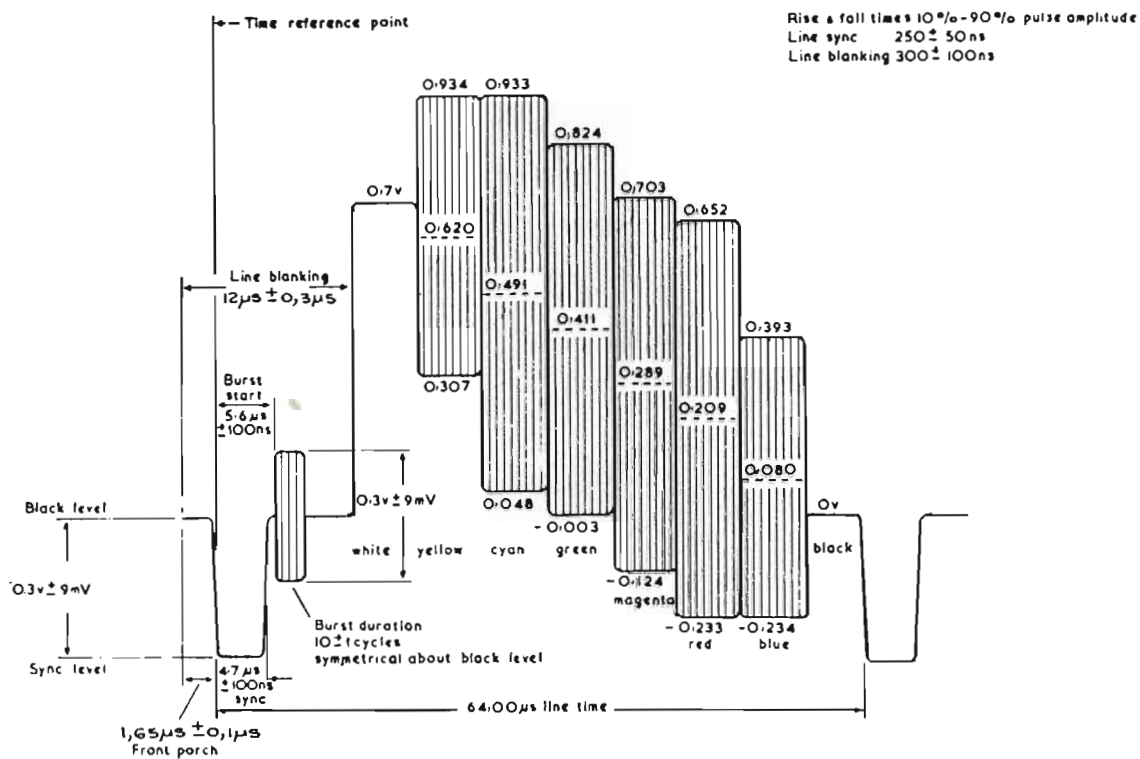


Fig. G.1 100-0-100-0 Colour Bar Video Signal

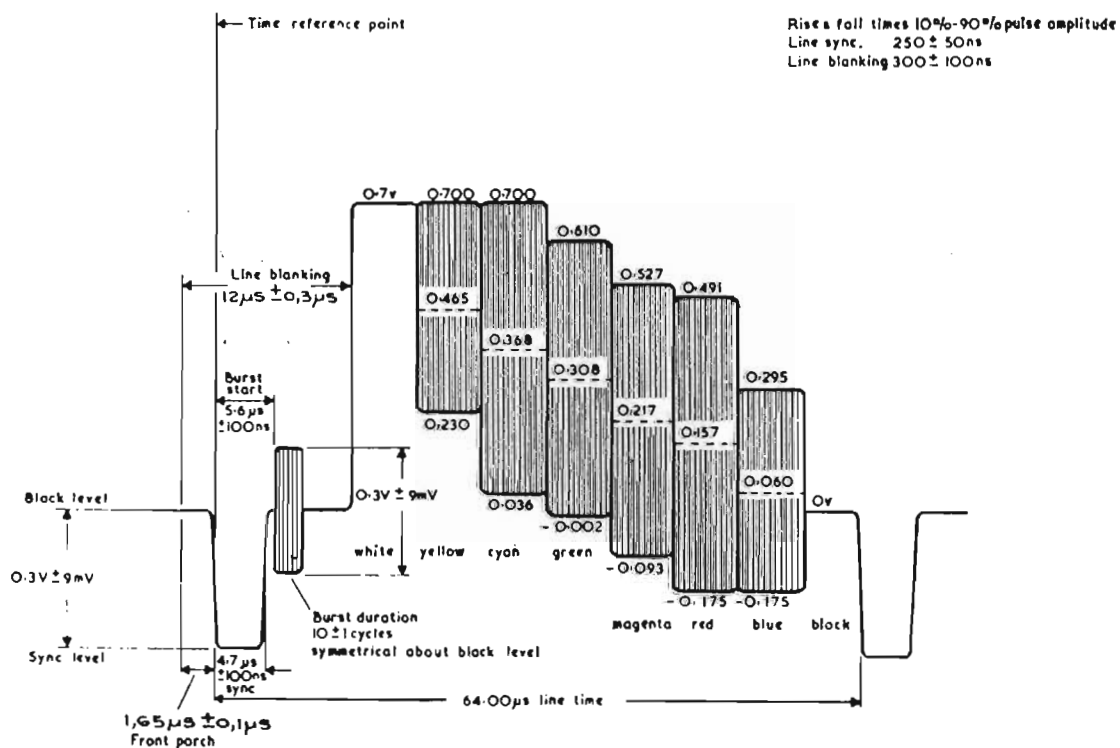


Fig. G.2 100-0-75-0 Colour Bar Video Signal

G.1.2 Field Sync Pulse Specifications

Field synchronisation waveforms which apply to Systems I/PAL and B+G/PAL follow in Figs. G.3 and G.4. These waveforms are of vital importance to the operation of the phase lock timing system as they identify pulse edges that occur with an unbroken period of T_H . These edges, which have the symbol “ \wedge ” below for indication, may therefore be used for synchronisation purposes. The data in Table G.1 applies to both Figs. G.3 and G.4.

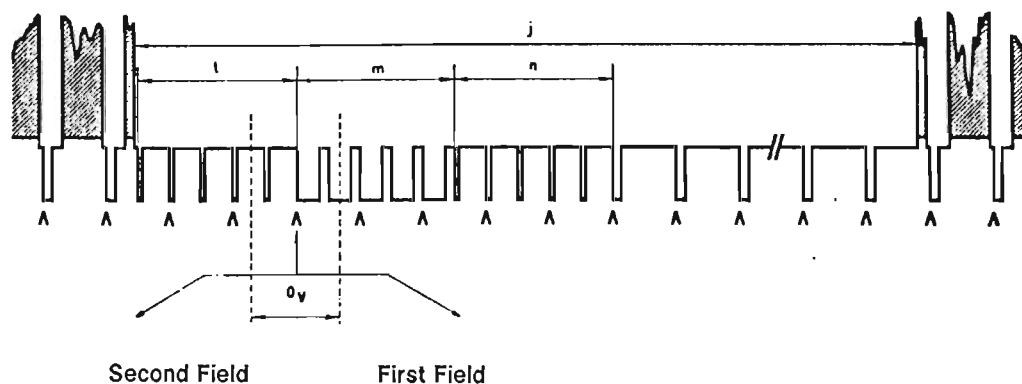


Fig. G.3 Field Synchronising Waveforms

Signal at the Beginning of each First Field
Applicable to Systems I/PAL and B+G/PAL but not M/NTSC

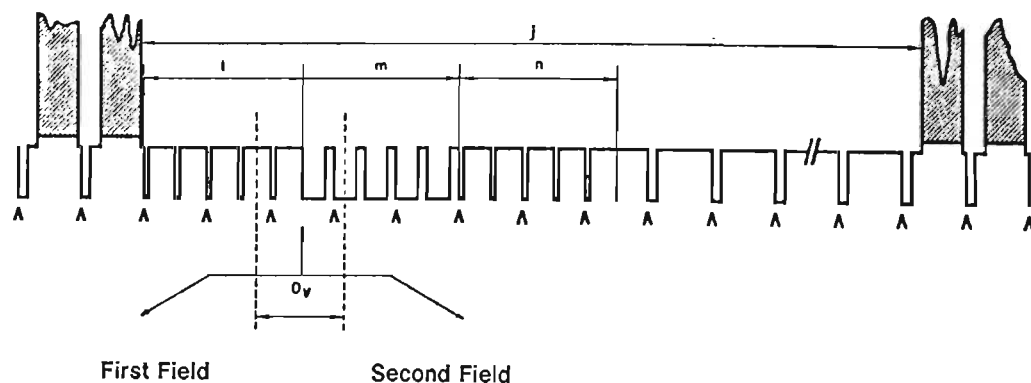


Fig. G.4 Field Synchronising Waveforms

Signal at the Beginning of each Second Field
Applicable to Systems I/PAL and B+G/PAL but not M/NTSC

Table G.1
Equalising Pulse Sequence Specifications

Duration of first sequence	$l = 2,5 H$
Duration of sequence	$m = 2,5 H$
Duration of second sequence	$n = 2,5 H$

Details of the field sync and equalising pulses are given in Fig. G.5 and the corresponding data in Table G.2 below.

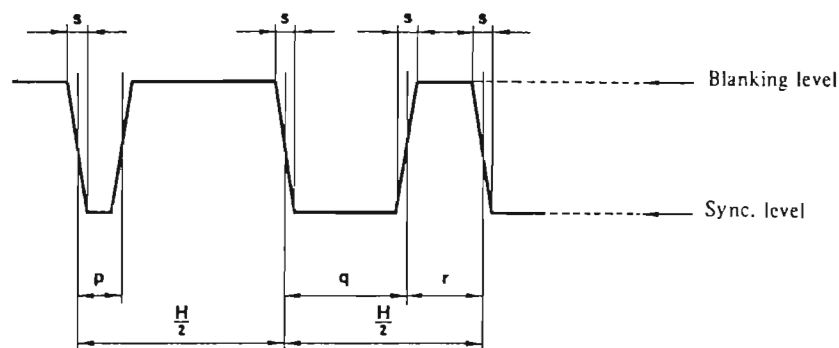


Fig. G.5 Field Sync and Equalising Pulse Details

Table G.2
Field Sync and Equalising Pulse Timing Specifications

Duration of sync pulse	$q = 27,3 \mu s$
Interval between sync pulses	$r = 4,7 \mu s \pm 0,2 \mu s$
Rise time of sync pulses	$s = 0,2 \mu s \pm 0,1 \mu s$
Duration of equalising pulse	$p = 2,35 \mu s \pm 0,1 \mu s$
Rise time of equalising pulses	$s = 0,2 \mu s \pm 0,1 \mu s$

The field synchronising signal for M/NTSC differs mainly in the number of equalising pulses, as may be seen in the relevant CCIR Report from which these waveforms were extracted [13].

G.1.3 Line Sync Pulse Specifications

All synchronisation in the sample pulse timing generator is aligned to the negative going leading edge of the line sync pulse, because the edge is continuously available at a constant repetition rate. These edges are identified by the symbols “ \wedge ” situated below the field synchronising waveforms in Figs. G.3 and G.4.

Line sync pulse specifications for the I/PAL System are given in Table G.3, which refers to the symbols in Fig. G.6. Corresponding specifications for the M/NTSC System are also included.

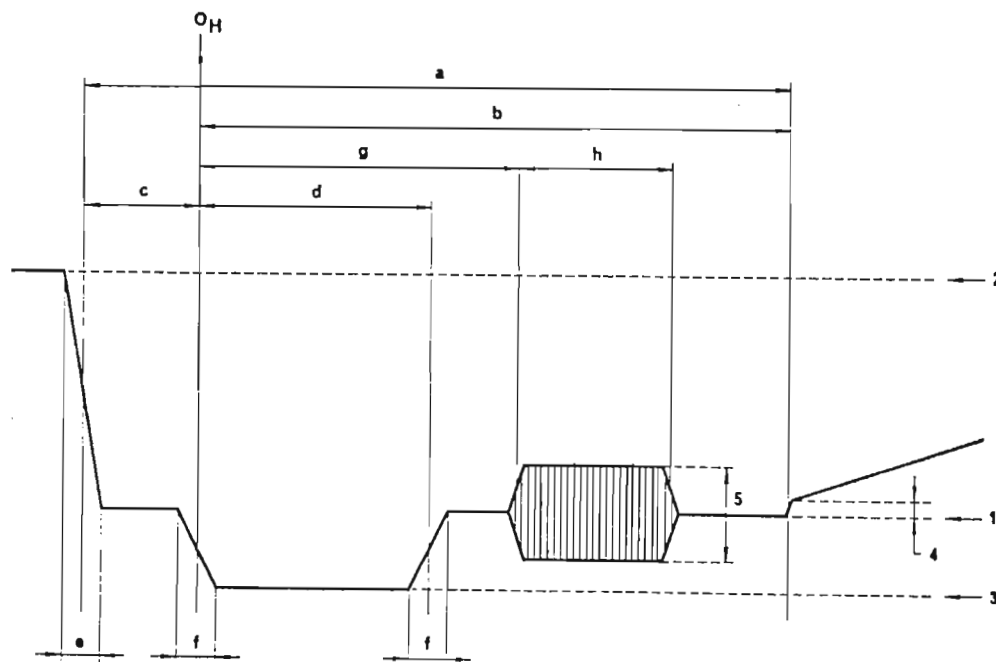


Fig. G.6 Line Sync Pulse Specifications

Table G.3
TV System Line Sync Specifications

TV SYSTEMS: I,B and G/PAL		
Nominal Line Period	$T_H =$	$64 \mu s$
Line-Blanking Period	$a =$	$12 \mu s \pm 0,3 \mu s$
Front Porch	$c =$	$1,5 \mu s \pm 0,3 \mu s$
Synchronising Pulse	$d =$	$4,7 \mu s \pm 0,2 \mu s$
Sync Pulse Rise Time	$=$	$0,2 \mu s \pm 0,1 \mu s$
Sync Pulse Amplitude	$=$	$300 mV \pm 9 mV$
TV SYSTEM: M/NTSC		
Nominal Line Period	$T_H =$	$63,5555 \mu s$
Line-Blanking Period	$a =$	$10,9 \mu s \pm 0,2 \mu s$
Front Porch	$c =$	$1,27 \mu s \rightarrow 2,22 \mu s$
Synchronising Pulse	$d =$	$4,7 \mu s \pm 0,1 \mu s$
Sync Pulse Rise Time	\leq	$0,25 \mu s$
Sync Pulse Amplitude	$=$	$300 mV \pm 9 mV$

G.1.4 Colour Burst and White Bar Specifications

Colour burst pulse, and white bar specifications relative to specified edge of the line sync pulse, are summarised in Table G.4 below. The burst width data was vitally important for determining the width of the sampling pulse and its position relative to the line sync pulse leading edge. Note that the line time reference point, at the beginning of the front porch of width $1,65 \mu s \pm 0,1 \mu s$, is used to specify the white bar leading edge position.

Table G.4
Colour Burst and White Bar Specifications

Burst Pulse Width	= 10 ± 1 cycles of subcarrier or = $2,2 \pm 0,2 \mu s$
Burst Amplitude	= $300 \pm 9 \text{ mV}$ peak-to-peak
White Bar Amplitude	= $0,7 \text{ V}$ peak
White bar position	= $12 \pm 0,3 \mu s$

G.2 ESTIMATED TOLERANCES IN EXPECTED INTERMODULATION PRODUCT FREQUENCIES

G.2.1 Introduction

CCIR Television System Specifications [13] indicate that tolerances of $\pm 1 \text{ kHz}$ are acceptable in sound subcarrier frequency f_s for Systems B/PAL and G/PAL, while $\pm 500 \text{ Hz}$ is acceptable in System I/PAL. Some of the older equipment used in Europe has these large frequency tolerances, but the SABC gave an assurance that the modern equipment installed in their transmitters had far smaller tolerances. As the prototype I.M. analyser was originally required for use on this modern equipment, the smaller tolerances were assumed to apply for the design.

G.2.2 Expected Frequency Tolerances

In this section, System I/PAL will be assumed throughout as this was the initial system design requirement. No corresponding values are available for TV systems in other countries.

Define the 1,57 MHz I.M. signal as:

$$v_{IM} = K \sin 2\pi (f_s - f_{sc})t \quad (G.1)$$

where K is a constant. Ideally, the frequency of the 1,57 MHz I.M. will be:

$$\begin{aligned} f_{IM} &= f_s - f_{sc} \\ &= 1,566381 \text{ MHz} \end{aligned} \quad (G.2)$$

Estimates of frequency tolerances associated with various types of modern TV broadcasting equipment were obtained from the Research Department of the SABC, and these are presented in what follows.

SBUF Test Transmitter:

$$f_s = 6 \text{ MHz} \pm 50 \text{ Hz} \quad (G.3)$$

TEKTRONIX Type 1411 Colour Bar Generator:

$$f_{sc} = 4,43361875 \text{ MHz} \pm 5 \text{ Hz} \quad (G.4)$$

Horizontal Line Frequency f_H :

$$\begin{aligned} f_H &= \frac{4f_{sc}}{(1135+4/625)} \text{ Hz} \\ &= 15625 \pm \frac{20}{(1135+4/625)} \text{ Hz} \\ &= 15625 \pm 0,0186 \text{ Hz} \end{aligned} \quad (G.5)$$

Therefore

$$\begin{aligned} f_{IM} &= 6 \text{ MHz} \pm 50 \text{ Hz} - 4,43361875 \text{ MHz} \pm 5 \text{ Hz} \\ &= 1,566381 \text{ MHz} \pm 55 \text{ Hz} \end{aligned} \quad (G.6)$$

The I.M. analyser automatically monitors both these frequencies with no external adjustments required by appropriate choice of local oscillator frequency. It also accommodates variations in the I.M. frequency of up to $\pm 55 \text{ Hz}$ with a resultant reading error of less than $\pm 0,25 \text{ dB}$.

G.3 COMPATIBLE PULSE TIMER SPECIFICATIONS

As the width of each colour bar is not determinable from the SABC Specification, their leading edges are not defined relative to the line sync pulse leading edge. This means that the sampling pulses used must be narrower than $6,4 \mu s$ and positioned within each bar in such a way that they cannot cross colour bar boundaries.

G.4 CONCLUSIONS

In view of the tighter specifications on frequency tolerances that have been assumed for the design of the prototype, it can be expected that the analyser will have problems when used on older transmitting equipment. Two solutions are possible.

Firstly, it is possible to extend the bandwidth of the active Sallen and Key low pass filters to say $2 kHz$. This would introduce more noise to the measurement system and reduce its dynamic range. A major portion of the noise will again be due to the $50 Hz$ sidebands of half-line frequency harmonics adjacent to the measurement window.

Alternately, an indication could be included to the effect that the frequency emerging from the low pass filters is within the $400 Hz$ band allowed. If not, the sound carrier frequency must either be adjusted or replaced by an accurate signal source. If this is not possible the measurement must be abandoned. This latter situation is not satisfying, but it would not be encountered often in practice and is therefore not too serious a problem.

APPENDIX H

Papers Published on the Sampling Type Intermodulation Distortion Analyser

This Appendix contains copies of two papers co-authored by the writer and referred to in references [8] and [9].

MEASURING TELEVISION TRANSPOSER INTERMODULATION DISTORTION

A D Broadhurst, P F Bower,

*Department of Electronic Engineering, University of Natal
Durban 4001, South Africa*

A L Curle

*South African Broadcasting Corporation, P O Box 8606,
Johannesburg, 2000, South Africa*

ABSTRACT

Intermodulation (I.M.) occurs in common amplification broadcast television transposers when the color subcarrier and the vision and sound carrier components interact in the presence of common amplifier non-linearities. Static measuring techniques, such as the three-tone method neglect the fact that a picture contains varying levels of luminance and chrominance information. This causes the I.M. level to vary from one instant to another, as the three carrier components experience different degrees of non-linearity during common amplification in the transposer.

This paper examines the behavior of the I.M. level during one line period and proposes a new measuring method allowing the use of a standard or a modified color bar test signal. The latter enables the non-linearity of the transposer to be minimized in the line synchronization region and this is shown to minimize vision/sound cross-modulation. Differential gain and phase can also be optimized. Measurements indicate that minimization of the I.M. level with the three-tone method (which corresponds to the carrier levels associated with the 100/0/75/0 cyan color bar in the South African television system) often causes unacceptable I.M. limits at other colors. The measurement technique is based upon sampling the demodulated color bar signal for short intervals corresponding to a selected color. This allows the simultaneous measurement of I.M. level at seven different points on the transposer's characteristic. The paper concludes that the internationally accepted three-tone test method appears to be inadequate.

1. INTRODUCTION

Intermodulation distortion occurs in common R.F. amplification television broadcast transposers, when the vision carrier, color subcarrier and sound carrier frequency components interact in the presence of amplifier non-linearities [1]. Fig.1 shows a typical characteristic of a 5 kW tetrode. When these non-linear devices are amplitude modulated by the video and sound signals, various spurious

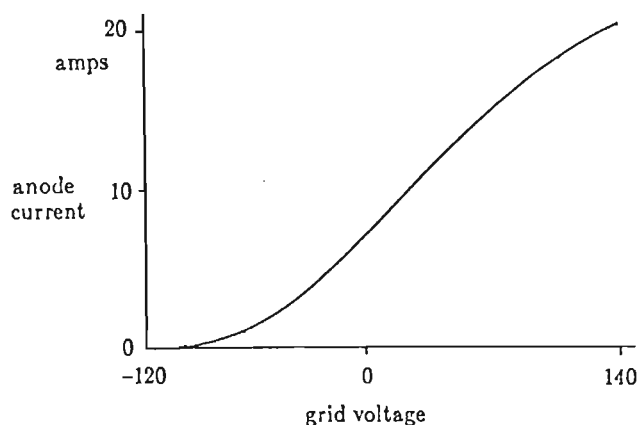


Fig.1 A typical characteristic of a 5 kW tetrode.

frequency components are generated as the excitation frequencies beat together or with their harmonics. If the three frequency components are represented as single frequencies f_v the vision carrier, f_{sc} the color subcarrier and f_s the sound carrier, two in-band intermodulation components occur, the most significant at a frequency of

$$\begin{aligned} f_{ip} &= f_v + f_s - f_{sc} \\ &= f_v + 920455.00 \text{ Hz for M/NTSC} \\ &= f_v + 1066381.25 \text{ Hz for B+G/PAL} \\ &= f_v + 1565981.25 \text{ Hz for I/PAL} \end{aligned} \quad (1.1)$$

which may cause perceptible interference patterns if the level of the intermodulation component is too high [1]. The maximum power which may be produced by a transposer [4] is limited by the permissible intermodulation level which is typically -53 dBp, i.e. 53 dB below the power transmitted during the synchronizing pulses.

Mathematical analyses [1,2,3,4] represent the transfer characteristic of the amplifier as a series containing 3 terms

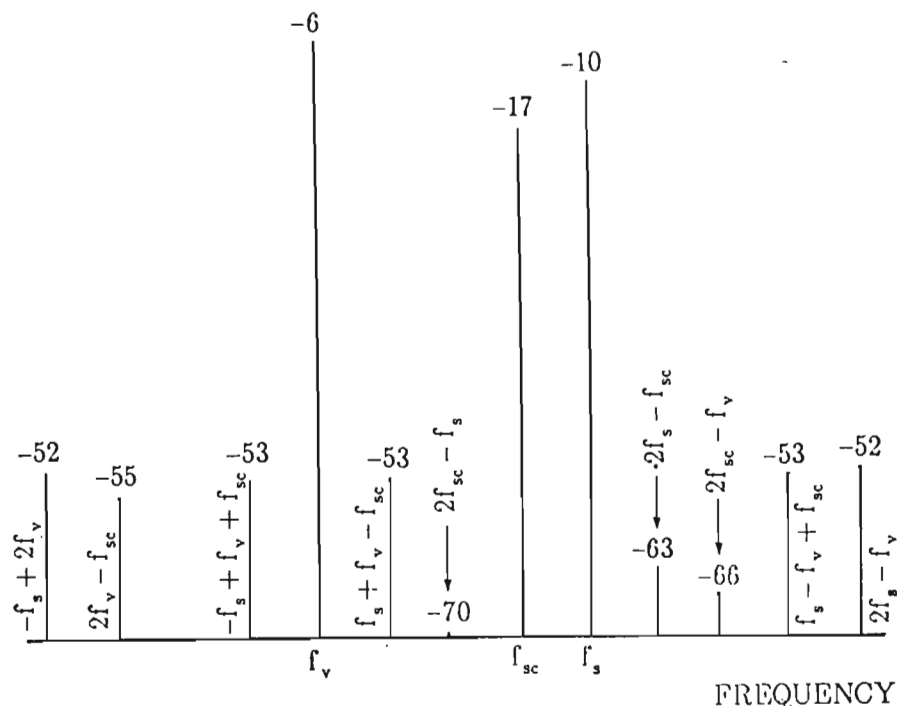


Fig.2 The three-tone test signal and third order intermodulation products calculated using [4] for the South African I-PAL system. An intermodulation level of -53 dBp is assumed.

$$e_s = K_1(e_i) + K_2(e_i)^2 + K_3(e_i)^3 \quad (1.2)$$

where K_1 , K_2 and K_3 are complex numbers which represent the gain and amplitude and phase distortion. The instantaneous input and output voltages are e_i and e_s respectively. When a simulated three-tone excitation signal of the form

$$e_i = A_v \cos \omega_v t + A_{sc} \cos \omega_{sc} t + A_s \cos \omega_s t \quad (1.3)$$

is applied to the amplifier various sidebands are produced. The even terms ($n=2,4$ etc) produce out of band distortion components, but the odd terms ($n=3,5$ etc) produce in-band components. The largest of these is that produced by the third term and most mathematical analyses neglect the higher order terms. The spectrum of the three-tone test signal and the third order intermodulation products are shown in Fig.2. The third order term produces two in-band intermodulation components given in Eqn.1.4 and it is the first term which is most visible, the second term being of much lower amplitude, typically 17 dB less.

$$e_{ip} = 1.5K_3A_vA_sA_{sc} \cos(\omega_v + \omega_s - \omega_{sc})t \quad (1.4)$$

$$+ 0.75K_3A_vA_s^2 \cos(2\omega_{sc} - \omega_s)t$$

Broadcasting authorities presently measure intermodulation distortion by applying a three-tone simulation of a composite video and sound signal to the transposer and then measure the relative amplitude of the major in-band intermodulation

product on a spectrum analyzer, referencing the level to the power transmitted during the synchronizing pulses. To perform the three-tone test the transposer is taken out of service and a signal applied which simulates the average video signal. Three signal generators are required to generate the three RF carriers, one having a frequency and amplitude equivalent to mid-gray at the vision carrier frequency. The amplitude of the second is equivalent to a large chrominance level of 0.7 V p.p., i.e. with the tips of the color subcarrier reaching the black and white levels. The third signal has an amplitude and frequency equivalent to the sound carrier.

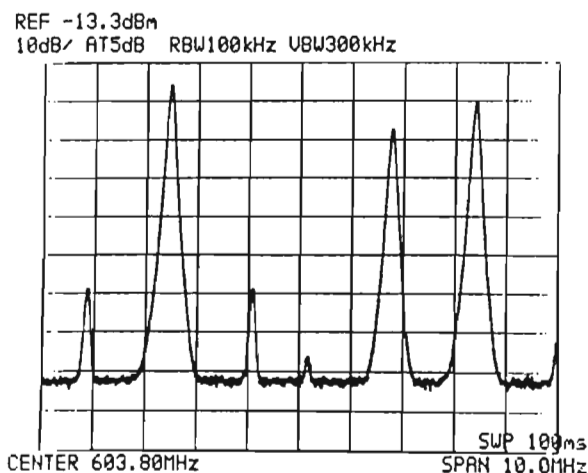


Fig.3

Typical three-tone spectrum at the output of the transposer showing the two in-band frequency components. The intermodulation level is -59 dBp. The reference level corresponds to peak sync. power.

The three levels and frequencies vary from system to system depending upon the percentage of peak power radiated during the black and white levels, and the power ratio between the peak vision and sound powers. Typical levels relative to peak sync power are -6 dB for the vision carrier, -10 dB for the sound carrier and -17 dB for the color subcarrier. These figures apply to the I-PAL system. Fig.3 shows a typical frequency spectrum, where the in-band and out-of-band intermodulation products are clearly visible. This three-tone method is slow and requires a skillful operator to achieve repeatable results. For maintenance work where less expensive spectrum analyzers are used, intermodulation levels are difficult to measure accurately because of their limited dynamic range, typically 60 dB.

The three-tone method tests the common r.f. amplification equipment at one luminance level and one chrominance level and therefore does not test the equipment over its full operating range. As far as the authors are aware only two broadcasting authorities, NHK (Japan Broadcasting Corporation) and IBA (Independent Broadcasting Authority), require the intermodulation performance of transposers to be measured at several luminance and chrominance levels. NHK[5] specifies that intermodulation should be measured at six points corresponding to the levels associated with the yellow, cyan, green, magenta, red and blue color bars of a color bar waveform and specifies that all intermodulation levels shall be less than -49 dBp. IBA[6] specifies the vision, chrominance and sound as -8 dBp, -17 dBp and -7 dBp respectively for the UK I-PAL system. The test is then repeated twice with vision levels of -3.5 dBp and -10.5 dBp. The worst figure is taken as the result.

These lengthy measurement procedures check the overall performance of a transposer, but are not convenient for adjusting the transposer's intermodulation precorrector. Intermodulation levels for the six colors are not available simultaneously and it has been found by the authors that a minimum at one color does not correspond to a minimum at another. See Appendix.

Only one other method has been proposed in the literature to measure intermodulation. Flor [7] uses insertion test line 331 in the B+G/PAL system and with this method the transposer does not have to be removed from service, because the levels of the luminance and color subcarrier are nearly the same as the three-tone test signals. The method relies upon filtering out the 1.07 MHz intermodulation product with a 200 kHz wide bandpass filter. The rise time of this filter is sufficiently small to respond to the 1.07 MHz intermodulation component during the duration of the color bar and so its amplitude may be measured with an oscilloscope. Unfortunately, many of the line spectra of the video signal are also present at the output of the bandpass filter, with the result that the dynamic range of the measurement is limited to about -45 dBp. Any attempt to reduce the bandwidth of the filter further prevents the 1.07 MHz component rising to its full amplitude during the duration of the color bar.

A new method [8] has been proposed by the authors which

appears to overcome many of the limitations of existing measuring techniques. In this paper we examine the intermodulation levels at different luminance levels using both the three-tone method (with different generator amplitudes) and the new method. The ratios of the levels are compared with theoretical differences calculated according to eqn.1.4. It is shown that it is not sufficient to measure the intermodulation component at one luminance level and that the differences are not fixed for all transposers as eqn.1.4 indicates. This is due to phase cancellation in multistage transposers and imperfections of precorrector circuits.

A need therefore exists for a measuring technique which will allow the simultaneous measurement of intermodulation at different luminance levels. This allows the overall performance of the transposer to be judged and assists with the adjustment of those transposers which employ precorrectors to minimize intermodulation distortion. It has been found that, while some precorrectors minimize the intermodulation level obtained with the three-tone measurement (corresponding to mid-gray or the color cyan), they may do so at the expense of the intermodulation levels at other luminance levels.

From an examination of the dynamic behavior of the intermodulation level during one line period, it is shown that a 100/0/75/0 composite full field color bar signal may be used to excite the transposer. Alternatively, a modified color bar test signal is proposed that enables the complete non-linearity of the transposer to be minimized, including the non-linearity in the line synchronization region and this is shown to minimize differential gain and phase, as well as the vision/sound cross-modulation.

The measurement technique is based upon sampling (at line frequency for NTSC systems and half line frequency for PAL systems) the demodulated color bar signal for short intervals corresponding to a selected color. This overcomes the limitations of Flor's method [7] and allows the simultaneous measurement of the intermodulation level at seven different points on the transposer's characteristic.

2. MEASURING INTERMODULATION WITH COLOR BARS

Intermodulation may be measured directly by the application of a color bar waveform via a test transmitter to the transposer. See Figs.4 & 5. However, the frequency spectrum at the output of the transposer cannot be examined directly, because of the narrow bandwidth required of the spectrum analyzer to separate the intermodulation component from the other line spectra. This narrow bandwidth results in the average level being measured for all the six colors, and, because of phase cancellation, will bear no relationship to the true intermodulation levels.

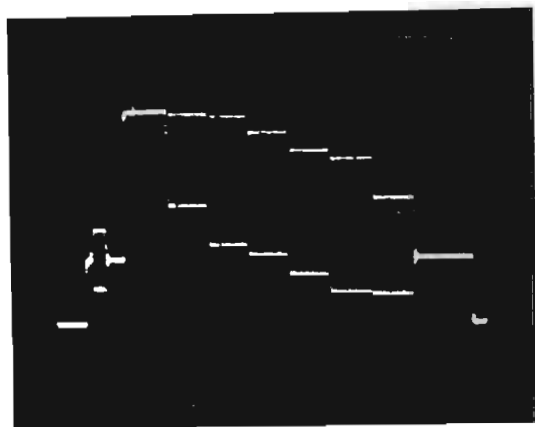


Fig.4 The line waveform of 100/0/75/0 color bars used to measure intermodulation distortion.

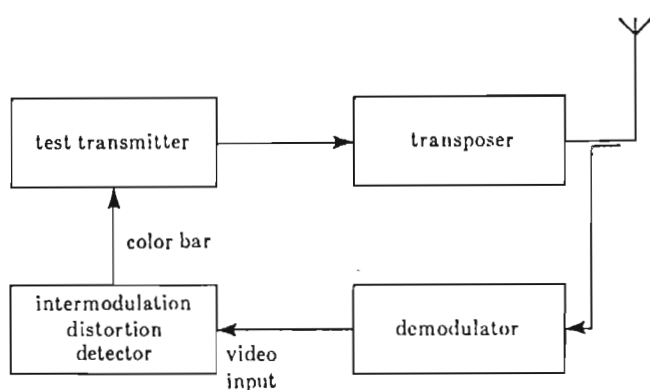


Fig.5 Block diagram of the test gear configuration used to measure intermodulation distortion with the color bar waveform shown in Fig.4.

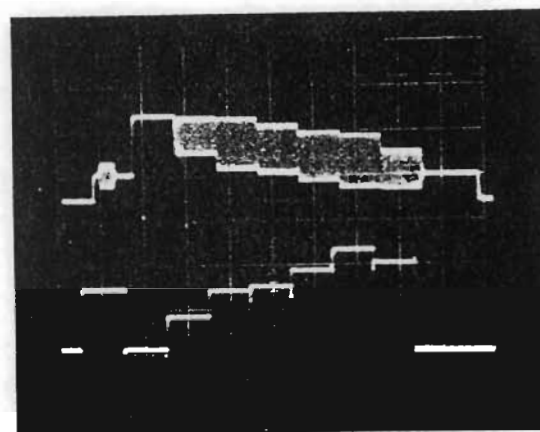


Fig.6 The histogram waveform of the intermodulation detector displaying intermodulation levels associated with the color burst, zero level (white), yellow, cyan, green, magenta, red, blue, zero level (black) and zero level (sync).

SYSTEMS	M/NTSC	B+G/PAL	I/PAL
Video Bandwidth B_v	4.2 MHz	5.0 MHz	5.5 MHz
Video rise time $t_{rv} = 1/B_v$	0.25 μ s	0.20 μ s	0.18 μ s
Chrom. Bandwidth B_{sc}	+0.62 MHz -1.30	+0.57 MHz -1.30	+1.07 MHz -1.30
Chrom. Rise time $t_{rsc} = 1/B_{sc}$	0.52 μ s	0.54 μ s	0.42 μ s
Rise time of I.M. $t_r = t_{rsc}$	0.52 μ s	0.54 μ s	0.42 μ s

Table 1. Estimated Rise Times of the Intermodulation Components

The dynamic behavior of the intermodulation level cannot be examined directly, but may be estimated from the rise time of the chrominance signal. The rise time of the luminance signal is small in comparison, as shown in Table 1. The sound subcarrier level is constant.

The duration of each of the color bars in Fig.4 is one tenth of the line period or 6.4 μ s. There is therefore ample time for the intermodulation component to reach its full value during each color bar. Measurements may be performed about 1 μ s from the beginning of each color bar. The color bars and sound carrier therefore apply the three tones to the transposer, changing levels in rapid succession and with suitable processing may be used to give all six intermodulation levels in histogram form as shown in Fig.6.

The processing is best implemented at baseband frequencies and a demodulator is employed to give a video signal as shown in Fig.5. The video signal is then applied to the intermodulation detector whose block diagram is shown in Fig.7. The signal is first bandpass filtered to remove most of the energy associated with the principal frequency components in the color bar waveform. These are the line frequency components associated with the luminance component and the color subcarrier sidebands. The sound carrier is removed by the demodulator. The passband used to select either the 920 kHz (NTSC), 1.07 MHz (B+G/PAL), or 1.57 MHz (I/PAL) intermodulation component is from 500 kHz to 2MHz.

The output signal from the bandpass filter is then fed to the mixer which samples the video signal for a short period (1.8 μ s) every line at a point corresponding to a particular color bar. See Fig.8. In this way the mixer is only excited with intermodulation components of constant amplitude and phase which do not vary from one line to the next. For PAL

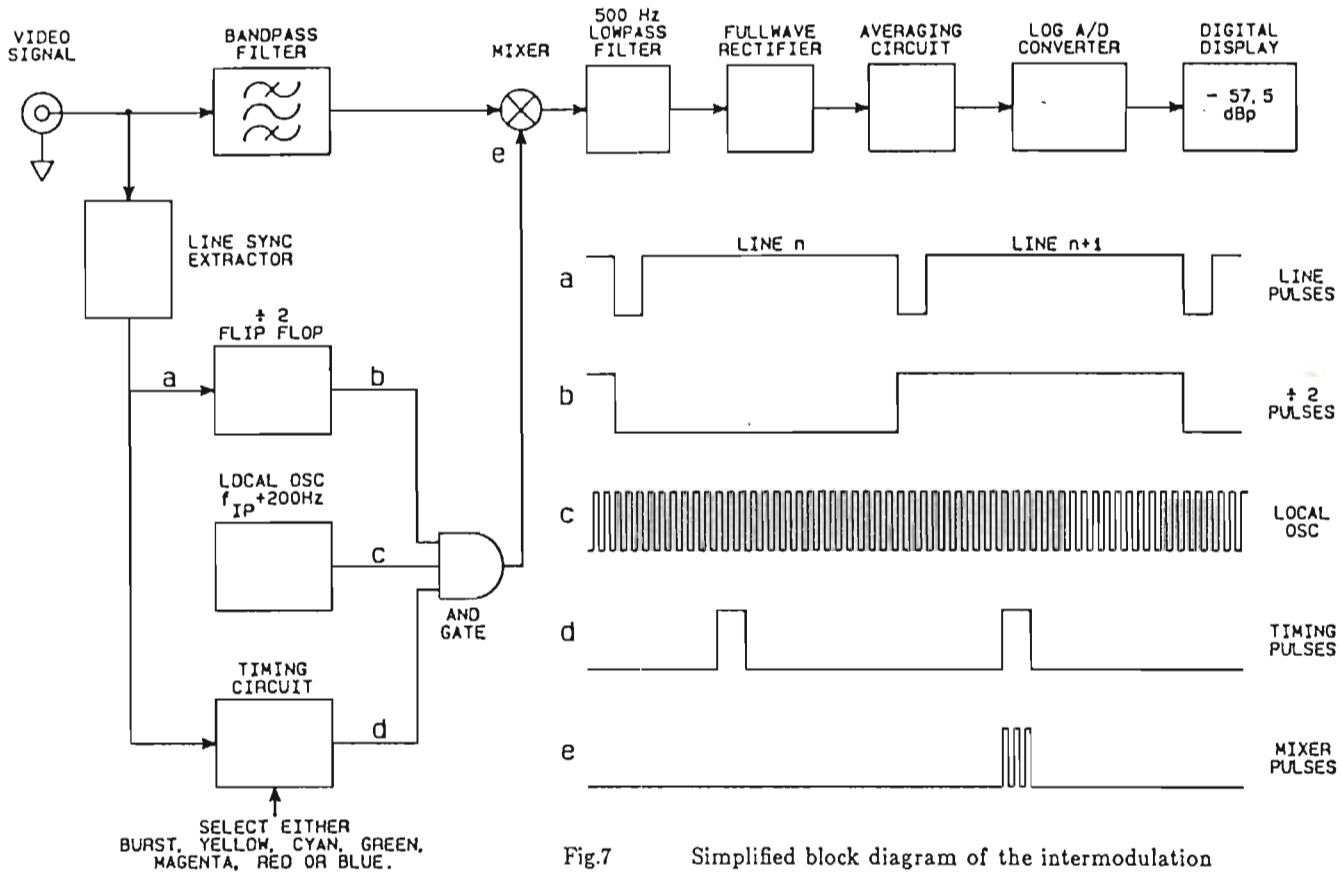


Fig.7 Simplified block diagram of the intermodulation detector.

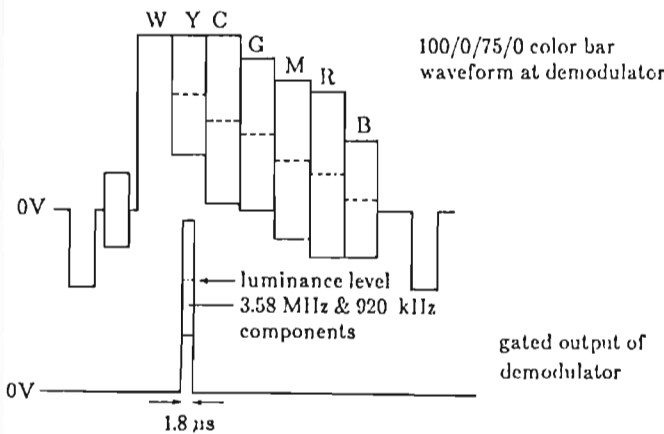


Fig.8 Sampling the color bar waveform from the demodulator for a short period during the yellow color bar.

systems, the alternating phase of the color subcarrier causes the phase of the intermodulation component to vary too. As this would cause significant errors, it is necessary to sample at half line frequency.

The input signal to the mixer $e_m(t)$ consists of three separate components, and, neglecting their phase relationships, is represented by eqn.2.1,

$$e_m(t) = e_y + e_{ip}\cos(\omega_s - \omega_{ic})t + e_{sc}\cos(\omega_{sc} - \omega_v)t \quad (2.1)$$

where e_y is a dc voltage corresponding to the luminance of the selected color bar, e_{ip} is the amplitude of the intermodulation product and e_{sc} is the amplitude of the subcarrier frequency. It should be noted that both the luminance and subcarrier components are small due to the attenuation of the bandpass filter.

In this implementation the mixer is an analog switch. Initially assume that the controlling signal to the switch consists of timing pulses "d" shown in Fig.7. The output of the mixer will then be its input signal multiplied by a periodic switching function of line period T or 2T(PAL).

$$e_{om}(t) = e_m(t) (d + 2d \sum_{n=1}^{\infty} (\sin(\pi nd)/(\pi nd) \cos(n\omega_1 t)) \quad (2.2)$$

$$e_{om}(t) = e_m(t) (d + 2d \sum_{n=1}^{\infty} (\sin(\pi nd)/(\pi nd) \cos(n\omega_1 t/2)) \quad (2.3)$$

where, t_d is the sampling duration, $d = t_d/T$ or $t_d/2T$ (PAL)

and $\omega_1 = 2\pi/T$ the line frequency.

In Tables 2 and 3 below, the frequency spectrum at the output of the mixer is evaluated for components in the vicinity of the intermodulation frequency for the M/NTSC and B+G/PAL systems respectively. The I/PAL system is very similar to the B+G/PAL systems except that the different sound-vision frequency spacing of 5999600 Hz gives intermodulation frequencies of about 1.57 MHz.

Examination of the frequencies in Tables 2 & 3 shows that a frequency component exists at the output of the mixer at the intermodulation frequency which is sufficiently separated from the other components to enable the amplitude of the intermodulation component to be measured. The component lies midway between the luminance components, a fact which is fundamental to television systems and is determined by the selection of the sound subcarrier, color subcarrier and line frequencies. In the case of the M/NTSC system the nearest line frequency is half a line frequency away or 7867 Hz. For

the B+G/PAL systems the spacing is about a quarter of a line frequency away or 3881 Hz. A similar frequency spacing exists for the I/PAL system.

Tables 2 & 3 also indicate that a color subcarrier component exists very much closer to the intermodulation frequency, but that its amplitude is much smaller. The function of the bandpass filter is to reduce this amplitude even further so that the intermodulation component can be isolated.

The measurement of e_{ip} may be performed using a frequency spectrum analyzer or by simply heterodyning the intermodulation component down to a lower frequency for measurement. This latter approach is shown in Fig.7, where the mixer is fed with a burst of pulses (signal "e") at a frequency of $f_{IP} + 200$ Hz. Assuming a square wave local oscillator, the peak amplitude of the 200 Hz component at the

Frequency Hz	Component	Amplitude Volts peak
888986	f_{IP} $n = 2$	0.0282 e_{ip}
896854	f_l $n = 57$	0.0105 e_y
904717	f_{SC} $n = 170$	0.0010 e_{sc}
904721	f_{IP} $n = 1$	0.0283 e_{ip}
912588	f_l $n = 58$	0.0099 e_y
920452	f_{SC} $n = 169$	0.0012 e_{sc}
920455	f_{IP}	0.0283 e_{ip}
928322	f_l $n = 59$	0.0093 e_y
936186	f_{SC} $n = 168$	0.0013 e_{sc}
936189	f_{IP} $n = 1$	0.0283 e_{ip}
944057	f_l $n = 60$	0.0086 e_y
951920	f_{SC} $n = 167$	0.0014 e_{sc}
951924	f_{IP} $n = 2$	0.0282 e_{ip}

Table 2. Frequency components at the output of the mixer shown in Fig.7 assuming the mixer is controlled by timing pulses "d". System M/NTSC with:

Video intermod. freq.:
 $f_{IP} = (f_s - f_{sc}) = 920455$ Hz

Line frequency:
 $f_l = 15734.28$ Hz

Sound vision spacing:
 $f_v - f_s = 4.5$ MHz

Color subcarrier spacing:
 $f_{sc} = f_{sc} - f_v = 3579545$ Hz

Sampling duration:
 $t_d = 1.8\mu s$

Duty cycle:
 $d = t_d f_l = 0.0283$

Frequency Hz	Component	Amplitude Volts peak
1050756	f_{IP} $n = 2$	0.0140 e_{ip}
1050806	f_{SC} $n = 433$	0.0002 e_{sc}
1054688	f_l $n = 135$	0.0000 e_y
1058569	f_{IP} $n = 1$	0.0141 e_{ip}
1058619	f_{SC} $n = 432$	0.0002 e_{sc}
1062500	f_l $n = 136$	0.0013 e_y
1066381	f_{IP}	0.0141 e_{ip}
1066431	f_{SC} $n = 431$	0.0001 e_{sc}
1070313	f_l $n = 137$	0.0011 e_y
1074194	f_{IP} $n = 1$	0.0141 e_{ip}
1074244	f_{SC} $n = 430$	0.0005 e_{sc}
1078125	f_l $n = 138$	0.0009 e_y
1082006	f_{IP} $n = 2$	0.0140 e_{ip}

Table 3. Frequency components at the output of the mixer shown in Fig.7 assuming the mixer is controlled by timing pulses "d". System B+G/PAL with:

Video intermod. freq.:
 $f_{IP} = (f_s - f_{sc}) = 1066381$ Hz

Line frequency:
 $f_l = 15625$ Hz

Sound vision spacing:
 $f_v - f_s = 5.5$ MHz

Color subcarrier spacing:
 $f_{sc} = f_{sc} - f_v = 4433618.75$ Hz

Sampling duration:
 $t_d = 1.8\mu s$

Duty cycle:
 $d = t_d f_l / 2 = 0.0141$

output of the mixer will be

$$e_o = e_{ip} d_i/\pi \tag{2.4}$$

The actual amplitude of the 200 Hz component is quite small because of the very small duty factor required to select a particular color bar. Like the three-tone method, the color bar method references the dBp level to peak sync. power. The voltage excursion between the sync. pulse level and the zero carrier level at the output of the demodulator, is 1.12 V dc for the M/NTSC system. Taking an example of an intermodulation level of -50 dBp, the input voltage to the mixer at the intermodulation frequency of 920 kHz will be

$$e_{ip} = 2 \times 1.12 \times 10^{-50/20} = 7.08 \text{ mV peak at } -50 \text{ dBp} \tag{2.5}$$

where the factor of 2 accounts for the 6 dB gain in the vestigial sideband filter in the demodulator at 920 kHz. The amplitude of the 200Hz component at the output of the mixer will be

$$e_o = 7.08 \text{ mV} \times d/\pi = 64 \text{ }\mu\text{V peak (at } -50 \text{ dBp for M/NTSC)} \tag{2.6}$$

where $d = 0.0283$

For the B+G/PAL and I/PAL systems the amplitude is about one half this level because the color bar can only be sampled every other line ($d=0.0141$). There are also small differences in the voltage excursion between the sync. pulse level and the zero carrier level (B+G/PAL 1.10V, I/PAL 1.25 V). Although small, with suitable amplification and lowpass filtering the 200 Hz component can be extracted to determine its amplitude. This amplitude is directly related to the amplitude of the intermodulation component. The authors used an eighth-order Butterworth filter with a -3 dB cut-off frequency of 500 Hz to achieve easily a measurement range of -70 dBp to -40 dBp with an accuracy of ± 0.5 dBp with a noise floor of -80 dBp. The output of the full wave rectifier in Fig.7 was averaged with a three second time constant and converted to a logarithmic scale to display the intermodulation level directly in dBp.

The histogram shown in Fig.6 was obtained by using time division multiplexing techniques. The mixer pulses in Fig.7 were aligned in turn with the color burst and each of the six color bars for a full field period (20ms) with the process repeating every seven field periods. The histogram was produced by sequentially scanning seven memories at the line repetition rate. The contents of the memories correspond to the intermodulation levels during the color burst, yellow, cyan, green, magenta, red, and blue drive levels and thus gave an apparently continuous display on an oscilloscope or

waveform monitor of the seven intermodulation levels. Thus the histogram was able to display amplitude changes smoothly in real time as the transposer was adjusted.

To perform the measurements it is necessary to interrupt the program and transmit color bars. During program transmissions, the level of intermodulation occurring during the duration of the color burst pulse can be monitored continuously. Modulation of the FM sound carrier causes a reduction in the indicated level of the intermodulation component, but during quiet moments the level may be assessed. A chart recorder may usefully be employed for this purpose. As the duration of the burst is only 2.25 μ s, the measurement during the burst under-reads by a fixed 3 dB. However, it provides a facility to continuously monitor the performance of a transposer while in service.

3. MEASUREMENTS

The color bar measurement technique has been tested extensively on TV transposers of the South African Broadcasting Corporation to see whether it is really easier to use than the three-tone method and whether it raises aspects of transposer performance obscure to the three-tone test. A 100/0/75/0 color bar waveform was used for all the intermodulation measurements. The luminance and chrominance levels in the cyan color bar correspond very closely to the levels used by the South African Broadcasting Corporation in their three-tone test. The system used is I/PAL and the three-tone intermodulation level of the specification is -53 dBp. Color bar and three-tone test readings agreed in all cases to ± 1 dB.

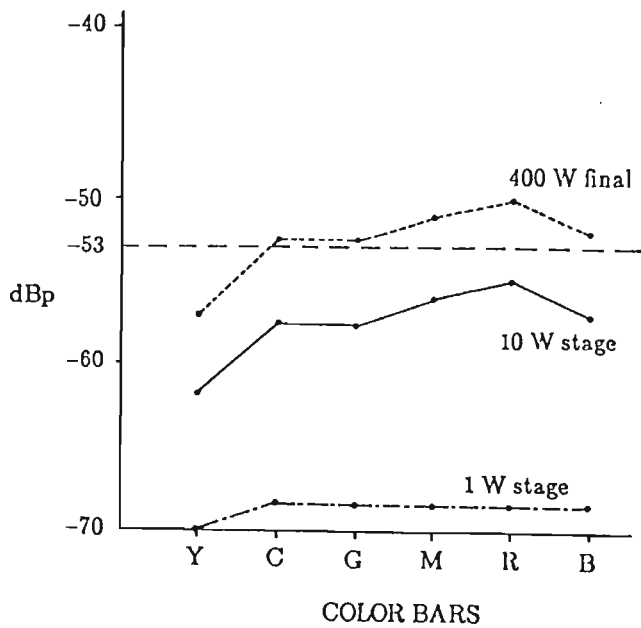


Fig.9 Intermodulation performance of a 400 W UHF tetrode output transposer measured using the color bar method.

Fig.9 shows the intermodulation performance of a 400 W UHF tetrode output transposer at the output of the 1 W, 10 W and 400 W stages. There is no precorrector used in this transposer. Fig.10 shows the performance of a 5 kW VHF common amplification transmitter with a history of visible intermodulation distortion on red and blue colors although its three-tone performance was well within specification. Using the histogram, the four controls of the intermodulation precorrector were quickly adjusted to minimize the distortion in this area.

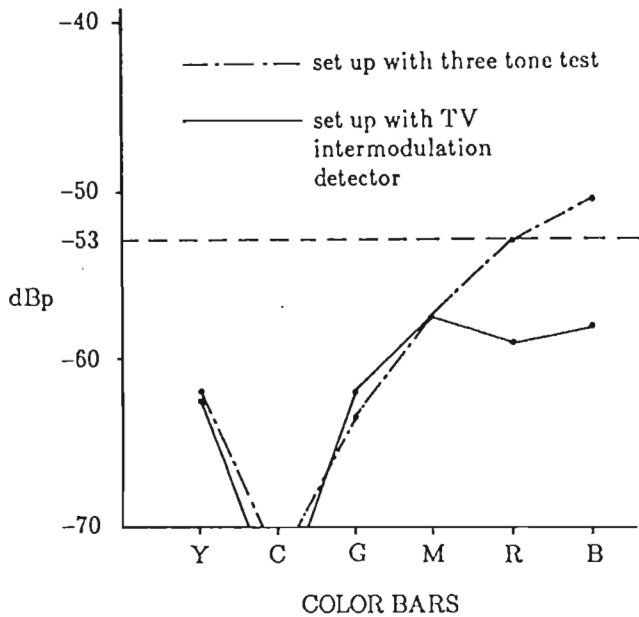


Fig.10 5 kW VHF transmitter intermodulation distortion levels before and after setting up with the intermodulation detector.

Fig.11 shows the performance of a 200 W UHF transistorized output transposer with no intermodulation precorrection. The level of the 200 W output stage is seen to be less than the 1 W driver stage showing clear evidence of phase cancellation for cyan, green and magenta colors, but phase addition for yellow, red and blue colors.

4. EVALUATION OF THE COLOR BAR MEASUREMENT TECHNIQUE

Eqn.1.4 suggests that it is not necessary to measure intermodulation at every color, as the level only depends upon coefficient K_3 , the sound carrier amplitude A_s which is constant, the luminance amplitude A_v and the subcarrier amplitude A_{sc} , which are both known variables. Thus knowing K_3 , A_s , and A_{sc} , it should be possible to predict the intermodulation levels for the other colors when that for one color is known. This notion is tested by comparing differences between the level measured with the cyan color (which corresponds to the three-tone test with the I/PAL system) and the levels at the five other colors. These differences are then compared with theoretical predictions based upon Eqn.1.4 using the carrier amplitudes corresponding to the 100/0/75/0 color bar. The results are given in Table 4.

Color	Luminance diff. dB	Chrominance diff. dB	Predicted diff. dB	Measured diff. dB Fig.9	Measured diff. dB Fig.11
Yellow	-1.6	-3.0	-4.6	-4.5	-0.5
Cyan	0.0	0.0	0.0	0.0	0.0
Green	0.9	-0.7	0.2	0.0	-2.0
Magenta	2.1	-0.6	1.5	1.5	2.5
Red	2.7	0.0	2.7	2.5	-0.5
Blue	3.7	-3.0	0.7	0.5	-1.5

Table 4. Differences between the six intermodulation levels are calculated using Eqn.1.4 for a 100/0/75/0 color bar waveform with the I/PAL system and compared with the measured differences for a 400 W UHF tetrode transposer (Fig.9) and a 200 W UHF transistorized transposer (Fig.11), both having no I.M. precorrection. Level differences for transposers with precorrection cannot be predicted (Fig.10).

There appears to be very good agreement between the predicted values in Table 4. and the measured values, especially in the case of the 400 W transposer shown in Fig.9. However, the 200 W transposer shown in Fig.11 has a final intermodulation level which is determined by the vector sum of several different stages and here the differences are not quite so predictable. Phase cancellation of intermodulation produced by the different stages appears to be primarily responsible. Furthermore, once a precorrector is used, the

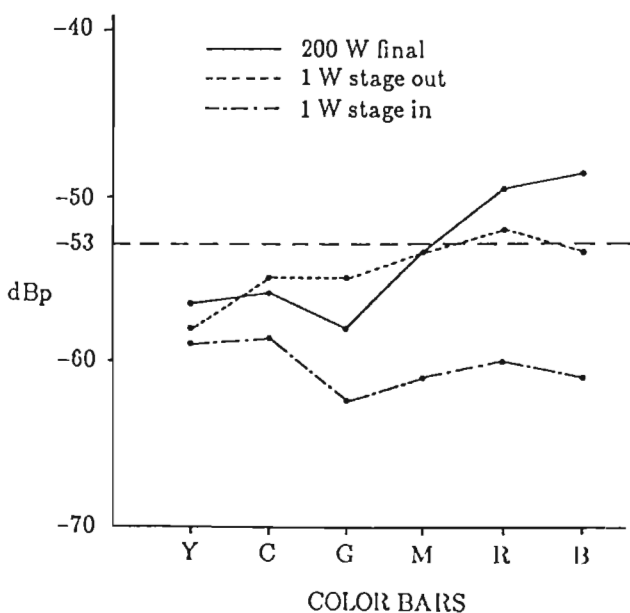


Fig.11 200 W transistorized output transposer with no intermodulation distortion precorrection.

differences are totally unrelated to Eqn.1.4. Finally, while K_3 is a constant for a given transposer it will vary between different types of transposers. It therefore appears essential to measure intermodulation at different luminance and color levels for all but the simplest of transposers.

5. WIDER APPLICATIONS OF THE COLOR BAR TECHNIQUE

The plethora of non-linear distortion measures used by the broadcaster suggests that there is no useful relationship between them. Some other non-linear distortion measures relevant to common amplification television transmitters are described below. However, theoretical studies [4] applied to the L/SECAM system show that for an amplifier represented by Eqn.1.2 this is not so and that all the parameters may be determined by the complex coefficients K_1 , K_2 and K_3 . Extending this theory to the NTSC and PAL systems, it is easily shown using Eqns.1.2 & 1.3 that the non-linear parameters are also directly related according to the Eqns. given below.

1. Differential gain

Differential gain is defined as the maximum variation of chrominance gain between black and white levels. The variation is caused by a distortion component at frequency f_{sc} . When added to the chrominance signal, it either increases or decreases the amplitude of the chrominance signal. Assuming the two components to be in phase, Eqn.5.1 gives the maximum differential gain error.

$$\Delta G = (1 + 1.5kA_v^2 + 1.5kA_c^2 + 0.75kA_{sc}^2) 100 \% \quad (5.1)$$

where $k = K_3/K_1$.

Differential phase

Differential phase is defined as the maximum variation in phase of the color subcarrier with different luminance levels. Assuming the two components to be 90 degrees out of phase, Eqn.5.2 gives the maximum differential phase error.

$$\Delta \phi = \arctan(1.5kA_v^2 + 1.5kA_c^2 + 0.75kA_{sc}^2) \quad (5.2)$$

where $k = K_3/K_1$

Vision/sound cross-modulation

Vision/sound cross-modulation is defined as the variation of the sound carrier amplitude caused by the variation of the vision carrier level and is particularly noticeable during the synchronization periods when

the vision carrier is at a maximum. It is normally expressed as a percentage of the sound carrier amplitude. The variation is caused by a distortion component at frequency f_s . When added to the sound carrier it modifies the resultant sound carrier amplitude modulating the carrier at the line frequency. The percentage distortion may be estimated using Eqn.5.3.

$$m = (1.5kA_v^2 + 0.75kA_s^2) 100 \% \quad (5.3)$$

where $k = K_3/K_1$.

4. Sync. pulse crushing

Sync. pulse crushing is defined as the change in the picture/sync amplitude ratio caused by non-linear distortion and is determined by the variation of luminance gain in the vicinity of the sync. pulses compared with a distortionless system. It may be estimated using Eqn.5.4.

$$\Delta S = 20 \log(1 + 1.5kA_v^2 + 0.75kA_s^2) \text{ dB} \quad (5.4)$$

where, $k = K_3/K_1$ and A_v is the mean value of the vision carrier in the sync. pulse region.

From the above analyses it is clear that for a transposer described by Eqn.1.2 all these non-linear parameters are related and determined by the coefficients K_1 and K_3 . However, when a transposer consists of several stages, or where several amplifiers are in parallel, phase cancellation may occur causing errors in these relationships. For transposers with precorrectors the relationships do not apply because of the complex nature of the phase cancellation of the intermodulation products.

The color bar method allows the intermodulation level to be measured over a number of luminance levels and the opportunity exists to also measure the intermodulation level which would occur if the luminance level extended into the synchronization region. This allows the complete transfer characteristic of the transposer to be investigated, simplifying the simultaneous satisfaction of the various non-linear distortion standards such as intermodulation and vision/sound cross modulation which are notoriously difficult to optimize simultaneously. The interaction of the two distortions is clearly visible by this means and has been found in practice to greatly simplify the adjustment procedure.

The modified color bar waveform shown in Fig.12 was adapted from the normal 100/0/75/0 color bar by converting the usual blue color bar to a blacker than black luminance level of -150 mV with a chrominance amplitude of 300 mV p.p. With the addition of this color bar it was possible to measure the intermodulation level at eight points on a transposer's characteristic. A comprehensive set of

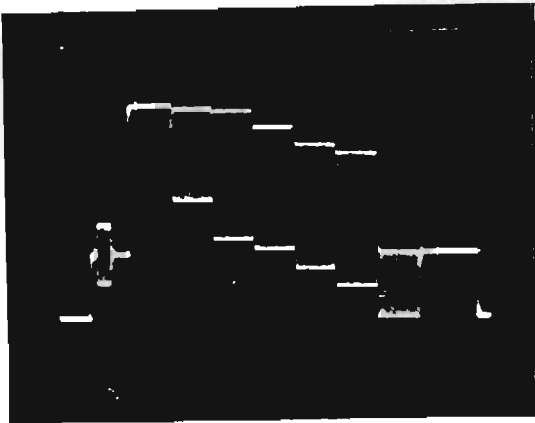


Fig.12 Modified blacker than black color bar waveform used to measure intermodulation in the synchronizing region.

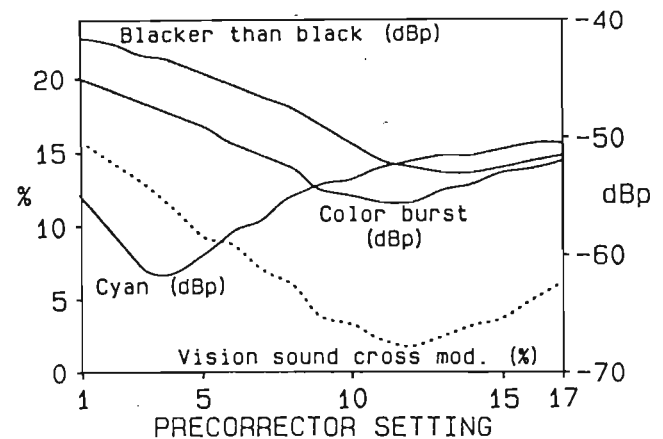


Fig.13 Vision/sound cross-modulation and intermodulation distortion levels of a 10 W transistorized transposer at different precorrector settings.

measurements were performed on a TEM 10 W solid state transposer. Eight intermodulation measurements were performed as well as conventional measurements of differential gain, differential phase and vision/sound cross modulation. These measurements were repeated seventeen times with different settings of the precorrector and the results are given in the Appendix. Some of the data is plotted in Figs.13 to 15.

From these figures it is apparent that minimizing the cyan color bar (three-tone test) is not the best way of minimizing differential gain, differential phase or vision/sound cross-modulation. A full statistical analysis of this data will be published later, but it would seem that the three different parameters that are most affected by the color bars are given in Table 5. It is therefore apparent that the equations relating the non-linear parameters are not valid for transposers employing precorrectors to minimize intermodulation distortion.

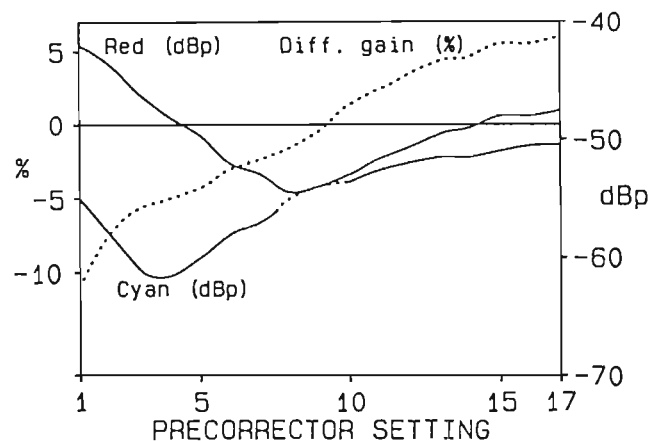


Fig.14 Differential gain and intermodulation distortion levels of a 10 W transistorized transposer at different precorrector settings.

Parameter	Color bars for best minimization
Vision/sound cross-mod	Burst, blacker than black
Differential gain	Blue, red and magenta
Differential phase	Blacker than black

Table 5. Optimization of the parameters shown above was best achieved with this 10 W transistorized transposer by optimizing the color bars shown.

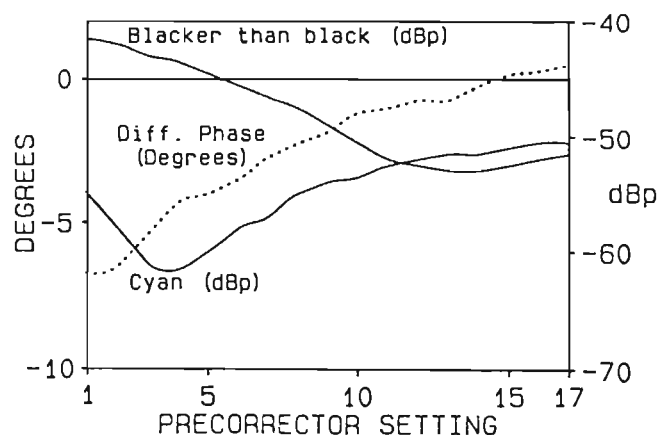


Fig.15 Differential phase and intermodulation distortion levels of a 10 W transistorized transposer at different precorrector settings.

6. CONCLUSIONS

A new method of measuring intermodulation distortion has been presented in this paper. The presently accepted three-tone method only tests the performance of a common amplification transposer at one luminance level. This is sufficient when a transposer's intermodulation performance is determined by one non-linear amplifier, but with several non-linear amplifiers phase cancellation of the intermodulation components occurs. It is then impossible to predict the intermodulation performance at various different luminance and chrominance levels. This also applies to transposers fitted with precorrectors.

It is therefore necessary to measure intermodulation at a number of different levels and the color bar waveform appears to be the obvious choice. Sampling techniques enable intermodulation to be measured simultaneously at seven different luminance levels assisting in optimizing transposer precorrector performance. In addition, it has been shown that it is not sufficient to minimize intermodulation at one luminance level and so minimize all the other non-linear parameters used by broadcasters. A blacker than black color bar has been found to be a useful addition to the color bar waveform, as it then also allows intermodulation to be measured in the synchronizing region. This gives control of all the non-linear parameters of a transposer.

ACKNOWLEDGEMENTS

The authors would like to thank the South African Broadcasting Corporation for permission to print this paper.

They also thank the University of Natal for the use of their laboratory facilities and Mr G Vath for his assistance in developing the prototype unit.

APPENDIX

The following measurements were made on a TEM 10 W transistorized transposer to determine the relationship between intermodulation and other non-linear measurement parameters for different settings of the single intermodulation precorrector control. The transposer was excited with an I-PAL 100/0/75/0 color bar waveform to perform the intermodulation measurements.

Table A.1 The table below gives all the eight intermodulation levels as well as the other non-linear measurement parameters at the seventeen different settings of the intermodulation precorrector control.

OBS Precorrector setting -- M marks the position of the minimum reading.

1.57 MHz Intermod. Levels in dBp

- X1 Burst
- X2 Yellow
- X3 Cyan
- X4 Green
- X5 Magenta
- X6 Red
- X7 Blue
- X8 Blacker than Black

Non-Linearity Measurement

- Y1 Differential Phase (Degrees)
- Y2 Differential Gain (%)
- Y3 Vision/Sound Cross-Modulation (%)

OBS	X1	X2	X3	X4	X5	X6	X7	X8	Y1	Y2	Y3
1	-45.0	-64.5	-55.0	-51.5	-46.0	-43.0	-42.5	-41.5	-6.8	-11.0	15.9
2	-46.0	-65.0M	-58.0	-54.0	-48.0	-44.5	-43.5	-42.0	-6.5	-7.2	14.5
3	-47.0	-64.0	-61.0	-56.5	-49.5	-46.0	-44.5	-43.0	-5.4	-5.7	13.0
4	-48.0	-62.0	-61.5M	-59.0	-54.0	-48.0	-46.0	-43.5	-4.3	-5.0	11.2
5	-49.0	-60.5	-60.0	-59.5 M	-54.0	-49.5	-47.5	-44.5	-4.0	-4.1	9.3
6	-50.5	-59.0	-58.0	-58.0	-55.5	-52.0	-49.0	-45.5	-3.5	-3.0	8.9
7	-51.5	-58.5	-57.0	-57.5	-56.5M	-53.0	-50.5	-46.5	-2.7	-2.2	7.0
8	-53.5	-57.5	-55.0	-55.5	-55.5	-54.5M	-52.5	-47.5	-2.3	-1.6	6.0
9	-55.5	-57.0	-54.0	-54.0	-54.5	-54.0	-53.5	-49.0	-1.9	0.1M	3.9
10	-56.0	-56.5	-53.5	-53.0	-53.0	-53.0	-54.0M	-50.5	-1.1	1.3	3.3
11	-56.5M	-56.0	-52.5	-52.0	-52.0	-51.5	-53.5	-52.0	-1.0	2.5	2.2
12	-56.5M	-55.5	-52.0	-51.5	-51.0	-50.5	-52.5	-52.5	-0.6	3.6	1.9M
13	-55.5	-55.5	-51.5	-51.0	-50.0	-49.5	-52.0	-53.0M	-0.6	4.3	2.6
14	-55.0	-55.5	-51.5	-51.0	-49.5	-49.0	-51.0	-53.0M	-0.3M	4.6	3.2
15	-54.0	-55.0	-51.0	-50.5	-49.0	-48.0	-50.0	-52.5	0.1M	5.7	3.9
16	-53.5	-55.0	-50.5	-50.0	-49.0	-48.0	-49.5	-52.0	0.3	5.7	5.0
17	-53.0	-55.0	-50.5	-50.0	-48.5	-47.5	-49.0	-51.5	0.5	6.0	6.1

REFERENCES

- [1] P. Shellswell, "The subjective effect of intermodulation distortion when sound and vision signals are amplified in a common amplifier," BBC Research Department Report No. RD 1974/35, 1974.
- [2] C.A.A. Wass, "A table of intermodulation products," Proc. IEE, vol. 33, pp. 31-39, 1948.
- [3] H.K.V. Lotsch, "Theory of non-linear distortion produced in a semiconductor diode," IEEE Trans. Electron Devices, vol. 5, pp. 294-307, 1968.
- [4] C. Cluniat, "Correction of non-linearity in low and medium power transmitters and transposers," Review Technique Thomson-CSF, Vol. 10, No. 2, June 1978.
- [5] Japanese Broadcasting Authority NHK, "TV translator manufacturing specification," BSS 03-6005.
- [6] Independent Broadcasting Authority, IBA Technical Review, London, May 1977, p.39.
- [7] W.Flor, "Intermodulationmessungen mit hilfe der prüfzeilentchnik," Fernsehund Kino-Technik, Vol.30 No. 10/1976, pp. 353-354, 1976.
- [8] A.D. Broadhurst, P.F. Bouwer, A.L. Curle, "TV Intermodulation measurement using a color bar waveform," 11th IBC, pp.369-372, Sept. 1986.

TV INTERMODULATION MEASUREMENT USING A COLOUR BAR WAVEFORM

A D Broadhurst, P F Bouwer

A L Curle

University of Natal, Republic of South Africa

South African Broadcasting Corporation,
Republic of South AfricaINTRODUCTION

A new measurement technique is proposed to determine the intermodulation distortion level which occurs in common r.f. amplification television broadcast transposers and transmitters, when the vision carrier, colour subcarrier and sound carrier frequency components interact in the presence of amplifier non-linearities.

Broadcasting authorities presently measure intermodulation distortion by applying a three tone simulation of a composite video and sound signal to the transposer and then measure the relative amplitude of the major in-band intermodulation product (nominally at vision carrier plus 1,57MHz in the 625 line PAL-1 system) on a spectrum analyser (Shelswell (1)). This method is slow and requires a skilful operator to achieve repeatable results. Furthermore it tests the common r.f. amplification equipment at one luminance level and one chrominance level and therefore does not test the equipment over its full operating range. Flor (2) describes a method of using test line 331 to avoid removing the transposer from service. The ratio of levels in the three tone method are approximately the same as those of the luminance and chrominance components of the active part of the line 331 signal. The intermodulation signal was extracted in (2) using a broadband bandpass filter at the intermodulation frequency (200kHz bandwidth at 1,07MHz for the PAL G system).

The method described in this paper uses either a 100/0/100/0 or 100/0/75/0 composite full field colour bar signal to excite the transposer via test transmitter as shown in Fig. 1. When testing a common amplification transmitter the colour bar signal is applied directly to its video input. The r.f. output of the transposer under test is demodulated in a precision demodulator and applied to the intermodulation detector as shown in Fig. 7. The detector measures, relative to peak sync level, the amplitude of the major in-band intermodulation component associated with each combination of luminance and chrominance level of the colour bar. The different distortion levels may be displayed as a histogram on an oscilloscope or TV waveform monitor, as shown in Fig. 2 and the transposer may be adjusted for optimum performance by attempting to minimise the height of each histogram bar. A digital display of selectable individual levels is provided on the front panel for logging results.

This paper describes the principle on which the intermodulation detector functions. The measurement technique has been tested extensively on TV transposers of the South African Broadcasting Corporation and the paper presents the results of some of these tests.

During these tests it was shown that the new technique requires minimal skill, has a wide dynamic range (-68dBp to -40dBp), high accuracy (+/- 0,5dB) and reveals anomalies in transposer performance not shown up by the three tone simulation method or the method described in (2). Furthermore, it allows transposer performance to be optimised over a wide range of luminance and colour levels not possible using any other currently available technique. The intermodulation level may also be monitored continuously while the transmitter is 'on the air' by displaying the intermodulation level occurring during the colour burst. The measurement technique is applicable to all PAL and NTSC television systems.

MEASUREMENT PRINCIPLE

Intermodulation distortion is measured by applying a colour bar test pattern to the transposer using a test transmitter. The output signal of the transposer is demodulated and the demodulated video signal is applied to the video signal terminal of the detector as shown on the simplified block diagram in figure 3. The signal is then bandpass filtered to remove most of the energy associated with the principal frequency components in the colour bar waveform. The pass band used to select the intermodulation product is from 500kHz to 2MHz for the 1,57MHz intermodulation product of the 625 line PAL-1 system.

The output signal from the bandpass filter is fed to the mixer whose function is to down-convert the intermodulation frequency, f_{ip} , of 1565381Hz to a frequency of about 200Hz. This is achieved using a local oscillator with a frequency $f_{ip} + 200$ Hz. The selective gating principle is explained later.

The output of the mixer is filtered and amplified by the low pass filter, which has a cut-off frequency of 500Hz. Only the intermodulation frequency components which fall within the narrow window created by the mixer and 500Hz low pass filter appear at the output of this filter. The window is narrow enough to allow the intermodulation frequency amplitude to be measured, but not wide enough to amplify the adjacent periodic frequency components of the line frequency. The output of the fullwave rectifier is averaged with a time constant of 3 seconds, and the dc voltage from the averaging circuit is measured and converted to a logarithmic scale, thus displaying the intermodulation level directly in dBp, i.e. referred to peak sync pulse power.

The digital pulses to the mixer, as shown in Fig. 3, consist of a burst of local oscillator pulses. The width of the burst is 1,8us and the position of the burst is arranged to coincide with a particular selected colour

on the colour bar test pattern. This allows the intermodulation amplitude to be determined at a particular section of the transmitter's characteristic or depth of modulation. During normal transmissions, the level of intermodulation occurring during the duration of the colour burst pulse can be continuously monitored. Modulation of the FM sound carrier causes a reduction in the measured level of the intermodulation component, but during quiet moments the level may be assessed. A chart recorder has been usefully employed for this purpose.

When monitoring a PAL transmission it is necessary to sample every alternate line, because the swinging phase of the colour subcarrier also causes the 200Hz intermodulation component from the mixer to swing in phase. Without this refinement, errors in the measured intermodulation levels would occur, the error being a function of the degree of phase swing of the colour subcarrier. The digital pulses to the mixer are therefore suppressed during alternative lines by the divide by 2 flip flop shown in Fig. 3.

The histogram shown in Fig. 2 is obtained by using time division multiplexing techniques. The mixer pulses are aligned in turn with the colour burst and each of the six colour bars for a full field period (20ms) with the whole process repeating every 7 field periods. The histogram is produced by sequentially scanning 7 memories at the line repetition rate. The contents of the memories correspond to the intermodulation levels during the colour burst, yellow, cyan, green, magenta, red and blue drive levels and thus gives an apparently continuous display on an oscilloscope or waveform monitor of the 7 intermodulation levels. The histogram display amplitude changes smoothly in real time as the transposer is adjusted.

FIELD TRIALS

The proposed measurement technique has been tested extensively on TV transposers of the South African Broadcasting Corporation to see whether it is really easier to use than the three tone test method and whether it raises aspects of transposer performance obscure to the three tone test. The test gear arrangement is shown in Fig. 1.

A 100/0/75/0 colour bar waveform was used for all the intermodulation distortion measurements. In this waveform the three tone levels of the cyan colour bar most closely approximate to those of the three tone test used by the South African Broadcasting Corporation. The intermodulation product produced by the cyan bar is of almost the same relative amplitude as that produced by the three tone test. Comparisons were made between the level recorded by the intermodulation detector during the cyan colour bar and those obtained using the three tone test method. The readings agreed in all cases to within ± 1 dB. The 3 tone test intermodulation level specification of the South African Broadcasting Corporation is -53dBp or better.

Figure 4 shows the intermodulation distortion performance of a 5kW VHF common amplification transmitter with a history of visible intermodulation distortion on red and blue picture signals while being well within the three

tone test specification. Using the intermodulation detector the four controls of the intermodulation distortion precorrector were quickly adjusted to minimise the distortion in this area.

Fig. 5 shows the I.P. levels of a 1000W UHF transposer while Fig. 6 shows the levels of a 1000W VHF transposer. These transposers are fitted with intermodulation distortion precorrectors of similar design. Their range of adjustment is shown in the figures. It would appear from these measurements that the VHF precorrector linearises the power amplifier transfer characteristic only up to carrier levels associated with the cyan colour bar. At carrier levels greater than these the precorrector has negligible effect.

CONCLUSIONS

The colour bar waveform is an attractive proposition for intermodulation distortion testing. It is more representative of an actual picture signal than the three tone simulation and the six colour bars have luminance and chrominance components of varying amplitude that exercise a television system over its full dynamic range.

This measurement technique has been shown to be as accurate as the three tone test method but much simpler to perform. In this implementation of the proposed measurement technique the intermodulation detector has a dynamic range allowing measurements down to -68dBp with an accuracy of ± 0.5 dB. Its ability to test the transmitter's transfer characteristic at seven different points may enable better precorrectors to be designed. Finally, this method allows the performance of a transposer to be monitored continuously at one point on the transmitter's transfer characteristic without the need for recalling the transmitter from service. This could assist in the maintenance of television transposers.

ACKNOWLEDGEMENTS

The authors would like to thank the South African Broadcasting Corporation for permission to print this paper.

They also thank the University of Natal for the use of their laboratory facilities and Mr. G. Vath for his assistance in developing the prototype unit.

REFERENCES

1. Shelswell, P., 1974, 'The subjective effect of intermodulation distortion when sound and vision signals are amplified in a common amplifier', BBC Research Department Report No. 1974/735
2. Flor, W., 1976, 'Intermodulationmessungen mit Hilfe der Prüfzeilentechnik', Fernseh- und Kino-Technik 30. Jahrgang Nr. 10/1976

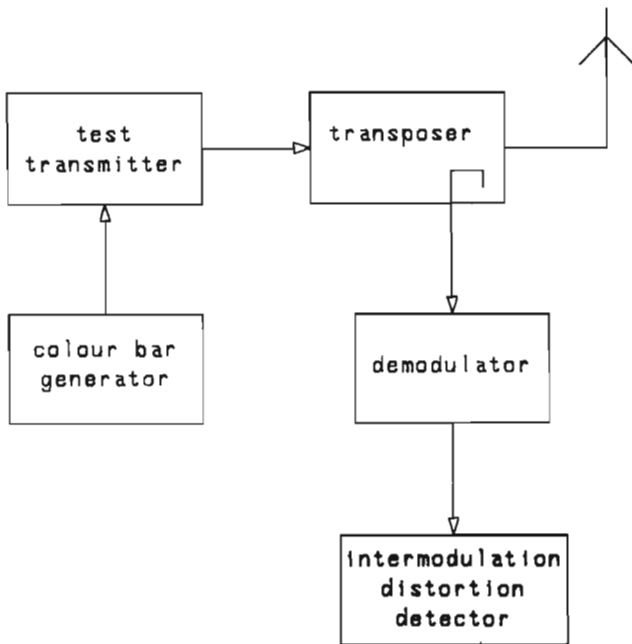
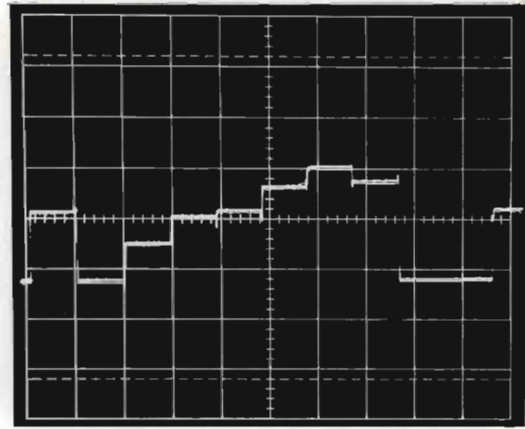


Figure 1 Test gear configuration for measuring a television transposer



100/0/75/0 colour bar intermodulation product levels displayed on a waveform monitor. Histogram bars, are from left to right, the i.p. levels associated with the colour burst, and the yellow, cyan, green, magenta, red and blue colour bars.

Figure 2 The histogram output of the intermodulation detector

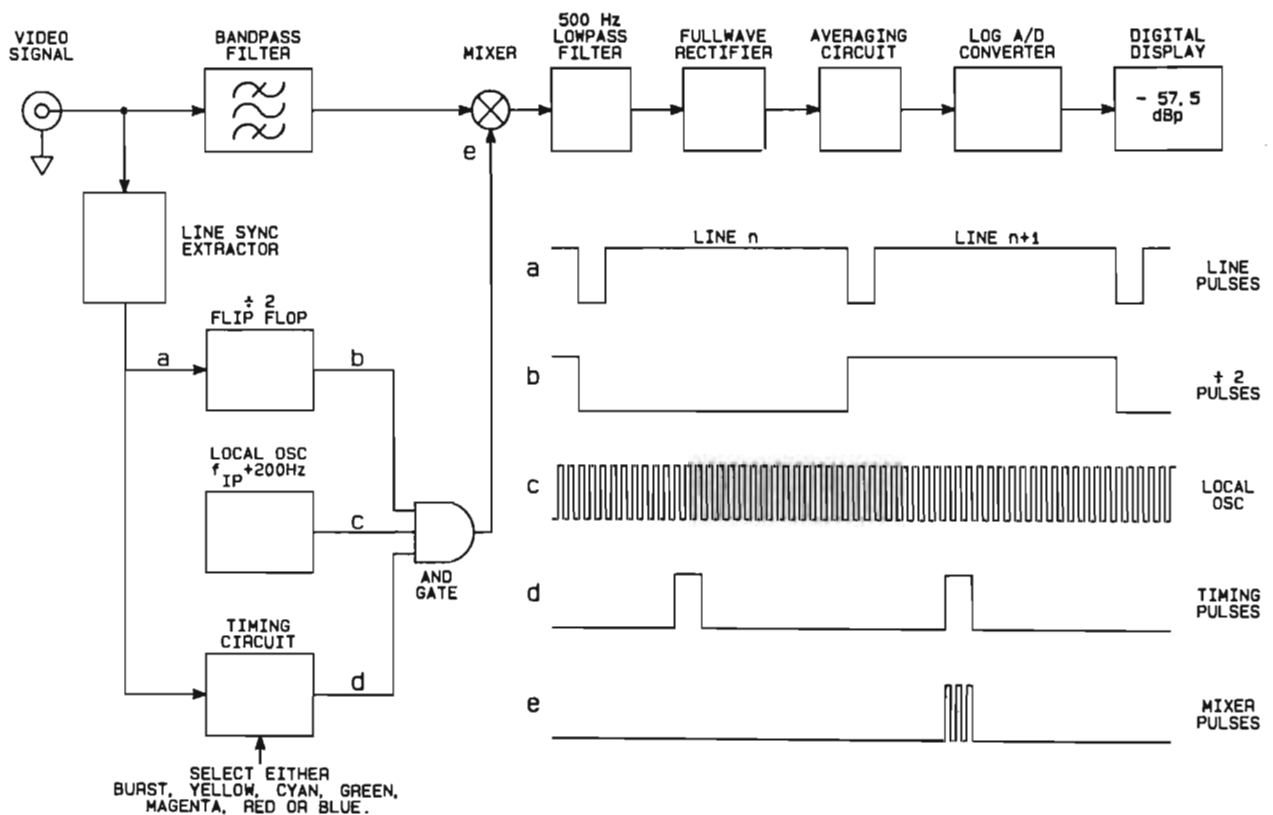


Figure 3 Simplified block diagram of the television intermodulation detector

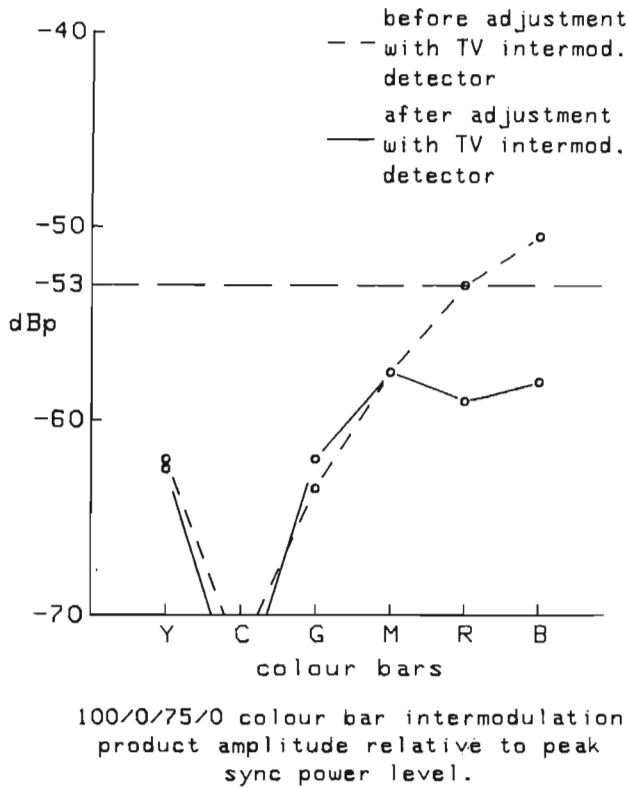


Figure 4 5kW VHF transmitter intermodulation distortion levels before and after setting up with the intermodulation detector

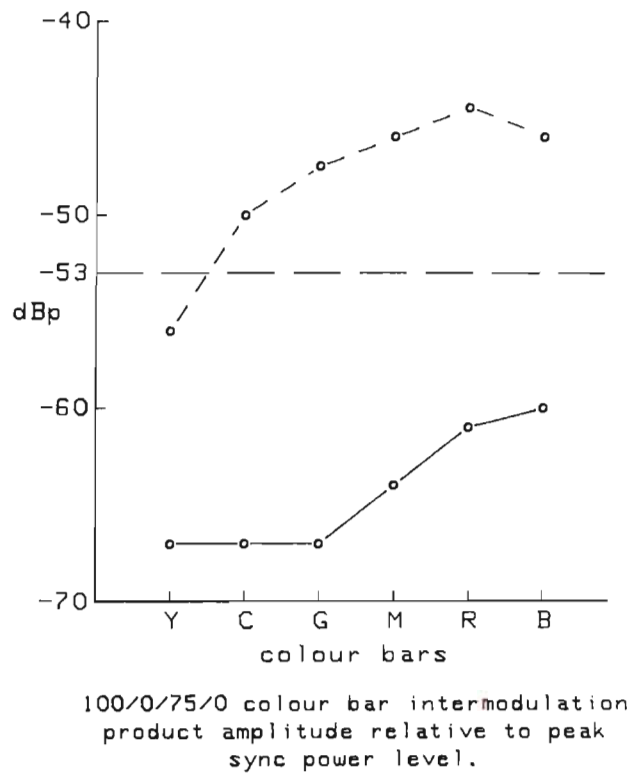


Figure 5 Range of intermodulation distortion precorrector adjustment on 1000W UHF television transposer

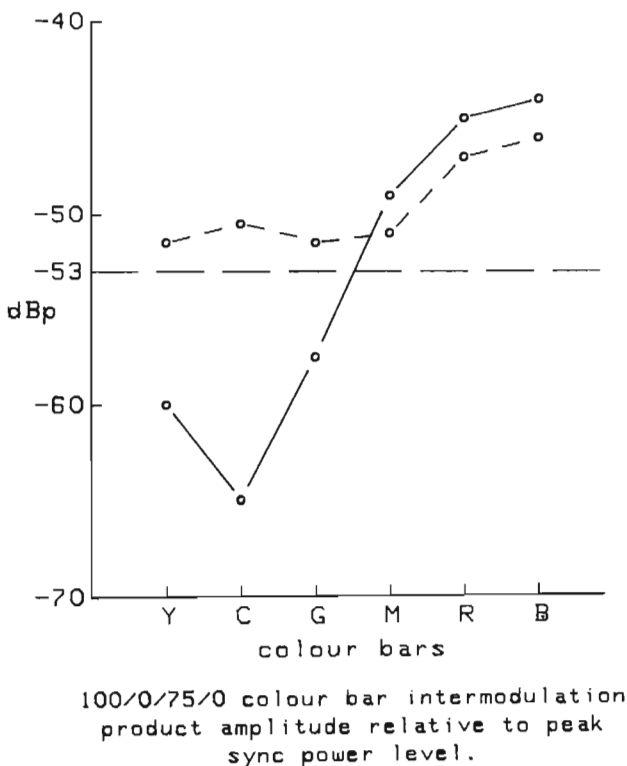


Figure 6 Range of intermodulation distortion precorrector adjustment on 1000W VHF television transposer

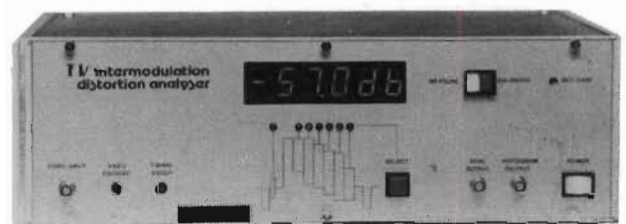


Figure 7 Prototype television intermodulation detector

REFERENCES

Intermodulation Distortion Effects and Measurements:

- [1] Broadhurst, A.D., "Measurement of Television Transponder Intermodulation Distortion Using Colour Bars", Internal Report to the SABC, 27th September 1982, (unpublished).
- [2] Flor, W., "Intermodulationsmessungen mit Hilfe der Prüfzeilentechnik", *Fernseh- und Kino-Technik*, 30 Jahrgang Nr. 10, 1976.
- [3] "An apparatus for measuring intermodulation distortion in TV broadcast equipment",
British Patent Application No. 8616838
U.S.A. Patent Application No. 879,928
R.S.A. Patent Application No. 85/5320
- [4] Shelswell, P., "The subjective effect of intermodulation distortion when sound and vision signals are amplified in a common amplifier", *BBC Report BBC RD 1974/35*.
- [5] Newell, G.F. and Geddes, W.K.E., "The visibility of small luminance perturbations on television displays", *BBC Research Department Report No. T-106*, Serial Number 1963/18, 1963.
- [6] Rösler, A., "Intermodulation und Kreuzmodulation in Fernseh-Antennenverstärkern", *Rundfunktech. Mitt.*, 11, 1967, pp.176-179.
- [7] Harvey, R.V., "Visibility of sound/chrominance pattern with the PAL system: dependence upon offset of intercarrier and upon sound modulation", *BBC Research Department Report No. G-102*, Serial Number 1966/30, 1966.
- [8] Broadhurst A.D., Bouwer, P.F. and Curle, A.L., "TV Intermodulation Measurement using a Colour Bar Waveform", *11th International Broadcasting Convention*, Brighton: 19-23 September 1986.
- [9] Broadhurst, A.D., Bouwer, P.F. and Curle, A.L., "Measuring Television Transponder Intermodulation Distortion", *IEEE Trans. Broadcasting*, vol. 34, Num. 3, September 1988.
- [10] Best, P., "Television Translator Testing Techniques Using a 3 Tone Test Oscillator", *ABU Technical Review*, July 1986.

- [11] Heydel, J. und Vogt, N., "*Fernsehumsetzer Ihre Technik und Untersuchung (Messung)*", Fachverlag Schiele & Schön GMBH, Berlin, Chapter 3.
- [12] Freemantle, S.W., "Performance of 'IP Test Set' During Temperature Stability Tests", Internal SABC Report on Measurements at BARCOMM, 18 September 1985.

Television Specifications:

- [13] "Characteristics of TV Systems", CCIR Report No. 624-2.
- [14] "Specification of Television Standards for 626-line system-I transmissions in the Republic of South Africa", South African Broadcasting Corporation, Revised Edition 1976.
- [15] "TV Translator Manufacturing Specification", Japanese Broadcasting Authority NHK, BSS 03-6005.
- [16] Independent Broadcasting Authority, IBA Technical Review, London, May 1977, p.39.
- [17] Swiss Institute of Posts, Telegraphs and Telephones, Report No. VD12 090 A, 23rd January 1987.

Television Fundamentals:

- [18] Carnt, P.S. and Townsend, G.B., "*Colour Television: Volume 2, PAL, SECAM and Other Systems*", Iliffe Books Ltd., London, 1969.
- [19] Patchett, G.N., "*Colour Television with Particular Reference to the PAL System*", Norman Price (Publishers) Ltd., Second Ed., 1970.

Pulse Response:

- [20] Angelo, E.J. Jr., "*Electronics, BJTs, FETs and Microcircuits*", McGraw-Hill Book Co. Inc., 1969.
- [21] Blinchikoff, H.J. and Zverev, A.I., "*Filtering in the Time and Frequency Domains*", John Wiley and Sons, 1976.
- [22] Clarke, K.K. and Hess, D.T., "*Communication Circuits: Analysis and Design*", Addison-Wesley Publishing Co., Inc., 1971, Chapter 3.
- [23] Glasford, G.M., "*Fundamentals of Television Engineering*", McGraw-Hill, 1955, Chs. 6 through to 8.

- [24] Valley, G.E. Jr. and Wallman, H., "*Vacuum Tube Amplifiers*", McGraw-Hill Book Co. Inc., New York, 1948.
- [25] Mc Collum P.A. and Brown B.F., "*Laplace Transform Tables and Theorems*", Holt, Rinehart and Winston, 1965.

Fourier Analysis and Spectra:

- [26] Burdic, W.S., "*Radar Signal Analysis*", Prentice-Hall Inc., 1968, Chs. 1 and 2.
- [27] Lathi, B.P., "*Communication Systems*", John Wiley and Sons, Inc., p.34.
- [28] Maurice, R.D.A., "*Convolution and Fourier Transforms for Communications Engineers*", Pentech Press, London, 1976 Ch. 10.
- [29] Panter, P.F., "*Modulation, Noise and Spectral Analysis*", McGraw-Hill, 1965.
- [30] Schwartz, M., "Information Transmission, Modulation, and Noise", McGraw-Hill, 1970 2nd Ed.
- [31] "Spectrum Analysis", *Application Note 63*, Hewlett-Packard, August 1968.
- [32] "Spectrum Analysis – Pulsed RF", *Application Note 150–2*, Hewlett-Packard, November 1971.
- [33] Spiegel, M.R., "*Fourier Analysis with applications to Boundary Value Problems*", Schaum Outline Series, McGraw-Hill, 1974.
- [34] Stark, H. and Tuteur, F.B., "*Modern Electrical Communications – Theory and Systems*", Prentice-Hall Inc., 1979.

Intermodulation Distortion Theory:

- [35] Chua, L.O. and Ng, C.Y., "Frequency domain analysis of nonlinear systems: general theory", *IEEE Journal of Electronic Circuits and Systems*, vol. 3, No. 4, July 1979, pp.165–185.
- [36] Cluniat, C., "Correction of Non-Linearity in Low and Medium Power Transmitters and Transposers", *Review Technique Thomson-CSF*, vol. 10, No. 2, June 1978, pp.1–46.
- [37] Dominguez, R., "Non-Linearity Measurement and Test System for Television Transmitters or Relay Equipment", *Laboratoire Général des Télécommunications*, a Thomson-CSF Publication.

- [38] Lotsch, H.K.V., "Theory of non-linear distortion produced in a semiconductor diode", *IEEE Trans. Electron Devices*, vol. 5, 1968, pp.294–307.
- [39] Lyner, A.G. and Shelswell, P., "UHF Amplifiers: Improvement of Linearity by Pre-Correction", *BBC Research Report RA-134*.
- [40] Procharzka, A., "Degradation of Performance Parameters in a Television Relay System-I", *IEEE Trans. on Broadcasting*, vol. BC-25, No. 3, September 1979, pp.90–100.
- [41] Riley, J.L., "Some Considerations on the Use of Pre-Amplifiers at Low-Power UHF Relay Stations", *BBC Engineering*, August 1977, pp.20–33.
- [42] Walker, H.P., "Sources of Intermodulation in Diode-Ring Mixers", *The Radio and Electronic Engineer*, vol. 46, No. 5, May 1976, pp.247–255.
- [43] Wass, C.A.A., "A Table of Intermodulation Products", *Proc. IEE*, vol. 33, 1948, pp.31–39.
- [44] Yousif, A.M and Gardiner, J.G., "Distortion effects in a switching-diode modulator with tuned terminations", *Proc. IEE*, vol. 119, No. 2, February 1972, pp.143–148.

Phase Lock Loop Techniques:

- [45] Egan, W.F., *"Frequency Synthesis by Phase Lock"*, John Wiley and Sons, 1981.
- [46] Frazier, J.P. and Page, J., "Phase-Lock Loop Frequency Acquisition Study", *IRE Transactions on Space Electronics and Telemetry*, September 1962.
- [47] Gardner, F.M., "Phase Lock Techniques", John Wiley and Sons, Inc., 1966.
- [48] Klapper, J. and Frankle, J.T., *"Phase-Locked and Frequency-Feedback Systems"*, Academic Press, Inc., New York, 1972.
- [49] Kuo, B.C., *"Automatic Control Systems"*, Prentice-Hall, Inc., New Jersey, 1962.
- [50] Lindsey, W.C. and Simon, M.K., Editors., *"Phase-Locked Loops and Their Application"*, IEEE Press, 1977.
- [51] Manassewitsch, V., *"Frequency Synthesizers Theory and Design"*, John Wiley and Sons, New York, 1980.

- [52] Nash, G., "Phase-Locked Loop Design Fundamentals", *Motorola Application Note AN-535*.
- [53] Rey, R.T., "Automatic Phase Control: Theory and Design", *Proc. IRE*, October 1960, pp.1760-1771 (Corrections: *Proc. IRE*, Mar. 1961).
- [54] Rohde, U.L., "*Digital PLL Frequency Synthesizers - Theory and Design*", Prentice-Hall Inc., 1983.
- [55] Soclof, S., "*Applications of Analog Integrated Circuits*", Prentice-Hall, Inc., New Jersey, 1985, Chapter 7.
- [56] "The RCA COS/MOS Phase-Locked Loop. A versatile Building Block for Micro-Power Digital and Analog Applications", *RCA CMOS Application Note ICAN-6101*.
- [57] Viterbi, A.J., "*Principles of Coherent Communication*", McGraw-Hill Book Co. Inc., New York, 1966.
- [58] National Linear Data Book, 1980.

Tolerances:

- [59] Stout, M.B. "*Basic Electrical Measurements*", Prentice-Hall Inc., 1960, Chapter 2.

Switched Capacitor Filters:

- [60] Tsividis, Y., "Principles of Operation and Analysis of Switched-Capacitor Circuits", *Proc. IEEE*, vol. 71, No. 8, August 1983.

Filter Theory and Design:

- [61] Dutta Roy, S.C. and Clark, P., "Design of sharp-cut-off filters with ripples in the pass-band", *The Radio and Electronic Engineer*, vol. 45, No. 6, June 1975, pp. 293-298.
- [62] Heulsman, L.P., "*Theory and design of Active RC Circuits*", McGraw-Hill Book Company, New York, 1968.
- [63] Heulsman, L.P., "*Active Filters: Lumped, Distributed, Integrated, Digital and Parametric*", McGraw-Hill Book Company, New York, 1970.

- [64] Kuo, F.F., "*Network Analysis and Synthesis*", John Wiley and Sons, Japan, pp.365-404.
- [65] Mitra, S.K., "Synthesizing Active Filters", *IEEE Spectrum*, vol. 6, January 1969, pp.47-63.
- [66] Moschytz, G.S. and Horn, P., "*Active Filter Design Handbook*", John Wiley and Sons, 1981.
- [67] Peless, Y. and Murakami, T., "Analysis and Synthesis of Transitional Butterworth-Thomson Filters and Bandpass Amplifiers", *RCA Review*, vol. 17, No. 1, March, 1957, pp.60-94.
- [68] Sallen, R.P. and Key, E.L., "A Practical Method of Designing RC Active Filters", *IRE Trans. Circuit Theory*, vol. CT-2, March 1955, pp.74-85.
- [69] Schoeffler, J.D., "The synthesis of minimum sensitivity networks", *IEEE Trans. Circuit Theory*, vol. CT-11, June 1964, pp.271-276.
- [70] Shea, R.F. (Editor), "*Amplifier Handbook*", McGraw-Hill Book Co, Inc., (no date), pp.5-11 to 5-12.
- [71] Stout, D.F. and Kaufman, M., "*Handbook of Microcircuit Design and Application*", McGraw-Hill Book Company, New York, 1980, Ch. 20.
- [72] Tedeschi, F.P., "*The Active Filter Handbook*", TAB Books, 1979, pp.113-121.
- [73] Daniels, R.W., "*Approximation Methods for Electronic Filter Design*", McGraw-Hill 1980.
- [74] Tow, J., "A step-by-step active filter design", *IEEE Spectrum*, vol. 6, December 1969, pp.64-68.
- [75] Van Valkenburg, M.E., "*Analog Filter Design*", Holt, Rinehart and Winston, 1982.

Filter Sensitivity:

- [76] Goldstein, A.J. and Kuo, F.F., "Multiparameter sensitivity", *IRE Trans. Circuit Theory (Corresp.)*, vol. CT-8, June 1961, pp.177-178.
- [77] Ilumoka, A. and Spence, R., "Reduction of Tolerance Effects in the 2nd-Order Sallen-Key Filter", *Proc. IEE, Part G, Number 4*, August 1981, pp.163-166.

- [78] Lueder, E. and Tilch, H.J., "Pole-Zero Assignment for RC-Active Filters with Minimised Sensitivity", *Proc. IEE*, Part G, vol. 128, No. 4, August 1981, pp.167–169.
- [79] Petrela, D.M. and Budak, A., "Design of Single-Voltage Amplifier Active Filters for Minimum Open-Loop Gain Sensitivity", *IEEE Transactions on Circuit Theory*, vol. CT-18, Number 6, November 1971, pp.631–636.
- [80] Rosenblum, A.L. and Ghausi, M.S., "Multiparameter Sensitivity in Active RC Networks", *IEEE Transactions on Circuit Theory*, vol. CT-18, Number 6, November 1971, pp.592–600.
- [81] Soderstrand, M.A. and Mitra, S.K., "Gain and Sensitivity Limitations of Active RC Filters", *IEEE Transactions on Circuit Theory*, vol. CT-18, Number 6, November 1971, pp.600–610.
- [82] Schoeffler, J.D., "The synthesis of minimum sensitivity networks", *IEEE Trans. Circuit Theory*, vol. CT-11, June 1964, pp.271–276.

Precision Rectifiers:

- [83] Tobey, G.E., Graeme, J.G., and Heulsman, L.P., "*Operational Amplifiers Design and Applications*", McGraw-Hill Kogakusha, Ltd., 1971, Chapter 9.
- [84] Antoniou, A., "Design of Precision Rectifiers using Operational Amplifiers", *Proc. IEE*, vol. 121, No. 10, October 1974, pp.1041–1044.

Monostable Multivibrator Design:

- [85] Paradise, J., "Using the CD4047A in COS/MOS Timing Applications", *RCA Application Note ICAN-6230*.
- [86] "CD4047A COS/MOS Low-Power Monostable/Astable Multivibrator", *RCA Data Bulletin*, File No. 623.
- [87] Dean, J.A. and Rupley, J.P., "Astable and Monostable Oscillators Using RCA COS/MOS Digital Integrated Circuits", *RCA Application Note ICAN-6267*.
- [88] "CMOS DATABOOK", *National Semiconductor Corporation*, Section 5.

Temperature Coefficients:

- [89] Dale-Lace, J., "Which Capacitor", *PULSE*, December 1975, p.33.
- [90] Dummer, G.W.A., "*Modern Electronic Components*", Sir Isaac Pitman and Sons, London, 2nd Ed., 1966.
- [91] "General Catalogue of Electronic Components and Materials", *Philips, Eindhoven*, Section C, p.C127, 1983.

Least Squares Curve Fitting:

- [92] Sokolnikoff, I.S. and Sokolnikoff, E.S., "*Higher Mathematics for Engineers and Physicists*", McGraw-Hill Book Co., 1941.

Thermistors:

- [93] Burke, A., "Linearizing thermistors with a single resistor", *Electronics*, June 2, 1981, pp.151-154.
- [94] Hyde, F.J., "*Thermistors*", Iliffe, London, 1971.

Noise:

- [95] Denny, H.W., "*Grounding for the control of EMI*", Don White Consultants, 1983.
- [96] Graeme, J., "Using op amps in low noise applications", Burr-Brown, Tucson, Ariz., *Application Note AN-68*, January 1975.
- [97] Letzter, S. and Webster, N., "Noise in Amplifiers", *IEEE Spectrum*, August 1970, pp.67-75.
- [98] Motchenbacher, C.D. and Fitchen, F.C., "*Low-Noise Electronic Design*", John Wiley and Sons, Inc., New York, 1973.
- [99] Rheinfelder, W.A., "*Design of LOW-NOISE transistor input circuits*", Iliffe Books Ltd., London, 1964.
- [100] Haus, H.A., "Representation of Noise in Linear Twoports", *Proc.I.R.E.*, vol. 48, 1960, pp.69-74.
- [101] Freeman, J.J., "*Principles of Noise*", John Wiley and Sons, Inc., 1958.
- [102] Davenport, W. and Root, W., "*Random Signals and Noise*", McGraw-Hill Book Co., Inc., 1958.

- [103] White, D.R.J., *"EMI Control in the Design of Printed Circuit Boards and Backplanes"*, Don White Consultants, 1980.
- [104] White, D.R.J., *"Electromagnetic Shielding: Materials and Performance"*, Don White Consultants, 1980.

Transmitting Facilities Design:

- [105] George, D.L. and Hiatt, J.F., "UHF Transmitting Facilities Design", *Proc. IEEE*, vol. 70, No. 11, November 1982.

Control Theory:

- [106] Luyben, W.L., *"Process Modeling, Simulation, and Control for Chemical Engineers"*, McGraw-Hill Kogakusha, Ltd., 1974, pp.366–371.

Operational Amplifiers:

- [107] Tobey, E.G., Graeme, J.G., and Heulsman, L.P., *"Operational Amplifiers Design and Applications"*, McGraw-Hill Kogakusha, Ltd., 1971, pp.51–89.